



# Assessing and Anticipating the Risks Associated with Nanoparticulate UV Filters Used in Sunscreens: A Life Cycle-Oriented Study.

Riccardo Catalano

## ► To cite this version:

Riccardo Catalano. Assessing and Anticipating the Risks Associated with Nanoparticulate UV Filters Used in Sunscreens: A Life Cycle-Oriented Study.. Environmental Sciences. Aix Marseille Univ., CEREGE, 2020. English. NNT : 2017AIXM0001 . tel-04526585

**HAL Id: tel-04526585**

**<https://theses.hal.science/tel-04526585>**

Submitted on 29 Mar 2024

**HAL** is a multi-disciplinary open access archive for the deposit and dissemination of scientific research documents, whether they are published or not. The documents may come from teaching and research institutions in France or abroad, or from public or private research centers.

L'archive ouverte pluridisciplinaire **HAL**, est destinée au dépôt et à la diffusion de documents scientifiques de niveau recherche, publiés ou non, émanant des établissements d'enseignement et de recherche français ou étrangers, des laboratoires publics ou privés.

# UNIVERSITE D'AIX-MARSEILLE

## ECOLE DOCTORALE « Science de l'environnement (ED 251) »

PARTENAIRE DE RECHERCHE

CEREGE/Environnement Durable

Institut Fresnel/CONCEPT

Thèse présentée pour obtenir le grade universitaire de docteur

Discipline : Science de l'environnement

Spécialité : Géoscience/Physico-chimie de l'environnement

**Riccardo CATALANO**

*Évaluer et anticiper les risques associés aux filtres UV  
nanoparticulaires employés dans les crèmes solaires: une  
étude orientée vers le cycle de vie.*

Soutenue le 30/06/2020 devant le jury :

Catherine MOUNEYRAC/ Université Catholique de l'Ouest

Céline PICARD/Université du HAVRE

Annalisa PINSINO/Consiglio Nazionale delle Ricerche (CNR)

Philippe PICCERELLE/Aix-Marseille Université - Timone

Jean-Claude HUBAUD/Helioscience

Mossadek TALBY/Directeur du Collège Doctoral d'Aix-Marseille Université

Jérôme LABILLE/CEREGE - Aix-Marseille Université

Myriam ZERRAD/Institut Fresnel – Aix-Marseille Université

Rapporteur

Rapporteur

Examineur

Examineur

Invité

Invité

Directeur de thèse

Co-directeur de thèse

Numéro national de thèse/suffixe local : 2017AIXM0001/001ED62





To Father, Mother and Brother  
To all the people I loved along the way  
To all the sunsets after a long journey



## Résumé

Les crèmes solaires interrogent de plus en plus quant à leur impact environnemental potentiel, car les ingrédients spécifiques qui la constituent, tels que les filtres UV, les tensioactifs, les épaississants, peuvent atteindre l'eau des rivières, des lacs, des côtes lorsque le produit est éliminé de la peau pendant la baignade. Les minéraux nanoparticulaires utilisés comme filtres UV sont susceptibles d'impacter ces systèmes. Des lacunes perdurent concernant la sécurité de ces nanomatériaux car peu d'études ont porté sur des filtres UV réels et leur cycle de vie à ce jour. Ce travail de thèse avait pour but de contribuer à combler ces lacunes en s'intéressant à plusieurs étapes clefs du cycle de vie: la caractérisation des filtres minéraux et l'optimisation de leur concentration dans le produit; l'écotoxicité marine à ces filtres UV minéraux ; dans le but de proposer des stratégies nouvelles pour anticiper et minimiser ces risques à travers une approche d'éco-conception.

Mots clés : évaluation du risqué, cycle de vie, nanotechnologie, éco-conception

## Abstract

Sunscreens are increasingly questioning their potential environmental impact, because the specific ingredients they contain, such as UV filters, surfactants, thickeners, can reach rivers, lakes, sea shore, and/or sewage treatment plants when the product is removed from the skin during bathing or daily cleansing. Nanomaterials (NMs) used in sunscreen formulation as UV filters may impact these systems. Knowledge gaps remain regarding the safety of these NMs, as few studies have been conducted on actual UV filters or on the life cycle of sunscreens to date. This thesis work aimed to contribute to filling these gaps by focusing on several key stages of the sunscreen life cycle: the characterization of nano-TiO<sub>2</sub> UV filters and the optimization of their concentration in the product, the exposure and marine ecotoxicity to these mineral UV filters; with the aim of proposing some new strategies to anticipate and minimize these risks through an eco-design approach.

**Keywords :** Lifecycle risk assessment, Nanotechnology, Eco-design



# Table of contents

|   |            |
|---|------------|
| <b>RÉSUMÉ.....</b>  | <b>III</b> |
| <b>ABSTRACT.....</b>  | <b>IV</b>  |
| <b>TABLE OF CONTENTS.....</b>   | <b>VI</b>  |
| <b>ACKNOWLEDGEMENTS.....</b>  | <b>IX</b>  |
| <b>CHAPTER I: INTRODUCTION .....</b>  | <b>1</b>   |
| <b>1.1 NANOTECHNOLOGY: DEVELOPMENT, PUBLIC CONCERN AND RISK ASSESSMENT.....</b>   | <b>1</b>   |
| 1.1.1 A RISING CONCERN ABOUT THE POTENTIAL ASSOCIATED RISK .....  | 1          |
| 1.1.2 A SPECIAL APPROACH NEEDED FOR NANOMATERIAL RISK ASSESSMENT .....  | 3          |
| 1.1.3 NANOMATERIAL REGULATION.....  | 4          |
| 1.1.4 CONCEPT OF LIFECYCLE AND ECO-DESIGNED NANOMATERIAL .....  | 5          |
| <b>1.2 LIFECYCLE RISK ASSESSMENT: THE SUNSCREEN NANOPRODUCT CASE STUDY.....</b>   | <b>7</b>   |
| 1.2.1 RELEASE IN THE ENVIRONMENT.....   | 9          |
| 1.2.2 UV FILTER ECOTOXICITY .....   | 13         |
| 1.2.3 FABRICATION AND USAGE.....  | 19         |
| <b>1.3 IMPORTANCE OF THE UV FILTER AGGREGATION STATE ALONG THE LIFECYCLE.....</b>   | <b>24</b>  |
| 1.3.1 EFFECTS OF THE UV FILTER AGGREGATION .....  | 24         |
| 1.3.2 SUNSCREEN STRUCTURAL CHARACTERISATION .....   | 26         |
| <b>1.4 THESIS OBJECTIVES AND LIST OF PAPERS.....</b>  | <b>28</b>  |
| <b>CHAPTER II: MATERIALS AND METHODS .....</b>  | <b>34</b>  |
| <b>2.1 MAIN METHODOLOGY .....</b>   | <b>34</b>  |
| <b>2.2 UV FILTERS SELECTION .....</b>   | <b>34</b>  |
| <b>2.3 SUNSCREEN FORMULATION.....</b>   | <b>36</b>  |
| <b>PART A: FABRICATION AND USAGE .....</b>  | <b>40</b>  |
| <b>CHAPTER III: CHARACTERIZATION OF NANOPARTICULATE UV FILTERS IN UNMODIFIED<br/>COSMETIC MATRIX.....</b>                                       | <b>42</b>  |
| <i>IN SITU</i> DETERMINATION OF NANOPARTICLE AGGREGATION STATE IN COSMETICS EMULSIONS. (TO BE SUBMITTED<br>TO ENVIRONMENTAL SCIENCE NANO) ..... | 44         |
| <b>CHAPTER IV: SAFER BY DESIGN: OPTIMIZATION OF UV FILTERS CONCENTRATION IN THE<br/>FORMULATION .....</b>                                       | <b>78</b>  |

|  |                |
|--|----------------|
| <b>PAPER II :</b> .....  | <b>79</b>      |
| OPTIMIZING THE DISPERSION OF NANOPARTICULATE TiO <sub>2</sub> -BASED UV FILTERS IN A NON-POLAR MEDIUM USED IN SUNSCREEN FORMULATIONS – THE ROLES OF SURFACTANTS AND PARTICLE COATINGS (PUBLISHED IN COLLOIDS AND SURFACE A) .....              | <b>79</b>      |
| <b>SUPPLEMENTARY INFORMATION CHAPTER IV</b> .....  | <b>91</b>      |
| <br><b><u>CHAPTER V: CHARACTERIZATION OF THE SCATTERING PROPERTIES OF THE NANOPARTICULATE UV FILTERS</u></b> .....   | <br><b>96</b>  |
| 5.1.....   | 96             |
| 5.1 PRINCIPLES OF SCATTERING FROM DIELECTRIC PARTICLES .....   | 96             |
| 5.2 PRINCIPLES OF ANGULAR SCATTERING MEASUREMENTS .....  | 100            |
| 5.3 MEASUREMENT TOOLS AND SET UP .....   | 103            |
| 5.4 MEASUREMENT AUTOMATION .....   | 105            |
| 5.5 CALIBRATION .....  | 107            |
| 5.6 SAMPLE MEASUREMENTS .....  | 108            |
| 5.7 TOTAL SCATTERING AND ABSORPTION CALCULATION.....   | 110            |
| 5.8 RESULTS DISCUSSION .....   | 111            |
| 5.9 CONCLUSIONS AND PROSPECTIVE.....   | 115            |
| <br><b><u>PART B: ENVIRONMENTAL RELEASE AND ECOTOXICITY</u></b> .....  | <br><b>117</b> |
| <br><b><u>CHAPTER VI: MINERAL UV FILTERS EXPOSURE IN THE MARINE ENVIRONMENT</u></b> .....  | <br><b>119</b> |
| <br><b>PAPER III :</b> .....   | <b>121</b>     |
| ASSESSING UV FILTER INPUTS INTO BEACH WATERS DURING RECREATIONAL ACTIVITY: A FIELD STUDY OF THREE FRENCH MEDITERRANEAN BEACHES FROM CONSUMER SURVEY TO WATER ANALYSIS (PUBLISHED IN SCIENCE OF TOTAL ENVIRONMENT) .....                        | <b>121</b>     |
| <br><b><u>CHAPTER VII: TiO<sub>2</sub> BASED UV FILTERS ECOTOXICITY: THE MEDITERRANEAN SEA URCHIN CASE STUDY</u></b> .....   | <br><b>138</b> |
| <br>PAPER IV: EFFECT OF NANO-TiO <sub>2</sub> (RUTILE)-BASED UV FILTERS USED FOR SUNSCREEN FORMULATIONS ON THE IMMUNOLOGICAL STATE AND EMBRYONIC DEVELOPMENT OF THE SEA URCHIN <i>PARACENTROTUS LIVIDUS</i> (SUBMITTED ON NANOMATERIALS) ..... | <b>140</b>     |
| <br><b><u>CHAPTER VIII: GENERAL CONCLUSIONS AND PROSPECTIVE</u></b> .....  | <br><b>165</b> |
| 8.1 CONCLUSIONS.....   | 165            |
| 8.2 PROSPECTIVE.....   | 172            |
| <br><b><u>REFERENCES:</u></b> .....  | <br><b>177</b> |





## Acknowledgements

I want to thank the DOC2AMU COFUND program for selected me as candidate for this project, and the financial supporters involved in it: European Union's Horizon 2020; Region SUD; Excellence Initiative of Aix-Marseille University - A\*MIDEX, the French "Investissements d'Avenir" program, through its associated Labex SERENADE project, and the contributors OSU-Institut Pythéas and IPR Innove. In particular I want to thank Sarah Sawyer and Prof. Mossadek Talby for have been following me since the first day.

I want to deeply thank my supervisor Jérôme Labille for believing in me, for always been present when I needed advices and help, for teaching me how to behave in the scientific research world and for always been calm, respectful and kind to me.

I want also to thank my Co-Supervisor Myriam Zerrad for her support and patience in teaching me how to work in the optics/light scattering domain, a subject in which I was (and mostly still am) a novice.

I want to thank all the scientist (and friends) of the groups Environnement durable (ED) and CONCEPT, respectively belonging to the two main labs where I had the pleasure to work: CEREGE and Fresnel Institute. Given the fact that I'm grateful to have meet each one of you during these years, I want to specifically thank some of you with whom I had the opportunity to relate more with: Danielle Slomberg; Armand Masion; Vladimir Vidal; Jerome Rose; Clement Levard; Melanie Auffan; Perrine Chaurand; Daniel Borschneck; Jean-Yves Bottero; Nicolas Roche; Blanche Colin.

Thanks also to all the friends I met in CEREGE and with whom I had the pleasure to spend many of my days in the last years. In particular: Jonathan Coutaz; Benjamin Bouriel; Ross Marchant; Valenti Rodellas; Maureen Le Bars, Julie Gattacceca; Andrea Carboni; Nithvon Cam; Wuhib Tamrat; Floriane Jamoteau; Solène Quero; Ali Ayadi; Meriem Djellali. Eugenie Perouse; Clement Outrequin; Clément Desormeaux; Hamed Pourkhorsandi; Chloé Paulin; Marie Protin; Amandine Jean; Marie Pons; Lisa Kramer; Agathe Toumoulin; Marie Laugié; Nicolas Lusinier. Nicolas Launey. Irene Puliti. Thomas Stieglitz; Aladin Andrisoa. Martina Cotena. Jesus Diaz; Alexandra Bivolaru; Alice Tagliati, Eleonore Paquier, Pierre Saraphin; Noemie Garron; Isabelle Hammad; Silvie Defreitas.

Thanks to the people who welcomed me in the other labs I had the privilege to work: Annalisa Pinsino & Andi Alijagic (CNR/IRIB); Nicolas Hucher & Celine Picard (Le Havre/URCOM); Francois Saint-Antonin (CEA/LITEN); Fabio Ziarelli & Andrea Campos(AMU/Spectropole). Thanks also to the industrial partner of the project Héliosscience in the person of Jean-Claude Hubaud.

Thanks to all my friends (old and new), especially to the new ones I met during these last four years in France (you know who you are), it wouldn't have been the same without you. I want to thank in particular: the **Culto Lovers** (Giorgio; Simone; Angelo and Fufo); Valeria; Francesca; Elena; Nicola; Michele; Stefania; Fabiana; Julia; Geoffrey; Théo; Alia; Livia; Luc; Gabriele; Ante; Fedo; Elsa; Andrea; Laura; Antonio; Conta; Disti; Lodi; Giupi; Giulia; Giorgia; Federica; Emilia; Alice; Ivan; Debba; Tony; Peppe; Auri; Sergio; Felix; Albert.

Last but not least, thanks to my Family: to Francesco, Daniela and Enrico. For support me and believe in me even when I don't. For the unconditional love you have always given to me.



## Chapter I: Introduction

### 1.1 Nanotechnology: development, public concern and risk assessment

The term *Nanotechnology* refers to the ability in manipulating matter at the nanoscale, which leads to new materials, products and devices that show new and unusual behaviour. A nanomaterial (NM) is defined as a material designed and produced to have at least one dimension of 100 nm or less<sup>1</sup>. This relatively young technology begins to grow between the end of the nineties and the early 2000 and, just five years later, was already promoted by press and scientific community as a major technological breakthrough, heralding the next industrial revolution<sup>2</sup>. Due to the exclusive benefits that nanoscale materials could provide to common daily-use products (ex: lighter and stronger objects; more effective batteries; antibacterial socks), the use of nanotechnologies spreads up at almost every industrial levels comprehending: food; agriculture; packaging; cosmetics; drugs; painting and medicine<sup>3-5</sup>. The global market value of nanotechnology is nowadays assessed between 64 and 76 billion U.S dollars<sup>6</sup> with a predicted growth of 17% until 2024<sup>7</sup>.

#### 1.1.1 A rising concern about the potential associated risk

Almost concurrently with its global diffusion, the concerns that these new nanotechnologies would bring about new risks for both human health and environment grew rapidly<sup>8</sup>, because of the bad examples of previous industrial revolutions that had been taught hard lessons on how rapid technological advances can impact on society. However, evaluating the risk associated to nanotechnology and nanomaterials is not a straightforward process. Because of

their small size, nanoparticles have many different physical-chemical properties (quantum confinement; surface plasmon resonance; super-magnetism effect) that differ from those of their bulk forms<sup>9</sup>. Also, nanomaterials are so diverse between one-another (**Figure 1.1**) (chemical composition; size; shape; dispersant phase), that a generical classification when it comes to evaluate their potential health impact is almost impossible.

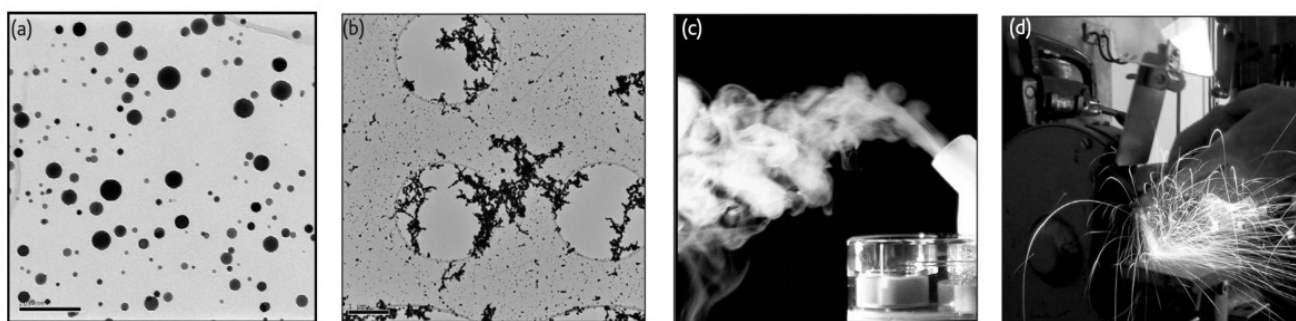


**Figure 1.1:** Examples of nanomaterials likely dangerous for human health (Maynard *et al.* 2005): (a) Unbound nanometer-diameter particles (in air or liquids). (b) Agglomerates of nanoscale particles (in powders, air, and liquids). (c) Aerosols of nanometer-structure particle suspensions, solutions, or slurries. (d) Particles released while working with or using nanostructured materials, through machining, grinding, or wear and tear.

For example, the cytotoxicity and immunological response of murine macrophages cells toward different types of nanoparticulate Ag or Au could be really different not only because of the different chemical composition of the materials but also because of different physical features such as primary particle size and shape<sup>10</sup>. The higher interest for human health associated to smaller sized nanomaterials (sub-100 nm) was already suggested in 2004 by the Royal Society and Royal Academy of Engineering<sup>11</sup>. However, the particle alone is not the only factor to look at when we consider a complex structured nanomaterial. Nanomaterials can in fact appear as aggregates composed of several nanoparticles and that can reach sizes far beyond the nano-meter scale. Some reports have suggested that when particle aggregation phenomena became significant, primary particle size should not be considered for assessing the toxicity effects<sup>12</sup> and that only the hydrodynamic size of the aggregates should be taken onto account<sup>13</sup>.

### 1.1.2 A special approach needed for nanomaterial risk assessment

Different nanoparticle transformation/modification (aggregation; agglomeration; sedimentation; dissolution) can indeed occur during the fabrication of the product where nanomaterials are employed (nano-product)<sup>14</sup>, during the product usage or at the end of the nano-product lifecycle when the nanomaterials inside it are released in the environment and are able to interact with organic matter or different microorganism leading to even more complex reactions<sup>15</sup>. These transformations can change the NM behaviour (surface properties; redox state; size) complicating the prediction of their transport, bioavailability and overall potential toxicity<sup>16</sup>.

Moreover, the full characterization of NMs inside complex matrix such as the initial product where they are incorporated, natural environments or inside biological systems is often a tricky process. For example, environmental relevant concentration of certain nanomaterials are really low and perhaps below the detection limits of many characterization techniques able to determine their concentration or their concentration or their aggregation state (ex. Dynamic Light Scattering; X-Rays absorption)<sup>17</sup>. Conventional electronic microscopies (TEM; SEM) are sometimes unsuitable to characterize NMs in complex matrix as they require extreme working condition that would alter the interactions between the NMs and the surrounding matrix<sup>17</sup>.

All these uncertainties and issues make difficult to generate standard protocols able to assess the toxicity of different nanoprodukt toward different organisms and environments as well as the hazard for product consumers<sup>18</sup>. Even-though certain standard protocols already exist for a wide range of aquatic invertebrates, fish and microbial organism<sup>19,20</sup>, these tests were established for traditional

chemicals but not for the NMs. The consensus is that the existing methods and framework for hazard assessment (standard test organisms, mortality, growth and reproduction endpoints) are generally fit for this purpose, but the details within each group of tests may require modification or optimization to work well with NMs<sup>21</sup>.

### 1.1.3 Nanomaterial regulation

One of the main aftermaths of the NMs complexity and diversity is the limited regulation and legislation. Regulators around the globe currently have little ability to identify and mitigate risk due to its associated scientific uncertainty<sup>22</sup>. Moreover, there is an intrinsic issue to create global regulation for the nano-product mostly because of lack of accordance between countries on NMs definition or quantification. For example, U.S countries consider NMs weight-based size distribution while other systems apply number-based size distribution criterion. Or again, U.S countries consider as NMs only the ones intentionally manufactured while European Commission (EC) includes also natural or incidental materials in the nanoscale range<sup>23</sup>.

To overcome all these problematics, the International Organization for Standardization (ISO), a non-governmental organization consisting of 156 nations' standardization institutes, has constructed a 27-nation committee to address nanotechnology standards<sup>24</sup>, which continue to develop a standardized framework for discussing and governing NMs. In addition to ISO, professional societies have devoted themselves to a global standard to be used in characterizing and regulating nanotechnology. As for example the American Society for Testing and Materials (ASTM) International, which formed a committee in 2005 to tackle issues of nanotechnology standardization and



guidance<sup>24</sup>. In Europe, the European Commission's regulation program Registration, Evaluation, Authorization and Restriction of Chemicals (REACH) is currently working on the regulation of products containing nanomaterials. The regulatory process normally requires a basic physicochemical characterization of the product (stability; purity; molecular weight; crystal structure) and, when it is necessary, a toxicological evaluation. (*in vivo* / *in vitro* toxicity tests)<sup>25,26</sup>

#### 1.1.4 Concept of lifecycle and eco-designed nanomaterial

Another fundamental aspect in the nanotechnology risk assessment is the consideration of the full product lifecycle. In 2006, in fact, the idea that new materials and compounds can be created first, with impact assessment made post manufacture and distribution became obsolete<sup>27</sup>. To become more proactive and to enable more holistic public health and environmental protection, adverse effects must be evaluated at the point of conception<sup>22</sup>. The life cycle assessment of NMs should include the full range of environmental effects assignable to products from raw-material production, manufacture, distribution, use and disposal<sup>27</sup>. The LCA defines also the boundaries for the conception of an environmentally-benign product and it constitutes the starting framework for the concept of eco-design, which focus more on the integration of environmental considerations in product development, conceiving ecological and economical tools for those designers involved in the making of the product<sup>28</sup>. Nonetheless, due to the complexity of the subject, the debate is still ongoing especially regarding the categorization of the different nanoproducts and the methodology to apply in order to determine a correct LCA for each one of them. Asmatulu *et al.*<sup>29</sup> attempted to categorize 1.094 nanoproducts (referring to the PEN CPI list<sup>30</sup>) into different classes based on their most probable end-of-life fate. They manage

to identify 9 categories of end-of-life groups: Recycle (ex. batteries); Ingestion (ex. chewing gums); Absorbed by skin then public sewer or water body (ex. lotions; sunscreens); Public sewer or water body (Laundry detergent); Burning then landfill (engine oil); Landfill; Air release (deodorant sprays); Air release then public sewer or water body (surface coatings); Others (plant grow mixture). Even-though the end-of-life stage is one crucial to assess the risk associated to a nanoproduct, it is not the only aspect to take onto account. In 2012, Gavankar *et al.*<sup>31</sup> reviewed the state-of-the-art on environmental impacts of nanomaterials and life cycle assessment studies on engineered nanomaterials (ENMs) and nanoproducts. They concluded that most of the works were incomplete, meaning that did not consider the whole lifecycle of the product but only one or two stages. In fact, while almost all of them did consider the manufacture or the environmental release, only a few were also concentrated on the nanoproduct usage stage. Also, wherever the nano-aspect was acknowledged as part of the discussion, its contribution was never evaluated quantitatively mostly because of the lack of information on the nanomaterial properties, toxicity and physical-chemical characterization model.

Since then, the knowledge on NMs and nanoproducts environmental risk assessment has certainly evolved especially concerning their release and toxicity at the end-of-life of the product<sup>32,33</sup>. More attention has been given to the chemical alterations of the ENMs in the environment, which is a crucial aspect to consider in order to better predict and assess the toxicity of a nanoproduct<sup>34,35</sup>. In this context, the aging of CeO<sub>2</sub>-based nanocomposites used as UV filter in wood paint was studied by Auffan *et al.*<sup>36</sup>. They analysed the long-term behaviour and stability of the ENMs in aqueous medium and demonstrated that the citrate coating of these ENMs is completely removed after 42 days of aging in water. This alteration was illumination dependent and caused colloidal destabilization of the

nanocomposites, which eventually leads to “new” CeO<sub>2</sub> NPs with surficial properties significantly different from the pristine ones, and thus with different fate transport in the environment as well as the impact toward the organisms. Recently, Scifo *et al.*<sup>37</sup> studied the dynamics of Ce release in aquatic environment from similar CeO<sub>2</sub>-acrylic nanocomposite designed for wood protection, revealing the presence of two different regimes of release, also influenced by the presence or absence of UV radiation. The release and fate of ENMs in aquatic environment was also approached by Botta *et al.*<sup>38</sup> and Kaegi *et al.*<sup>39</sup>, in the case of nanoparticulate TiO<sub>2</sub> used in sunscreens and building facades respectively. In both cases, a significant ENMs release was observed, especially in freshwater mediums, although both were preliminary studies realised in controlled lab conditions and needed further analysis and developments. Each one of these works taken as examples, are of course focused on just one stage of a selected nanoproduct lifecycle. It is anyway fundamental to gather and summarize the knowledge provided in the state-of-the-art on a particular nanoproduct and cross it with the regulatory and industrial data, in order to better formulate the nanoproduct LCA. This will also contribute to define a starting network for an eco-design of the nanoproduct, that is the integration of environmental considerations in product development. An effort in this direction was recently made by Walker *et al.*<sup>40</sup> in the context of the LCA of nano-enabled pesticides. However, nanoproduct LCA oriented studies are still rare and definitely need further investigations.

## 1.2 Lifecycle risk assessment: The sunscreen nanoproduct case study

Among products enabled by nanotechnology, sunscreens are of emerging concern. They provide effective protection against the damages caused by exposure to ultraviolet radiation (UVR)<sup>41</sup> which is dangerous for human skin,

causing burns, aging, and even cancer<sup>42</sup>. UVR can be split into two main contributions: UVA (400-320 nm) and UVB (320-280 nm). UVC (280-100 nm) are also present but are not a concern in sunscreen protection as they are mainly absorbed by the ozone layer in the atmosphere<sup>43</sup>. UVB typically induces erythema and direct DNA damage, whereas UVA is associated with tanning and photoaging. UVA also generates excess reactive oxygen species which indirectly damage DNA<sup>44</sup>.

These cosmetic products are highly consumed by the worldwide population as the sun care market constitutes 3% of the overall market of personal care products<sup>45</sup>. From a physical-chemical point of view, sunscreens are essentially emulsions of water and oil in which are dispersed specific components, called UV filters, able to screen the user skin from UV radiations. These filters could be organic molecules (avobenzene; benzophenones), which screen UV light mainly through absorption mechanisms, or inorganic minerals like  $\text{TiO}_2$  or  $\text{ZnO}$  (employed in micrometric or nanometric forms) which screen UV radiations through both physical (scattering and/or reflection) and absorption mechanisms. The UVR screening efficiency of a sunscreen is defined by the Solar Protection Factor (SPF), which can be evaluated through *in vitro*<sup>46</sup> or *in vivo* tests. The latter are generally costly and time consuming, thus not practical for routine sunscreen evaluation contrariwise to *in vitro* ones, which are based on diffuse transmission spectroscopy and are widely used by companies as credible alternatives<sup>47</sup>. In such type of tests, a thin film of product is applied to a suitable UV transparent substrate (generally a PMMA plate) and then UV radiation transmitted through this film is measured by a spectrophotometer equipped with an integrating sphere<sup>48</sup>.

Sunscreens are increasingly questioning on their potential environmental impact, because the specific ingredients they contain, such as UV filters, surfactants, thickeners, can reach the water of rivers, lakes, sea shore, and/or sewage treatment plants when the product is removed from the skin during bathing or daily cleansing. Such compounds may impact these systems, even-though a precise evaluation of the impact degree is not a straightforward process.

The risk assessment of a certain product should require a hazard evaluation for each component and for the entire mixture, as well as its doses response and exposure assessments (*NAS/NRC 1983*). If we want to evaluate the risk associated to nanoparticulate UV filters used in a sunscreen formulation, assess the toxicity of the ENMs alone is not enough. At each stage of the product lifecycle, physical-chemical transformations can take place, which could modify the ENMs reactivity. These alterations can have repercussions on the performance of the nanoproduct during the usage, but also on the subsequent transportation, bioavailability (exposition) and eco-toxicity (hazard) after its release in the environment. An extensive analysis of the ENMs transformation and reactivity at each lifecycle stage of the nanoproduct is thus required.

### 1.2.1 Release in the environment

After the usage, sunscreens are washed off the skin mainly via bathing activities or domestic wastewater pathway (e.g. after shower). The fate of nanoparticulate UV-filters depends on the extent and routes of the aging process and determines their potential impact on the environment. The propensity of the products to be dispersed in the aqueous phase as nanoparticles or colloids is a point that eco-design should seek to minimize.

In general, environmental release of ENMs could be determined through two different approaches: field sampling (local scale) or model estimation (varying scale). The latter allows to overcome some technical and practical issues which normally affect a field sampling and was thus widely developed in the last years. Besides many knowledge gaps (e.g. on ENM production, application and release) still affect the modelled values, an order of magnitude of the environmental concentrations of ENMs used in cosmetics was reached and agreed in many cases<sup>49-52</sup>. In 2007, Boxall *et al.*<sup>52</sup> presented the first quantitative study, where they predicted realistically concentrations of various ENMs used in cosmetics, fuel additives and paints, in soil, water and sludge. They obtained ranges of 24-245 µg/L and 76-760 µg/L for TiO<sub>2</sub> and ZnO in water, respectively. Gottschalk *et al.*<sup>49</sup> developed a probabilistic method to compute the distributions of Predicted Environmental Concentrations (PEC) in nanomaterials based on flow modelling and Monte-Carlo simulation, in order to deal with the uncertainty in the model parameterization related to lack of knowledge on transfer, partitioning coefficients and emission factors. The modelled PEC values proposed in the literature are not always comparable due to the different scenarios considered and nanoparticle characteristics used. A dozen of those existing models was reviewed in 2013 in order to clarify those key parameters that determine the modelled values<sup>53</sup>. One year later, Keller *et al.*<sup>51</sup> estimated the ENM release from personal care products (PCP) into soils, water, air, and landfills in California and China. They accomplished this by surveying consumer's habits and analyzing container sizes and ENM concentration in each product. The total sunscreen consumption in the USA was estimated at 90,000 metric tons per year, involving 2,300-2,700 mt/yr of ENMs. Authors revealed that sunscreen is the most intensive ENM application among PCPs, with 81-82% of the total ENM mass flow, and that ZnO and TiO<sub>2</sub> are the most commonly used ENMs, representing together 94% of the ENM use in PCPs. From the overall sunscreen usage, including

everyday use and recreational activities, they predicted that the amount of sunscreen directly released from the skin to the bathing area water levels at 5%. The rest of the consumed products was mostly used out of recreational activity, giving about 60 to 90% washed off during showering and flowed to the wastewater treatment plant (WWTP). The efficiency of the WWTP for ENM removal from the wastewater controls the ENM partitioning between the downstream compartments soil and surface water.

Field sampling approach was always limited and dependent to ever evolving detection methods<sup>54</sup>, thus a few studies were addressed on the detection of UV filters in coastal waters to date, most of them concentrated in the last 7-8 years<sup>55-57</sup>. While the presence of organic UV filters is commonly observed in the ng/L range in areas with recreational activities, it is still unclear how these molecules partition and degrade within the different environmental compartments, and how this will impact their resulting lifetime. Degradation is mainly induced by photoisomerization and photodegradation processes in the presence of sunlight, processes which are known to be influenced by the presence of certain water constituents, such as natural organic matter, chlorides, nitrates, and bicarbonates<sup>58,59</sup>.

For mineral UV filters, the scenarios of environmental fate can be different and pose new scientific questions. The detection of anthropogenic TiO<sub>2</sub> and ZnO minerals (nano or non-nano) in aquatic environments where both Ti and Zn elements naturally occur in varying background concentrations remains an analytical challenge. Different proxies have been tested to distinguish the natural, terrigenous materials from those that are man-made. Al and Si are the most often used elements in mineral UV filter coatings, but are difficult to use as a proxy for anthropogenic emission due to their abundance in natural systems<sup>16,60</sup>. The

available analytical methods are often not sensitive enough for current environmentally relevant concentrations and cannot distinguish natural materials in the nanoscale size range from manufactured nanomaterials<sup>61,62</sup>.

An alternative to traditional proxies can be considered based on the simultaneous release of mineral and organic UV filters in bathing water. Both filter types may be found together in the environment, as a result of being associated in a common sunscreen or originating from different products. The organic UV filters, which are not present in the natural background, can be detected more easily and may be used as a proxy for the mineral filters. Indeed, the co-evolution of organic and mineral UV-filters has been measured in near shore fresh waters with time-dependent concentrations<sup>63,64</sup>. However, a lack of knowledge remains regarding the respective environmental fate and persistence of these two types of UV-filters, which may be contrasting. The fate of mineral UV filters depends on both their solubility and their tendency to disperse or aggregate and sediment<sup>65</sup>. In addition, the hydrophilic or hydrophobic character of the particle surface will also affect its propensity to remain individually dispersed in the aqueous environment or to adsorb to the surface of natural suspended matter<sup>58</sup>.

Overall, despite the rising interest in the environmental concern of UV filters, very few data are available on the quantification of the source of UV filter inputs in the field. Social surveys on consumer sunscreen use in recreational areas are needed to better understand the relation between the quantities of sunscreen used and the environmental concentrations of the UV filters actually detected in the water. Nonetheless, knowing the release and realistic concentration of the UV filters in the different environments is anyway crucial in order to assess their ecotoxicological impact.



### 1.2.2 UV filter ecotoxicity

Until now, the toxicity of a wide range of UV filters toward different model organisms, belonging to salty or fresh water environments was extensively investigated, especially in the case of organic UV filters<sup>12,66,67</sup>. Some studies investigated the toxicity of different commercial sunscreens, mainly towards corals and phytoplankton<sup>63,68</sup>. Although this knowledge is certainly important, such type of studies often does not permit to understand the contribution of the different components of the formulation in the biological effects observed. Recent reports have been focused on the impact of just certain organic filters, highlighting the potential impact of benzophenones and camphor on the marine environment, particularly on coral reef (bleaching) and in marine organisms such as Crustaceans, Echinoderms, Algae<sup>69–71</sup>.

In this context of emerging concern for the potential sunscreen ecotoxicity, the status of mineral and nanoparticulate UV-filters remains under consideration. Once released into the environment, these ENMs could undergo through various physical-chemical transformations, which would likely modify their subsequent transport and reactivity. In general, nanoparticles may remain in suspension as individual particles, dissolve, or aggregate and form larger particles that are subsequently deposited on sediment. Moreover, they may adsorb onto various components in marine waters (e.g., dissolved organic matter, DOM), and transform chemically based on reduction-oxidation (redox) reactions, or transform biologically in the presence of biota (e.g., microorganisms) in the marine environment<sup>72</sup> (**Figure 1.2**). The environmental fate of these ENMs is thus controlled by their physical, chemical and biological transformations<sup>73</sup>. Physical factors include for example degradation of surface coating, advection, dispersion, aggregation, disaggregation, deposition and resuspension<sup>15,74,75</sup>. Aggregates of

nanoparticles usually have a higher chance to deposit on sediments. The reduction of nanoparticle aggregates from the water column through deposition or sedimentation lowers the concentration of bioavailable fraction for pelagic species such as fish. Although these aggregates become less mobile, uptake by sediment-dwelling organisms or filter feeders is possible<sup>76</sup>, transferring potential effects to other ecosystem compartments.

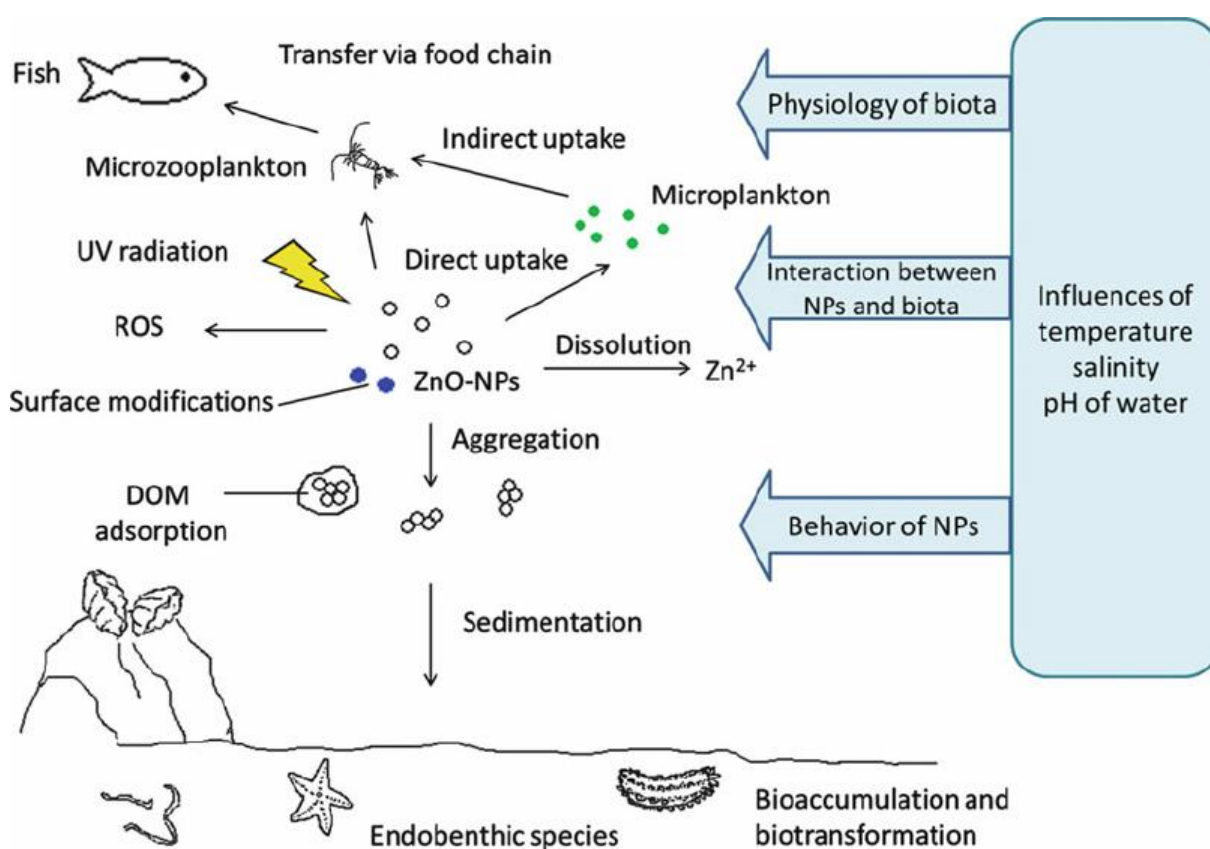


**Figure 1.2:** Schematic illustration of the behaviour and transport of ZnO-NPs (nano particles) in the marine environment (Yung *et al.* 2015)

Multiple Physical and Chemical factors can affect the ENMs distribution, persistence, and toxicity. Physicochemical characteristics of a nanoparticle, together with the conditions of the surrounding environment (e.g. temperature, oxygen level and natural organic matter), can determine the behaviour and

transport of nanoparticles in the environment<sup>75</sup>. Moreover, these reactions and transformations occurring on ENMs after sunscreen is washed-off the skin do not only depend on the local conditions, they are also dependent of the formulation process used at the early fabrication stage of the product. Finally, each stage of the entire sunscreen lifecycle is likely to influence the bioavailability and toxicity of ENMs to aquatic organisms<sup>77</sup>. Once internalised into living organisms, the ENM surface chemistry can lead to some preferential interaction with some organs, which may lead to varying distribution and excretion within an organism<sup>78</sup>. In this context, Slikerman and Keur<sup>79</sup>, have recognized four main mechanism of ENMs reactivity which would affect organism: *physical damage*; *dissolved ions*; *ROS generation*; *carrier function*.

*Physical damage* includes the effects from the particle itself via interaction of the particle and the organism. Depending on size and form, the effects and pathways can differ. For example, nano-ZnO particles attached onto the exoskeleton of the *T. japonicus* nauplii hampered their movement<sup>80</sup>, while the same particles can accumulate into gills and digestive gland tissues of marine oysters, possibly leading to ineffective feeding<sup>81</sup>.

*Dissolved ions* are generated when minerals like ZnO and TiO<sub>2</sub> are involved in redox reactions, leading to an increased ionic-metal concentration. Dissolved ions are more bioavailable than the particle-form counterpart, and could easily be accumulated by aquatic organisms<sup>77</sup>. For this reason, nano-ZnO is generally considered more toxic than nano-TiO<sub>2</sub>, because of its faster ionization in aqueous medium which increase bioavailability and accumulation into aquatic organisms<sup>76,82</sup>

*Photo excitation* from inorganic UV particles (such as TiO<sub>2</sub> and ZnO) under solar radiation produces hydrogen peroxide (H<sub>2</sub>O<sub>2</sub>), a typical Reactive Oxygen Species (ROS). This has been shown to induce oxidative stress to marine phytoplankton

and negatively affect their growth rate<sup>83</sup>. Toxicity of nTiO<sub>2</sub> is mainly associated with this type of mechanism<sup>84</sup>.

The *carrier function* pathway is mainly associated with the interactions between organic toxicants and ENMs in the aquatic environment. Recent studies report that TiO<sub>2</sub> can interact with co-occurring pollutants (mainly through adsorption reactions), resulting in an increase or decrease of pollutant bioavailability<sup>85,86</sup>. Ecotoxicity studies performed agree that nTiO<sub>2</sub> have no expected effects at field concentration toward a wide range of tested model organisms<sup>87</sup>. Marine bacteria (*V. fischeri*) showed no effect towards nano-TiO<sub>2</sub> within the concentration range tested from >100 to >20,000 mg/L<sup>72,88</sup>. Although the responses were species specific, algae did not show effects up to levels of 1 mg/L<sup>72,88</sup>. For rotifers (28 days chronic test) the effects levels were in the same ranges as for algae<sup>89</sup>. The Japanese Medaka fish embryos appears to be one of the most sensitive organisms to bare nano-TiO<sub>2</sub> exposure. The harmful effects observed include reduction of hatching time, altered swimming activity and malformations at concentrations starting at 0.03 mg/l. Unhatched embryos exposed to levels of 7 and 14 mg/L were fully encapsulated in TiO<sub>2</sub> material by study completion, possibly resulting in oxygen stress<sup>90</sup>. Even, zebrafish larvae exposed to assumed environmentally relevant concentrations (1–10 mg/L) of nano-TiO<sub>2</sub> showed neurologic adverse symptoms, such as locomotor alteration, and alterations in mRNA. The authors observed TiO<sub>2</sub> accumulation in brain and oxidative stress, with cell death in the hypothalamus<sup>91</sup>.

After bacteria and mollusks, echinoderms are one of the most studied model organisms regarding nano-TiO<sub>2</sub> aquatic ecotoxicity<sup>87</sup>. Among echinoderms, sea urchin is globally distributed in almost all depths, latitudes, temperatures, and environments in the ocean. Due to its dominant role in structuring and functioning of the rocky reef ecosystem, it is of strong interest as a potential model

to monitor the state of marine environmental health<sup>92</sup>. The potential immunotoxicity of a few metal oxide nanoparticles, including TiO<sub>2</sub> was investigated in vivo, pointing out the potential pathway that can be involved in the interaction with immune cell<sup>93,94</sup>. In analogy, TiO<sub>2</sub> nanoparticle activates suppressive mechanisms by down-regulating the expression of genes encoding immune-related and apoptotic proteins, elicits metabolic rewiring by boosting the immune cell antioxidant activity and restores homeostasis by keeping at physiological levels some key immune-related proteins, in vitro<sup>95</sup>.

Based on the current literature, TiO<sub>2</sub> based UV filters are generally considered the safer UV blockers to be used in sunscreen formulation, even-though further elucidations are still required. Minetto *et al.*<sup>87</sup> in 2014 reviewed more than 200 articles analyzing the eco-toxicity of nano-TiO<sub>2</sub> toward a wide range of aquatic organisms. They highlighted how most of the scientific production (74 %) concern the impact of nano-TiO<sub>2</sub> toward fresh water organisms while only the 15% toward salt water organisms (**Figure 1.3**). The authors claimed that this could be ascribed to the higher complexity of saltwater testing medium, which due to its high salt content and ionic strength, leads to enhanced ENMs instability,

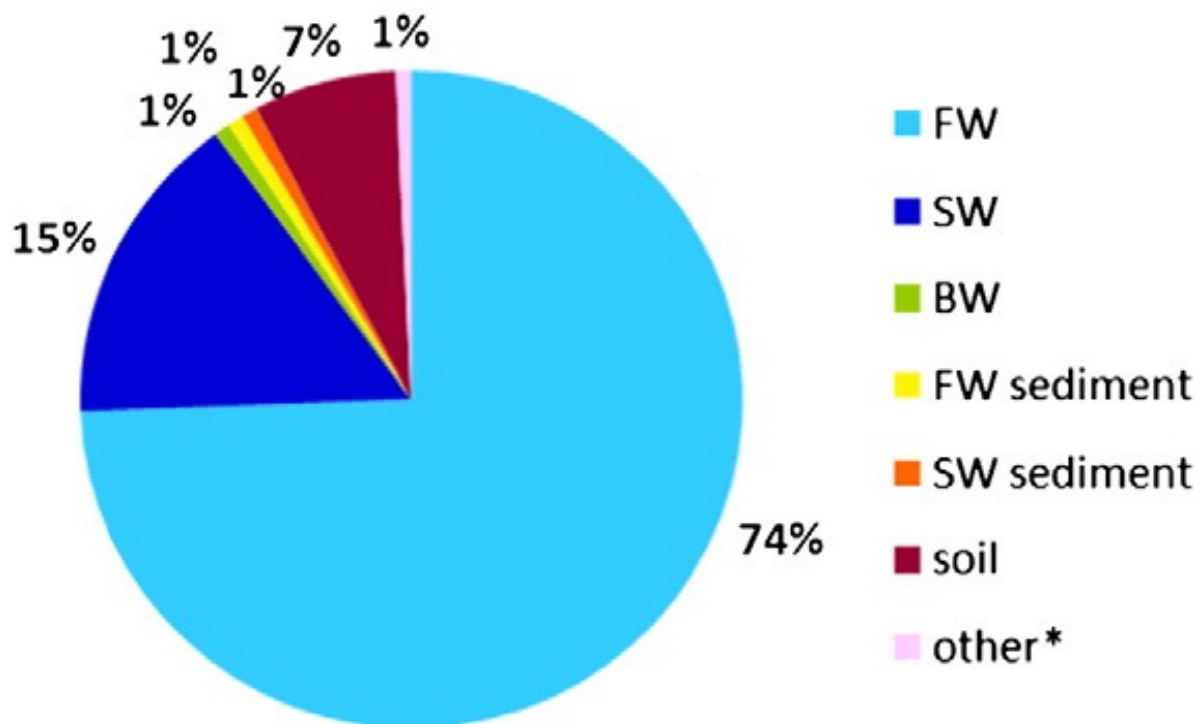


**Figure 1.3:** Publication distribution about nTiO<sub>2</sub> toxicity, depending on the different matrices used in the test for the organism exposure. The publications are related to both in vivo and in vitro tests (n = 129). FW = freshwater, SW = saltwater, BW = brackish water. \*other: interior paints and ceramic pellets. (Minetto *et al.* 2014)

promoting the formation of agglomerates and precipitates in a short time compared to freshwater<sup>96,97</sup>. As the extent of such alterations is arduous to evaluate with the current characterization techniques, especially at low (ppm) ENMs concentrations<sup>17</sup>, determining a specific ENMs toxicity pathway is often impossible. Another issue in the literature revealed by the same review, was the type of ENMs globally used for the toxicological tests. In most of the scientific production, TiO<sub>2</sub> based ENMs were in fact used in the form of pure anatase or P25 (mix of rutile and anatase), which are different from the rutile phase normally used in cosmetic formulations. Also, ENMs used for the tests were in the form of bare particles<sup>87</sup>, without any protective coating, as in the case of the commercial mineral filters used in real sunscreen formulations. Although bare TiO<sub>2</sub> nanoparticles could be considered as analogues of the final aging stage of the mineral UV filters normally used in sunscreens, using them to assess mineral UV filters toxicity does not correspond to a realistic exposure scenario.

Finally, considering the lack of knowledge on environmental release and analytical concentration of these ENMs in the environment, a lot of works (especially the oldest) performed experiments using nano-TiO<sub>2</sub> concentrations far above the field relevant ones<sup>87</sup>. Large knowledge gaps thus remain regarding the marine eco-toxicity of relevant mineral UV-filters.

### 1.2.3 Fabrication and usage

As previously mentioned, sunscreens are emulsion of oil and water. Based on the ratio between these two phases, the emulsion can be water-in-oil (W/O) or oil-in-water (O/W), depending if the dispersing medium is the oil (W/O) or the water (O/W). Among the high diversity of texture available on the market, lotions and creams/gel still remain the preferred form, with approximately 60% of the most recently introduced market products irrespective of the region, even-though in Europe emulsion sprays are still very popular<sup>98</sup>. The main ingredients of a standard sunscreens are emollients, emulsifiers and UV filters (**Figure 1.4**).

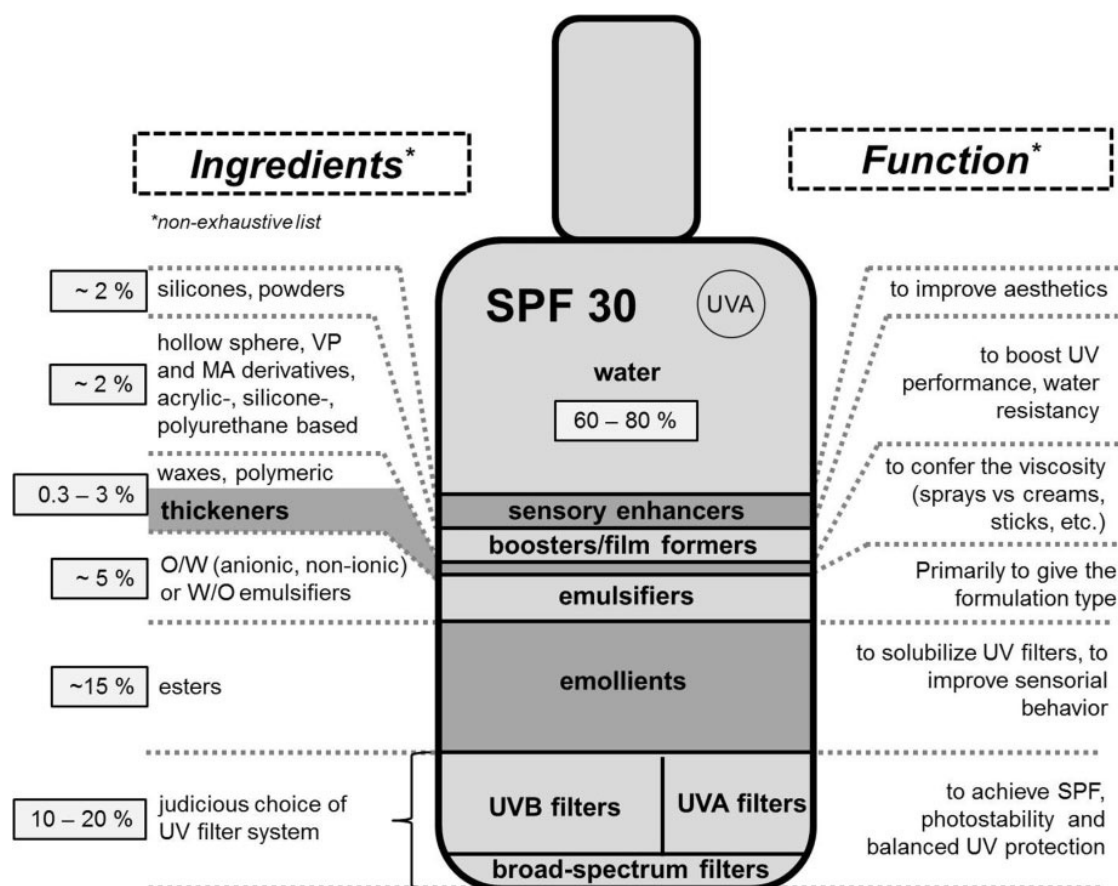


**Figure 1.4:** The ingredients of a typical sunscreen and its functions (Osterwalder *et al.* 2014).

Emollient oils play a triple role in sunscreen formulations: crystalline UV filters<sup>99</sup> and mineral UV filters<sup>100</sup> dispersion; photo-stabilization of photo-unstable UV filters and sensorial enhancing on the user's skin. Concerning the photo-stabilization role, organics UV filters, especially avobenzone (BMBM), were shown to undergo molecular breakdown under UV irradiation, leading to non-absorbing by-products<sup>101</sup>. Some emollients have quenching efficacy with regard to the excited state of BMBM that prevents the molecule photodegradation<sup>102</sup>.

The nature of the emulsifier used in the formulation defines the type of sunscreen emulsion. Anionic emulsifiers, such as potassium cetyl phosphate, sodium cetearyl sulfate, C20–22 alkyl phosphate emulsifiers are generally used to stabilize O/W emulsion, while combination of anionic and non-ionic emulsifiers,



including PEG-100 stearate and glyceryl stearate, allows the stabilization of W/O emulsions. One of the most used surfactants were anionic sulfate- based  $R-SO_4$  ( $C_{14}-C_{22}$ ) which are highly effective and economical, but no longer very utilized nowadays in formulation as bio-sourced surfactants are preferred. Moreover, their production has a high environmental impact, as the sulfuric acid needed for the synthesis uses sulfur from underground origin<sup>103</sup> which, after extraction becomes bioavailable at the earth surface and subject to radiolysis reactions potentially producing toxic byproducts<sup>104</sup>.

O/W emulsions types are generally preferred due to their easy spreading and lighter skin feel. On the other hand, W/O emulsion allow the achievement of higher Solar Protection Factor (SPF) values and improved water resistance<sup>45</sup>. UV filters are the active ingredients used to achieve the UV protection properties of the product. Regardless of the type, they are generally dispersed in the oil phase of the formulation with the required emollient, although water soluble or hydrophilic filters are also available to overcome some issues related to overloaded oil phase stabilization and homogeneity of the filters on the skin after the application<sup>105</sup>.

Although there are many types of organic UV filters, they are always molecules which contain an aromatic moiety (Avobenzone; Octocrylene; Oxybenzone; Octisalate). The presence of conjugated systems as aromatic rings, in fact, allow these molecules to adsorb light radiations in the UV region (400-100 nm). To modulate absorption range of the organic molecule, the aromatic rings substituents are of crucial importance. They could have electron releasing (+M) or electron withdrawing (-M) properties which shift the maximum of absorbance wavelength of the organic filter. Most efficient are di-substituted systems with a +M and a -M group in para position. Thanks to such type of substitutions, it is

possible to synthesize organic UV filters specifically absorbing UVA (400-320 nm) or UVB (320-280 nm), as function of the extent of the maximum of absorbance shift determined by the substitution group <sup>106</sup>.

Among all the mineral compounds that are able to absorb UV light, TiO<sub>2</sub> and ZnO are the only ones allowed in sunscreen formulations by the existing sunscreen regulations (e.g. US FDA, EU cosmetic regulation). Both types of filters attenuate UV radiation mainly through scattering and absorption, even-though the latter seems to be predominant<sup>107</sup>. The efficient absorption of UV wavelengths by ZnO or TiO<sub>2</sub> is enabled via the excitation of the outermost electrons of the constituting atoms. However, this comes with the generation of reactive oxygen species (ROS) when the electrons come back to a stable state. This so-called photocatalytic feature has to be eliminated in sunscreen products in order to prevent any induced oxidative stress on the skin or damage of the lotion<sup>66,108</sup>. For this reason, the less photocatalytic rutile form of TiO<sub>2</sub> is preferred to the anatase form in cosmetic applications<sup>109</sup>. In addition to this, a further photo-passivation of TiO<sub>2</sub> or ZnO is achieved by precipitating an inert mineral layer at the nanoparticle surface. The most common photo-passivating coatings found in sunscreen are alumina and silica<sup>65,110</sup>.

Mineral UV filters are normally loaded in the oil phase of the formulation (event-though they can be also found in the water phase in certain types of formulation)<sup>45</sup> and to be effective in the UVR screening they need to be finely dispersed. To enhance their dispersion capacity, mineral UV filters are coated with a second external coating that could have hydrophobic or hydrophilic properties<sup>111</sup>. Most commons hydrophobic coatings are silane-type polymers, like polydimethyl siloxane (PDMS), or stearic acid<sup>65</sup>, while polyacrylic acid or bare silica coating typically favor aqueous dispersion<sup>112,113</sup>. Amphiphilic properties of the filters

could also be obtained with e.g. simethicone coatings (PDMS + SiO<sub>2</sub>) which favor mineral particles dispersion in both aqueous and oily phases<sup>111,114</sup>.

Nanoparticulate UV filters are preferred to the micrometric ones, because they provide different advantages, such as higher screening efficiency and transparency on the skin<sup>115</sup>. When used together, nano-ZnO and nano-TiO<sub>2</sub> provides a good broad-spectrum of photo-protection, as the first one has a broad UVA-UVB absorption curve, while the latter provides better UVB absorption and a UVA protection depending on the particle size<sup>116,117</sup> (**Figure 1.5**). Nano-TiO<sub>2</sub> UVA protection, in fact, is due to scattering effects that are likely to occur when the diameter of the particles is approximately half the wavelength of the light to be scattered<sup>118</sup>.

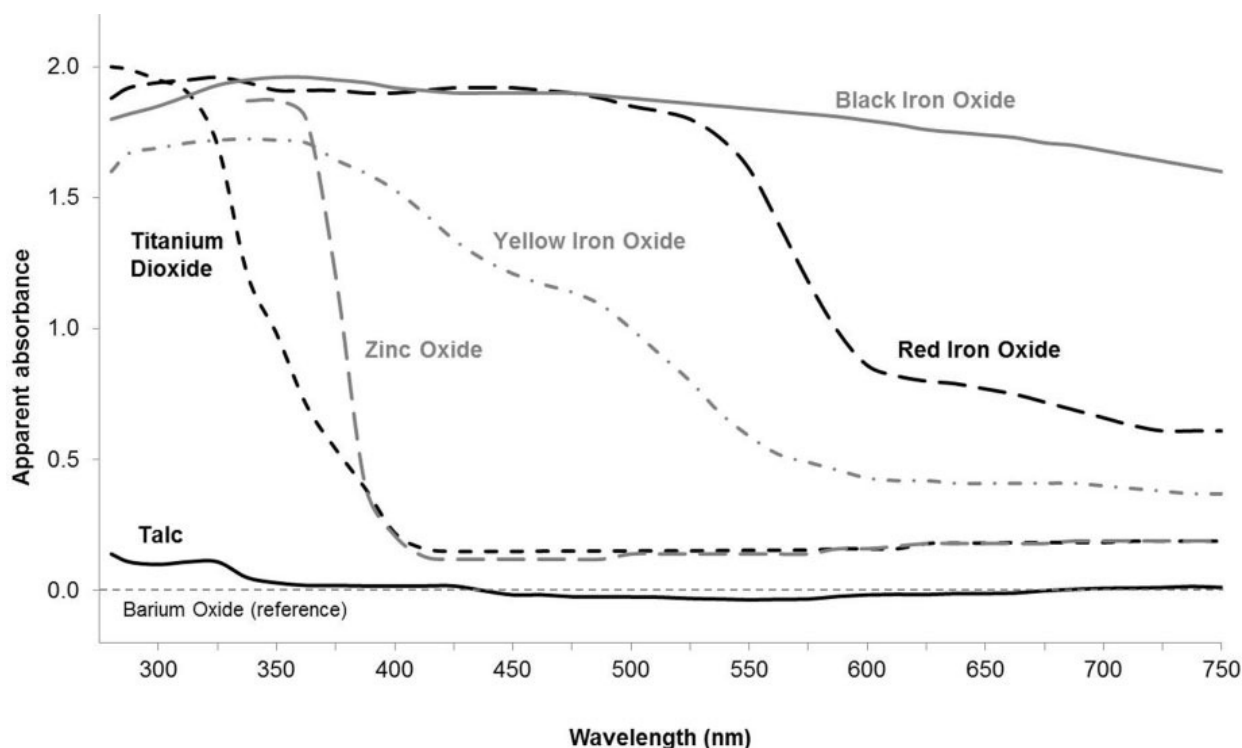


**Figure 1.5:** UV-Vis absorption of different inorganic UV filters (Osterwalder *et al.* 2014)

### 1.3 Importance of the UV filter aggregation state along the lifecycle

#### 1.3.1 Effects of the UV filter aggregation

In order to assure their screening efficacy, nanoparticulate mineral UV filters need to be finely dispersed in the formulation. When nanoparticles are aggregated, their screening capacity decrease<sup>119</sup>, likely because particles are able to cover a smaller surface on the user skin, as schematized in **Figure 1.6**, and thus allow greater percentage of UVR to reach the skin surface.

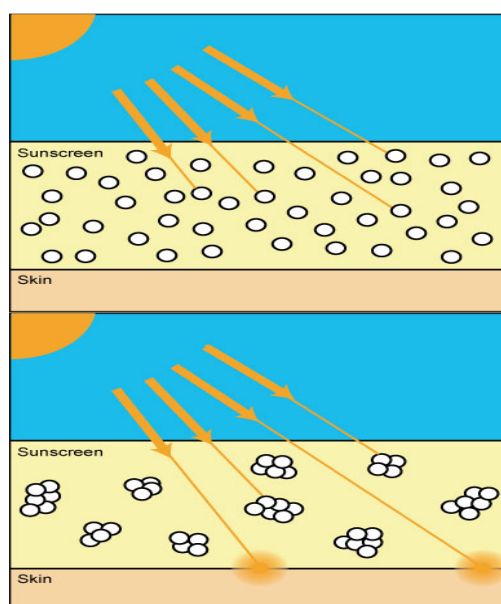


**Figure 1.6:** Schematic representation of hypothetical effect of NP aggregation on sunscreen UVR protection efficiency.

It is fair to say that it takes a lower concentration of finely dispersed nanoparticles in the formulated product than needed with large aggregates to reach a given solar protection factor. This reduced metal “load” in the formulation is an interesting point in lowering both the product cost and its environmental footprint after use. Although these two aspects are not directly related to the LCA, they represents instead central tasks of the eco-design conception of a product<sup>120</sup>. Control the ENMs dispersion in the formulation with the aim of minimize any

aggregation phenomena became thus crucial in the optics of re-styling sunscreens nanoproducts in a more sustainable way.

The causes behind ENMs aggregation could be mainly ascribed to their different coatings, their interactions with the surrounding medium and the aging stage of the sunscreen<sup>121</sup>. As already mentioned, sunscreens are complex systems which contain many components, such as emulsifying, thickening and preservative agents, all aimed at maximizing the stability of the final product. Although mineral UV filters are also employed to stabilize the sunscreen emulsion under certain condition<sup>122,123</sup>, little is known about the role of the different product components in stabilizing the mineral UV filters themselves. Surfactants used in emulsifying agents can surely play a role by interacting at ENMs surface and stabilize their dispersion, however such properties were mostly investigated only in water mediums<sup>124–126</sup>, while studies performed in oil or sunscreen emulsions are still scarce in literature<sup>45,123</sup>. Moreover, in line with what is already raised in section 1.2.2, such mixture effect does not interest only the fabrication stage but also the further lifecycle stages, because certain ingredient combinations affect weathering and environmental dispersion of the product<sup>38,127</sup> and thus the ENMs transportation, bioavailability and toxicity into the aquatic environment, as it was already argued for other nanoproduct<sup>128</sup>.

Besides its influence on sunscreens UVR screening performances, it was also argued that the aggregation state can also influence ENMs internalization inside the user skin, as dermal penetration is one of the main pathways for ENMs to reach human organism<sup>1, 75</sup>. It was observed that nanoparticulate mineral UV filters are able to penetrate through user's skin and reach the stratum corneum (SC), especially in sunburned skins<sup>76</sup>. This may pose a risk for users, as it was recently reported that TiO<sub>2</sub> ENMs has adverse effects on Human Epidermal

Keratinocytes<sup>131</sup>. Moreover, as it was already argued in the case of Au-based ENMs, aggregation phenomena would also influence the ENMs harmful effects toward the same types of Keratinocytes, even-though the mechanisms and extent of affection still need further elucidation, and could be also ascribable to co-effects of the ENMs coating and shape<sup>132</sup>.

Knowing the aggregation state of ENM UV filters is thus crucial in order to assess the nanoproduct efficiency and minimize the risk associated at the fabrication and usage lifecycle stages. Although the physicochemical characterization of the raw nanomaterials (size; shape; aggregation state; chemical composition) prior its integration into the product is relatively straightforward<sup>133</sup>, it is often more challenging to measure these characteristics in the final nano-enabled product because of the matrix complexity.

### 1.3.2 Sunscreen structural characterisation

Tyner *et al.*<sup>134</sup> compared more than 20 analytical methods to characterize nanomaterials in sunscreen formulations; concluding that just four of them were capable to give insights on some specific characteristics without changing the composition of the original product. X-ray diffraction (XRD) is suitable for the characterization of the primary particle crystalline structure and size. Variable pressure scanning electron microscopy (VPSEM) provides a surface characterization. Laser-scattering confocal microscopy (LSCM) is able to give insight on the presence of nanoparticles and their average dispersion state, but owing the diffraction-limit resolution of optical microscopy and low optical contrast, the particles cannot be detected or sized accurately. Finally, atomic force microscopy (AFM) is able to detect nanomaterials inside the formulation and gives insight on morphological features, even though for the bulk characterization a phase imaging is required. Because AFM is really sensitive to topographical

changes, height analysis can be complicated because of artifact arising from sample preparation.

One of the main experimental issues is related to the oily nature of the product, which impedes a complete drying of the sample. Therefore, size, structure and chemical analyses using Transmission Electron Microscopy (TEM) in regular mode are not possible, because this works under a complete vacuum, and can eventually lead to sample aspiration which could damage the instrument<sup>134</sup>. Dilution of the cream with an organic solvent is often used prior to the analysis in order to avoid this effect with conventional TEM, as well as for size measurement by Dynamic Light Scattering (DLS)<sup>135</sup>. Such sample preparation can substantially change the raw nanomaterial characteristics and its interaction with the formulation ingredients, leading to artefact results. Scanning Electron Microscopy can be a suitable method to characterize the surface of a sunscreen sample but it still requires pre-drying under vacuum and cannot thus provide a precise information about the dispersion state of the nanoparticles in the bulk of the formulation<sup>136</sup>.

To avoid the sample aspiration or drying during a TEM analysis, Butler *et al.*<sup>137</sup> used an high pressure freezing substitution of the creamy medium with a suitable resin. The resulting images allowed a finer characterization of particle size, shape and aggregation state. However, this experimental set-up is very time-consuming (3 days) and the resin addition could likely change the interaction of the nanoparticles with the surrounding medium. Recently, Philippe *et al.*<sup>138</sup>, performed a TEM analysis on different commercial sunscreens in cryogenic mode. This technique was already evoked by Schilling *et al.*<sup>139</sup> as suitable to obtain finer electron microscopy images of nanoparticles in sunscreen formulations without altering the original composition of the product. Although Cryo-TEM is able to

give insight on the size and shape of primary particles and aggregates, the images are rarely representative of the entire product morphology (i.e. nanoparticles aggregation or agglomeration state; inhomogeneities), because of the very confined portion of the sample observed.

In sum, an extensive study of nanoparticulate UV filters behavior inside the formulation, at the sunscreen fabrication and usage stage, is essential in order to determine the LCA of this nanoproduct. The coating design is crucial in order to maximize the homogeneity of the filter dispersion in the dispersant medium, as finer colloidal dispersion allow formulation with less NPs content but equal SPF, eventually leading to a nanoproduct with lower environmental footprint. Homogeneity and aggregation state of the nanomaterials should be evaluated *in situ*, trying to avoid any preparation protocol that would alter the original formulation matrix. Furthermore, the influence of the different components of the mixture on the NPs stability must be evaluated, taking also into account the mechanism behind each interaction. This will not only allow a better control of the nanoparticle dispersion, but also a more realistic prediction of their transport, bioavailability and eco-toxicity at the end-of-life stage of the product.

#### 1.4 Thesis objectives and list of papers

The scope of the present PhD thesis was to contribute to filling the gaps in the LCA of TiO<sub>2</sub> based nanomaterials used as UV blockers in sunscreens formulation, by analyzing and developing different key stages of the nanoproduct lifecycle (**Figure 1.7**). Following a safe by design approach, a first part of this thesis was focused on the sunscreen fabrication stage, with the aim of minimizing the risk associated to ENMs, while maximizing the product efficacy.



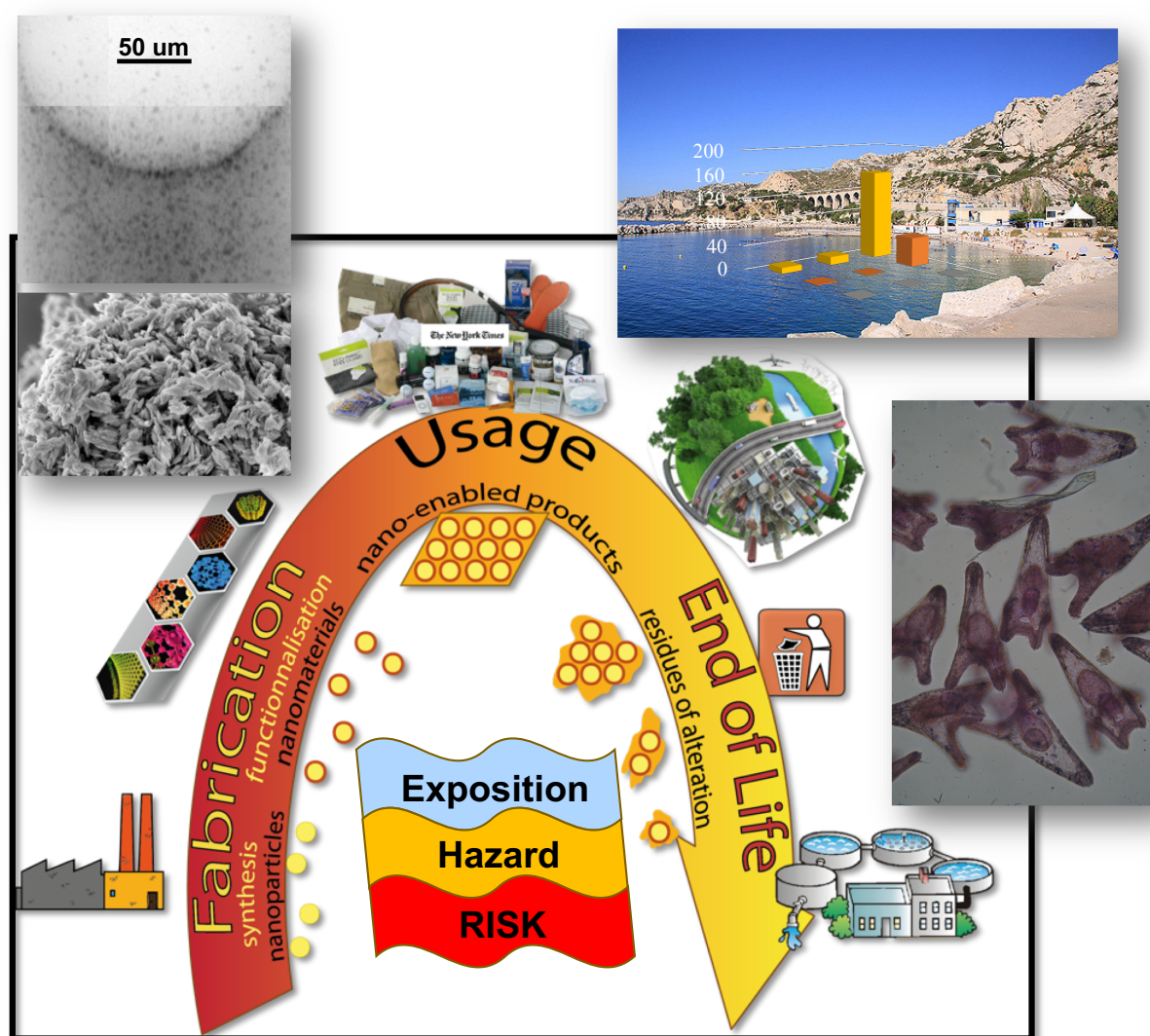


**Figure 1.7:** Integrating the entire lifecycle of the sunscreen product from fabrication to end of life enables to anticipate the environmental release and impact of the involved ENMs, and tune the product in a safe-by-design approach to minimise the risk posed.

In this context, particular attention has been paid to the characterization of nano-TiO<sub>2</sub> based UV filters inside a realistic home-made sunscreen formulation. The aim was to evaluate the aggregation state of different commercial filters without significantly modifying the original matrix of the formulation. In order to reach this goal, a new methodology based on 2 Dimensional X-Rays Nano-Tomography (2D XRNT) was developed. It allowed us to analyse and quantify the aggregation state of two different commonly used TiO<sub>2</sub> ENMs and their influence on the homogeneity of the entire formulation. This methodology was also compared

with another one based on cryogenic-Transmission Electron Microscopy (Cryo-TEM), which was able to provide more detailed images of the particle inside the formulation. The relation between aggregation state of the filters and the UVR protection efficiency of the respective formulation was also investigated highlighting the importance of such knowledge in the optimization of mineral sunscreen formulations. The set of these results is reported in the article *“In situ determination of nanoparticle aggregation state in cosmetics emulsions.”* presented in **Chapter III**.

In order to develop a safe by design approach, the particle aggregation state of ENMs should not only be measured in-situ in the sunscreen formulation, it should also be controlled and optimized. In this aim, the dispersion of four different nano-TiO<sub>2</sub> based UV filters was studied at the early stage of the formulation, in a bio-sourced sunscreen oil phase. The roles of particle coating and the interaction between the different component of the oil phase (emollients and emulsifiers) and the nanoparticle surfaces were evaluated through a novel methodology of extraction and characterization based on solid state Nuclear Magnetic Resonance. This part of the work is reported in the article *“Optimizing the dispersion of nanoparticulate TiO<sub>2</sub>-based UV filters in a non-polar medium used in sunscreen formulations - the roles of surfactants and particle coatings.”* presented in **Chapter IV**.

Understanding the photoprotection mechanism of mineral UV filters is another key point in the safe by design approach of sunscreen nanoproducts. Since mineral UV filters are known to screen UVR via both absorption and scattering, knowing the respective contributions of these two mechanisms in the overall photoprotection obtained could help future UV filters improvements by orientating toward optimal properties (e.g. particle size and shape). Moreover,

quantifying the amount of UVR screened by absorption mechanism is also important in the risk assessment of TiO<sub>2</sub> ENMs as UV absorption can lead to the production of ROS through photocatalytic activity<sup>140</sup>, which is the main pathway of TiO<sub>2</sub> toxicity toward living organisms. In order to achieve this goal, a novel analytical tool able to measure the angular UV scattering profile of ENMs was designed and developed. It allowed the distinction of UVR scattered, reflected and absorbed by ENMs dispersed in a realistic sunscreen oil phase. These results are presented in detail in **Chapter V**.

The second half of this thesis was focused on the lifecycle stages of sunscreen beyond usage. In order to give insight on the UV filters release in marine environment through bathing activity, a field sampling campaign was realized in three major beaches of Marseille seashore. The main challenges of this part of the work were: to estimate the daily flux of sunscreen and UV filters transferred from beachgoers into the bathing water on a standard summer day; to study the possible co-occurrence of organic and mineral UV filters in seawater, both in the water top surface layer and water column; to determine, for the first time, the patterns of UV filter occurrence in the bathing water at three French Mediterranean beaches. The results of this work are reported in the article “Assessing UV filter inputs into beach waters during recreational activity: A field study of three French Mediterranean beaches from consumer survey to water analysis.”, presented in **Chapter VI**.

Some of the information obtained in the field campaign (i.e. release and environmental relevant concentrations of TiO<sub>2</sub> in the environment) were used to perform more realistic eco-toxicity tests on the Mediterranean Sea-urchin (*Paracentrotus Lividus*). We decided to focus on this particular biological model for many reasons: is globally distributed in almost all depths, latitudes,

temperatures, and environments in the ocean; it is very sensitive to minimal environmental changes and capable of rapidly adapt to them; it is a relatively easy handle invertebrate, less subjected to ethics regulations. Due to its dominant role in structuring and functioning of the rocky reef ecosystem, it is of strong interest as a potential model to monitor the state of marine environmental health<sup>92</sup>. The effect of three different commercial nano-TiO<sub>2</sub> rutile-based UV filters on development and immune response of the sea urchin were evaluated in comparison with bare rutile NPs. Two media typically used as oil or water phase of the sunscreen formulation, were used as UV filters pre-dispersant liquid. Hydrophilic ENMs were dispersed in the water and hydrophobic ENMs were dispersed in the oil. These suspensions were exposed to sea urchin at varying concentrations. The ecotoxicity results of this work are reported in the article “Effect of nano-TiO<sub>2</sub> (rutile)-based UV filters used for sunscreen formulations on the immunological state and embryonic development of the sea urchin *Paracentrotus lividus*”, presented in **Chapter VII**.



## Chapter II: Materials and methods

### 2.1 Main methodology

Among all the different types of ENM UV filters, TiO<sub>2</sub> based ones are generally considered the safer and the elective candidates for eco-friendly sunscreens nano-enabled products. Given the limited knowledge on both fabrication and end-of-life stages of these commercial ENMs, we decided to focus our research on this type of mineral UV filters in order to better assess, minimize and anticipate its risk associated and contribute to develop safer formulations. We also decided to equip the lab with all the tools needed to be able to fabricate realistic in-house sunscreen formulations. This choice was dictated by the need to control the fabrication stage and be certain of the formulation composition, as commercial sunscreens suppliers are rarely fully precise on such information, which is instead fundamental for any decent interpretation of experimental results. Moreover, being able to control all the steps of the formulation process, allowed us to adapt the sunscreen emulsion to different experimental conditions, e.g. break-up the formulation into simplified ENMs/oil dispersions more suitable for certain analysis or to mimic environmental sunscreen degradation during the eco-toxicological tests.

### 2.2 UV filters selection

Four nano-TiO<sub>2</sub> UV filters were selected as case studies during this work. They are graphically represented in **Figure 3.1** while the chemical composition provided by the different suppliers is reported in **Table 3.1**. Three of the four filters, T-S; T-Lite; T-2000, had hydrophobic surface properties given by their different external coatings, respectively stearic acid, dimethicone and simethicone, and had an internal coating of aluminium hydro(oxide). The fourth filter (T-AVO) had instead hydrophilic surface

properties given by its only surface coating  $\text{SiO}_2$ . In the first section of this PhD work dealing with the characterisation of the sunscreen at the design stage, we mostly focussed on the hydrophobic filters, as they are the most used in commercial formulations, usually pre-dispersed in the non-polar oily phase of the emulsion, as already mentioned in Chapter 1.2.3. The hydrophilic filter has been tested against the hydrophobic ones in the section on the ecotoxicological impact, where the effect of a polar vs. apolar dispersing medium was studied together with the ENM coating.

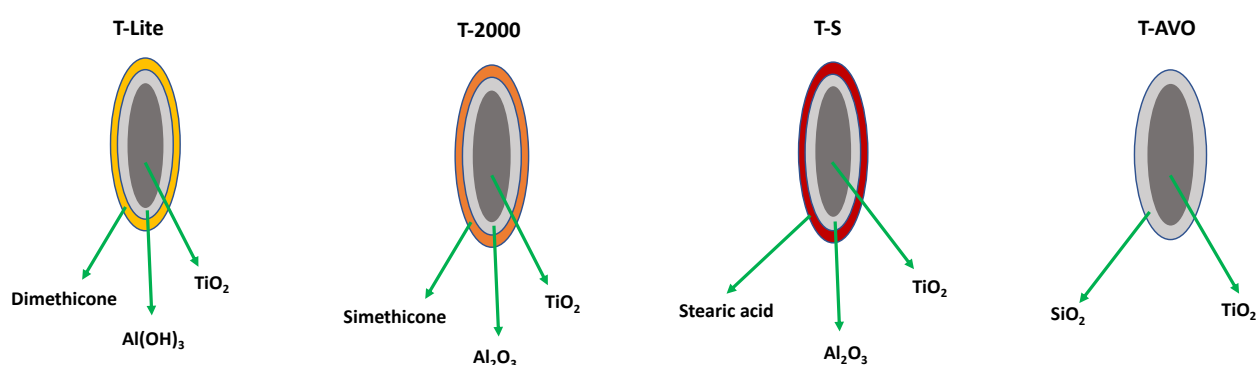


**Figure 2:** Schematic representation of the four commercial nano- $\text{TiO}_2$  based UV filters selected, with the green arrows indicating the compositions of the different ENMs layers.

The three hydrophobic filters were selected based on the nature and characteristics of their organic external coatings. Stearic acid (T-S) and dimethicone (poly-dimethyl siloxane - PDMS) are two of most common coatings used in commercial cosmetic formulations to ease the ENMs dispersion and stability. Nonetheless these two compounds are characterized by contrasted origins, as stearic acid is a bio-sourced fatty acid that could be found in nature and obtained from the saponification of fats and oils, while dimethicone is a polymer obtained by hydrolysis of dimethyl-chlorosilane which is a synthetic compound. It was thus interesting for us to evaluate the effect on performances and hazard given by these two coatings to the ENM UV filters and eventually select the most efficient and eco-friendly one. Simethicone differs from dimethicone by the presence of amorphous silica in the mixture PDMS giving it an amphiphilic nature. For this reason, we also selected T-2000 ENMs characterized by

the presence of dimethicone on the surface, to evaluate the effects and eventual advantages that an amphiphilic coating can bring during the fabrication stage of a sunscreen nanoproduct. Silica coated ENMs (T-AVO) were chosen for several reasons. First to have a hydrophilic filter to be used as control for the hydrophobic ones, during the studies of dispersion optimization in non-polar medium, discussed in Chapter IV. Second, because the only presence of a mineral coating layer represents a realistic intermediate aging stage of UV filters ENMs in the environment, making T-AVO an interesting candidate for the eco-toxicological tests discussed in Chapter VII. Third, because  $\text{SiO}_2$  coating, aside of  $\text{Al}_2\text{O}_3$ , is one of the main internal coating used as ENMs passivating agent in commercial cosmetics.

**Table 2.1:** Name, manufacturer and chemical composition of the four filters selected for the experiments.

| Product Name   | Manufacturer | Chemical composition   |
|----------------|--------------|--|
| T-Lite SF      | BASF         | $\text{TiO}_2$ (79-89%)/ $\text{Al}(\text{OH})_3$ /Dimethicone |
| Eusolex T-AVO  | Merck        | $\text{TiO}_2$ (79.6%)/ $\text{SiO}_2$                         |
| Eusolex T-2000 | Merck        | $\text{TiO}_2$ (80.3%)/ $\text{Al}_2\text{O}_3$ /Simethicone   |
| Eusolex T-S    | Merck        | $\text{TiO}_2$ (73-79%)/ $\text{Al}_2\text{O}_3$ /Stearic Acid |

## 2.3 Sunscreen formulation

Among all the types of formulation present in the market, (ex: sprays, gels; creams; lotions), we decided to focus on a water in oil (W/O) creamy emulsion only containing  $\text{TiO}_2$  based ENMs as UV blockers, with an average oil content of 15% w/w and 70% w/w on water. Even if sprays are very popular in Europe, current regulations do not allow the presence of ENMs inside this type of formulation, to avoid their possible inhalation by the users. The higher amount of oil phase in W/O emulsions compared with O/W ones, allow the dispersion of higher amounts of inorganic UV filters and are thus able to reach higher Solar Protection Factors<sup>106</sup>. This property gave us the opportunity to test different ENM concentration without over saturate the formulation due to mineral load. Also, W/O sunscreen emulsions guarantee a higher waterproof effect and thus a lower environmental release during bathing activity, making it an



interesting candidate for the development of eco-designed formulations. All the components of the sunscreen emulsions were bio-sourced and directly provided by the suppliers and their chemical composition is reported in **Table 2.2**. The original formulation recipe was originated by Alexandra Lopez, founder of *Laboratoire CNB* based in Marseille, and its preparation methodology will be presented in detail in Chapter III. Another characteristic of this recipe is the unnecessary heating of the sunscreen after the formulation, which is interesting in the context of energy economy.

**Table 2.2:** Trade name, chemical composition and formulation function of the components used to fabricate in-house sunscreens.

| <b>Commercial Name</b> | <b>Supplier</b> | <b>Composition</b>  | <b>Function</b>       |
|------------------------|-----------------|---|-----------------------|
| <b>SEPIPLUS 400</b>    | SEPPIC          | Polyacrilate; Polyisobutene Polysorbate 20; Water; Sorbitan; Isooctadecanoate | Gelling agent         |
| <b>EASYN OV</b>        | SEPPIC          | Octyldodecanol; Octyldodecyl Xyloside; PEG30 Dipolyhydroxystearate            | Emulsifier            |
| <b>CETIOL LC</b>       | AMI CHIMIE      | Coco-Caprylate/Caprata  | Emollient             |
| <b>TEGOSOFT P</b>      | EVONIK          | Isopropyl Palmitate   | Emollient             |
| <b>EUXYL PE 9010</b>   | SCHUELCKE       | Phenoxyethanol; Ethylhexylglycerine   | Cosmetic preservative |

Coco-caprylate (Cetiol LC) and isopropyl palmitate (Tegosoft P) are widely used bio-sourced oils used as emollients in various cosmetics. Notably, the supplier indicated Tegosoft P as a good dispersant phase for both organic and minerals filters. Easynov on the contrary is a common used bio-sourced emulsifier, used to stabilize high oil content W/O emulsions. It is composed of two different surfactants, one polymeric (PEG30 dipolyhydroxystearate) and one non-ionic glycosidic (octyldodecyl xyloside), both solubilized into an octyldodecanol solvent. Sepiplus 400 is a liquid polymer used as gelling agent in cosmetics in place of silicone-based oils, and it is composed of various bio-sourced chemicals. The only non-bio-sourced compound employed in smaller quantity in the in-house formulated sunscreens, was the Euxyl PE 9010, a cosmetic preservative with anti-bacteria activity. Even-though it exists other “bio”

preservatives, they aren't always as effective, and we decided to still use the phenoxyethanol-based one.



## **Part A: Fabrication and usage**



## **Chapter III: Characterization of nanoparticulate UV filters in unmodified cosmetic matrix**

In this chapter we focus on the evaluation of nanoparticle dispersion and aggregation state after the formulation stage of sunscreens nanoproduct. As discussed in Chapter 1.2.3, at this lifecycle stage it is a fundamental to determine whether the UV filters are stable or not in the emulsion, because such feature will ultimately influence not only the screening efficiency of the product but also its potential impact at the usage and end-of-life stages. Overall, better knowing the ENMs behaviour after loading in the final formulation, is a key point to develop a nanoproduct safer-by-design. One of the main issues in this purpose, is that the characterization techniques and the methodologies explored to date, are affected by several limitations such as: alteration of the original matrix which will eventually modify the NMs aggregation state and eventually lead to biased results; time consuming and expensive set up of the analysis; non-quantitative information. To overcome these obstacles, here we propose a new methodology of characterization based on 2 Dimensional X-Rays Nano-Tomography (2D XRNT). We selected and characterized the surface properties of two different commercial nano-TiO<sub>2</sub> based UV-filters (T-S and T-Lite ENMs), which differ in the external organic coating they contain (Stearic acid or Dimethicone). Then we formulated in-house sunscreens loaded with these filters (one at a time) at increasing concentrations, and we evaluated their dispersion state and screening efficiency of the formulation as a function of the ENM coatings and concentrations. The methodology developed proved to be able to determine quantitatively the aggregations state of the ENMs and in turn the homogeneity of their dispersion in the formulation. The nature of the organic coating was seen to dramatically affect the dispersion state of the ENMs. Moreover, a proportional correlation was

observed between homogeneity of the formulation and its UVR screening efficiency.

## ***Paper I :***

### ***In situ* determination of nanoparticle aggregation state in cosmetics emulsions.** (To be submitted to Environmental Science Nano)

Riccardo Catalano; Jerome Labille; Danielle Slomberg; Vladimir Vidal; Celine Picard; Nicolas Husher; Francois Saint-Anonin; Jerome Rose; Myriam Zerrad; Jean-Claude Hubaud.

#### **1.Introduction**

In the last 20 years, nanotechnology has been widely used in different areas such as cosmetics, painting, medical, packaging and food<sup>2,141</sup>. Together with the higher efficiency of the so called *nano-products*, there has been a corresponding concern toward their potential hazardous effect for the consumers and the environment as well<sup>142,143</sup>. The European Commission's regulation program Registration, Evaluation, Authorization and Restriction of Chemicals (REACH) is currently working on the regulation of products containing nanomaterials. The regulatory process normally requires a basic physicochemical characterization of the product (stability; purity; molecular weight; crystal structure) and, when it is necessary, a toxicological evaluation. (*in vivo* / *in vitro* toxicity tests)<sup>25,26</sup>

Although the physicochemical characterization of the raw nanomaterials (size; shape; aggregation state; chemical composition) prior its integration into the product is relatively straightforward<sup>133</sup>, it is often more challenging to get it on the final nano-enabled product because of the matrix complexity. It is nevertheless necessary to determine these characteristics inside the final product because the aggregation state or the chemical properties of the nanomaterials



may be altered during the formulation, leading to unexpected effects on product efficiency and/or. (eco)toxicity<sup>9,119</sup>.

Cosmetic products, like sunscreen, often contain nanoparticulate TiO<sub>2</sub> or ZnO, minerals, used as UV filters. These engineered nanomaterials (ENM) are normally coated with specific components (Al<sub>2</sub>O<sub>3</sub>; SiO<sub>2</sub>; Dimethicone; Stearic acid) able to decrease their photocatalytic activity and/or to increase their dispersion in the formulation. They are preferred to the corresponding micro-sized particulate filters because of their better screening efficiency and transparency on the skin<sup>106</sup>. Along with that, an increasing concern has been expressed in the literature regarding the potential higher toxicity of these nanomaterials due to higher active surface and bioavailability<sup>77,79</sup>. It was also argued that these nanoparticulate mineral filters could penetrate the human skin, and may cause cytotoxicity<sup>1,129,130</sup>. Consequently, the determination of nanoparticles size and dispersion state (i.e. aggregation; agglomeration) inside a cosmetic formulation is crucial step in order to assess the safety and the efficiency of these products.

Tyner *et al.*<sup>134</sup> compared more than 20 analytical methods to characterize nanomaterials in sunscreen formulations. They concluded that just four of them were capable to give insights on some specific characteristics without changing the composition of the original product. X-ray diffraction (XRD) is suitable for the characterization the primary particle crystalline structure and size. Variable pressure scanning electron microscopy (VPSEM) provides a surface characterization. Laser-scattering confocal microscopy (LSCM) is able to give insight on the presence of nanoparticles and their average dispersion state, but owing the diffraction-limit resolution of optical microscopy and low optical contrast, the particles cannot be detected or sized accurately. Finally, atomic force microscopy (AFM) is able to detect nanomaterials inside the formulation and give

insight on morphological features, even though for the bulk characterization a phase imaging is required. Because AFM is really sensitive to topographical changes, height analysis can be complicated because of artifact arising from sample preparation.

One of the main experimental issues is related to the oily nature of the product, which impedes a complete drying of the sample. Therefore, size, structure and chemical analyses using Transmission Electron Microscopy (TEM) in regular mode are not possible, because this works under a complete vacuum, and can eventually lead to sample aspiration which could damage the instrument<sup>134</sup>. Dilution of the cream with an organic solvent is often used prior to the analysis in order to avoid this effect with conventional TEM, as well as for size measurement by Dynamic Light Scattering (DLS) <sup>135</sup>. Such sample preparation can substantially change the raw nanomaterial characteristics and its interaction with the formulation ingredients, leading to artefact results. Scanning Electron Microscopy can be a suitable method to characterize the surface of a sunscreen sample but it still require a pre-drying under vacuum and cannot thus provide precise information about the dispersion state of the nanoparticles in the bulk of the formulation<sup>136</sup>.

To avoid the sample aspiration or drying during a TEM analysis, Butler *et al.*<sup>137</sup> used an high pressure freezing substitution of the creamy medium with a suitable resin. The resulting images allowed a finer characterization of particle size, shape and aggregation state. However, this experimental set-up is very time-consuming (3 days) and the resin addition could likely change the interaction of the nanoparticles with the surrounding medium. Recently, Philippe *et al.*<sup>138</sup>, performed a TEM analysis on different commercial sunscreens in cryogenic mode. This technique was already evoked by Schilling *et al.*<sup>139</sup> as suitable to obtain finer

electron microscopy images of nanoparticles in sunscreen formulations without altering the original composition of the product. Although Cryo-TEM is able to give insight on the size and shape of primary particles and aggregates, the images are rarely representative of the entire product morphology (i.e. nanoparticles aggregation or agglomeration state; inhomogeneities), because of the very confined portion of the sample observed.

In the present work two different nano-TiO<sub>2</sub> based commercial UV filters were used at three different concentrations to formulate 6 in-house Sunscreens. The Solar Protection Factor (SPF) of each formulation was evaluated, and was explored as a possible indicator of the UV filter distribution in the formulation. A novel methodology based on 2D X-Rays Nano-Tomography is proposed to rapidly characterize the nanoparticles aggregation and dispersion state in the sunscreen product, together with the formulation homogeneity. Cryo-TEM was also used to measure particle size, shape and dispersion state in the emulsion in order to give insights on the advantages and limitations of both methods for sunscreen characterization.

## **2. Materials and methods**

### **UV filters studied**

T-Lite and T-S UV filters were directly purchased from the supplier as dry powders (Table 1). Chemical speciation of the pristine powders (NMR; EDX; Elemental analysis) together with the evaluation of the primary particle sizes and shapes are reported elsewhere<sup>144</sup>.

**Table 1:** Trade names and chemical composition of the two nano-TiO<sub>2</sub>-based UV filters employed in the in-house sunscreen formulations.

| Nanoparticle type   | Composition  |
|---------------------|--|
| Eusolex T-S (Merck) | TiO <sub>2</sub> (73-79%)/Al <sub>2</sub> O <sub>3</sub> /Stearic Acid |
| T-Lite SF (BASF)    | TiO <sub>2</sub> (79-89%)/Al(OH) <sub>3</sub> /Dimethicone             |

### Contact angle measurement and Surface Free Energy calculation

T-Lite and T-S NPs were directly purchased from the supplier as dry powders (*Table 1*) and were mixed with pure KBr powder (*Sigma-Aldrich*) in order to obtain a solid dispersion at 20 % w/w NPs concentration. For each solid dispersion, 9 pellets were prepared by compacting the powders under 3 tons using a high-pressure press. The sessile-drop method was conducted on each pellet with a *Digidrop* goniometer (*GBX*, Dublin, Ireland) and the software *Windrop*<sup>++</sup> (1.18.04), in order to evaluate the contact angle between different liquids droplets and the pellets surface. Contact angle measurement were conducted with three reference liquids characterized by different polar/dispersive component: ultrapure water; diiodomethane and formamide. In order to obtain information also about the affinity of the two UV filters for the sunscreen oil phase, the contact angle between the oil phase droplets and the different pellets was measured. The measurements with each liquid were performed in triplicates after 4 seconds from the droplet deposition. The surface energy components (dispersive and polar) were then calculated using the Van Oss–Chaudhury–Good equation<sup>145</sup>.

## Sunscreens formulation

Water in Oil (W/O) sunscreen emulsions with different NPs types and concentrations were prepared based on the receipt provided by *SEPPIC*<sup>®</sup>. The emollients, emulsifier and preservative components used for the formulation were directly purchased from the supplier (*Table 2*). The continuous oil phase of the sunscreen was prepared by mixing two emollient oils and one emulsifying agent in 2:2:1 ratio and gently homogenized for 20 min through stirring agitation. The resulting phase is called *Phase D*. To formulate the sunscreens at a NPs concentration of 10 % w/w, 10 g of either T-S or T-Lite NPs were dispersed in 15 g of the *Phase D* under mechanical agitation (1000 rpm) for 10 minutes, using a *Heidolph Hei-Torque 400* stirrer equipped with a pitcher blade impeller. The resulting dispersion is called *Phase C*. Meanwhile, 70.3 g of MQ water were mixed with 3 g of glycerol (*Sigma Aldrich*) using a *Turbotest evo* agitator (VMI 181086) equipped with a deflocculator, at 400 rpm agitation speed. The resulting solution is called *Phase A*. Keeping the stirring on, 1.2 g of gelling agent (Sepiplus 400) was added to the *Phase A* while increasing the agitation speed to 1600 rpm for 10 min. The resulting gel is called *Phase B*. Then, the rotor/stator was mounted in place of the deflocculator, and the *Phase B* was mixed with the *Phase C* at 2000 rpm agitation speed, until the two phases where well mixed. Then, 0.5 g of preservative Euxyl PE 9010 was added to the emulsion and dispersed through mechanical agitation for 10 min at 1000 rpm with the deflocculator. A total of seven sunscreen formulations was prepared using the same procedure (*Table 3*). For sunscreens with lower NPs concentrations, the loss in weight of NPs was replaced with MQ water.

**Table 2:** List of chemicals used to formulate the in-house sunscreens.

| Commercial Name | Supplier   | Composition   | Function              |
|-----------------|------------|---|-----------------------|
| SEPIPLUS 400    | SEPPIC     | Polyacrilate; Polyisobutene Polysorbate 20; Water; Sorbitan; Isooctadecanoate | Gelling agent         |
| EASYNOV         | SEPPIC     | Octyldodecanol; Octyldodecyl Xyloside; PEG30 Dipolyhydroxystearate            | Emulsifier            |
| CETIOL LC       | AMI CHIMIE | Coco-Caprylate/Caprata  | Emollient             |
| TEGOSOFT P      | EVONIK     | Isopropyl Palmitate   | Emollient             |
| EUXYL PE 9010   | SCHUELCKE  | Phenoxyethanol; Ethylhexylglycerine   | Cosmetic preservative |

**Table 3:** Chemical composition (% w/w) of the sunscreens formulated in-lab.

| Sunscreens  | Composition (% w/w)   |
|-------------|---|
| TLite-S-2.8 | T-Lite SF NPs (2.8), Easynov/Cetiol LC/Tegosoft P (15), Glycerol (3), Sepiplus (1.2), Water (77.5), Euxyl PE 9010 (0.5)   |
| TLite-S-5   | T-Lite SF NPs (5), Easynov/Cetiol LC/Tegosoft P (15), Glycerol (3), Sepiplus (1.2), Water (75.3), Euxyl PE 9010 (0.5)     |
| TLite-S-10  | T-Lite SF NPs (10), Easynov/Cetiol LC/Tegosoft P (15), Glycerol (3), Sepiplus (1.2), Water (70.3), Euxyl PE 9010 (0.5)    |
| TS-S-2.8    | Eusolex T-S NPs (2.8), Easynov/Cetiol LC/Tegosoft P (15), Glycerol (3), Sepiplus (1.2), Water (77.5), Euxyl PE 9010 (0.5) |
| TS-S-5      | Eusolex T-S NPs (5), Easynov/Cetiol LC/Tegosoft P (15), Glycerol (3), Sepiplus (1.2), Water (75.3), Euxyl PE 9010 (0.5)   |
| TS-S-10     | Eusolex T-S NPs (10), Easynov/Cetiol LC/Tegosoft P (15), Glycerol (3), Sepiplus (1.2), Water (70.3), Euxyl PE 9010 (0.5)  |
| Control-S   | Easynov/Cetiol LC/Tegosoft P (15), Glycerol (3), Sepiplus (1.2), Water (80.3), Euxyl PE 9010 (0.5)                        |

### Solar Protection Factor (SPF) measurement

The SPF of each sunscreen formulation was measured using the method of spectral transmittance defined by the equation (1):

$$(1). \quad \frac{\int_{290}^{400} E_{\lambda} s_{\lambda} d\lambda}{\int_{290}^{400} E_{\lambda} \tau_{\lambda} s_{\lambda,er} d\lambda}$$

Where  $E_{\lambda}$  is the spectral irradiance of “standard sun” corresponding to COLIPA “SPF method”;  $s_{\lambda}$  is the erythema action spectrum (CIE 1987) at wavelength  $\lambda$  and  $\tau_{\lambda}$  is the spectral transmittance of the sunscreen.  $E_{\lambda}$  and  $s_{\lambda}$  are tabulated values, while the  $\tau_{\lambda}$  is calculated by transmittance measurement performed as follow.

UV transmitting PMMA plates (50x50 mm) with a 5  $\mu\text{m}$  medium roughness were used as substrate mimicking skin. Between 1.2 and 1.4  $\text{mg}/\text{cm}^2$  of product was spread on the substrate, weighing accurately the amount deposited before and after evaporation occurred. By using light finger pressure, the amount of cream was spread all around the surface until a homogeneous distribution was achieved and left settle for 15 min at room temperature to ensure a self-leveling of the formulation. Another bare PMMA plate was used as blank. The transmittance of each sample was measured in the UV range (400-290 nm) using a spectrophotometer (*Kontron UVIKON – UVK lab*) equipped with an integrating sphere behind the sample. For each sunscreen sample, the measurements were repeated 9 times at different location of the PMMA plate.

### Cryogenic Microtome/Cryogenic Transmission Electron Microscopy

A droplet of either T-S or T-Lite sunscreens at 2.8% w/w was settled on a metallic support and frozen at -100 °C in the cryochamber of a *Leica EMFC7* ultramicrotome. Once the sample was homogeneously frozen and stable on the support, the temperature was raised to -80 °C to soften up the sample and ease the cutting procedure. The samples were cut in thin slices of 80 nm thickness and 1-2 mm length (cut-speed = 1 mm/s; FEED = 80 nm) using a diamond cutting-knife. The slices were placed in a suitable sample holder and stored in liquid nitrogen overnight. The frozen samples were placed on an Agar C-166-3 lacey carbon grid, inside a cryo-holder (*ThermoFisher*) filled with liquid nitrogen. The samples were then transferred into the microscope (*ThermoFisher* Tecnai Osiris) and analysed operating a 200kV voltage. Scanning-Transmission Electron Microscopy (STEM) mode was chosen instead of standard TEM to record the images, as it allowed a clearer detection of the nanoparticles. To attempt to distinguish more precisely the different phases of the formulation (oil; water; TiO<sub>2</sub>), elemental chemical analysis of the samples was performed using Energy Dispersive X-Ray (EDX) detector mounted inside the microscope. The EDX images were then processed with ESPRIT software (Bruker), in order to treat and minimize the background.

### 2D X-Rays Nano-Tomography

Each sunscreen formulation was pumped into a 249 µm diameter Kapton capillary, using a disposable syringe fit with a needle. The portion of the capillary not filled with the sample was cut-off and the extremities were closed with epoxy glue, to avoid sample evaporation. 2D X-Ray nano-Tomography (XRNT) analysis was performed using a UltraXRM-L200 (*Zeiss Xradia*). A mosaic of 5x5 images was



recorded in large field of view (64.5x64.5  $\mu\text{m}$ ), to be able to cover the entire sample area, with a pixel resolution of 60x60 nm. Each sample measurement took only 25 min, which is likely to avoid any aging of the sample structure.

### Images and data treatment

The original 2D XRNT images (8bit) were treated with *ImageJ* software in order to process a greyscale composed of 256 shades of grey, in which the black (maximum X-Ray absorption) is at 0 and the white (no X-Ray absorption) is at 256. In order to be sure to observe sample portions of the same thickness (249  $\mu\text{m}$ ), the areas corresponding to the edges or the cream-air interface in the image were avoided, and only the central bulk area of the sample was taken in consideration. In order to be able to distinguish accurately the nanoparticles contribution in the sample images, each greyscale distribution was deconvoluted with three gaussian curves using *Fityk* software. Each gaussian contribution would likely represent portions of the sample having a respective nanoparticle density (high, medium, low, see *Additional information*). To better visualize these three respective areas in the 8-bit images, the greyscale distribution range displayed was limited within max and min values corresponding to the intersection point values between the gaussian curves. The sizes high nanoparticle density portions in each sample image was then evaluated by measuring their longer size length, in order to better define then UV filters aggregation state in the formulation.

To give insight on the homogeneity of nanoparticle dispersion in each sunscreen formulation, the threshold area of ideally dispersed nanomaterials in each sample was estimated, knowing that the transmission of X-Rays through a slab of thickness  $d$  is given by equation (2)<sup>146</sup>:

$$(2). \quad T = \exp(-n\mu_a d)$$

where  $n$  is the number of atoms per unit volume,  $\mu_a$  is the atomic photo-absorption cross section. at a given wavelength and  $d$  is the distance travelled by the beam inside the sample. The factor  $n$  was calculated based on the brute formula of each sunscreen components and on their nominal proportions inside the different formulations. The factor  $\mu_a$  can be obtained from the relation with the unreal scattering factor  $f_2$  given by equation (3)<sup>147</sup>:

$$(3). \quad \mu_a = 2 r_0 \lambda f_2$$

where  $r_0$  is the classical electron radius, and  $\lambda$  is the wavelength of the incident beam. The factor  $f_2$  can be in turn obtained, knowing the index of refraction  $n_r$  of the sample, by the equation:

$$(4). \quad n_r = 1 - \frac{1}{2\pi} N r_0 \lambda^2 (f_1 + i f_2)$$

The index of refraction of each sample was obtained using the calculation tool provided by the Center of X-Ray Optics (CXRO/ <http://www.cxro.lbl.gov>). In order to calculate the index of a certain material we need to know its density. In a three-phasic emulsion like a sunscreen formulation, the various components (water; oil; gelling agent; nanoparticles) has significantly different densities. The calculation of an average density for uneven distributed mixtures as sunscreens it was beyond the scope of this work. However, the obstacle was exceeded by separately calculate the index of refraction (and thus the corresponding  $f_2$  value) of each component of the formulation for which the density was known (i.e.: Phase A; Water; Sepiplus 400; Glycerol; Rutile). Then, the average  $\mu_a$  for the entire sunscreen formulation (ideally dispersed) was derived by linear combination of each component contribution weighted by their nominal ratio in the mixture.

A 5 % error on the nanoparticles proportion was applied in the calculation of the average  $\mu_a$  factor for each sunscreen sample, in order to obtain a T value range for ideally dispersed nanoparticles with 95 % confidence interval. This calculated X-rays transmission range limits of ideally dispersed nanoparticles in each sunscreen formulation, was applied to the distribution greyscale of the correspondent sample and the area under the curve portion defined by the range limit was calculated using the trapezoid approximation rule. Therefore, the percent of *ideal dispersed nanoparticles* in the different sunscreen formulations was calculated by dividing the area defined by the calculated limit range of ideal dispersion to the total greyscale distribution area (see *Additional information*).

### 3. Results and discussion

#### Surface free energy of the nanoparticles:

The contact angle ( $\theta$ ) results obtained with the different liquid for T-S and T-Lite pellets are reported in **Figure 1**.  $\theta_{TLite-D} \ll 90^\circ$  ( $18^\circ$ ), with the oil phase (Phase D) and T-Lite confirms the high affinity of this UV filter for the sunscreen oil. T-S NPs also showed a good affinity for the Phase D, but the higher contact angle ( $\theta_{TS-D} = 25^\circ$ ) compared to T-Lite, suggests that the latter has a slightly more effective interaction with the oil phase used for the sunscreen formulations. These observations were overall supported by the further results obtained using three standard liquids (ultrapure water, diiodomethane and formamide) to calculate the surface free energy components (**Table 4**).

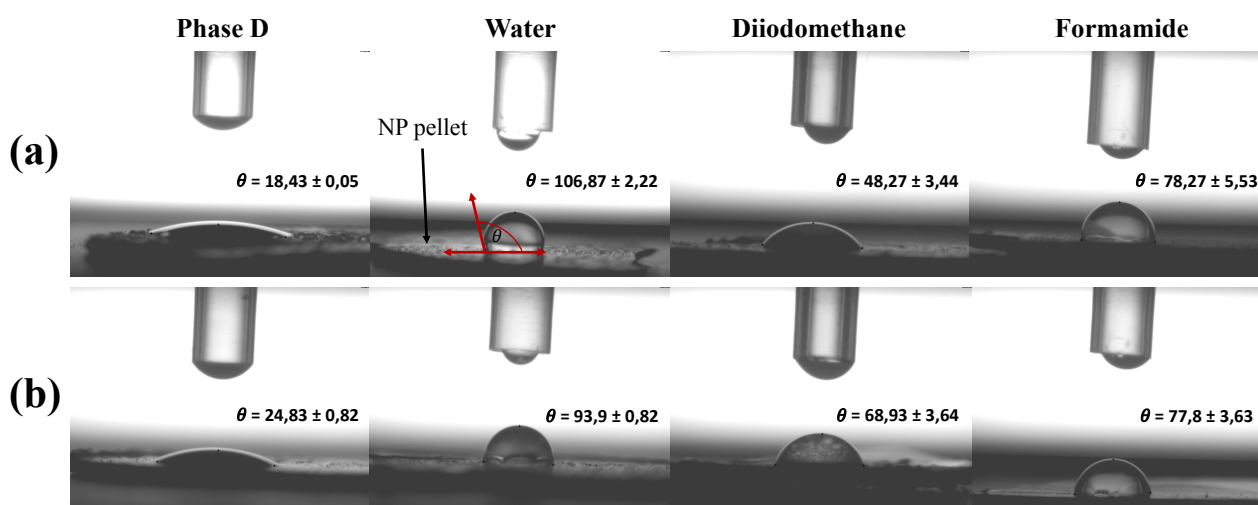


**Figure 3:** Contact angle measurements ( $\theta$ ) between different liquids and the T-Lite **(a)** or T-S **(b)** nanoparticles pellets, using sessile drop method.

**Table 4:** Surface free energy components values calculated using the Van Oss–Chaudhury–Good equation.

| Nanoparticulate UV filters | Interfacial Lifshitz-Van der Waals component ( $\gamma^{LW}$ ) | Lewis base component ( $\gamma^-$ ) | Lewis acid component ( $\gamma^+$ ) | Surface free energy ( $\gamma^s$ ) (mN/m) |
|----------------------------|--|-------------------------------------|-------------------------------------|---|
| T-Lite                     | $35.3 \pm 1.4$   | $0.1 \pm 0.1$                       | $0.4 \pm 0.2$                       | $37.5 \pm 1.5$                            |
| T-S                        | $21.3 \pm 2.0$   | $3.9 \pm 1.5$                       | $0.4 \pm 0.4$                       | $23.1 \pm 1.8$                            |

The interfacial Lifshitz-Van der Waals component of the surface free energy ( $\gamma^{LW}$ ), describes the likelihood of a compound surface to establish apolar interactions<sup>145</sup>, while the Lewis base components value ( $\gamma^-$ ) describes the likelihood to interact with polar components.  $\gamma^{LW}$  is higher for T-Lite NPs (35 mN/m) compared to T-S NPs (21.3 mN/m), while  $\gamma^-$  is higher for T-S NPs (4 mN/m). The reason behind these differences of surface properties can be ascribed to the different organic coatings of the two ENMs. The carboxylic group of stearic acid coating of T-S NPs can indeed act as an electron donor (Lewis base) and determine a small capability to interact with polar molecules, although we do not have any information about the stearic acid chains orientation and type of adsorption on the NPs surface, which is a crucial information in order to verify the availability of the carboxylic

group to interact with external components. T-Lite NPs, contrarywise, contain a dimethicone (polydimethyl siloxane) coating that would not favor polar interactions, because of lack of electron donor (or acceptor) moiety in the molecule.

These considerations will eventually explain the small differences in affinity for the ultrapure water observed in **Figure 1** between the two ENMs. T-S NPs, although still preserving a hydrophobic character, showed a slightly higher affinity for ultrapure water ( $\theta_{TS-w} = 93.9^\circ$ ) compared to T-Lite NPs ( $\theta_{TLite-w} = 106.9^\circ$ ). This is certainly due to the relatively more polar feature of T-S NPs, suggesting that the wettability for the Phase D should be mostly influenced by the apolar interactions with the NPs surface, that would be stronger with T-Lite NPs based on the  $\gamma^{LW}$  component.

### Solar protection efficacy and formulation texture of the sunscreens

The Solar Protection Factors (SPF) of the different sunscreens, formulated with T-S or T-Lite NPs, were measured in-vitro and are reported in **Figure 2**. Overall, at every NP concentration tested, the sunscreens formulated with T-Lite UV filter show greater protection performances than those formulated with T-S UV filter. Moreover, this difference increases with the NP concentration (**Figure 2**, *dashed line*).

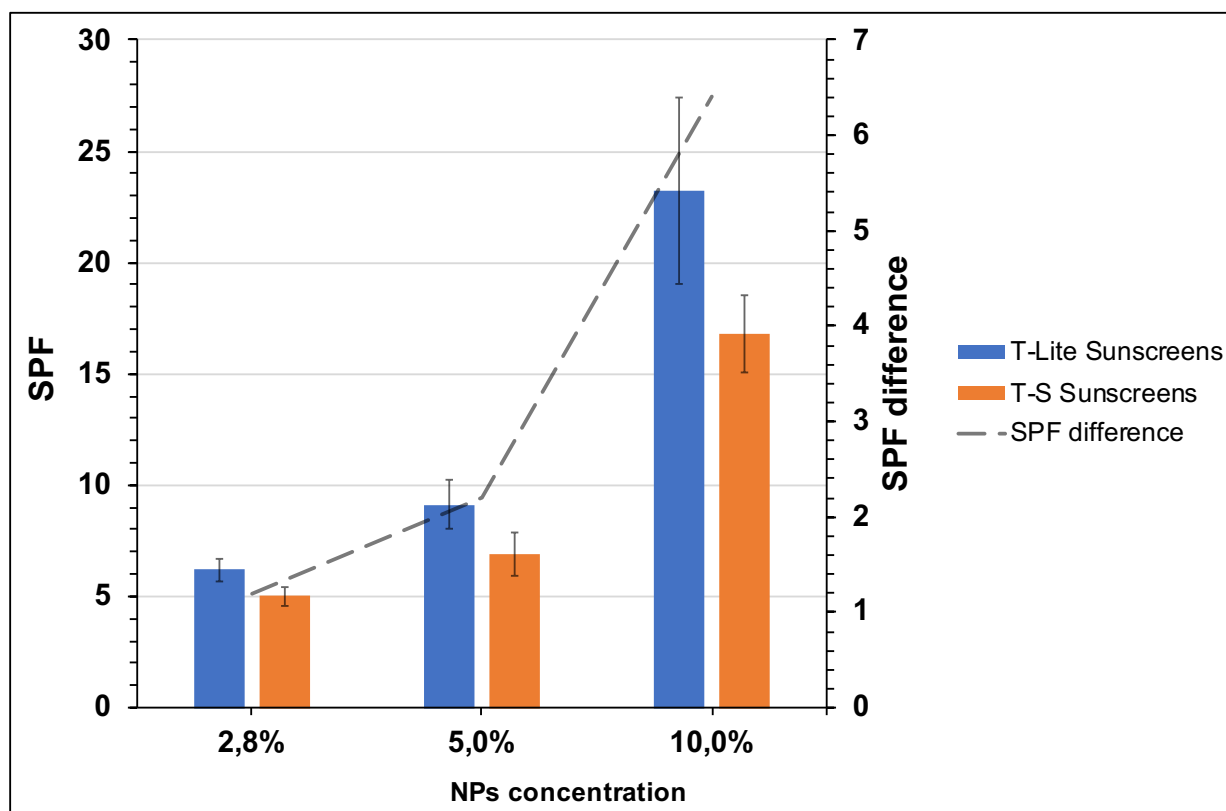


**Figure 4:** SPF values for T-S and T-Lite sunscreens for each NPs concentration. The dashed line represents the SPF differences between T-Lite and T-S sunscreens at each concentration.

The SPF value being proportionally correlated to the UV absorbance<sup>148</sup>, this trend cannot be biased by the calculation method. It could also unlikely be due to any size difference between the primary particles constituting T-S and T-Lite NPs (*Table 1*), because this would not lead to such dependence with the NP concentration. It is our hypothesis that such differences in the SPF between the formulations arises from varying aggregation state of the nanoparticulate UV filters in the formulation. It is well-known that particle aggregation increases proportionally with the particle concentration<sup>149</sup> and leads to lower sunscreen screening efficacy<sup>150</sup>. Increase the particle concentration, in fact, lead to a higher probability of particle interaction and thus aggregation. Aggregation phenomena determine inhomogeneities of the particle distribution inside the formulation, with the formation of “holes” of low filter content that are more transparent to UV radiation. It is thus crucial to determine the particle aggregation in sunscreen

product, using a methodology that does not alter the original formulation matrix. In an attempt to do achieve this result, each formulation was characterized using 2D X-Rays Nano-Tomography (XRNT) in large field of view. The unmodified 8bit mosaic images are presented in **Figure 3**.

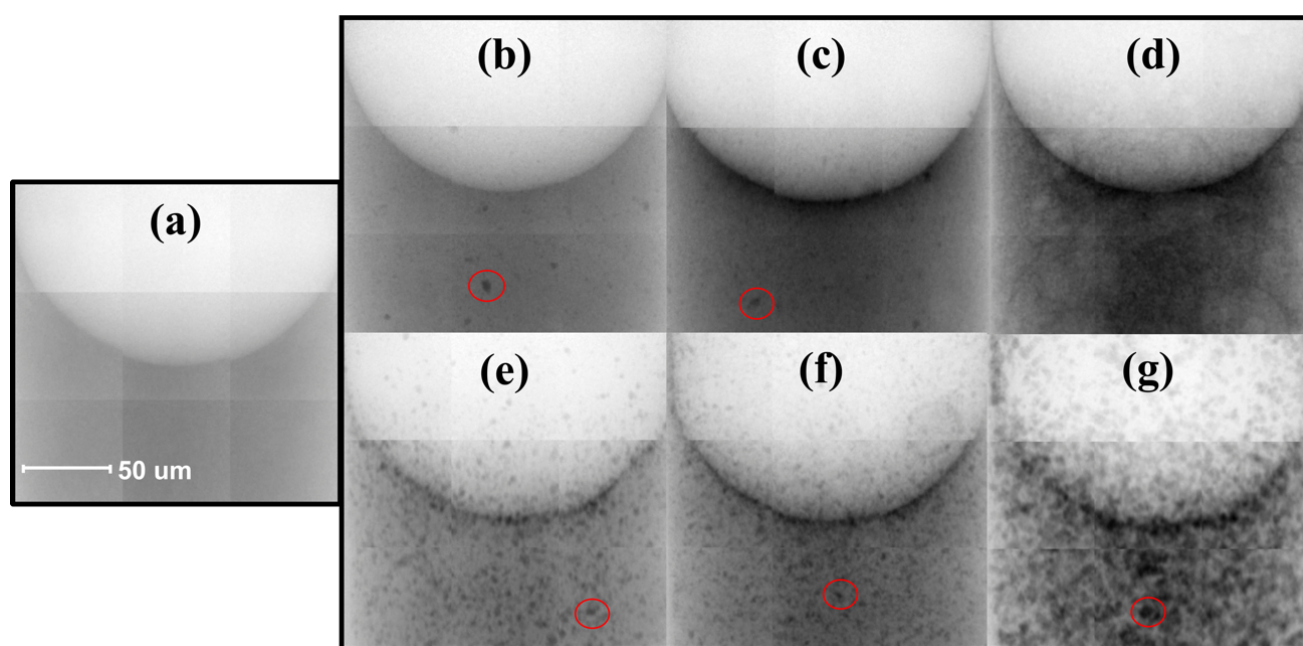


**Figure 5:** 2D X-Ray Nano-Tomography (raw data) on sunscreens: Blank Sunscreen (a); T-Lite sunscreens 2.8; 5; 10 % w/w (b-d); T-S Sunscreens 2.8; 5; 10 % w/w (e-g)

In each greyscale image, darker shades correspond to higher X-rays absorbing zones while brighter shades to the lower X-rays absorbing ones. Denser materials, like  $\text{TiO}_2$ , are stronger X-Rays absorber than aqueous or oily sunscreen component. Black dots of few micrometer size (red circles) in NP-containing sunscreens (b-g), can be thus easily associated to NP aggregates, as they are also not detected in the control sunscreen free of NP (a). It appears clearly at each NP concentration, that the T-Lite sunscreens contain less micro-sized aggregates than the T-S sunscreens. The formulation texture appears overall darker with T-Lite than with T-S, indicating a more homogeneous dispersion of the NPs. If for

the same filter selection, the textures at 2.8 and 5 % NP concentrations look similar, the highest NP concentration testes of 10% w/w seems to dramatically affect the homogeneity of the dispersion. In TS-S-10 (**g**) this appears related to an increasing particle aggregation, which results in larger aggregate size. In T-Lite-S-10 (**d**), although the presence of discrete micro-sized aggregates is not observed, the texture itself appears less homogeneous compared to lower T-Lite concentrations, with the presence of brighter zone (on sides) cohabitating with darker zones (concentrated in the center and near the meniscus interface). This nanoparticles accumulation at the air-cream interface is also observed in T-Lite-S-5 and in all the TS-S samples. It is probably due to a higher affinity of the NPs for the air phase than for the sunscreen dispersing medium, which leads the NPs to accumulate at the air-cream interface in order to minimize the area of interaction with the oil. Such type of reactions are normally observed in aqueous colloidal dispersion with hydrophobic particles and usually accompanied by particle aggregation/coagulation<sup>151</sup> and could likely increase at greater particle concentration. The fact that this phenomenon is already observed at the lowest particle concentration in TS-S-2.8 sample suggests that this ENM is more unstable in the formulation system compared to T-Lite NPs. This is in accordance with the contact angle measurement observations discussed in the previous section, which showed a higher capability of T-Lite NPs to interact with apolar medium and a higher affinity for the oily dispersant phase (Phase D). The hypothesis, expressed so far, that the differences in the screening performances between T-S and T-Lite sunscreens could be related to diversified aggregation/agglomeration phenomena of the two UV-filters is overall corroborated by the XRNT observation presented in **Figure 3**.



### Nanoparticles dispersion state and aggregate size

In order to obtain more precise and quantitative information about the size of the aggregates and the nanoparticle dispersion in the formulated sunscreens, we treated the grayscale distributions of each images, taking onto account only the central bulk portion of the capillary, in order leave side effects apart (see detailed methodology in supplementary material, Figure S\*\*). The results are reported in **Figure 4**. The three gaussian deconvolutions performed on the greyscale distribution of each image, could be attributed to three contributions in the sample texture, having respective contrasts in X-ray absorption.

It is important to underline that the images obtained by XRNT are 2D projections of a 3D sample, where each pixel thus results from the sum of the projected voxels.  $\text{TiO}_2$  NP is the most X-Rays absorbent component of the formulation, cohabitating with the aqueous and oil components. Nevertheless, the lowest absorption areas observed in XRNT may not represent an absence of NPs, but parts of the cream through which the incident X-Ray beam encountered mostly water or oil phase and less  $\text{TiO}_2$ . Thus, the distribution greyscale limits (max and min value), intensities and width depend on the NP concentration and aggregation state in the volume analysed. Therefore, each of the three greyscales contributions can define distinct area portions of the sample characterized by different  $\text{TiO}_2$  NPs densities. We defined these contributions as High, Medium and Low  $\text{TiO}_2$  density areas (HTD; MTD; LTD). The % of each contribution in the sample images is reported in the distribution pies next to each density map (Figure 4).

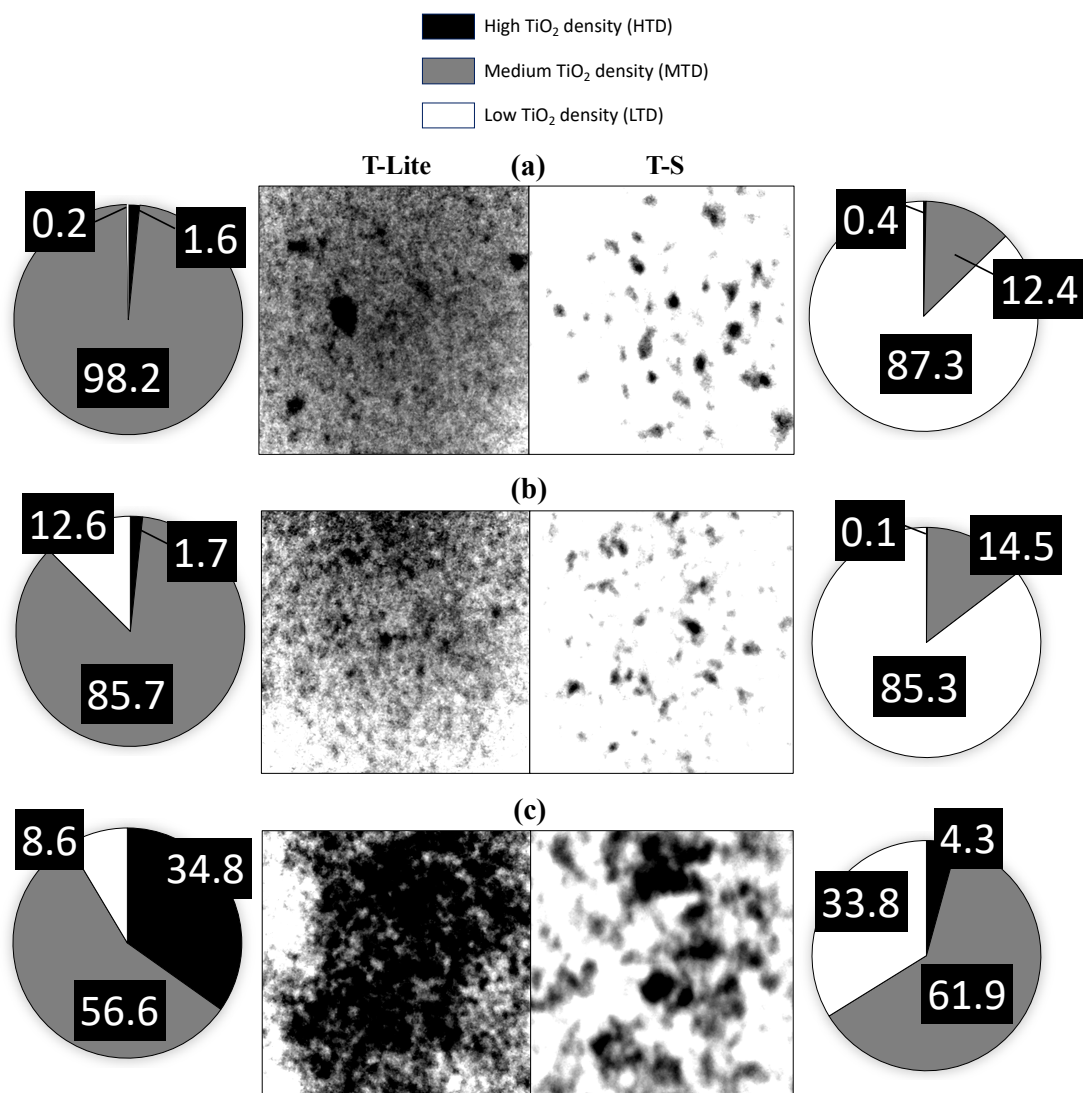


**Figure 6:** Density maps of the  $\text{TiO}_2$  NPs in the sunscreen, obtained from the deconvolution of the XRNT greyscale in three contribution with high, medium and low  $\text{TiO}_2$  density. The surface area % of each contribution is plotted in pies. T-Lite and T-S sunscreen at 2.8% (a); 5% (b) and 10% (c) NPs concentration

HTD areas (black) are generally organized in spots of few micrometers size and can be attributed to NP aggregates. MTD areas (grey) can be considered representative of the average nanoparticle dispersion state in the formulation, where both NPs and liquid phases contribute optimally to the cream texture. These greyscale contributions (HTD; MTD; LTD) are not absolute but relative, meaning that they can be compared with each other only between samples containing the same nominal NP concentration. This is because greyscales

distributions of samples containing significantly different nominal NPs concentration are not superimposable.

In TLite-S-2.8 (**Figure 4 a**), the MTD area is observed as a homogeneous matrix that represent the 98% of the entire image, in which particulate units are not distinguished from the rest of the formulation. In TS-S-2.8, instead, the MTD areas are observed as discrete units not really distinct in size and shape from the HTD areas containing particle aggregates. We hypothesize that these MTD areas can also be attributed to particle aggregates, but that these small aggregates cohabitate with neighbor areas of lower density (i.e. less superposition between particles), tending to attenuate the X-Ray absorption signal to MTD level. These MTD areas represent only the 12% of the entire image for TS-S-2.8. The image is actually mostly composed of LTD areas (87%). This comes in agreement with the major aggregation of the T-S NPs in this sample, that generates inhomogeneities in the emulsion, and thus large areas of lower nanoparticles content. LTD areas are almost undetected in TLite-S-2.8 while few HTD zones of aggregation are clearly distinguished. In the XRNT image of TS-S-5 (**Figure 4 b**) the dispersion state of the sample seems similar to that in TS-S-2.8 sample, while in the TLite-S-5 image the MTD area is less homogeneously distributed compared to the TLite-S-2.8 together with an increase of the LTD area (18%). This may be due to an inception of particle aggregation in TLite-S-5 sample due to the increasing NP content.

A drastic change in the homogeneity of the formulation is instead observed at 10% of nominal filter content in both types of sunscreens (**Figure 4 c**). In the TLite-S-10 image, a dramatic increase of the HTD areas (35%) is observed, together with the presence of larger particle aggregates, mostly confined in the central part of the image while the edges are dominated by LTD (8.6%) and MTD

(56.6%) areas. The texture appears overall significantly less homogenous compared to the lower concentrated T-Lite sunscreens, probably because of emulsion oversaturation at a NPs concentration of 10% w/w that would destabilize the colloidal dispersion. In the TS-S-10 image, although the NPs dispersion state does not seem to be altered compared to the lower concentrated TS sunscreens, the size of the NPs aggregates (HTD areas) is clearly increased. The presence of MTD areas is also increased (62%) due likely to the higher NPs content in the formulation, even though their distribution in the image does not appear homogenous but localized in discrete units. As it was argued for the previous T-S samples, these discrete units can be associated to particle aggregates as well as the HTD areas. The size (longest side length) of the units associated to particle aggregates was measured and divided into arbitrary size classes as reported **Figure 5**.

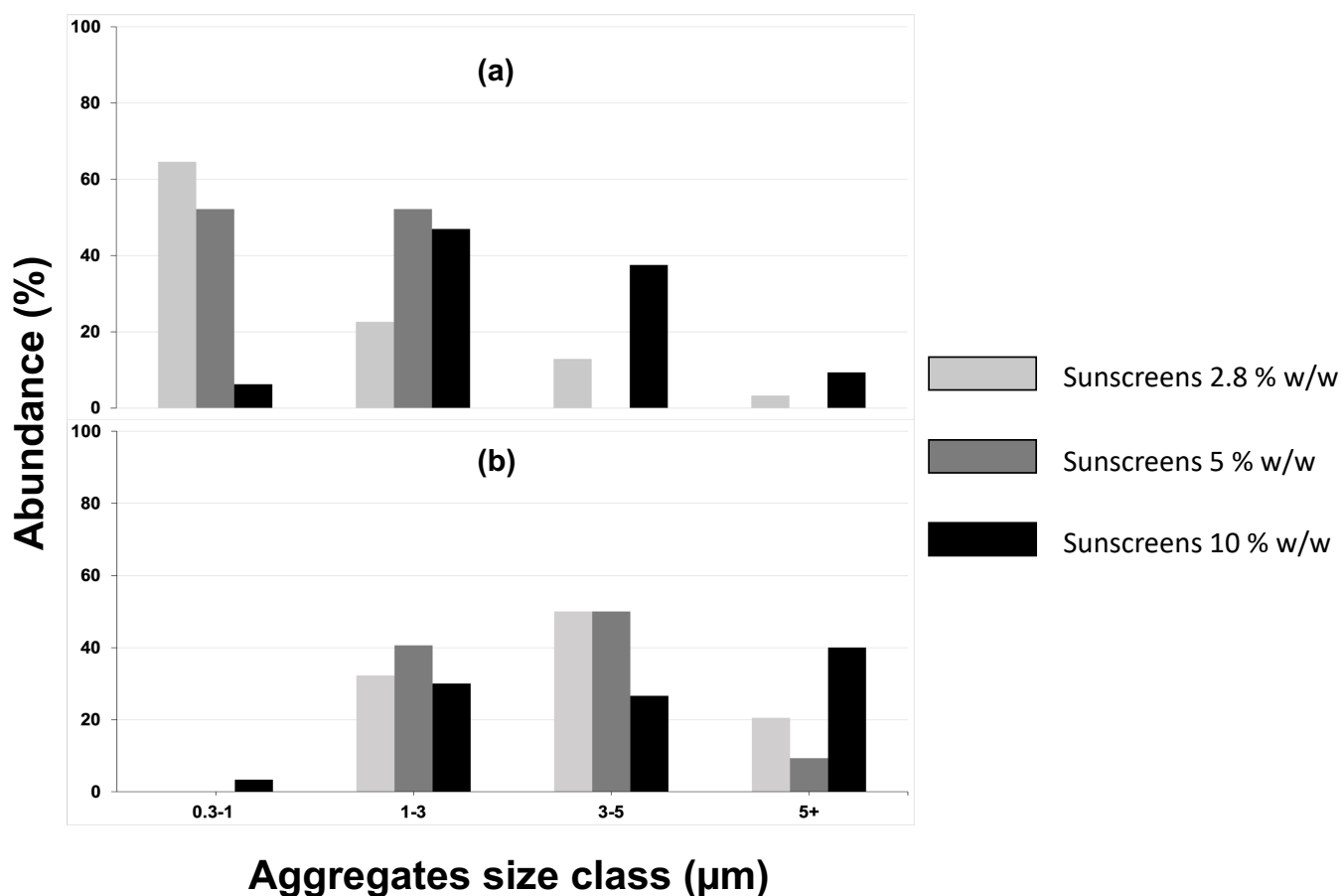


**Figure 7:** TiO<sub>2</sub> aggregates size class distribution in T-Lite **(a)** and T-S **(b)** sunscreens

In T-Lite sunscreens (**Figure 5 a**) at 2.8 and 5 % NPs concentration, the most abundant aggregate size classes are the 1<sup>st</sup> (0.3-1 μm) and 2<sup>nd</sup> (1-3 μm). Especially in T-Lite-S-2.8 sample (light grey), most of the aggregates are below the micrometer size while in the more concentrated T-Lite-S-5 (dark grey) the 1<sup>st</sup> and 2<sup>nd</sup> size classes are equally populated. Increasing the NPs concentration up to 10% in T-Lite-S-10 (black) shifts most of the aggregates into higher size classes (2<sup>nd</sup> and 3<sup>rd</sup>) leaving the submicron class almost absent, together with the detection of few aggregates in the 4<sup>th</sup> size class (> 5 μm). In T-S sunscreens (**Figure 5 b**), instead, particle aggregates of submicron size are almost undetected at every NP concentration. No particular differences of the aggregation state are observed at increasing NP concentration except for the dominant presence of 4<sup>th</sup> size class

aggregates in TS-S-10 sample (black). Overall, in T-S sunscreens, the aggregates are larger than in T-Lite sunscreens at every NPs concentrations. In sum, the speculations over the lower colloidal stability of T-S NPs and the greater nanoparticle aggregation in overloaded sunscreens are refined by the results showed in **Figure 5**.

The effects of particle aggregation on the homogeneity of the formulation is clarified by the results reported in **Figure 6**. From each image reported in **Figure 4**, the area in which the NPs are ideally dispersed was calculated. This was achieved by estimating the theoretical X-ray absorbance that would correspond to a formulation in which the NPs are homogeneously dispersed at a given concentration. In T-Lite-S-2.8 almost 80% of the NPs are ideally dispersed, which means that the nominal ratio between the formulation ingredients and the NPs is preserved in 80% of the analysed area. Going through higher concentrated T-Lite sunscreens, the % of ideals dispersion decreases proportionally with the NP content. This is consistent with the increasing aggregation phenomena highlighted in **Figure 5a** and with the decrease of MTD area % observed in the results reported in **Figure 4**. Areas of ideal dispersion are very low in TS-S-2.8 (20%) and almost absent in T-S sunscreens at 5% and 10 % NP concentration, which is in line with the higher aggregation state observed already at lowest T-S ENM concentration. (**Figure 5b**).

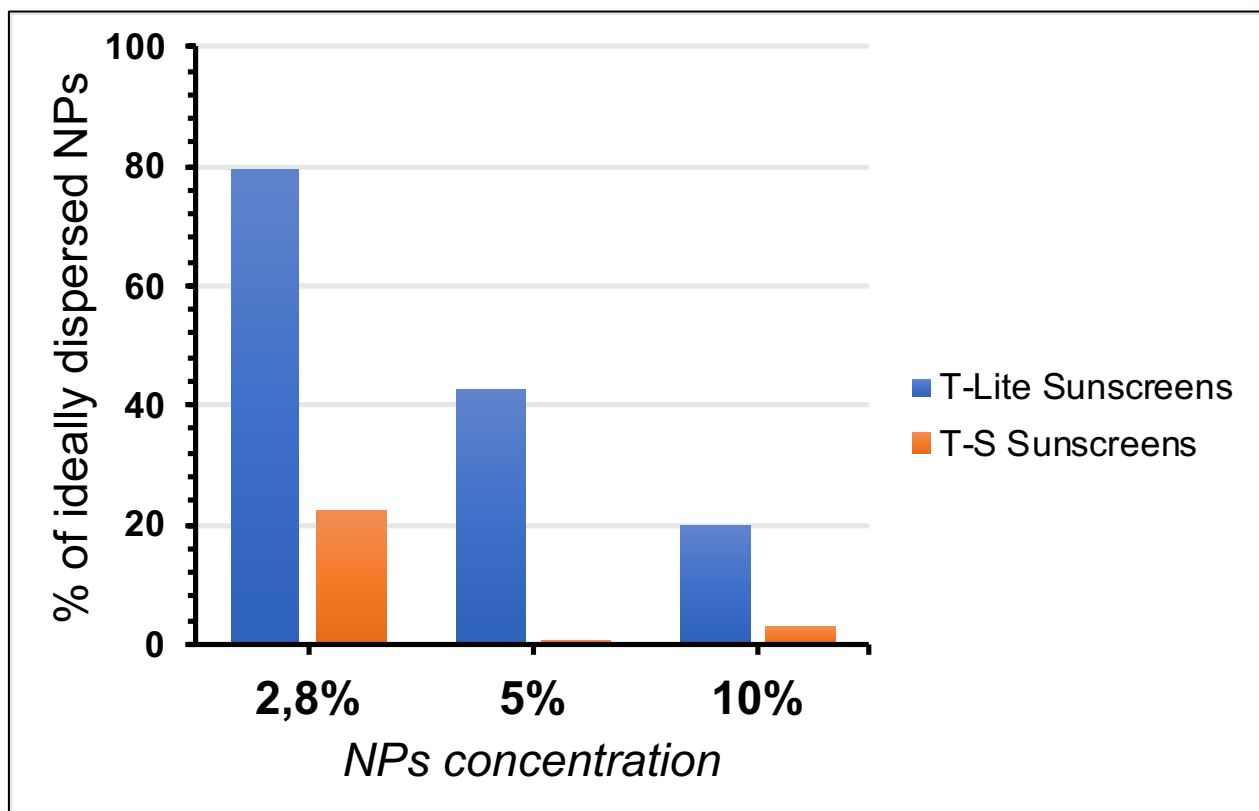


**Figure 8:** % of ideal nanoparticle dispersion for T-Lite (blue) and T-S (orange) sunscreens at increasing nanoparticles concentrations

In highly concentrated sunscreens, TEM images may be saturated in ENM, which will make it difficult to observe the differences in aggregation and dispersions state between samples. For this reason, only TLite-S-2.8 and T-S-S-2.8 samples were selected to be further analyzed with Cryogenic-STEM. The results are reported in **Figure 7** (TS-S-2.8) and **Figure 8** (TLite-S-2.8). In both samples, the presence of titanium-based nanoparticles was confirmed by the EDX analysis reported right next each original image. The elemental analysis of titanium is mapped in red, together with the one of carbon in green and oxygen in blue. It is our hypothesis that the areas dominated by the presence of carbon in the EDX map could be associated to the sunscreen oil phase while the ones dominated by the presence of oxygen could be associated with the aqueous phase. Superimposition of different emulsion phases, which can usually affect the data interpretation of TEM image, is minimized in the ultrathin sample slices of 80 nm

thickness obtained through the ultramicrotome procedure used here, and ultimately allows a more accurate distinction of the emulsion phases.

In TS-S-2.8 sample (**Figure 7**), presence of brighter contrasting objects is attributed to nanoparticle aggregates of  $\cong 2\ \mu\text{m}$  size are clearly visible in the image **7a**. This is confirmed in the corresponding EDX chemical map (**Figure 7b**), with the concentration of titanium (red dots) in the same area. In the second slice (**7c**) the NP dispersion seems to be more homogenous with the presence of smaller aggregates of less than  $1\ \mu\text{m}$  size. In both slices, the presence of the water/oil emulsion is clearly distinguished in the two EDX maps (images **7b** and **7d**) by the presence of high carbon signal zones (oil) and high oxygen zones (water). The detection of titanium NPs only inside the areas of high presence of carbon (images **7b** and **7d**), is in accordance with the hydrophobic property of the NPs together with the formulation procedure that involved NP dispersion in the oil phase first. It is interesting to notice that in the zones **(1)** and **(2)** of the images **7c** and **7d**, NPs appear more concentrated at the interface between water and oil phase (blue arrows). This can be related to the phenomenon known as Pickering effect where finely dispersed particles can interact at the interface between two liquid phases leading to the emulsion stabilization<sup>152</sup>, even-though there are not enough images to analyze and compare in order to fully support this speculation.



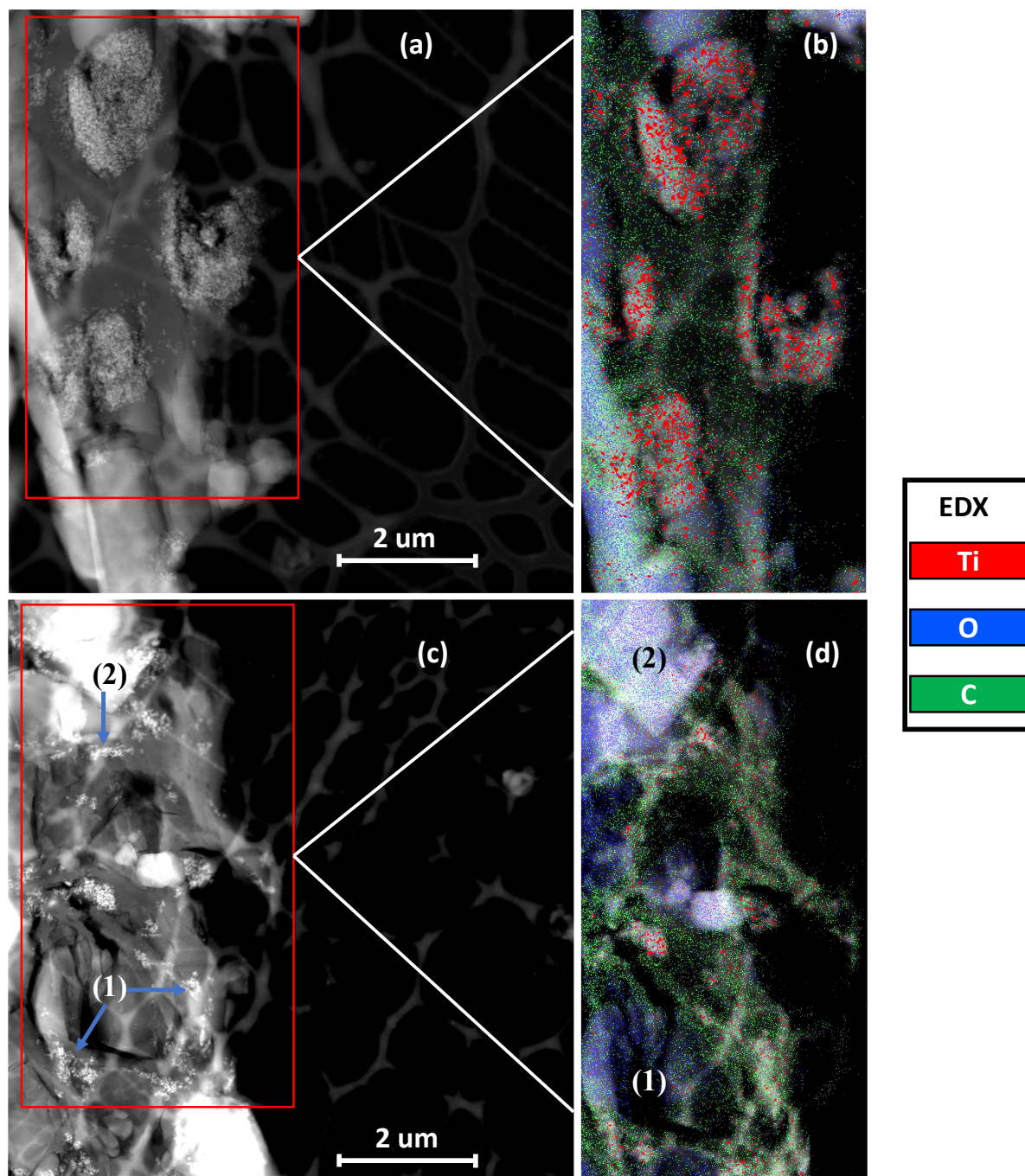


**Figure 9:** (a; c) Cryo-TEM images on TS-S-2.8. (b; d) related EDX analysis of Titanium; Oxygen and Carbon.

The Cryo-STEM images for TLite-S-2.8 sample are reported in **Figure 8**. In both slices (images **8a** and **8d**) the presence of solid  $\text{TiO}_2$  particles is confirmed by the EDX detection of titanium in the same areas (images **8c** and **8f**). Compared to TS-S-2.8, the particles appear better dispersed with most of the aggregates observed  $< 1 \mu\text{m}$ . As it was not possible to well distinguish in the same maps the titanium

signal from the carbon and oxygen ones, the EDX maps for each slice are presented in superimposition of C and O signals to highlight the emulsion structure (Figures **8b,e**), and in superimposition of O and Ti signals to visualize the NP dispersion (Figures **8c,f**). The lower detection of titanium in the EDX spectrum compared to the TS-S-2.8 sample could be related to the lower size of the aggregates, i.e. lower X-ray absorbance, that led to a lower contrast in the image compared to the O and C contributions. Some titanium agglomerates are however visible in the image **8c**.

Regarding the emulsion structure, the EDX maps of the two slices show oil and water phases hardly distinguishable in TLite-S-2.8, while they were clearly separate in TS-S-2.8 sample. In TLite-S-2.8 carbon signal prevailed over the oxygen, suggesting a prevalence of the oil phase, even-though the excess O in the zone **(1)** of **Figure 8(a-c)** could be probably due to the presence of an emulsion water droplet. In the slice of TLite-S-2.8 reported in the image **8d** the EDX map (**8e**) shows a prevalence of oxygen over the carbon, suggesting an excess of the water phase with regard to the oil. These differences in the emulsion structure between the two slices in TLite-S-2.8 sample could be explained by considering the slices size. If we compare, in fact, the longer side length of each of the slices reported in **Figure 8** with the ones reported in **Figure 7**, it can be noted that TLite-S-2.8 slices are, in average, half the size of the TS-S-2.8 ones. Which means that the slices of TLite-S-2.8 are maybe too small to allow the coexistence of both aqueous and oily phases and thus a clear visualization of the emulsion structure. In the area analyzed here, the nanoparticles are clearly visible as bright objects in the original STEM image, but they are barely detected with the EDX analysis (image **8f**). This could maybe be ascribed to a finer dispersion of the particles which leads to less dense particle agglomerates, eventually resulting in a less intense Titanium signal in the EDX map.

Especially in the zones **(1)** and **(2)** of the image **8(d;e)** the aggregates seem to be stuck at the interface between the water and the oil phase of the emulsion, similarly to what was already seen in TS-S-2.8 sample (**Figure 7c**), that could be ascribed to the Pickering effect discussed so far. However, the low presence of carbon detected through EDX (**Figure 8e** (1) blue arrows), sometimes also undistinguished from the underling carbon grid (**Figure 8e** (2)), lead to an uneasy distinction of the emulsion phases and particle location, preventing any further speculations.

Although this physical property was not accurately evaluated in the present work, it should be noticed that the primary particle size of both types of UV-filters in the Cryo-STEM images does not appear significantly different. This corroborates the hypothesis, advanced so far, that the higher aggregate size of T-S UV filters in the sunscreen formulation, compared to the T-Lite one, is related to their respective surface properties presented in section 3.1 and not to different size of the nanoparticle units composing the aggregates.

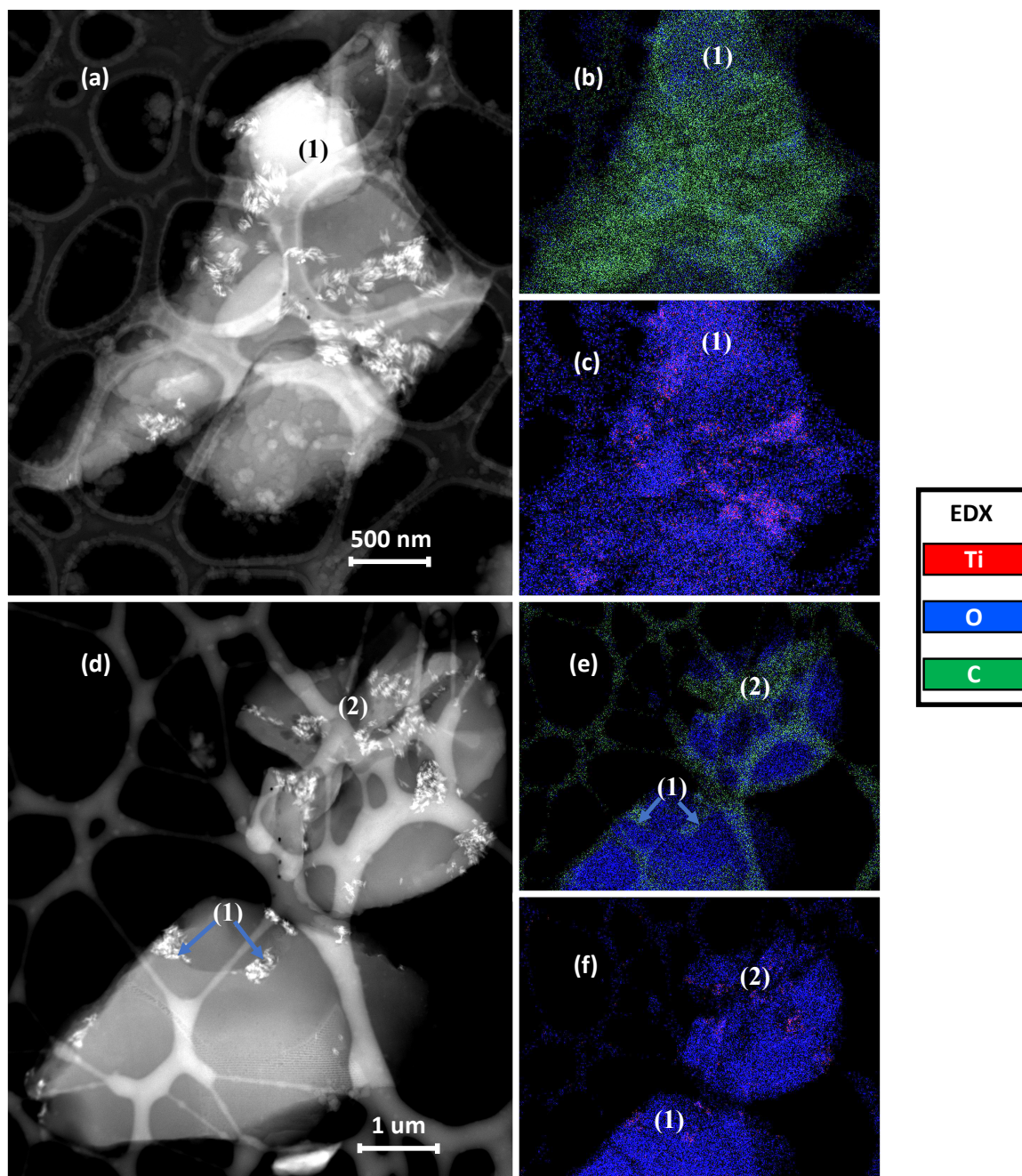


**Figure 10:** (a) Cryo-TEM image on T-Lite sunscreen 2.8% w/w formulation. (b-c) EDX analysis of Oxygen/Carbon and Oxygen/Titanium image (a)

## 4. General discussion and conclusions

As it was already evoked in section 1., the determination of primary size, shape and aggregation state of nanomaterials inside cosmetic formulations like Sunscreens is essential to evaluate the product efficacy to absorb UV rays, the internalization of NPs through the consumer's skin, their interactions with biological systems, and their environmental fate and impact. Evaluate these physical-chemical properties *in situ* in the original product without modifying the structure of the matrix (ex. dilutions; dehydrations) is crucial in order to not generate artefact results.

X-Rays Nano-Tomography (XRNT) proved to be a powerful technique to determine the aggregation state of diverse nanoparticulate mineral UV filters in a W/O sunscreen formulation without altering the characteristics of the original product. Direct observation of the raw images gives useful information on the product characteristics. The distinctions of NP aggregates, larger than 300 nm, from the rest of the emulsion appeared to be straightforward (**Figures 3**). Despite the nanometric scale resolution of XRNT (pixel size: 60x60 nm), nanoparticle aggregates smaller than 300 nm and primary particles sizes couldn't be distinguished from the rest of the formulation, due to their lower contrast to X-rays. In the raw image, the absence, or low detection, of nearly micrometer aggregates can be used as an undirect proof that the NPs are well dispersed in the formulation at a nanometric scale. Further analysis of the raw XRNT images also enables to measure the relative extent of NP dispersion in the formulation (**Figure 4**). The deconvolution of the greyscale distribution allowed to quantitatively distinguish the areas with different NP densities, and thus a finer evaluation of the formulation homogeneity, a precise visualization of the particle aggregates or UV filters lacuna, and their eventual size measurement. The



operating conditions adopted during the XRNT measurements (constant X-Ray energy; fixed sample thickness; fast measurement analysis; known samples nominal composition), allowed a precise calculation of the ideal NP dispersion threshold that can be used as a reference to optimize the sunscreen formulation (**Figure 6**). The sensitivity of X-Rays to the higher density of the mineral UV-filters dispersed in the formulation makes of XRNT a powerful tool to provide more precise information compared technique such as Multi-Photon Tomography (MPT) or Laser Scanning Confocal Microscopy (LSCM) used in previous studies<sup>136,137</sup> to characterize similar colloidal systems. Indeed, these methods were capable to provide qualitative information on the dispersion state of the nanomaterials in the formulation at the micrometer scale. However, due to resolution limits of the techniques, the authors could not provide a quantitative description of the size of the particles or aggregates and on the homogeneity of the formulation.

Ultramicrotome/Cryo-TEM results on the lower concentrated sunscreens, were capable to provide a clearer visualization of particle aggregates and primary particles, corroborating the observations made with XRNT. Compared to previous studies using cryogenic<sup>138</sup> or freeze-substitution TEM<sup>137</sup>, the preparation of ultrathin (80 nm) sample slices using a cryogenic ultramicrotome, prior the Cryo-TEM analysis, allows a finer visualization of the emulsion phases and nanoparticles dispersion characteristics after EDX analysis (**Figure 7**). However, due to the smaller observation field compared to XRNT, Cryo-TEM method could not give insight on the dispersion state and homogeneity of the overall product neither on the presence of large micrometric aggregates (2  $\mu\text{m}$ ) that give evidence of a bad formulation. Moreover, any variability on the NP aggregate size when a heterogenous sample is analyzed lead to a lack of reproducibility at this scale of observation as seen with TS sample in this work (images **7a** and **7c**). All these

considerations about Cryo-TEM taken together with the high time-consumption and expansive cost, suggest that it should be employed only when the determination of the primary particles size and shapes inside the products is required. However these physical information can be also obtained by mean of normal electron microscopy routines (SEM/TEM) which, although require dilution/drying<sup>135</sup> of the sample, are methodologically more simple and accessible.

The determination of the aggregates size of NPs inside a cosmetic formulation is not only essential for the biological/environmental risk assessment of the product but also to optimize the product design. The relation between the aggregation state of the NPs in the formulation (**Figures 3 and 4**) and the solar protection efficiency (**Figure 2**) noticeable in the present work, confirmed what was already observed by Tyner et al.<sup>119</sup> for mineral UV filters in a liquid suspension: finer dispersed nanoparticles lead to higher SPF of the sunscreen. Particle aggregation also leads to more heterogenous formulations that eventually provoke a more heterogenous UV screening on the users-skin, i.e. with protection lacuna. The 2D-XRNT based methodology hereby discussed, is capable to quantify these physical-chemical properties (**Figure 5 and 6**) and eventually to help to determine the most effective type of mineral UV-filter and its optimal concentration inside a product.

T-Lite NPs proved to have a more effective dispersion properties and higher protection efficiency compared to T-S NPs, in the present sunscreen formulation. This is certainly related to their higher surface hydrophobicity and affinity for the dispersant oil phase. However, we could also evidence in this work that at the highest concentrations (10 % w/w), T-Lite NPs begin to aggregate, due to mineral overload in the formulation, causing a significant decrease of sunscreen homogeneity. Thus, in perspective, it is fair to say that an optimal lower

concentration which would keep an effective SPF without excessively decrease the homogeneity of the formulation should be found. This would eventually allow the preparation of sunscreens with lower NPs load, that would have a lower environmental footprint at the end of the product lifecycle. Indeed, optimizing the efficiency of NP UV-filters in sunscreen by maximizing its dispersion helps to minimize the dosage in the formulation for a desired SPF, which can ultimately lead to lower environmental release and contribute to design a product safer for the environment. Our results proved that 2D-XRNT indeed could be a useful tool to reach this goal.





## Chapter IV: Safer by Design: Optimization of UV filters concentration in the formulation

As it was discussed in the previous chapter, controlling the ENMs dispersion in sunscreen formulation in the aim of minimizing the aggregation and maximizing the homogeneity of the emulsion, is a crucial step for the eco-design of nano-enabled sunscreens with a lower economic and environmental impact. Nonetheless, the academic knowledge on this subject is still scarce, especially in the case ENMs dispersed in the oil phase of the formulation. In this chapter, we present a novel methodology to evaluate the effects of the different components of a bio-sourced sunscreen oil phase on the stability of four commercial nano-TiO<sub>2</sub> based UV filters. The filters were selected as a function of their hydrophobic/hydrophilic character as well as the nature of their photo-passivating coating. We deliberately chose to focus only on the ENMs dispersion in the oil phase, which represent the first step of formulation, in order to avoid any interferences coming from the water and the gelling agent during the emulsification step.

In this work, we could evidence that the dispersion state of the ENMs was strongly affected by the emulsifying agent. In particular, the octyldodecyl xyloside surfactant (ODX) was seen to have a specific interaction with the ENMs surface, enhancing the UV filter dispersion in the oil. The UVR efficiency of each colloidal dispersion was dramatically affected by the ENMs aggregation state, ultimately proving the importance of understanding the factors controlling the stability of ENMs dispersion in sunscreen formulation. Such knowledge will eventually allow to optimize formulations safer by design, with minimum ENMs content and lower environmental footprint.

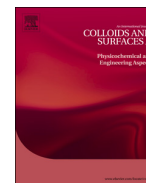
***Paper II :***

Optimizing the dispersion of nanoparticulate TiO<sub>2</sub>-based UV filters in a non-polar medium used in sunscreen formulations – The roles of surfactants and particle coatings (Published in Colloids and Surface A)



Contents lists available at ScienceDirect

Colloids and Surfaces A

journal homepage: [www.elsevier.com/locate/colsurfa](http://www.elsevier.com/locate/colsurfa)

## Optimizing the dispersion of nanoparticulate TiO<sub>2</sub>-based UV filters in a non-polar medium used in sunscreen formulations – The roles of surfactants and particle coatings

Riccardo Catalano<sup>a</sup>, Armand Masion<sup>a</sup>, Fabio Ziarelli<sup>b</sup>, Danielle Slomberg<sup>a</sup>, Jérôme Laisney<sup>c</sup>, Jason M. Unrine<sup>c</sup>, Andrea Campos<sup>d</sup>, Jérôme Labille<sup>a,\*</sup>

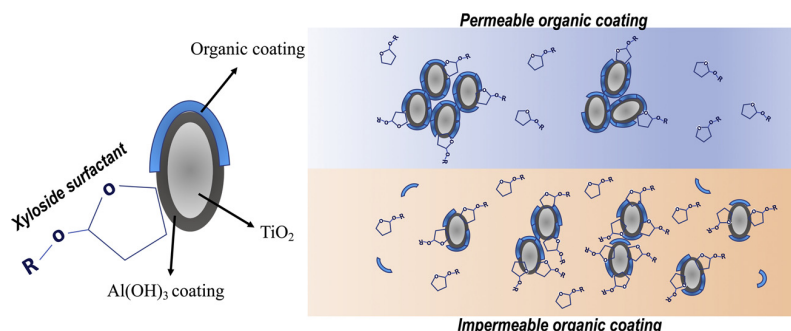
<sup>a</sup> Aix Marseille Univ, CNRS, IRD, INRA, Coll France, CEREGE, Aix-en-Provence, France

<sup>b</sup> Aix-Marseille Univ, CNRS, Centrale Marseille, FSCM, 13397 Marseille, France

<sup>c</sup> Univ Kentucky, Dept Plant & Soil Sci, 1100 S Limestone St, Lexington, KY 40546 USA

<sup>d</sup> Aix Marseille Université, CNRS, Centrale Marseille, FSCM, CP2M, 13397 Marseille, France

### GRAPHICAL ABSTRACT



### ARTICLE INFO

**Keywords:**  
Nanoparticle  
Oil dispersion  
Safe-by-design  
Colloidal suspension  
Octyldodecyl xyloside  
NMR

### ABSTRACT

Manufactured TiO<sub>2</sub> nanoparticles are widely used in cosmetics as UV blockers. The environmental risk associated with these Engineered Nanomaterials (ENMs) strongly depends on their concentration, aggregation state, and surface chemistry. Controlling these parameters in the sunscreen formulation is crucial in order to optimize the ENMs content and better understand their fate, transport, and toxicity at the product's end-of-life.

In the present work, the dispersion in sunscreen oil phase of four nanoparticulate UV filters having different coating characteristics was studied as a function of the oil composition. All the UV filters had a nano-TiO<sub>2</sub> core. Three of them were coated with a primary layer of aluminum (hydro)oxide and a secondary external layer of different polymers giving a hydrophobic character. The fourth UV-filter was coated with SiO<sub>2</sub> only, giving a hydrophilic character. The oil phase was composed of emollient oils and an emulsifying agent containing two surfactant molecules: Octyldodecyl xyloside (ODX) and PEG30 dipolyhydroxystearate (DHS). The ENMs were dispersed in the oil in the presence or absence of the emulsifying agent. Their aggregates size was evaluated, together with the speciation of the surface chemistry before and after the dispersion in oil.

We observed that the dispersion in oil of all the UV filters was enhanced by the emulsifying agent, as they were all more aggregated in the emollient oil free of emulsifier. The ODX surfactant played a major role in the ENM stabilization compared to the other oil phase components. The extent of interaction between nanoparticles

\* Corresponding author.

E-mail address: [labille@cerge.fr](mailto:labille@cerge.fr) (J. Labille).

<https://doi.org/10.1016/j.colsurfa.2020.124792>

Received 27 November 2019; Received in revised form 26 March 2020; Accepted 27 March 2020

Available online 20 April 2020

0927-7757/ © 2020 The Author(s). Published by Elsevier B.V. This is an open access article under the CC BY-NC-ND license

(<http://creativecommons.org/licenses/by-nc-nd/4.0/>).

surface and ODX surfactant appeared to be mediated by the chemistry and the stability of both internal and external coatings of the ENM. The highest affinity was evidenced with the  $\text{Al}(\text{OH})_3$  / dimethicone surface.

## 1. Introduction

Sunscreens provide effective protection against the damage caused by exposure to ultraviolet radiation (UVR) [1] which is dangerous for human skin, causing damages such as burns, aging, and even cancer [2]. These cosmetic products are highly consumed by the worldwide population as the sun care market constitutes 3% of the overall market of personal care products [3]. In order to absorb or reflect UVR, sunscreens contain UV filters, which can be organic (e.g., Avobenzone, Octocrylene) or mineral ( $\text{TiO}_2$ ,  $\text{ZnO}$ ) and are dispersed in the formulation [4].

Contamination of the aquatic environment by UV filters is an increasing public concern due to the secondary effects of pharmaceuticals and personal care products potentially released in receiving aqueous systems, which may reach detectable and even toxic concentration levels [5,6]. Among these systems, contamination of the seawater environment is a crucial issue that needs to be studied [7], especially considering the increasing coral bleaching concerns in the recent years [8,9]. Between 6000 and 14,000 tons of sunscreen lotion are estimated to be released into coral reef areas each year bringing at least 10 % of the global reefs at risk of exposure, and approximately 40 % of coral reefs located along coastal areas at risk of exposure [10,9].

Mineral UV-filters are the only type of UV filter accepted in sunscreens labelled as BIO (or Natural) because they are considered safer for the consumer and the environment [11]. Moreover, the market of mineral-based sunscreens has largely shifted to nano-sized particles, not only because of their higher efficiency but also because of their transparency on the consumer's skin [12]. Nevertheless, their environmental impact still needs further investigation [11].

Some biological models have shown harmful effects in the presence of pure  $\text{TiO}_2$  nanoparticles, at nearly field relevant concentrations [13,14]. The mineral filters used in sunscreens are usually coated with an internal mineral layer that prevents photocatalytic activity (e.g.  $\text{Al}_2\text{O}_3$ ;  $\text{SiO}_2$ ) and an external layer aimed at enhancing dispersion in the sunscreen formulation (e.g. PDMS; Stearic acid). Pure  $\text{TiO}_2$  nanoparticles could thus be considered as analogues of the final aging stage of the mineral UV filters normally used in sunscreens. Indeed, it was shown that the external PDMS coating of certain mineral UV filters undergoes oxidation and desorption soon after contact with water, causing favored dispersion and thus higher bio-accessibility of the newly hydrophilic nanoparticles [15–17].

In this context of anthropic impact on the aquatic environment, a challenge remains in minimizing the risk associated with nanoparticulate mineral UV filters, i.e., decreasing their environmental hazard or exposition. While this could be achieved by modifying the chemistry of the filters or reducing their content in the formulation, altering the product efficacy to screen the UVR is not a feasible option. A compromise can be found by optimizing the nanoparticle dispersion in the formulation, since smaller primary particle sizes and finer particle dispersions were shown to result in a higher solar protection factor [18]. Controlling these parameters during the formulation is a crucial step in optimizing the efficiency of the nanoparticulate UV filters and it is certainly also an objective of cosmetic companies for economic reasons, because it allows a lower nanoparticle content with no decrease in the SPF. Following this approach, a lower environmental footprint can be obtained, and a safer-by-design product is developed. While the dispersion of nanoparticles in aqueous media has been well described by the theory of Deryagin, Landau, Verwey and Overbeek (DLVO), it is still challenging to model and optimize the dispersion of high-concentration nanoparticle suspensions in organic media [19]. Although

the coating selection is certainly one of the main strategies to achieve this, it was also observed that  $\text{TiO}_2$  ENMs dispersion in organic media could be modulated by the adsorption of some specific molecules from the medium that would modify the ENMs interaction with the surrounding medium. This was evidenced for example with  $\text{TiO}_2$  ENMs dispersion in a silicone oil, enhanced in the presence of agents bearing a perfluoroalkyl group [20].

Indeed, the interactions with the different sunscreen formulation ingredients can also influence the UV filter dispersion, as well as the stability of the entire product through particle-droplet interactions at the emulsion microstructure scale [21]. The actual extent of ENMs aggregation or dispersion strongly depends on the affinity of the filter surface, i.e. the external coating, for the dispersing medium or the surrounding components inside. Depending on the formulation composition and desired properties, sunscreen can be an oil in water (O/W) or water in oil (W/O) emulsion [22]. For the most common lipophilic UV filters, an optimal dispersion is normally obtained in the oil phase where the emollient assumes high chemical affinity for the ENM. Surfactants (emulsifying agents) are also present, aimed at stabilizing the oil-water interface [23].

Although it is well known that certain surfactants are able to stabilize  $\text{TiO}_2$  particles in aqueous phase [24–26], a knowledge gap remains at the design stage of the sunscreen where the surface interactions between mineral particles and surfactants take place in an oil medium, and may determine the efficacy of the entire product. As it was already argued for other types of ENMs [27], such interactions may also modify the transport and reactivity of manufactured nanoparticles in the aqueous environment, and thus their exposure and hazard at the end of product life cycle.

Our work was aimed at studying the dispersion capacity of nano- $\text{TiO}_2$  based UV filters in a common bio-sourced sunscreen oil, in order to give insights on the role of the emulsifier at the initial stage of the sunscreen development and on how it may control the nanoparticle behavior. In order to avoid any interference coming from the interaction with the other sunscreen components, such as water, we decided to focus on the oil phase, as it represents the first dispersing medium in which nanoparticles are introduced during the formulation process. We studied four commercial UV filters characterized by different external coatings, and analyzed the surface interactions with the components of the dispersing medium, such as emollient and emulsifier. The dispersion state of the filters in the oil was evaluated using Dynamic Light Scattering (DLS). The chemical characterization of the nanoparticle surface, before and after interaction with the sunscreen oil phase, was performed through Solid State Nuclear Magnetic Resonance ( $^{13}\text{C}$  and  $^{29}\text{Si}$ ) and Transmission Electron Microscopy equipped with Energy Dispersive X-ray Spectroscopy (TEM EDS). A novel methodology to recover and dry the aged nanoparticles after dispersion in the oil phase is hereby proposed.

## 2. Material and methods

### 2.1. Commercial nano $\text{TiO}_2$ based UV filters

Four commercial  $\text{TiO}_2$ -based sunscreen UV filters were selected here, based on contrasted surface coatings. They were provided by the manufacturers as a dry powder. Scanning Electron Microscopy in high resolution (HR-SEM) was performed to characterize the primary particle sizes. 3–4 mg of each dry powder were dispersed on a carbon adhesive tab and analysed using Zeiss Gemini500-Field emission SEM (see *Supplementary information*). Images were recorded at low voltage

(1–5 kV) to be able to obtain surface sensitive image at nanoscale resolution. In order to evaluate the primary particle size of the different filters, the longer side length of 50 particles in the images was measured using ImageJ software. The primary particle sizes obtained for each commercial UV filter are reported in Table 1, together with the respective trade name, abbreviation and chemical compositions provided by the manufacturers. All have a heterogenous but comparable primary particle size, between 50 and 65 nm in average. They consist of a TiO<sub>2</sub> nanoparticulate core, coated with dimethicone (T-dim), simethicone (T-sim), stearic acid (T-ste) or silica (T-S) as the external layer. An internal mineral layer made of aluminum (hydr)oxide was also found on the hydrophobic candidates T-dim, T-sim and T-ste, sandwiched between the TiO<sub>2</sub> surface and the grafted polymer.

## 2.2. Oil dispersing medium preparation

The components constituting the typical sunscreen oil phase used in this work are reported in Table 2. They were provided by the respective suppliers. They consist of two emollient oils: *Cetiol LC*<sup>™</sup> (Coco-Caprylate/Caprate) and *Tegosoft P*<sup>™</sup> (Isopropyl palmitate) [28], and one emulsifying agent: *Easynov*<sup>™</sup> [29]. Isopropyl palmitate is broadly used in cosmetics as a dispersing agent for both organic and mineral UV filters [30]. The emulsifying agent contains two types of surfactant: one polymeric, PEG30 dipolyhydroxystearate (DHS), and one glycoside non-ionic surfactant octyldodecyl xyloside (ODX). It is typically used to stabilize W/O cosmetic emulsions.

Tegosoft, Cetiol and Easynov were mixed together in a 2:2:1 ratio. The oil mixture (Phase A) was gently homogenized by magnetic stirring for 10 min. The nanoparticulate UV filter was then added to the oil phase in order to reach a concentration of 2.5 % w/w and was dispersed by mechanical agitation at ambient temperature for 10 min at 1000 rpm (which turned out to be the optimal speed in order to break particle aggregates; see *Supplementary Information*) using a *Heidolph Hei-Torque* 400 stirrer equipped with a pitcher blade impeller. For comparison, the same procedure was repeated in an oil phase free of emulsifier, in which the two emollient oils were mixed together with a 1:1 ratio (Phase B).

## 2.3. Elemental carbon analysis

In order to evaluate the % of carbon present in the three hydrophobic UV filters, a few milligrams (between 7–16) of the three pristine powders were placed in tin nacelles and analyzed using a Thermo-Fisher Scientific *FlashSmart*<sup>™</sup> elemental analyzer. A soil reference and aspartic acid, both provided by Thermo-Fisher, were used as calibration standards. The % of organic coating for each ENM was then calculated knowing the % of carbon and the molecular weight of the respective organic coating.

## 2.4. UV filter size distribution and UV absorbance in oil phase dispersions

Dynamic Light Scattering (DLS) intensity distributions of each UV filter suspension in oil were recorded right after the agitation step, in order to minimize any potential reaggregation before size measurement. A *Malvern Zetasizer Nano* (Malvern Instrument) was used. A 2 mL volume of the dispersion was analysed in a standard plastic disposable

cuvette. The measurements were performed in triplicates at 25 °C with 11 runs per measurement and 0.01 cumulant fit error tolerance. The viscosity used in the Stokes – Einstein relation, to calculate the hydrodynamic size of the UV filters dispersed in oil were measured as follows. Phases A and B were analysed through rheology measurement using an *Advanced Rheometer 1000* (TA Instrument) equipped with a 60 mm steel cone with 2° angle tip. The measurements were run in continuous speed rate from 0 to 100 s<sup>-1</sup> in 3 min. The measured viscosities were 7.45 ± 0.42 mPa for Phase A and 8.71 ± 0.24 mPa for Phase B.

The UV absorbance of each oil dispersion was also evaluated using the following methodology: ≈ 60 mg of the oily dispersion were deposited on a UV transmitting PMMA plate (50 × 50 cm; 5 μm medium roughness) and spread by light finger pressure all around the surface until a homogenous distribution was achieved. Absorbance spectra were then recorded in the UV range (270–400 nm) using a *Jasco v650* spectrophotometer equipped with an *ISV-922 60 mm diameter* Integrating Sphere. Each sample was analysed 4 times, rotating the PMMA plate a quarter turn between each replicate.

Single absorbance values at the fixed wavelength of 270 nm are presented in the results for each oily dispersion. Even-though these values do not equal the exact Solar Protection Factor (SPF), they give a rapid indication of the UV-screening efficacy of the nanoparticle-in-oil dispersion, since the SPF is proportional to the absorbance in the UV ray range [31].

## 2.5. Nanoparticle recovery after aging in the oil phase

Within dispersion in the oil, any component from the dispersing medium having high affinity for the UV filter surface may likely adsorb to it. In order to investigate such change in the ENM surface chemistry, an extraction protocol, adapted from Roweczyk et al. [32], was developed to recover and dry the nanoparticulate UV filters after aging in oil. The ENMs in oil dispersion was centrifuged at 11,200 g for 30 min (Jouan BR4i, Thermo). The pellet was separated from the oil supernatant and re-dispersed in 10 mL cyclohexane (Sigma Aldrich) in order to wash the oil components not strongly attached to the ENM surface. The ENMs were then centrifuged again for 30 min at 11,200 g. The pellets were separated from the supernatant and dried for 48 h using a Thermo Fisher freeze dryer. This drying procedure was required to have a particle powder enough withered to be suitable for a solid-state (ss) NMR analysis. Washing the ENMs with cyclohexane was essential, as the freeze-drying procedure alone was not able to remove the excess of oil phase from the pellets.

## 2.6. Chemical characterization of the oil and UV filters

Nuclear Magnetic Resonance (NMR) was used to characterize both the oil phases (<sup>13</sup>C NMR) and the nanoparticle coating before and after aging (<sup>13</sup>C and <sup>29</sup>Si NMR). For all the characterizations, ~100 mg of nanoparticle powder was placed in the rotor and analysed using a Bruker Advance III WB 400 solid state NMR spectrometer. In order to verify the chemical composition of the oil phases, <sup>13</sup>C NMR spectra were recorded using low power decoupling sequence (lpdec) with d1 = 10 s, number of scans (NS) = 2k, 3 kHz spin rate. <sup>29</sup>Si CPMAS

**Table 1**

Product name and chemical composition provided by the manufacturer for each of the four mineral UV filters together with their respective primary particle size measured by HR-SEM.

| Product Name   | Abbreviation | Manufacturer | Chemical composition   | Primary particle size (nm) |
|----------------|--------------|--------------|--|----------------------------|
| T-Lite SF      | T-dim        | BASF         | TiO <sub>2</sub> (79–89%)/Al(OH) <sub>3</sub> /Dimethicone             | 58.3 ± 10.8                |
| Eusolex T-AVO  | T-sil        | Merck        | TiO <sub>2</sub> (79.6%)/SiO <sub>2</sub>                              | 51.0 ± 10.6                |
| Eusolex T-2000 | T-sim        | Merck        | TiO <sub>2</sub> (80.3%)/Al <sub>2</sub> O <sub>3</sub> /Simethicone   | 65.5 ± 12.8                |
| Eusolex T-S    | T-ste        | Merck        | TiO <sub>2</sub> (73–79%)/Al <sub>2</sub> O <sub>3</sub> /Stearic Acid | 64.4 ± 11.4                |

**Table 2**

Trade name and chemical composition provided by the manufacturer for each component of the oil phase.

| Product name | Manufacturer | Function          | Chemical composition  |
|--------------|--------------|-------------------|---|
| Tegosoft P   | Evonik       | Emollient oil     | Isopropyl Palmitate   |
| Cetiol LC    | BASF         | Emollient oil     | Coco-Caprylate/Caprates   |
| Easynov      | SEPPIC       | Emulsifying agent | Octyldodecanol; Octyldodecyl Xyloside; PEG-30 Dipolyhydroxystearate |

were recorded at 79.5 MHz, 10 kHz spin rate.  $^{13}\text{C}$  Cross-Polarization Magic Angle Spinning (CPMAS) spectra were recorded at 100.7 MHz, 10 kHz spin rate, 20k NS. Spectra simulations of oil phase components and particles organic coatings, together with peak integrations and gaussian fits of the experimental spectra, were performed using *Mest-ReNOVA* software (see *Supplementary Information*).

### 2.7. Elemental mapping and composition of the UV filters

The  $\text{TiO}_2$  nanoparticles were examined by transmission electron microscopy (TEM) and scanning transmission electron microscopy (STEM) using a Talos F200X analytical electron microscope (Thermo Scientific, Waltham, MA, USA), operated at 200 keV and equipped with a four-element silicon drift detector (SDD)-based EDS system for quantitative chemical composition analysis and elemental distribution

mapping. Sample preparation was performed by dipping lacey carbon grids (Ted Pella, Redding, CA, USA) in 100 mg/L suspensions of nanoparticles previously sonicated for 15 min at maximum amplitude using a Misonix S-4000 cup-horn sonicator (Newton, CT, US) to ensure the optimal dispersion of the nanoparticulate powders.

## 3. Results and discussion

### 3.1. Emulsifying agent stabilizing UV filters dispersion

The size distributions of the nanoparticulate UV filters dispersed in Phase A are reported in Fig. 1 (solid lines). In all cases, they are relatively large and above the primary particle size, indicating polydisperse aggregation of the nanoparticles. The ENMs coated with stearic acid (a) or silica (b) are more aggregated than those coated with dimethicone

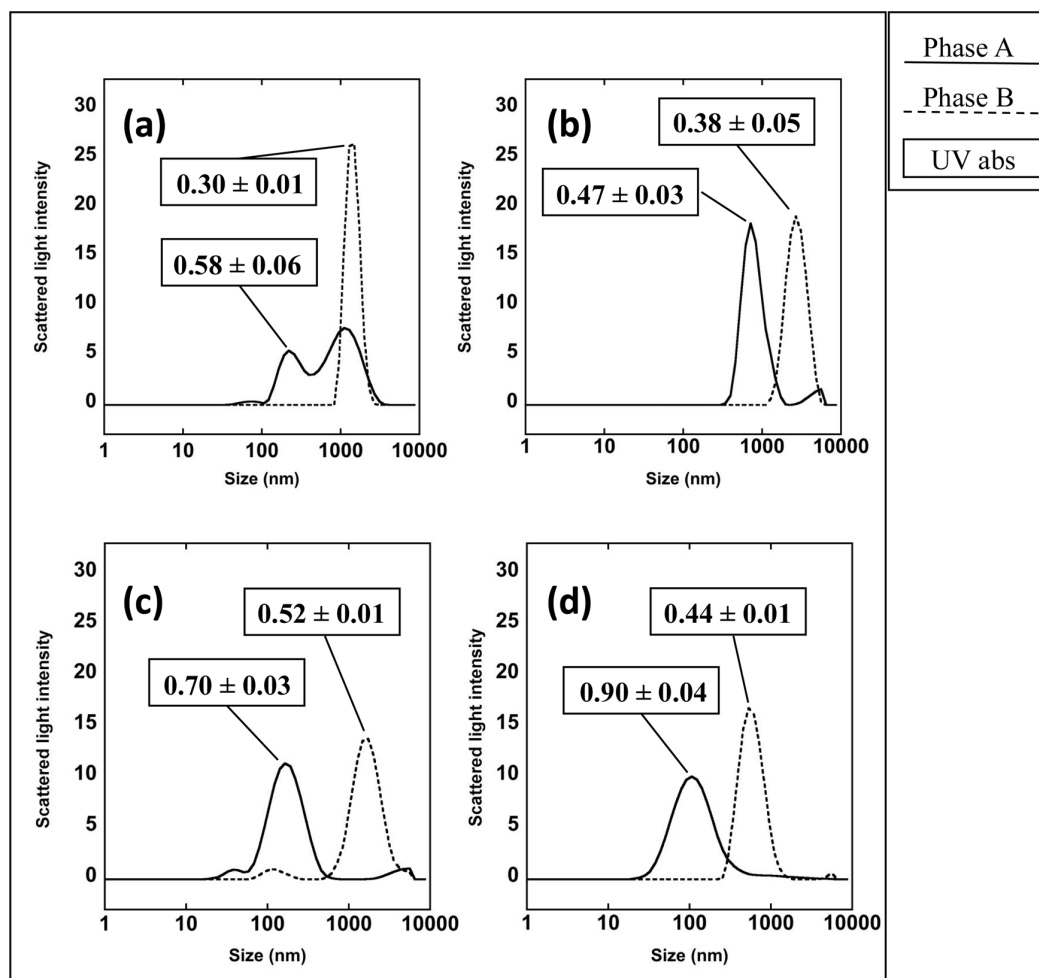


**Fig. 1.** Average hydrodynamic size distributions of the UV filters dispersed in Phase A (solid line) and Phase B (dashed line) for: (a) T-ste; (b) T-sil; (c) T-sim; (d) T-dim. Measurements were realised by DLS and are shown in intensity weight. The respective UV absorbances at 270 nm of the colloidal suspensions are reported inside the boxes for each distribution.



(c) or simethicone (d). The T-ste distribution appears bimodal at 220 and 1100 nm and the T-sil gives one peak at 800 nm, while the T-sim and T-dim distributions are centered on lower sizes around 100–200 nm. Significant aggregation was expected with the silica-coated nanoparticle, due to its hydrophilic surface, since in the oil dispersing medium there is no amphoteric surface charge driving any electrostatic inter-particle repulsion. However, the large aggregation of the T-ste UV filter is more surprising since the stearic acid coating is hydrophobic and was expected to have high affinity for the emollient components present in the oil (Isopropyl Palmitate; Coco-Caprylate).

The size distributions in the oil free of emulsifier (Phase B) (Fig. 1, dashed lines) clearly showed a general increase of the aggregate sizes for all the 4 UV filters compared to phase A. The narrower distributions in phase B suggest a more homogeneous aggregated state where the finer dispersed units around 100 nm have been totally incorporated into the larger ones of up to 1–2  $\mu\text{m}$  in size. However, the aggregate sizes approached the nano-DLS detection limit, and the distribution widths are less trustworthy and thus impede an accurate signal interpretation.

Based on the Intensity mean values in the four DLS distributions, the shift of the aggregate size between Phase A and Phase B seems to depend on the UV filter type. The size shift is more pronounced in the case of T-sim (from 370 nm to 1719 nm) and T-dim (from 170 nm to 647 nm) while it is less evident for T-sil (from 1000 nm to 2700 nm) and T-ste (from 857 to 1437 nm). It is worthwhile noting that the presence of the emulsifier leads to a finer dispersion of the ENMs coated with simethicone or dimethicone (T-sim and T-dim) than for T-ste or T-sil, while without the emulsifier agent the four ENMs show similar aggregation states. The large aggregate size in phase B for all the four ENMs, suggests a relatively weak affinity of their respective surface coatings for the emollient oil used here. Yet, isopropyl palmitate is particularly recommended by the suppliers as a good dispersant oil phase for hydrophobically coated pigments in cosmetics preparations [28]. It should be noted that the agitation speed used to prepare the oil dispersion (1000 rpm) was high enough to break down the aggregates and bring most of the nanoparticles in contact with the solvent. As clearly shown by the UV absorbance (at 270 nm) values reported in Fig. 1, a loss of UV absorption is associated to the increasing ENMs aggregation state in all the Phase B formulations. The most important loss in UV absorbance with regard to values in Phase A, is measured for T-dim ENMs (- 45 % UV abs.), while for the other three filters the average loss is around 18 %. T-dim showed the best UV protection performances in Phase A formulation, likely because of their finest dispersion in this medium. These greater performances in Phase A could eventually explain the singular loss of screening efficacy of T-dim in Phase B medium compared with the other three UV filters. Nonetheless, the general trend of ENMs aggregation and UV absorbance of the formulations are in line with the previous findings of Tyner et al. [18]. Moreover, the large variability range in UV absorbance up to 45 %, confirms the need for optimal component coupling in the sunscreen formulation in the aim of minimizing the ENM aggregate size for maximizing the solar protection factor.

### 3.2. Characterization of the oil phases components

The oil phases A and B and the emulsifier used in this work were analysed using  $^{13}\text{C}$  NMR spectroscopy, as shown in Fig. 2. The peak assignment was performed by comparing the experimental spectra with the predicted spectra of each component generated with *Mest-Re NOVA* software (see Supplementary Information).

The fingerprints of the two surfactants constituting the Easynov emulsifier are clearly seen in Fig. 2 (top). The signal at 100 ppm is attributed to the resonance of the anomeric carbon of the sugar moiety present in the ODX molecule. The small peak at 105 ppm is probably due to the resonance of the same anomeric carbon in a different conformation. The signal at 173 ppm is attributed to the resonance of the carboxylic carbon of the polymeric surfactant DHS. The other signals

between 75 and 60 ppm are due to the resonance of hydroxyl or ether groups present in both surfactant structures. The signal at 65 ppm is likely attributed to the hydroxyl group of the octyldodecanol, which is the solvent of the emulsifier agent. The ratio between the peak area of the anomeric carbon and the sum of the area of all the peaks of the emulsifying agent was used to determine the ratio of the ODX in the mixture. The same procedure was used to determine the ratio of the DPH, using the signal of its carboxylic carbon. This analysis revealed that the two surfactants and the octyldodecanol solvent, in the emulsifying agent, are in a ratio 1:1:8.

The  $^{13}\text{C}$  NMR spectrum of the Phase B, containing only the two emollient oils, is reported in Fig. 2 (middle). The resonance of the carbonyl carbon is at 172.2 ppm for the caprate (Cetiol LC) and at 171.8 ppm for the isopropyl palmitate (Tegosoft). The peak at 67 ppm could be assigned to both the secondary C–OH group of the caprate and to the carbon next to the oxygen of the ester group isopropyl palmitate. The two signals at 64 ppm and 60 ppm are respectively assigned to the carbon next to the oxygen of the ester group and to the terminal C–OH group of the caprate oil. The spectrum of the Phase A, which is the mixture between the two emollient oils and the emulsifier, is reported in Fig. 2 (bottom). The region between 75 and 50 ppm is dominated by the two peaks at 67 and 64 ppm, which are likely associated to the isopropyl palmitate and caprate emollients. The other prominent signal at 70 ppm is assigned to octyldodecanol hydroxyl group (see Supplementary Information). The signals associated to the emulsifier are less intense and visible than in the top spectrum (Fig. 2 top), which is understandable as the Easynov constitutes 20 % w/w of the entire Phase A. Considering that each surfactant constitutes approximately 10 % of emulsifier, the concentration of each surfactant in the Phase A should be around 2% w/w. That is probably the reason why the ODX fingerprint at 100 ppm is barely visible in the Phase A spectrum.

### 3.3. Characterization of the pristine nanoparticulate UV filters

$^{13}\text{C}$  NMR spectra of the pristine UV filters are shown in Fig. 3 a–d (bottom). For T-ste (Fig. 3 a), the presence of the stearic acid coating was confirmed by comparing the experimental spectra with the simulated Stearate spectra. The signal at 182 ppm is attributed to the carboxylic carbon resonance of the stearic acid molecule, together with the 6 peaks in the alkyl region associated to  $\text{CH}_2$  and  $\text{CH}_3$  groups of the stearate chain. The PDMS coating of T-sim and T-dim (Fig. 3 c,d) is

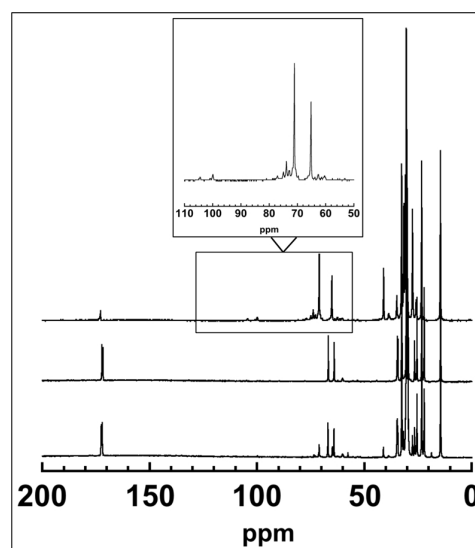
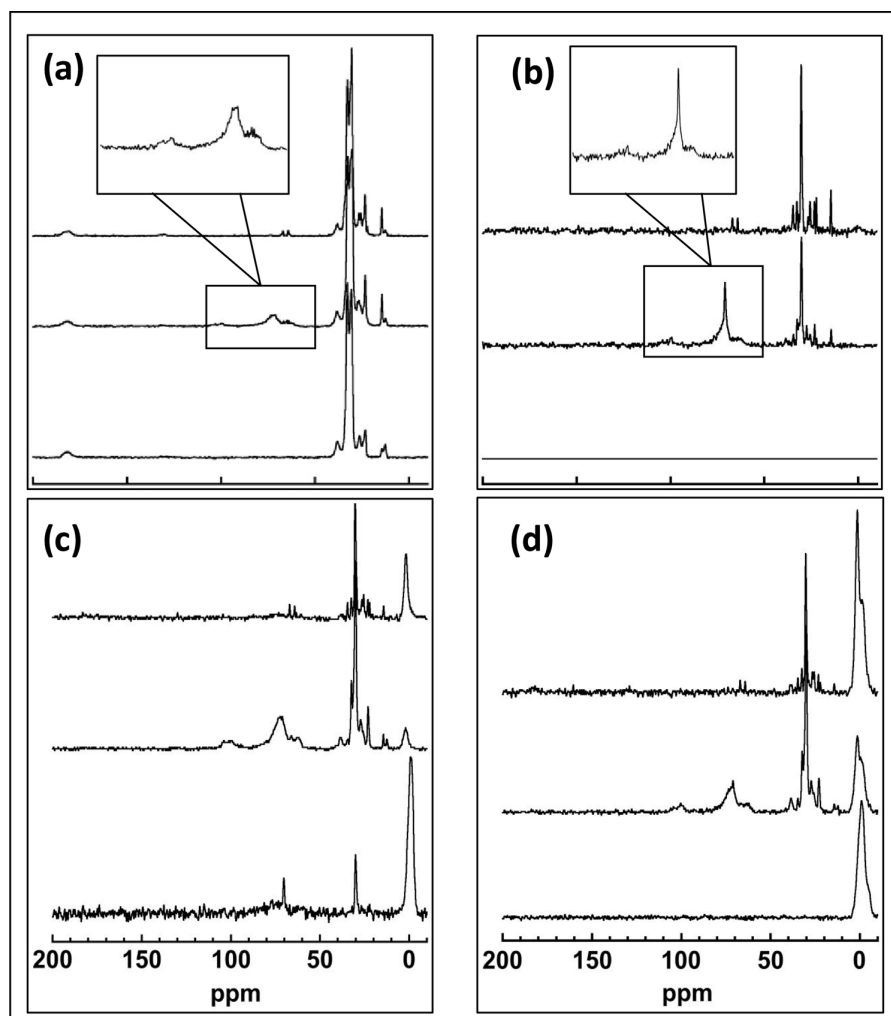


Fig. 2.  $^{13}\text{C}$  NMR spectra of the Phase A oil (bottom); the Phase B oil free of emulsifier (middle); and the Easynov emulsifier (top).





**Fig. 3.**  $^{13}\text{C}$  NMR spectra for T-ste (a); T-sil (b); T-sim (c); and T-dim (d) UV filters; recorded on pristine ENMs (bottom), after aging treatment in Phase A (middle), or after aging treatment in Phase B (top).

confirmed by a clear signal at -0.9 ppm associated to the methyl groups bound to the  $\text{SiO}_2$  units. In the T-sim spectra, the presence of two small signals at 70 and 30 ppm, could be due to propanol pollution. As expected, no carbon resonance signal was detected in the original T-sil spectra (Fig. 3 b), as they do not contain any organic coating.

$^{29}\text{Si}$  NMR spectroscopy was performed on the UV filters containing silicon either in the form of silica or of PDMS (T-sil; T-dim; T-sim) and provided further characterization (Fig. 4). For T-dim filters (Fig. 4b), the resonance at 0 ppm corresponds to  $\text{Si}(\text{CH}_3)_3$  terminal group and the resonance at -22 ppm is associated with  $\text{SiO}(\text{CH}_3)_2$  main chain units of the PDMS polymer, while at -44 ppm the resonance signal is attributed to Si-O-Al linkages with the underlying  $\text{Al}(\text{OH})_3$  coating. These results are in accordance with the findings of Auffan et al. on the same  $\text{TiO}_2$  based UV filters [16]. For T-sil (Fig. 4c), the presence of the silica coating is confirmed by the resonance at -100 ppm associated to  $\text{SiO}_2$  units. Surprisingly, the signal at -100 ppm of  $\text{SiO}_2$ , which is a claimed component of commercial simethicone (PDMS +  $\text{SiO}_2$ ), is missing in the spectrum of T-sim (Fig. 4a). Such absence of any  $\text{SiO}_2$  signal was also confirmed using ATR-FTIR which provides a lower detection limit (data not shown). Furthermore, the signal at -44 ppm attributed to Si-O-Al linkages is missing, suggesting that the simethicone coating is not covalently bound to the ENM surface, but more likely weakly adsorbed.

#### 3.4. The roles of emulsifier components and particle coatings

The  $^{13}\text{C}$  NMR spectra for the four UV filters after aging in Phase A are reported in Fig. 3 (a,b,c,d) (middle). For each of the four ENMs, some signals related to organic molecules adsorbed to the ENM surface are clearly visible. These compounds were strongly attached to the nanoparticle surface considering that they remained bound through the treatment with cyclohexane followed by 48 h freeze drying. However, not all of the components of the phase A were visible in the spectra of the aged nanoparticles. Mainly the ODX molecule fingerprints was clearly distinguished, with the signal at 100 ppm of the anomeric carbon of the sugar moiety.

On the other hand, the missing signals in the carbonyl region of the NMR spectra, could exclude the presence of the other surfactant DPH as well as the two emollient oils. As all the oil phase components contain similar alkyl chains, with similar chain length and chemical structures, it is probable that the higher affinity for the nanoparticle surface of the ODX surfactant could come from its particular xyloside sugar moiety. In the aged T-sil spectrum, Fig. 3 (b – middle), the two narrow peaks at 70 and 30 ppm could also be associated to propanol contamination as in the pristine T-sim spectrum, Fig. 3 (c – bottom). This presumable contamination is covering part of the signals in the hydroxyl/ether region between 60 and 80 ppm and prohibited a quantitative analysis of the

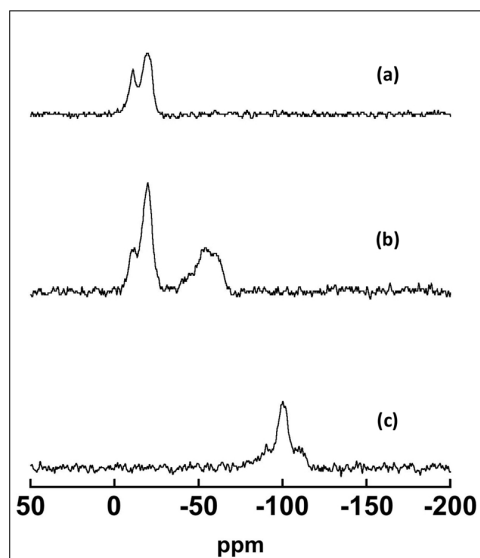


Fig. 4.  $^{29}\text{Si}$  CPMAS NMR spectra of the pristine T-sim (a); T-dim (b); T-sil (c) UV filters.

spectra. This was however performed on the three other aged UV filters.

The peak integration in T-sim and T-dim aged spectra, Fig. 3 (c; d) (middle), enabled further understanding of the underlying mechanisms. The number of carbons associated to each peak was estimated based on the hypothesis that the signal at 100 ppm is only due to the resonance of the single anomeric carbon of the ODX sugar moiety attached to the ENM surface. This resulted in a number of carbons not related to the coating estimated at 20 in T-sim spectrum and 22 in T-dim spectrum. Even if we assume that all these carbons are only related to the surfactant molecule, this quantity is below the 25 carbons of the original ODX surfactant. We thus hypothesize that the surfactant molecule was partially degraded into smaller units.

It was not possible to clearly determine the mechanism that caused such degradation during the aging time or the extraction procedure. However, it is very unlikely that the addition of hexane during the washing procedure could have caused such type of reaction, as it is considered an inert solvent. It is instead more likely that the reaction could take place at the surface of the ENMs during the initial dispersion in oil. Further speculation about this hypothesis are handled afterwards.

In the spectrum of the T-ste UV filters aged in phase A, the stearic acid coating signal in the alkyl region partially covers the pattern of the organic molecules from phase A attached to the ENMs surface. It was thus impossible to determine the number of carbons associated to these compounds.

The  $^{13}\text{C}$  NMR spectra for the ENMs aged in Phase B are shown in Figs. 3a–d (top). The two small peaks between 70–60 ppm are most likely due to the resonance of the alkyl carbons bound to the oxygen of the ester group of the two emollient oils: coco-caprylate and isopropyl palmitate. Even though, the signal associated to the resonance of the ester carbons itself was never present in all the four spectra. The reason could be that the quantity of emollients oils adsorbed on the ENMs surface was probably so low that ester signal could not be seen. Also, the similar shape and the intensity of these two peaks in all the 4 spectra suggest that the interaction does not change as function of the particle coating. This is in accordance with the size distribution of the ENMs in Phase B (Fig. 1) which showed similar aggregation state for the 4 types of nanoparticles and a larger size than in phase A. Nevertheless, the persistence of the emollient oil signals even after the recovery procedure, indicates that the interaction with the ENM surface is strong

enough to resist the recovery and drying procedure. This was not observed through aging in phase A, where only surfactant was added compared to phase B, but which resulted in a net ODX signal in the aged nanoparticles Fig. 3 (middle). This further supports the hypothesis that the prevalence of ODX signals in the spectra of the ENMs aged in Phase A, is due to a higher affinity of this surfactant for the ENM surface at the expense of the other component of the Phase A and not to a procedural artefact.

The resonance of the anomeric carbon of the octylidodecyl xyloside (100 ppm) was more pronounced in the T-sim and T-dim spectra, while it was less detected in the T-ste spectrum and barely visible in T-sil spectrum. In the spectra of the three hydrophobic UV filters aged in phase A, (Fig. 3 a, c, d middle), which did not contain any impurity signal, the area of each peak was determined using a gaussian fit. In each spectrum, the peak area of the anomer carbon was then divided by the total peak area in order to get the ratio of anomer signal and to compare its respective weight between the three candidates. The % of anomer signal ratio was 5.1 for T-sim, 3.8 for T-dim, and 3.2 for T-ste. The coating signal ratio, on the other hand, showed the opposite trend. The dimethicone signal ratio was 6.2 % in T-sim spectrum and 34 % in T-dim spectrum while the stearic acid ratio should be around 58 % in T-ste spectra, based on the signal ratio of the carboxylic carbon at 182 ppm. Thus, as the coating ratio decreases, the anomer ratio increases. This suggests that the interaction of the sugar moiety of the ODX may occur in the internal surface layer of the ENMs rather than over the organic outermost coating.

It is thus our hypothesis that the sugar moiety of the ODX interacts with the  $\text{Al}(\text{OH})_3/\text{Al}_2\text{O}_3$  coating of the nanoparticles. Vilg -Ritter et al. already observed that aluminum polychlorosulfate PACS could selectively remove polysaccharide molecules from river waters [33]. Yang et al. and Chang et al. showed that  $\text{Al}^{3+}$  ions could strongly bind to the polysaccharide motifs of cell wall in pectin from Tobacco and Rice plants [34,35]. Efficient adsorption behavior of different monosaccharides onto Alumina surface were seen by Singh & Mohan [36,37] in aqueous solution. They reasoned that different types of interactions between the monosaccharides and the alumina surface could occur during the adsorption process, such as: electrostatic attraction (or repulsion) and hydrogen bonding. They also hypothesized that sucrose molecules can coordinate to Al atoms of “water coordinated”  $\text{AlOH}_2^+$  groups by substitution of a water molecule, forming an organometallic complex.

How  $\text{Al}(\text{OH})_3/\text{Al}_2\text{O}_3$  surfaces dispersed in oil here differ from the  $\text{Al}^{3+}$  ions and  $\text{Al}(\text{OH})_3$  studied elsewhere in aqueous solution is not clear, as a knowledge gap remains on this latter systems. It is fair to say that electrostatic interactions (dipolar or ionic) would be more difficult, as an oil medium is less capable to allow acid-base equilibrium and ion stabilization. Hydrophobic bonding could also occur, but does not explain why the other components of the oil phase, which do contain hydrophobic tails, did not interact efficiently with the alumina surface. We thus hypothesize that complexation interaction between the aluminum oxide surface and the sugar moiety of ODX will be more probable in this oily system. Such type of bonding would also be more in accordance with the hypothesis of a partial breakdown of the surfactant molecule previously mentioned.

Moreover, considering the persistence of the signal at 100 ppm in Fig. 3 (middle), we assume that the rupture in the surfactant molecule should occur in the octylidodecyl chain. This would keep the O–C–O group intact, even if it is not certain whether the xyloside moiety was preserved or whether the pentose ring was successively opened generating an acetale group, which has similar chemical shift of anomer carbons.

Although proposing a mechanism for the surfactant break-down reaction was not the goal of this study, some hypothetical reactions are proposed here. The rupture of the molecule could be caused by a heterogeneous reaction at the  $\text{Al}(\text{OH})_3/\text{Al}_2\text{O}_3$  surface. Organic reactions at the alumina surface are well established in literature and are very

useful in lab-scale synthesis because of their high selectivity and mild reaction conditions (ex: ambient temperature) [38]. While no specific studies on mono/di-saccharides degradation on aluminum oxides surfaces was already described, the formation of monosaccharides due to acetaldehyde polymerization (formose reaction) catalysed by  $\text{Al}_2\text{O}_3$  was observed by Gabel & Ponnampertuma in aqueous medium [39]. It is still unclear if alumina can also catalyse breakdown reactions of sugars, even if Reid & Orgel observed sugar degradation right after the formose reaction in similar conditions but using a carbonate-apatite catalyst [40].

Concerning the stabilization mechanism of the colloids in Phase A, we suppose that the ODX surfactant can act as charge control agent (CCA) on the ENM surface. CCAs increase the ionic conductivity of the system by creating free charges in solution or at particle surfaces. Surfactants are indeed capable of acting as charge control agents, affecting the interparticle interactions and the stability of the suspension in a non-polar system [41–43]. Yet, the mechanism leading to the particle charge stabilization is ambiguous [44]. In our system, particle aggregation being prevented by electrostatic repulsion should be the more realistic scenario considering the surfactant molecule breakdown at the  $\text{Al}_2\text{O}_3$  surface, which would eventually reduce the alkyl tail length and minimize its hydrophobic stabilization within the oily medium or any steric hindrance between particles.

Due to the presence of propanol impurities in the aged T-sil  $^{13}\text{C}$  NMR spectrum, it was not possible to perform a quantitative analysis that would define the potential break-down of the surfactant molecule on the silica surface. Nevertheless, such reaction was not expected here, since heterogeneous catalysis with pure  $\text{SiO}_2$  has not been evidenced in the literature. Although the anomer carbon peaks in the spectrum of T-sil aged in phase A (100 ppm) appear feeble and less resolved, it is fair to say that the ODX molecule interacts with the silica surface, since a finer aggregation state of T-sil ENMs was measured in Phase A compared to Phase B (Fig. 1 b). Kwon et al. [45] studied the adsorption behavior of polysaccharide polymers (dextran) on silica and alumina surfaces. They observed that the mass of retained dextran was higher with alumina (83 ng/cm<sup>2</sup>) than with silica (9 ng/cm<sup>2</sup>), suggesting a higher affinity for the alumina. This agrees with our results showing ODX surfactant less detected on the T-sil surface than on T-dim or T-sim after aging in phase A.

The three UV filters T-dim, T-sim and T-ste all have an aluminum oxide coating which could likely favor such interaction with the sugar moiety of the ODX surfactant. Nevertheless, they displayed contrasted fates. This could be related to the stability of the respective polymer coatings. As previously mentioned, aged T-sil filters showed the lower coating signal ratio (6.2 %) compared to aged T-dim (34 %) and T-ste (58 %). This can be associated to a loss of the simethicone coating from the ENM surface during the dispersion stage. Indeed, the simethicone coating was not strongly bound to the particle surface, as seen from  $^{29}\text{Si}$  NMR results (Fig. 4a) where no covalent linkage between the simethicone coating and the underlying alumina coating was detected, leading most likely to a lower stability of this external coating that could be partially removed during the dispersion procedure. Of note, even if a potential involvement of the cyclohexane washing procedure in the coating removal could not be excluded here (further investigation are needed to clarify this aspect), such effect would take place after the ENM aging in oil, and the preferential surface interaction with the ODX observed here would not be affected. The same process may take place in a lower extent with the T-dim ENMs, for which part of the dimethicone coating was covalently bound to the  $\text{Al}(\text{OH})_3$  layer (Fig. 4b) constituting a more stable external layer. The stearic acid coating of T-ste probably constituted a denser and more stable surface layer, corroborated by its higher organic coating/ $\text{TiO}_2$  ratio (Table 3). This may prevent the surfactant molecules from diffusing and reaching the underlying  $\text{Al}(\text{OH})_3$  surface. Higher steric hindrance may likely occur in the case of T-ste ENMs, because of the longer and bulkier  $\text{C}_{18}$  chains of the stearic acid coating in comparison with dimethicone single methyl

groups, although we do not have any information about the orientation of the different external coatings on the ENMs surface. In turn, the T-ste ENMs dispersion was less affected by the presence of the emulsifier agent (Fig. 1) and the pattern of this latter was less detected in the  $^{13}\text{C}$  NMR spectra after aging in Phase A.

HR-TEM images of pristine and aged ENMs are presented in Fig. 5 (a;b;c;d). No significant differences in the size and shape are observed between the samples. T-sim ENMs aged in oil phase (Fig. 5 d), however, show a peculiar layer surrounding the particle surface that is not detected in the T-dim sample aged in Phase A. We do not have enough data to tell the nature and the origin of this layer even-though its thickness, and the fact that it is present just in the aged samples suggests that it could be an oil phase residue remaining attached to the particle surface. EDX characterization map of titanium, oxygen and aluminum on T-dim and T-sim ENMs before and after aging are presented in Fig. 5 (a1; b1; c1; d1). The mass ratio of aluminum in the sample areas analysed is reported in the red framed boxes. For both T-dim and T-sim ENMs, it remained unvaried before and after aging in Phase A (Fig. 5a1-b1 and Fig. 5c1-d1), suggesting that the aluminum oxide was not degraded during the whole aging and recovery processes. These results corroborate our previous hypothesis on the preferential interaction of the sugar moiety of the ODX surfactant with the aluminum oxide coating of the ENMs, which eventually constitutes a stable surface of interaction.

A sketched dispersion mechanism in Phase A medium is proposed in Fig. 6 for the four  $\text{TiO}_2$  UV filters studied, based on these assumptions. Simethicone and Dimethicone coated ENMs (Fig. 6 (red)) showed the finer dispersion capacity. During the dispersion in oil, they could lose part of their coating, leaving a higher aluminum oxide surface available to interact with the ODX sugar moieties, which leads to a higher ENM dispersion stability. On another hand, the stearic acid coating on the T-ste ENMs (Fig. 5 (blue)) is more stable and remains mostly intact at the ENMs surface during the dispersion in oil. This leads to a lower extent of ODX surfactants reaching the alumina surface, and to a weaker particle dispersion stability in Phase A, i.e. larger aggregation. In T-sil ENMs (Fig. 6 (green)) there is no aluminum oxide but a  $\text{SiO}_2$  coating. In absence of a secondary organic coating in the pristine material, this surface is fully accessible to the ODX molecules, nevertheless a weaker affinity takes place with silica compared to the aluminum oxide surface, resulting in a limited amount of adsorbed ODX and in a low dispersion stability, i.e. large aggregation.

#### 4. Conclusions

The emulsifying agent Easynov™ favored the dispersion of four different commercial nanoparticulate UV filters in a realistic sunscreen oil phase. The extent of dispersion was shown to be influenced by the surface coating properties of the nanoparticles. Specific interaction between the octyldodecyl xyloside molecule and the four UV filters among the other oil phase components were observed, suggesting a key role of this surfactant in the stabilization of the colloidal system. This stabilization happened to be more efficient with mineral UV filters containing simethicone/dimethicone external coatings. After aging in the oil of the hydrophobic coated nanoparticles, an inverse relation was observed between the amount of external coating remaining at the ENMs surface and that of xyloside adsorbed. Thus, a specific interaction

**Table 3**

% of carbon and % of organic coating in the three UV filters T-dim, Tsim and T-ste.

| Product name | % of carbon | % of organic coating |
|--------------|-------------|----------------------|
| T-dim        | 1.11        | 3.42                 |
| T-sim        | 1.08        | 6.35                 |
| T-ste        | 7.38        | 9.21                 |

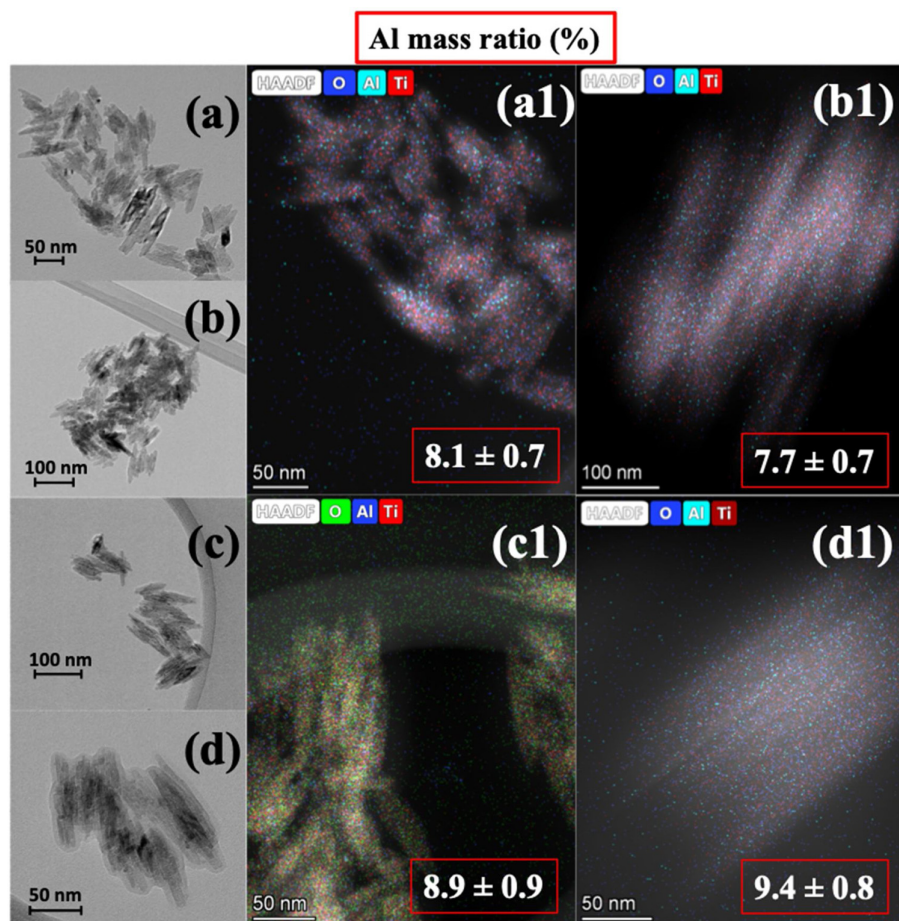


**Fig. 5.** HR TEM images of T-dim and T-sim pristine powders before (a; b) and after aging in Phase A (c; d). The respective EDX maps of oxygen; aluminum and titanium elements are reported in the images with a “1” label. The mass ratio (%) of aluminum in each area analysed is reported in the red framed boxes. (For interpretation of the references to colour in this figure legend, the reader is referred to the web version of this article).

with the internal  $\text{Al}_2\text{O}_3/\text{Al}(\text{OH})_3$  coating was proposed.

In this work, surfactants normally used to stabilize W/O emulsions were highlighted to be also fundamental in stabilizing the nanoparticulate UV filters dispersions. A compromise needs to be considered between the stability of the mineral UV filter's external coating and its capability to let the surfactant molecules diffuse into the inner spheres of the nanoparticle. In this light, T-dim ENMs showed the best

performance, given that the external PDMS coating was stable and not significantly degraded during the dispersion procedure but permeable enough to allow the diffusion of the ODX surfactant through the surface, leading to a finer ENMs dispersion and to an enhancement of the UV absorbance almost by a factor 2. This work brings light on the necessary step to optimize the use of nanomaterials in sunscreen product. Decreasing the amount of nanoparticulate UV filters in a sunscreen

### Coating

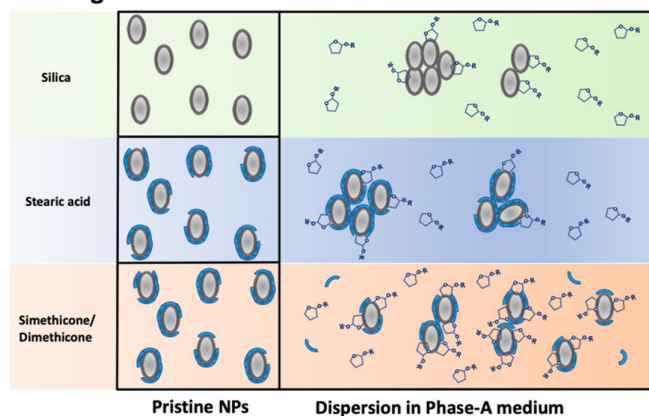


**Fig. 6.** Schematic representation of the different dispersion behaviors for the four tested UV filters: T-sim and T-dim (red); T-ste (blue); T-sil (green). The external coating is represented with blue blocs while the alumina or silica coating are the dark grey ovals. Differences on the quantity of blue pales between PDMS and stearic acid coated pristine ENMs, are used to emphasize the different capability of the two types of coating in shielding the inner spheres on the nanoparticle. (For interpretation of the references to colour in this figure legend, the reader is referred to the web version of this article).



formulation and better predicting their environmental fate and toxicity are key levers in the approach of minimizing the associated risk.

#### CRedit authorship contribution statement

**Riccardo Catalano:** Conceptualization, Data curation, Formal analysis, Investigation, Writing - original draft, Writing - review & editing. **Armand Masion:** Conceptualization, Data curation, Validation, Writing - original draft, Writing - review & editing. **Fabio Ziarelli:** Data curation, Formal analysis, Resources, Software. **Danielle Slomberg:** Conceptualization, Writing - original draft. **Jérôme Laisney:** Formal analysis. **Jason M. Unrine:** Resources, Software. **Andrea Campos:** Formal analysis, Resources, Software. **Jérôme Labille:** Conceptualization, Funding acquisition, Project administration, Resources, Supervision, Validation, Writing - original draft, Writing - review & editing.

#### Declaration of Competing Interest

The authors declare that they have no known competing financial interests or personal relationships that could have appeared to influence the work reported in this paper.

#### Acknowledgments

This work has received funding from the European Union's Horizon 2020 research and innovation programme under the Marie Skłodowska-Curie grant agreement No713750. It has also received funding from Excellence Initiative of Aix-Marseille University - A\*MIDEX, a French "Investissements d'Avenir" program, through its associated Labex SERENADE project. This work is also a contribution to the OSU-Institut Pythéas and IPR Innove. The authors also acknowledge the CNRS for the funding of the PICS n°08322 SODA Light. The authors also want to thank: Nithavong Cam, Caroline Orneto and Helioscience in the person of Jean-Claude Hubaud for their precious contribution to this work.

#### Appendix A. Supplementary data

Supplementary material related to this article can be found, in the online version, at doi:<https://doi.org/10.1016/j.colsurfa.2020.124792>.

#### References

- [1] B.L. Diffey, Sunscreens and melanoma: the future looks bright, *Br. J. Dermatol.* 153 (2) (2005) 378–381, <https://doi.org/10.1111/j.1365-2133.2005.06729.x>.
- [2] A. Krickler, B.K. Armstrong, D.R. English, Sun exposure and non-melanocytic skin cancer, *Cancer Causes Control* 5 (4) (1994) 367–392, <https://doi.org/10.1007/BF01804988>.
- [3] U. Osterwalder, M. Sohn, B. Herzog, Global state of sunscreens: global state of sunscreens, *Photodermatol. Photoimmunol. Photomed.* 30 (2–3) (2014) 62–80, <https://doi.org/10.1111/phpp.12112>.
- [4] T.X. Hoang, I. Popa, Innovation in Inorganic UV Filters in Sunscreen, (2014).
- [5] P. Gago-Ferrero, M.B. Alonso, C.P. Bertozzi, J. Marigo, L. Barbosa, M. Cremer, E.R. Secchi, A. Azevedo, J. Lailson-Brito Jr., J.P.M. Torres, O. Malm, E. Eljarrat, M.S. Díaz-Cruz, D. Barceló, First Determination of UV Filters in Marine Mammals. Octocrylene Levels in Franciscana Dolphins, *Environ. Sci. Technol.* 47 (11) (2013) 5619–5625, <https://doi.org/10.1021/es400675y>.
- [6] H. Sharifan, D. Klein, A.N. Morse, UV Filters Interaction in the Chlorinated Swimming Pool, a New Challenge for Urbanization, a Need for Community Scale Investigations, *Environ. Res.* 148 (2016) 273–276, <https://doi.org/10.1016/j.envres.2016.04.002>.
- [7] J. Labille, D. Slomberg, R. Catalano, S. Robert, M.-L. Apers-Tremelo, J.-L. Boudenne, T. Manasfi, O. Radakovitch, Assessing UV filter inputs into beach waters during recreational activity: a field study of three french mediterranean beaches from consumer survey to water analysis, *Sci. Total Environ.* 706 (2020) 136010, <https://doi.org/10.1016/j.scitotenv.2019.136010>.
- [8] S.F. Heron, J.A. Maynard, R. van Hooidonk, C.M. Eakin, Warming trends and bleaching stress of the world's coral reefs 1985–2012, *Sci. Rep.* 6 (1) (2016) 38402, <https://doi.org/10.1038/srep38402>.
- [9] R. Danovaro, L. Bongiorno, C. Corinaldesi, D. Giovannelli, E. Damiani, P. Astolfi, L. Greci, A. Pusceddu, Sunscreens cause coral bleaching by promoting viral infections, *Environ. Health Perspect.* 116 (4) (2008) 441–447, <https://doi.org/10.1289/ehp.10966>.
- [10] C. Wilkinson, Status of Coral Reefs of the World, Global Coral Reef Monitoring Network and Reef and Rainforest Research Centre, Townsville, 2008.
- [11] D.M.E. Slijckerman, M. Keur, Sunscreen Ecoproducts: Product Claims, Potential Effects and Environmental Risks of Applied UV Filters, Wageningen Marine Research report C056/18, 2018, <https://doi.org/10.18174/457209>.
- [12] D.M. Berube, Rhetorical gamesmanship in the nano debates over sunscreens and nanoparticles, *J. Nanopart. Res.* 10 (S1) (2008) 23–37, <https://doi.org/10.1007/s11051-008-9362-7>.
- [13] G. Paterson, J.M. Ataria, M.E. Hoque, D.C. Burns, C.D. Metcalfe, The toxicity of titanium dioxide nanopowder to early life stages of the japanese medaka (*Oryzias latipes*), *Chemosphere* 82 (7) (2011) 1002–1009, <https://doi.org/10.1016/j.chemosphere.2010.10.068>.
- [14] Q. Fang, X. Shi, L. Zhang, Q. Wang, X. Wang, Y. Guo, B. Zhou, Effect of titanium dioxide nanoparticles on the bioavailability, metabolism, and toxicity of penta-chlorophenol in zebrafish larvae, *J. Hazard. Mater.* 283 (2015) 897–904, <https://doi.org/10.1016/j.jhazmat.2014.10.039>.
- [15] C. Botta, J. Labille, M. Auffan, D. Borschneck, H. Miche, M. Cabié, A. Masion, J. Rose, J.-Y. Bottero, TiO<sub>2</sub>-based nanoparticles released in water from commercialized sunscreens in a life-cycle perspective: structures and quantities, *Environ. Pollut.* 159 (6) (2011) 1543–1550, <https://doi.org/10.1016/j.envpol.2011.03.003>.
- [16] M. Auffan, M. Pedetour, J. Rose, A. Masion, F. Ziarelli, D. Borschneck, C. Chaneac, C. Botta, P. Chaurand, J. Labille, J.-Y. Bottero, Structural Degradation at the Surface of a TiO<sub>2</sub>-Based Nanomaterial Used in Cosmetics, *Environ. Sci. Technol.* 44 (7) (2010) 2689–2694, <https://doi.org/10.1021/es903757q>.
- [17] J. Labille, J. Feng, C. Botta, D. Borschneck, M. Sammut, M. Cabie, M. Auffan, J. Rose, J.-Y. Bottero, Aging of TiO<sub>2</sub> Nanocomposites Used in Sunscreen. Dispersion and Fate of the Degradation Products in Aqueous Environment, *Environ. Pollut.* 158 (12) (2010) 3482–3489, <https://doi.org/10.1016/j.envpol.2010.02.012>.
- [18] K.M. Tyner, A.M. Wokovich, D.E. Godar, W.H. Doub, N. Sadrieh, The state of nano-sized titanium dioxide (TiO<sub>2</sub>) may affect sunscreen performance: nano-sized TiO<sub>2</sub> and sunscreen performance, *Int. J. Cosmet. Sci.* 33 (3) (2011) 234–244, <https://doi.org/10.1111/j.1468-2494.2010.00622.x>.
- [19] H. Kamiya, M. Iijima, Surface modification and characterization for dispersion stability of inorganic nanometer-scaled particles in liquid media, *Sci. Technol. Adv. Mater.* 11 (4) (2010) 044304, <https://doi.org/10.1088/1468-6996/11/4/044304>.
- [20] Y. Hanada, M. Nomura, H. Suzuki, H. Kamiya, Analysis of the dispersion behavior of surface-modified titanium dioxide nanoparticles in silicone oil using the colloid probe AFM method, *J. Soc. Powder Technol. Jpn.* 52 (3) (2015) 139–144, <https://doi.org/10.4164/sptj.52.139>.
- [21] M. Rossano, N. Hucher, C. Picard, D. Colletta, F. Le Foll, M. Grisel, Effects of aging on structure and stability of TiO<sub>2</sub> nanoparticle-containing oil-in-Water emulsions, *Int. J. Pharm.* 461 (1–2) (2014) 89–96, <https://doi.org/10.1016/j.ijpharm.2013.11.039>.
- [22] SaNogueira, J. P. (73) Assignee: Playtex Products, Inc., Westport, CT. 26.
- [23] D. Terescenco, N. Hucher, G. Savary, C. Picard, From interface towards organised network: questioning the role of the droplets arrangements in macroscopically stable O/W emulsions composed of a conventional non-ionic surfactant, TiO<sub>2</sub> particles, or their mixture, *Colloids Surf. Physicochem. Eng. Asp.* 578 (2019) 123630, <https://doi.org/10.1016/j.colsurfa.2019.123630>.
- [24] T. Imae, K. Muto, S. Ikeda, The pH dependence of dispersion of TiO<sub>2</sub> particles in aqueous surfactant solutions, *Colloid Polym. Sci.* 269 (1) (1991) 43–48, <https://doi.org/10.1007/BF00654658>.
- [25] F. Loosli, S. Stoll, Effect of surfactants, pH and water hardness on the surface properties and agglomeration behavior of engineered TiO<sub>2</sub> nanoparticles, *Environ. Sci. Nano* 4 (1) (2017) 203–211, <https://doi.org/10.1039/C6EN00339G>.
- [26] E. Núñez-Rojas, H. Domínguez, Computational studies on the behavior of sodium dodecyl sulfate (SDS) at TiO<sub>2</sub>(Rutile)/Water interfaces, *J. Colloid Interface Sci.* 364 (2) (2011) 417–427, <https://doi.org/10.1016/j.jcis.2011.08.069>.
- [27] S. Skoglund, T.A. Lowe, J. Hedberg, E. Blomberg, I.O. Wallinder, S. Wold, M. Lundin, Effect of laundry surfactants on surface charge and colloidal stability of silver nanoparticles, *Langmuir* 29 (28) (2013) 8882–8891, <https://doi.org/10.1021/la4012873>.
- [28] Evonik. Tegoseft P - Technical Information, (2018).
- [29] SEPPIC. Easynov - Liquid Emulsifier, (2011) [www.sepic.com](http://www.sepic.com).
- [30] Schlossman, M. L. PIGMENTS AND BASES INTO PRODUCTS CONTAINING OIL AND WATER PHASES. 6.
- [31] J. Chou, T.J. Robinson, H. Doan, Rapid comparison of UVB absorption effectiveness of various sunscreens by UV-vis spectroscopy, *J. Anal. Bioanal. Tech.* 08 (02) (2017), <https://doi.org/10.4172/2155-9872.1000355>.
- [32] L. Rowenczyk, C. Duclairoir-Poc, M. Barreau, C. Picard, N. Hucher, N. Orange, M. Grisel, M. Feuillol, Impact of coated TiO<sub>2</sub>-Nanoparticles used in sunscreens on two representative strains of the human microbiota: effect of the particle surface nature and aging, *Colloids Surf. B Biointerfaces* 158 (2017) 339–348, <https://doi.org/10.1016/j.colsurfb.2017.07.013>.
- [33] A. Vilg  -Ritter, A. Masion, T. Boulang  , D. Rybacki, J.-Y. Bottero, Removal of natural organic matter by coagulation-flocculation: a Pyrolysis-GC-MS study, *Environ. Sci. Technol.* 33 (17) (1999) 3027–3032, <https://doi.org/10.1021/es981232p>.
- [34] Y.-C. Chang, Y. Yamamoto, H. Matsumoto, Accumulation of aluminium in the cell wall pectin in cultured tobacco (*Nicotiana tabacum* L.) cells treated with a combination of aluminium and Iron, *Plant Cell Environ.* 22 (8) (1999) 1009–1017, <https://doi.org/10.1046/j.1365-3040.1999.00467.x>.
- [35] J.L. Yang, Y.Y. Li, Y.J. Zhang, S.S. Zhang, Y.R. Wu, P. Wu, S.J. Zheng, Cell wall polysaccharides are specifically involved in the exclusion of aluminum from the rice root apex, *Plant Physiol.* 146 (2) (2008) 602–611, <https://doi.org/10.1104/pp.107>.

- 111989.
- [36] K. Singh, S. Mohan, Adsorption Behavior of Selected Monosaccharides onto an Alumina Interface, *J. Colloid Interface Sci.* 270 (1) (2004) 21–28, <https://doi.org/10.1016/j.jcis.2003.05.002>.
  - [37] K. Singh, S. Mohan, Kinetic studies of the sucrose adsorption onto an alumina interface, *Appl. Surf. Sci.* 221 (1–4) (2004) 308–318, [https://doi.org/10.1016/S0169-4332\(03\)00950-4](https://doi.org/10.1016/S0169-4332(03)00950-4).
  - [38] G.H. Posner, Organic reactions at alumina surfaces, *Angew. Chem. Int. Ed. Engl.* 17 (7) (1978) 487–496, <https://doi.org/10.1002/anie.197804871>.
  - [39] N.W. Gabel, C. Ponnampuruma, Model for origin of monosaccharides, *Nature* 216 (5114) (1967) 453–455, <https://doi.org/10.1038/216453a0>.
  - [40] C. Reid, L.E. Orgel, Synthesis of sugars in potential prebiotic conditions, *Nature* (216) (1967) 455, <https://doi.org/10.1038/216453a0>.
  - [41] A. Noel, D. Mirbel, E. Cloutet, G. Fleury, C. Schatz, C. Navarro, G. Hadzioannou, CyrilBrochon, Tridodecylamine, an efficient charge control agent in non-polar media for electrophoretic inks application, *Appl. Surf. Sci.* 428 (2018) 870–876, <https://doi.org/10.1016/j.apsusc.2017.09.171>.
  - [42] S.K. Sainis, V. Germain, C.O. Mejean, E.R. Dufresne, Electrostatic interactions of colloidal particles in NoENMolar solvents: role of surface chemistry and charge control agents †, *Langmuir* 24 (4) (2008) 1160–1164, <https://doi.org/10.1021/la702432u>.
  - [43] P.G. Smith, M.N. Patel, J. Kim, K.P. Johnston, T.E. Milner, Electrophoretic mobility measurement by differential-phase optical coherence tomography, *J. Phys. Chem. C* 111 (6) (2007) 2614–2622, <https://doi.org/10.1021/jp0645723>.
  - [44] I.D. Morrison, Electrical charges in nonaqueous media, *Colloids Surf. Physicochem. Eng. Asp.* 71 (1) (1993) 1–37, [https://doi.org/10.1016/0927-7757\(93\)80026-B](https://doi.org/10.1016/0927-7757(93)80026-B).
  - [45] K.D. Kwon, H. Green, P. Bjöörn, J.D. Kubicki, Model bacterial extracellular polysaccharide adsorption onto silica and alumina: quartz crystal microbalance with dissipation monitoring of dextran adsorption, *Environ. Sci. Technol.* 40 (24) (2006) 7739–7744, <https://doi.org/10.1021/es061715q>.

## Supplementary information Chapter IV

### Primary particle size determination by HR-SEM

The primary particle size (longer side length) for each type of TiO<sub>2</sub> based UV filter was determined based on the HR SEM images reported in **Figure S1**.

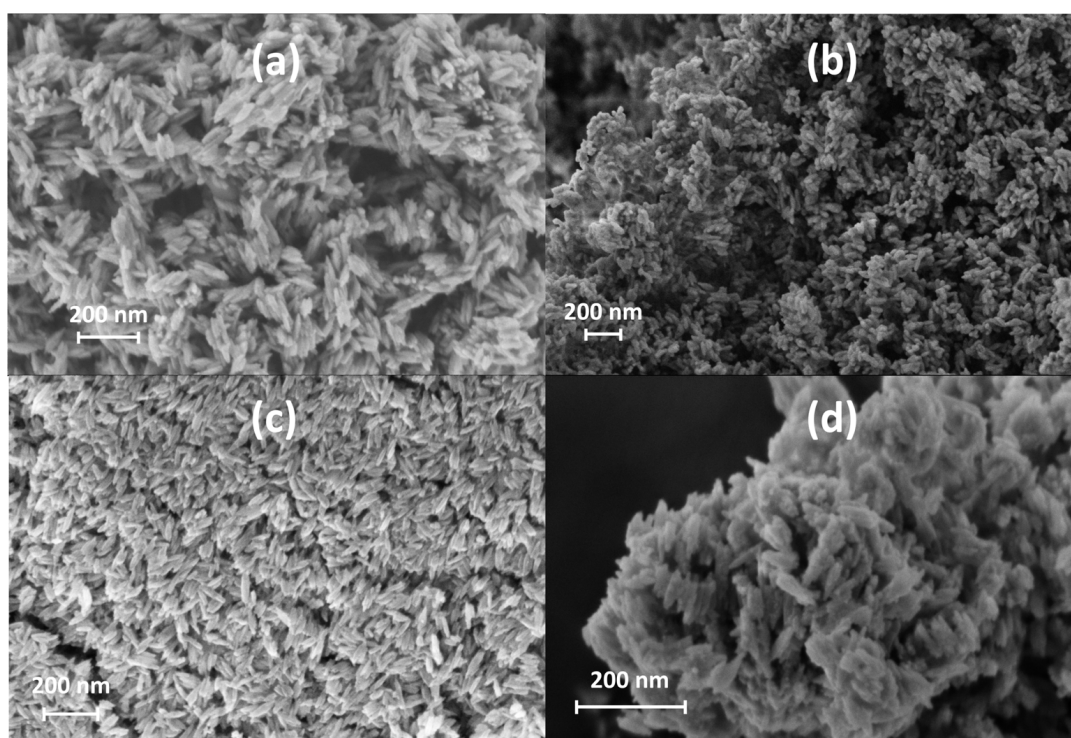


**Figure S11:** High Resolution Scanning Electron Microscopy images of pristine NPs: T-sim (a); T-sil (b); T-ste (c) and T-dim (d).

### Aggregate size vs agitation speed test

It possible to see that for T-dim and T-sim NPs agitation speed does not influence the aggregate size while in the case of T-sil and T-ste increase the agitation speed is needed to break-up the aggregates, until a size comparable to the ones of T-dim and T-sim. Small differences in the mean size values showed in this figure,

compared with the intensity mean size values of the results showed in in the manuscript, are due to the fact that in this case we used the number weighted representation, which minimize bimodal distributions and allow to have just one mean size value for each colloidal dispersion. Number distributions normally over-weight smaller aggregates

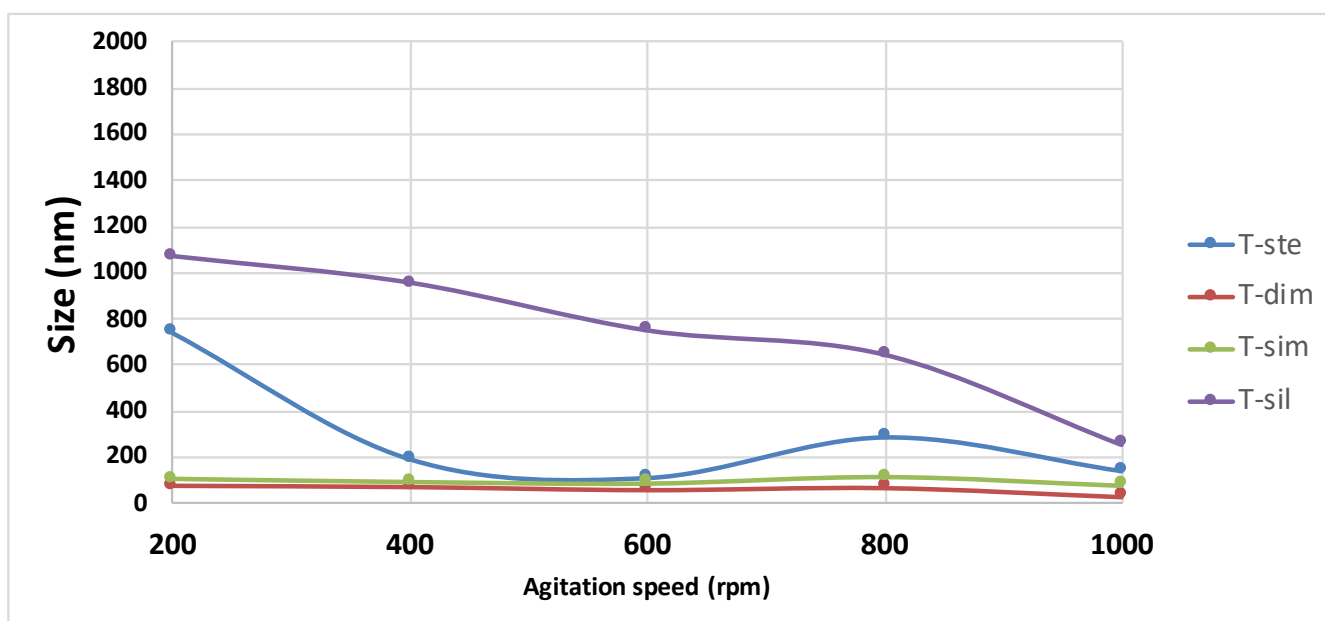


**Figure S12:** Aggregate size (DLS number distribution) of the four UV filters in Phase A, as function of the palette agitation speed.



## NMR data treatment

In order to ease the peak assignment in the NMR spectra of the different oil phase components, simulated  $^{13}\text{C}$  NMR spectra were produced using MestRE Nova software. The simulated spectra are reported in **Figure S2**.

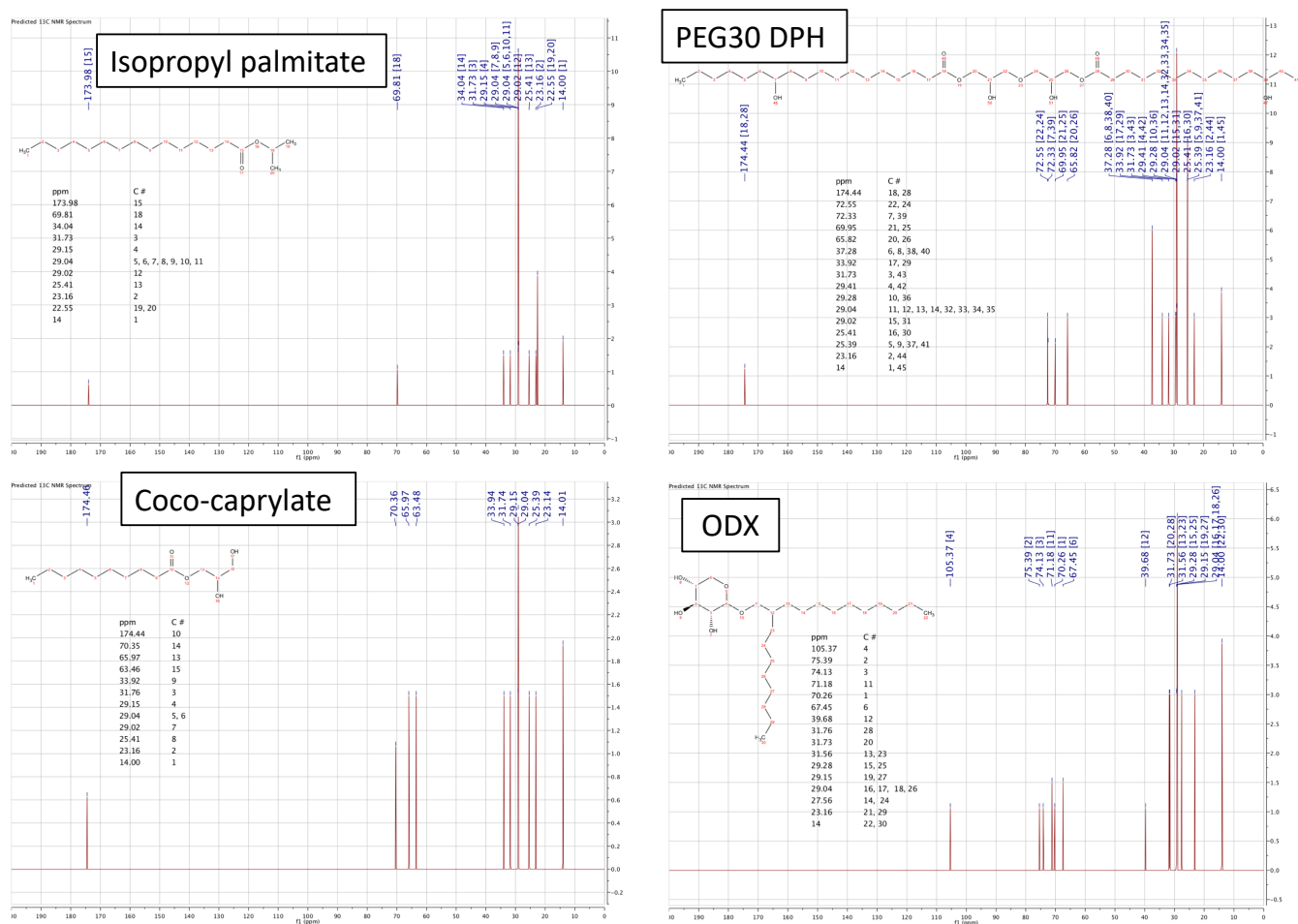


**Figure S13:** Simulated  $^{13}\text{C}$  NMR spectra for the two emollient oils (coco-caprylate and isopropyl palmitate) and the two surfactants (PEG30 dipolyhydroxystearate-DPH and Octyldodecyl Xiloside-ODX) composing the oil phase (Phase A).

$^{13}\text{C}$  NMR spectrum peak integration of Easynov<sup>TM</sup> emulsifier was performed with MestRE Nova software using the Gaussian fit method and is reported in **Figure S4**. It allowed the quantification of the ODX ratio in the emulsifier mixture and proved the sensibility of the technique to all C present in the system. The same method was used also to determine the total number of C atoms of the compounds remains attached on T-sim and T-dim NP surface after the aging in Phase A (**Results and discussion** – The roles of emulsifier components and particle coatings).

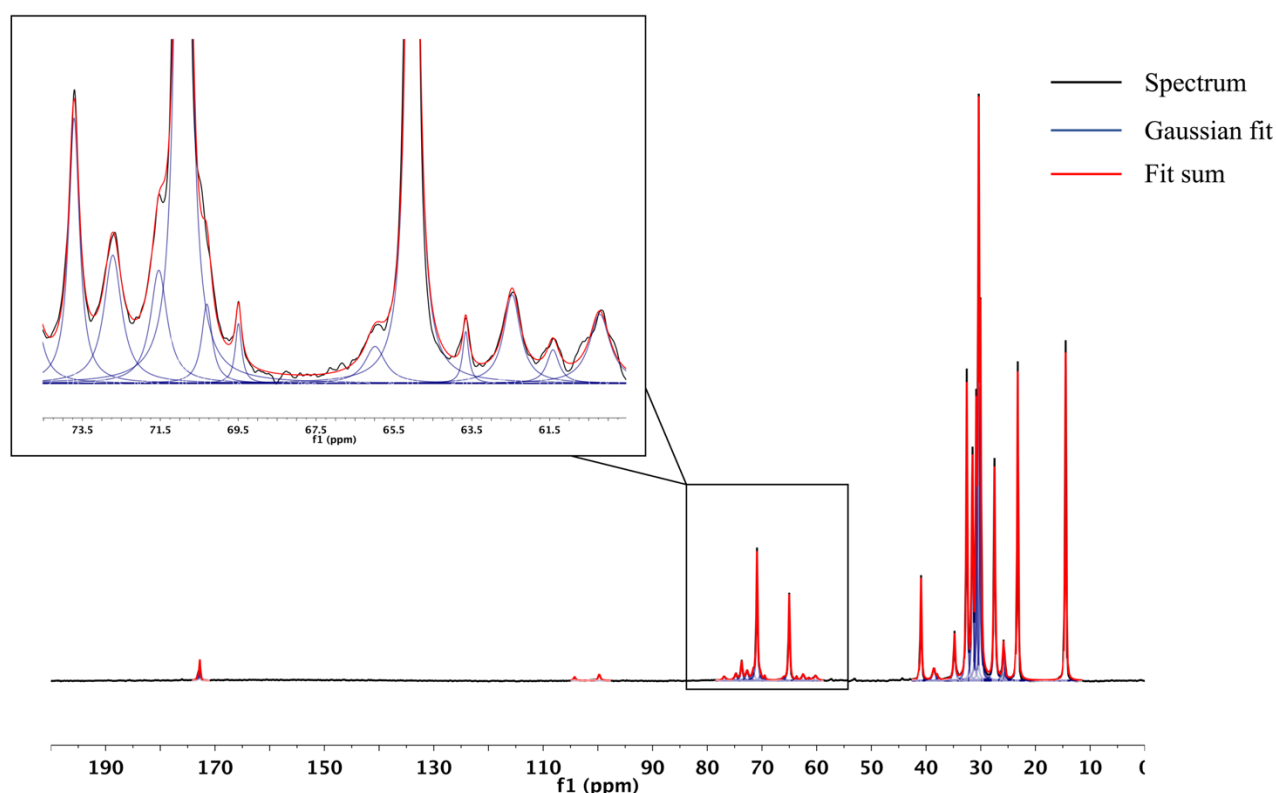


**Figure S14:** Line fitting of the C-13 NMR spectrum of Easynov performed with the MestReNova software. **black:** spectrum; **blue:** peak fit; **red:** Fit sum



## Chapter V: Characterization of the scattering properties of the nanoparticulate UV filters

### 5.1 Principles of scattering from dielectric particles

The amount of radiation blocked by a single semiconductor (like  $\text{TiO}_2$  or  $\text{ZnO}$ ) particle within a population of particles, and hence, the UV attenuation by inorganic sunscreens is affected by both scattering and absorption. The attenuation,  $(dI)$  of an incident beam of intensity,  $(I)$  by a dilute suspension of particles, volume fraction  $(f)$  over a small distance,  $(dx)$  may be written as follows<sup>118,153</sup>.

$$-\frac{dI}{I} = f q_{ext} dx \quad (1)$$

where  $q_{ext}$ , the total attenuation coefficient per unit volume of particles, is the sum of the coefficients of scattering and absorption and may be rewritten as follows:

$$q_{ext} = q_{sca} + q_{abs} \quad (2)$$

In the simplest case, that of a non-absorbing particle, with a diameter smaller than one-tenth of the radiation wavelength, the scattering efficiency is given by the Rayleigh Equation:

$$q_{sca} = \frac{C}{V} = \frac{KV}{\lambda^4} \quad (3)$$

Where  $C$  is the scattering cross-section,  $K$  is a constant whose size is a function of  $m$ , the ratio of the refractive index of the particle,  $m_p$ , to the refractive index,  $m_m$ , of the medium,  $V$  is the particle volume and  $k$  is the wavelength of the incident light in the medium ( $k = k_0/m_m$  where  $k_0$  the wavelength in vacuo).

When the particle diameter exceeds  $\sim\lambda/4$ , the Rayleigh equation is no longer applicable. Instead, Mie theory may be used. The light extinction cross-section of isolated spheres  $q_{ext} = C/V$  is then given by equation (4).

$$C = \frac{\lambda^2}{2\pi} \sum_{n=1}^{\infty} (2n+1) \{[a_n]^2 + [b_n]^2\} \quad (4)$$

Where  $a_n$  and  $b_n$  are complex functions, depending not only on wavelength and refractive index but also on the particle diameter, assuming that the spheres are optically isotropic, meaning that the refractive index is the same in all directions. Both Equations (3) and (4) show that  $q_{sca} = C/V$ , is a sensitive function of both the wavelength,  $k$ , and the refractive index  $m$ . The latter is a complex quantity and may be written as  $m = n - ik$ . Light scattering depends on the difference between the real part,  $n$ , of the particle and the surrounding liquid, whereas absorption depends on both  $n$  and the imaginary part,  $k$ . Scattering and absorption cross-sections can be calculated by substituting the real and apparent parts of the refractive index into the Mie equations, allowing afterwards the calculation of the total extinction cross section from equation (2). Both scattering and absorption cross section value are strictly correlated with the particle diameter. In the case of Rayleigh scattering, a  $d^3$  variation is expected, while Mie scattering has a more complex relation<sup>118</sup> with  $d$ . Although the attenuation of particulate suspensions can, in principle, be calculated from Mie Theory, there are significant practical challenges. Corrections for optical anisotropy and for the spread of rutile crystal sizes have already been introduced but further factors must be considered. One is that the calculations assume that the scattering by each particle is unaffected by

scattering from its neighbors; individual particles must be sufficiently far apart that there is no interference with the nearby scattered light. The higher the concentration of inorganic UV filter, the less well this condition is satisfied. A second complication is that practical dispersions never consist only of single particles; they always contain some agglomerates of two or more basic particles (aggregates). Therefore, even if all the inorganic crystals have an identical size, the formulated dispersion will contain a distribution of sizes. The details of this distribution will depend not only on the nature of the absorber and whether it has been treated at the surface, but also on such factors as the milling conditions and dispersant additions used to prepare the final formulation. Finally, for the concentrations of inorganics typical of mineral sunscreens, some of the initially scattered light will be multiply scattered, that is it will be further scattered during subsequent interactions with further particles. A complete experimental study would require attenuation measurements to be made as a function of concentration<sup>118</sup>.

As already claimed in **Chapter 1.3**, from a safer-by-design approach, providing a full quantitative description of the absorptive versus the scattering and reflecting properties of the mineral UV filters, is essential if one want to optimize their performances and better anticipate and minimize their possible risk toward marine environment. Until the 80ies, mineral filters were thoughts to had a purely reflective/scattering interaction with UVR<sup>107</sup>. In 1986, Kollias *et al.*<sup>154</sup>, recognized for the first time the absorption properties of mineral filters in the UV region, but without providing any quantitative description of the phenomena. More recently, different studies were able to provide this quantitative description and distinguish between scattering and absorption pathway of photoprotection, mainly by means of UV spectrophotometers coupled with *integrating sphere*

tools<sup>107,118</sup> (**Figure 5.1**), concluding that mineral filters protect from UVR mainly through absorption.

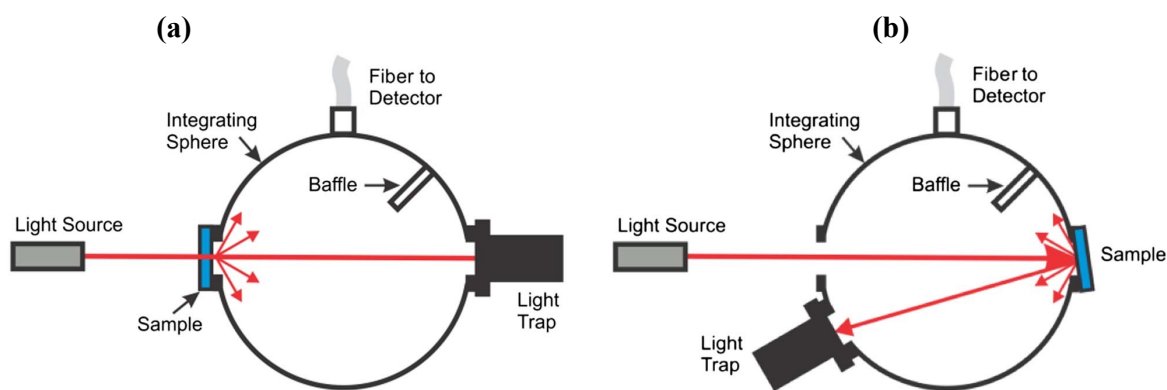


**Figure 5.1:** Integrating sphere arrangements for measurement of total integrated transmittance scatter **(a)** and total integrated reflectance scatter **(b)**. (adapted from Payne *et al.* 2015)

As far as this methodology certainly allows a quantitative description of absorptive and scattering properties of mineral filters, it also affected by intrinsic uncertainties deriving from the instrumental set-up that, although can be minimized, are unavoidable (e.g. misfit between sample and sphere surface; inhomogeneity of the sphere coating)<sup>155,156</sup>. Common integrating spheres (Beckman model) will lead to incorrect results for any sample which is not an ideal diffuse reflector<sup>157</sup> (as in the case of mineral UV filters). Also, backscattering near the direction of the incident light ( $\sim$  reflection) is lost during the measurement<sup>118</sup>. It was instead observed that reflected and transmitted scattering characteristic of nanomaterials can be accurately determined by means of Angular Resolved Scattering (ARS) measurement carried out at single wavelength<sup>158</sup> (**Figure 4.2**), in which the scattered light is collected into a collimator rotating around a single plane around the sample, avoiding lack

information on the angular dependence of scattered light for non-ideal diffusor materials.

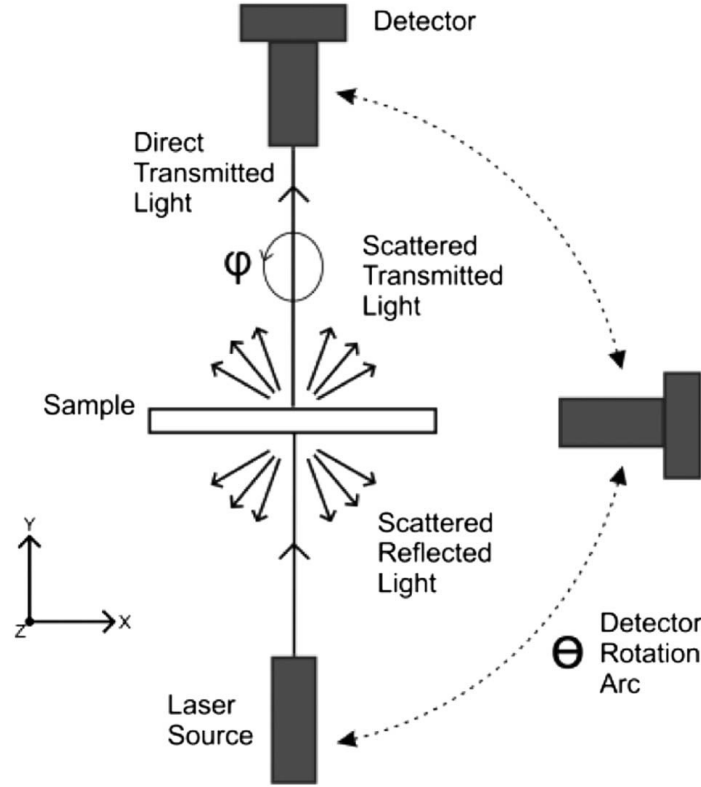


**Figure 5.2:** Illustration of ARS measurement process for reflected and transmitted scatter (Payne et al. 2015).

## 5.2 Principles of angular scattering measurements

The scattered intensity, or ARS, is defined in the space around the sample by :

$$I(\theta, \phi) = ARS(\theta, \phi) \quad (5)$$



Where  $\theta$  is the angle measured from the sample normal and  $\phi$  is the polar angle, as shown in **Figure 5.3**. Thus, from this relation,  $I(\theta; \phi)$  represent the light intensity scattered in a  $(\theta; \phi)$  direction of the space, or the scattered radiation for solid angle unit, normalized to the incident radiation. The notion *Bidirectional Scattering Distribution Function* (BSDF) is also often utilized, and it is defined by the relation described in equation (6):

$$I(\theta, \phi) = BSDF(\theta, \phi) \cos \theta \quad (6)$$

BSDF have thus the dimension of the inverse of a solid angle ( $\text{steradian}^{-1}$ ). depending on whether we consider the half space reflected or transmitted, we can respectively use the nomenclature BRDF and BTDF for *Bidirectional Reflectance Distribution Function* and *Bidirectional Transmittance Distribution Function*.

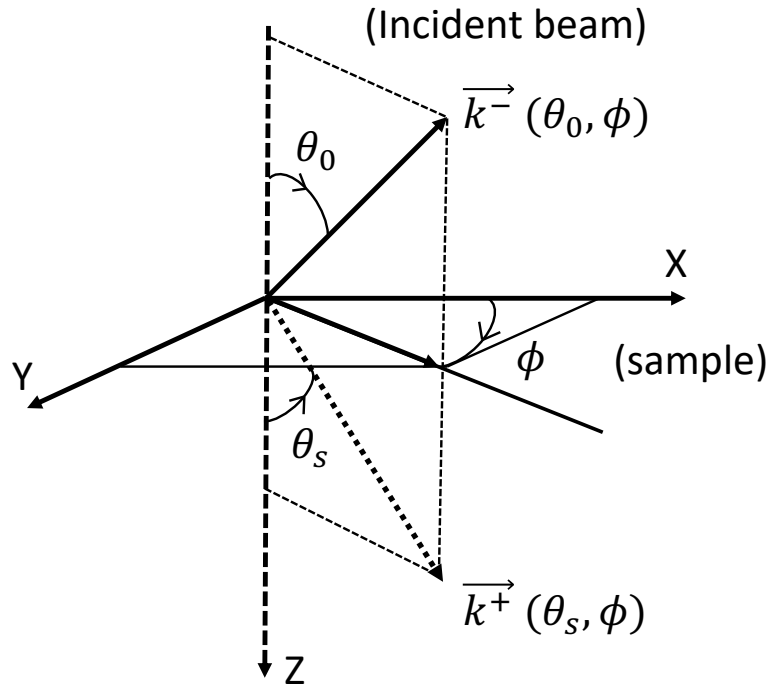


**Figure 5.3:** Definition of the scattering angles  $\theta$  and  $\phi$

In **Figure 5.3** the wave vectors of the transmitted and reflected scattered light are respectively defined by  $\vec{k}^+$  and  $\vec{k}^-$ , and their tangential projection into the plane Oxy is the spatial pulsation  $\sigma = 2\pi\nu$ , where  $\nu$  is the spatial frequency. We thus have that:

$$\vec{\sigma} = \frac{2\pi n_0}{\lambda} \sin \phi \begin{pmatrix} \cos \phi \\ \sin \phi \end{pmatrix} = 2\pi \vec{\nu} \quad (7)$$

$$\vec{k}^- = \frac{2\pi n_0}{\lambda} \begin{cases} \sin \theta \cos \phi \\ \sin \phi \sin \phi \\ -\cos \theta \end{cases} \quad (8)$$

$$\vec{k}^+ = \frac{2\pi n_s}{\lambda} \begin{cases} \sin \theta \cos \phi \\ \sin \phi \sin \phi \\ \cos \theta \end{cases} \quad (9)$$

Where  $n_0$  is the index of the incident medium and  $\lambda$  is the wavelength of irradiation.

### 5.3 Measurement tools and set up

With the aim of measure the angular scattering profile of different colloidal oily dispersion of commercial nanoparticulate mineral UV filters, an angular scatterometer was built-up at the Institut Fresnel, directly inspired from previous works<sup>159</sup>. The different tools used and the instrument set-up are schematized in **Figure 5.4**.

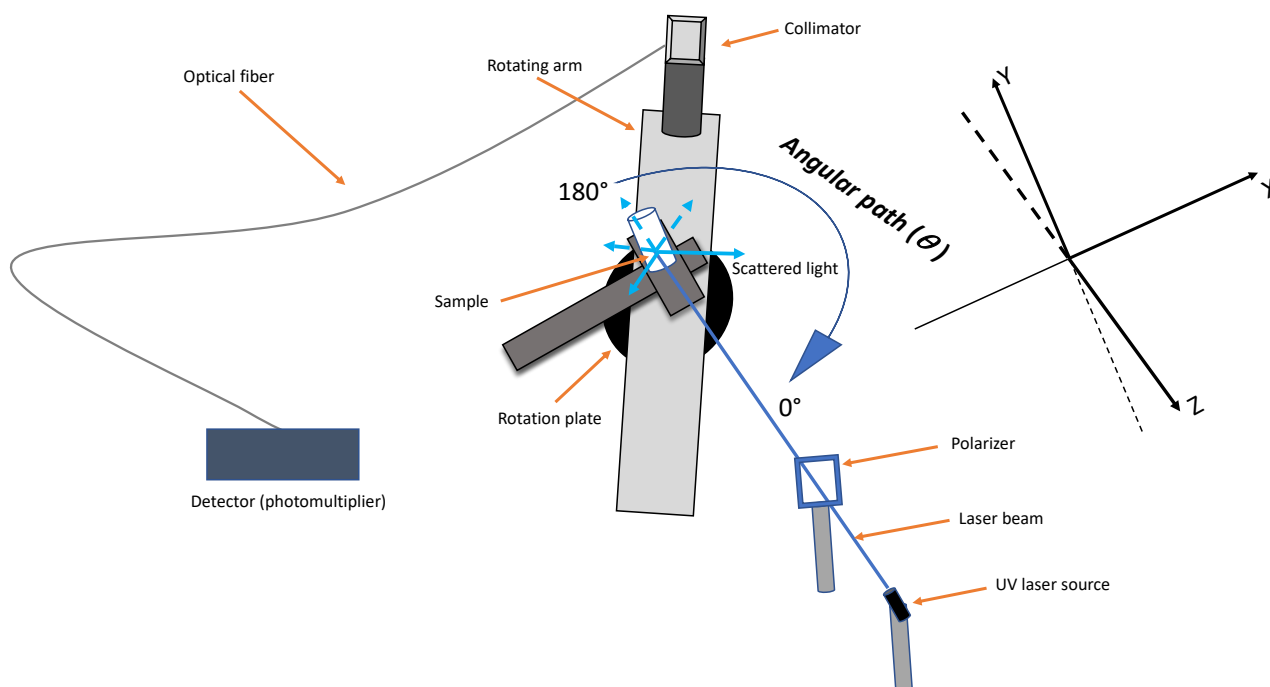


**Figure 5.4:** Schematized set-up of the angular scatterometer developed for the scattering measurements of the colloidal dispersions.

A photo of the instrument is also reported in **Figure 5.5**, to give insight of its real dimensions.

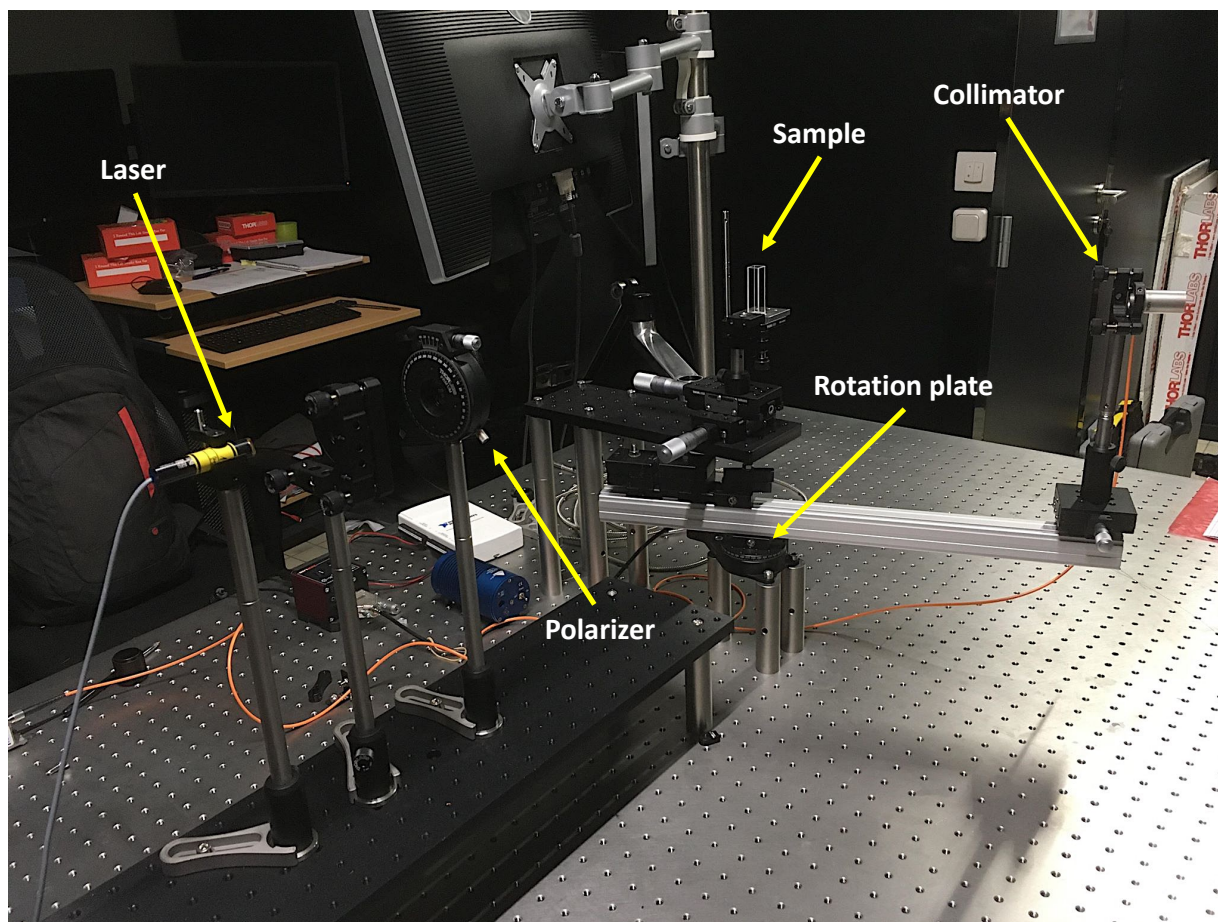


**Figure 5.5:** Photography of the instrument. Yellow flashes indicate the main component of the set-up.

Two different light sources were employed for the analysis, one LED lamp emitting at wavelength of 300 nm (M300L4 - *Thorlabs*) and one fiber-coupled laser diode emitting at 405 nm (K41 - *Laser Components*). This wavelength was chosen based on the maximum absorbance region observed in the UV-vis measurements performed in Chapter III. To give insight of the polarization dependence scattering intensity of the samples (i.e. aggregates shapes and polydispersity), an adjustable polarizer filter is interposed in the beam path between the light source and the sample. The incident laser beam is perpendicular to the XY plane of the sample, which is in turn placed on a Kinematic Platform Mounts (KM100B/M-*Thorlabs*), that is a sample holder with two axes of adjustment (X and Y of **Figure 5.4**) allowing a precise alignment of sample plane and the incident beam. Below the sample holder a rotation plate goniometer

connected to a motor stage controller (KPRMTE/M-*Thorlabs*) is placed. A 1m length aluminium arm (XT34-*Thorlabs*) is fixed on the rotation plate and on one extreme of the arm, a reflective and fibered collimator (RC02SMA-F01 *Thorlabs*) is mounted to provide an illumination at a working wavelength between 250 and 450 nm. The arm is thus able to rotate around the sample, allowing the collimator to collect the scattered radiation on the XZ plane (**Figure 5.4**). The scattered light collected by the collimator during the measurement is sent through an optical fiber (M100L02S-UV-*Thorlabs*) to a photodetector (OE-200-UV-FC – *FEMTO*), able to convert and adjust the receiving signal gain from  $10^3$  up to  $10^{11}$  V/W. This functionality is essential in order to amplify weak scattering response of the sample ( $\theta \approx 90^\circ$ ), otherwise undetectable, or attenuate strong excessively strong signals ( $\theta \approx 0^\circ ; 180^\circ$ ) which will saturate the detector.

#### 5.4 Measurement automation

In order to automate the ARS measurements, an instrument control interfaced through PC was programmed in G graphical language, using LabVIEW® software. The final scope was to have a user interface in which define the measurement parameters (e.g. angle range; number of measurements), launch automate measurements, acquiring and saving data in transferable formats (e.g. excel files). A simplified block diagram representing the organigram of the code enabling automate measurements is reported in **Figure 5.6**.

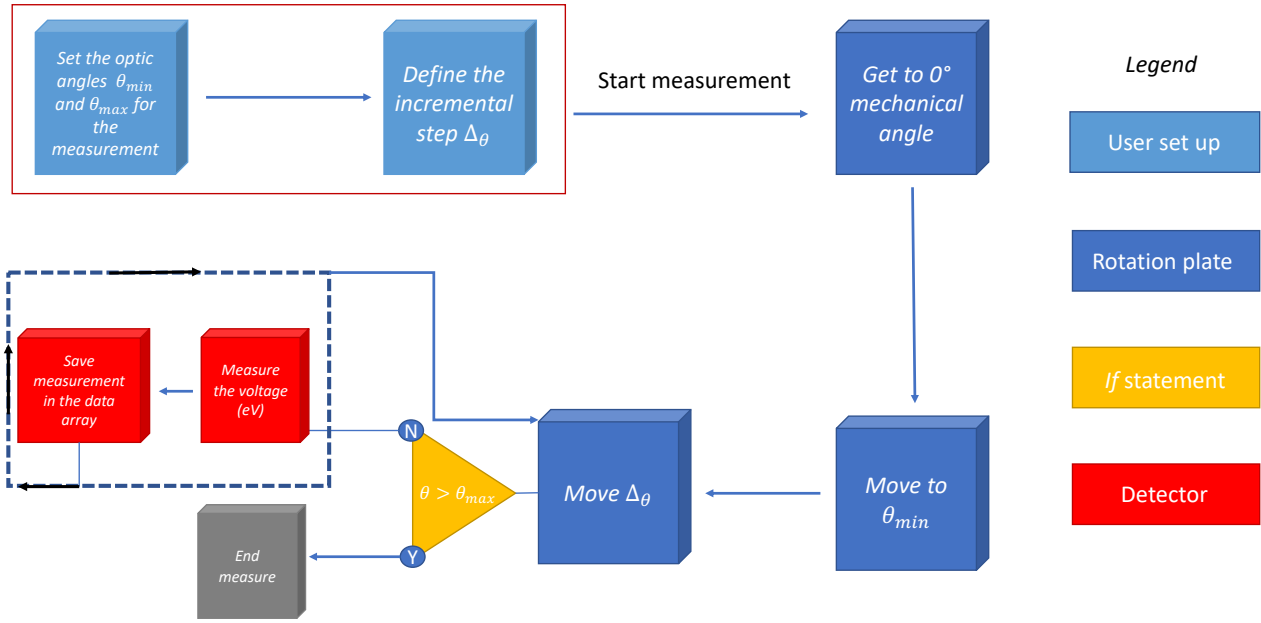


**Figure 5.6:** Block diagram representing the organigram of the algorithm which controlled the automation of the ARS measurement.

Each ARS measurement required the definition of two main parameters: the optical angles  $\theta_{min}$  and  $\theta_{max}$ , which defines the range of angular rotation of the goniometer plate; the incremental step  $\Delta_\theta$  done by the goniometer to reach  $\theta_{max}$ . As at each step a measure of the light intensity scattered by the sample is performed, the more  $\Delta_\theta$  is short, the more the ARS measurement will be precise at the end. Once defines these parameters we could launch the automated ARS measurement. In the first place, the goniometer needs to find the mechanical 0 angle to further goes to the defined  $\theta_{min}$  angle. When the goniometer moves of an incremental step  $\Delta_\theta$  to reach  $\theta_{max}$ , a logical restriction is activated in the algorithm: if after the increment  $\theta < \theta_{max}$ , then a measurement of scattered light intensity is registered by the instrument and saved into an appended array. If this condition is not maintained, instead, the measurement routine is stopped.

## 5.5 Calibration

Before starting the measurements, the instrument must be calibrated to be able to deliver an absolute value of the light intensity scattered by the sample. This means determine the constant  $K_c$ , which binds the observable voltage signal  $V(\theta)$  to the characteristic chosen to quantify the scattering intensity  $I(\theta)$ . This constant is determined by means of a standard Lambertian sample whose total scattering  $S_c$  is known, determined by the U.S *National Institute of Standards and Technology*, and has a value of 98% at a wavelength of 400 nm. Moreover, the ARS of the calibration sample is known to follow a Lambertian scattering law which is :

$$I(\theta) = \frac{0.98}{\pi} \cos \theta (rad) \quad (10)$$

was measured for a  $\theta$  going from 5 to 90° and the constant  $K_c$  was determined using the equation (10):

$$K_c = \frac{S_c \cdot \cos \theta (rad)}{\pi \cdot V_\theta} \quad (10)$$

In order to validate the accuracy of the calibration, the experimental ARS was compared to the ideal ARS of the standard, verifying that the two curves were superimposable with minimal deviations. The theoretical ARS was plotted using the  $V_t(\theta)$  intensities, calculated in accordance to equation (11):

$$V_t(\theta) = \frac{S_c \cdot \cos \theta (rad)}{\pi} \quad (11)$$

An example of calibration measurement is reported in **Figure 5.7**, using a 400 nm incident laser radiation with horizontal polarization.

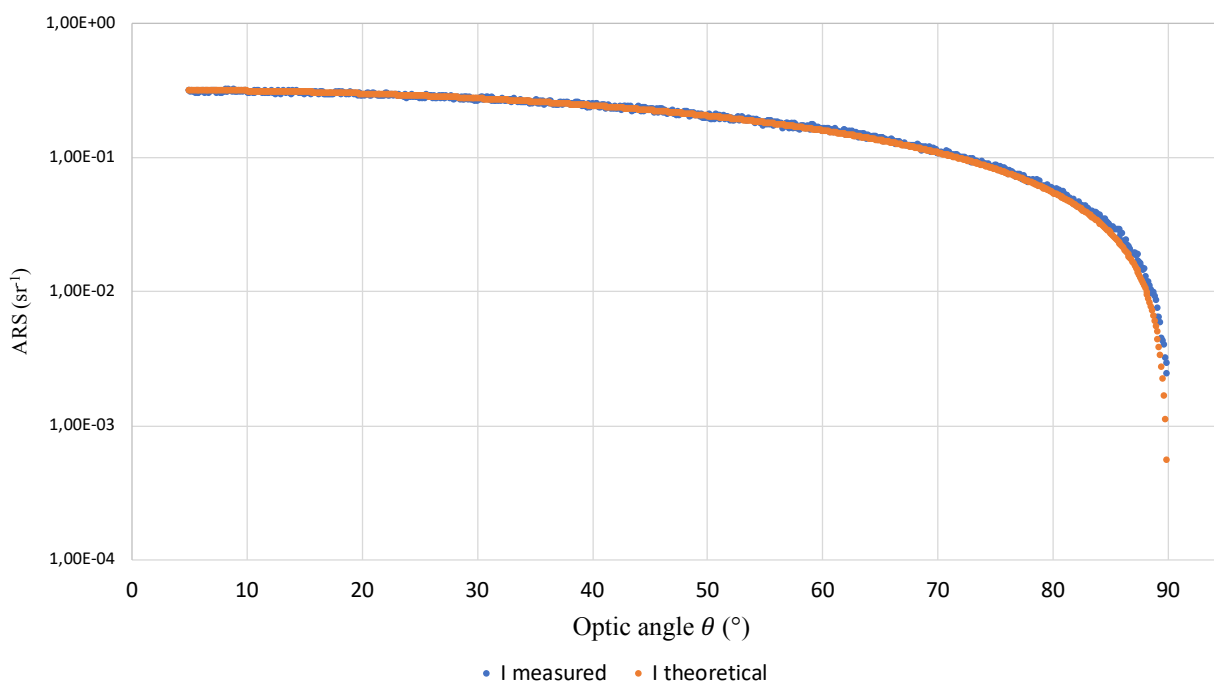


**Figure 5.7:** Theoretical (orange) and experimental (blue) ARS calibration curves using a Lambertian sample

This calibration routine was performed before each measure, in order to take into account random instrumental oscillations, and the new  $K_c$  derived each time was multiplied to  $V(\theta)$  to obtain the absolute scattering value  $I(\theta)$ . To give insight of the detection limits of the instrument and determine the shape of the incident beam, a sample free measurement was also performed for an optic angle  $\theta$  going from  $5^\circ$  to  $185^\circ$ .

## 5.6 Sample measurements

Measurements were performed on ENMs oily dispersions at 2.8 % w/w concentration, prepared with the same methodology presented in Chapter III. We selected two filters for this experiment, T-S and T-Lite ENMs, as they contain contrasted organic external coatings, both theoretically enhancing their dispersion in non-polar mediums as sunscreen oil phases. Nonetheless, in



Chapters III and IV we showed how these two coatings leads to unexpected and opposites fates of ENMs dispersion. T-S filters were more unstable in the formulation compared to T-Lite filters, determining highest ENMs aggregation and ultimately lead to a lower UVR screening efficiency of the final product. In the present chapter we attempt to evaluate the effects that such differences in the aggregation state can produce on the scattering and absorption properties of the ENMs dispersions.

Preliminary experiments using the LED lamp at 300 nm in the set-up were not able to detect any angular scattering signal of the samples. We argued that two main factors could have affected the measurements: the LED source was too weak to induce a detectable scattering signal; at 300 nm wavelength, light is mostly absorbed by the sample and thus unable to reach the detector. With the aim of avoiding both issues, we decided to use the laser diode source at 405 nm wavelength to validate the whole set-up, which guaranteed a more powerful beam and a minimal ENMs absorption. For the analysis, the ENMs oily dispersions were placed inside a quartz cuvette transparent to the near UV radiation. In order to distinguish the contribution of ENMs from the rest of the sample components, the same measurements were also performed on the empty cuvette and on the cuvette filled with just pure oil phase. Analysis were performed in both vertical and horizontal polarization, with  $\theta_{min}=3^\circ$ ,  $\theta_{max}=240^\circ$  and a  $\Delta\theta=0.1^\circ$ . The results are reported in **Figure 5.8**, together with the calibration measurement performed earlier between  $5^\circ$  and  $185^\circ$ .

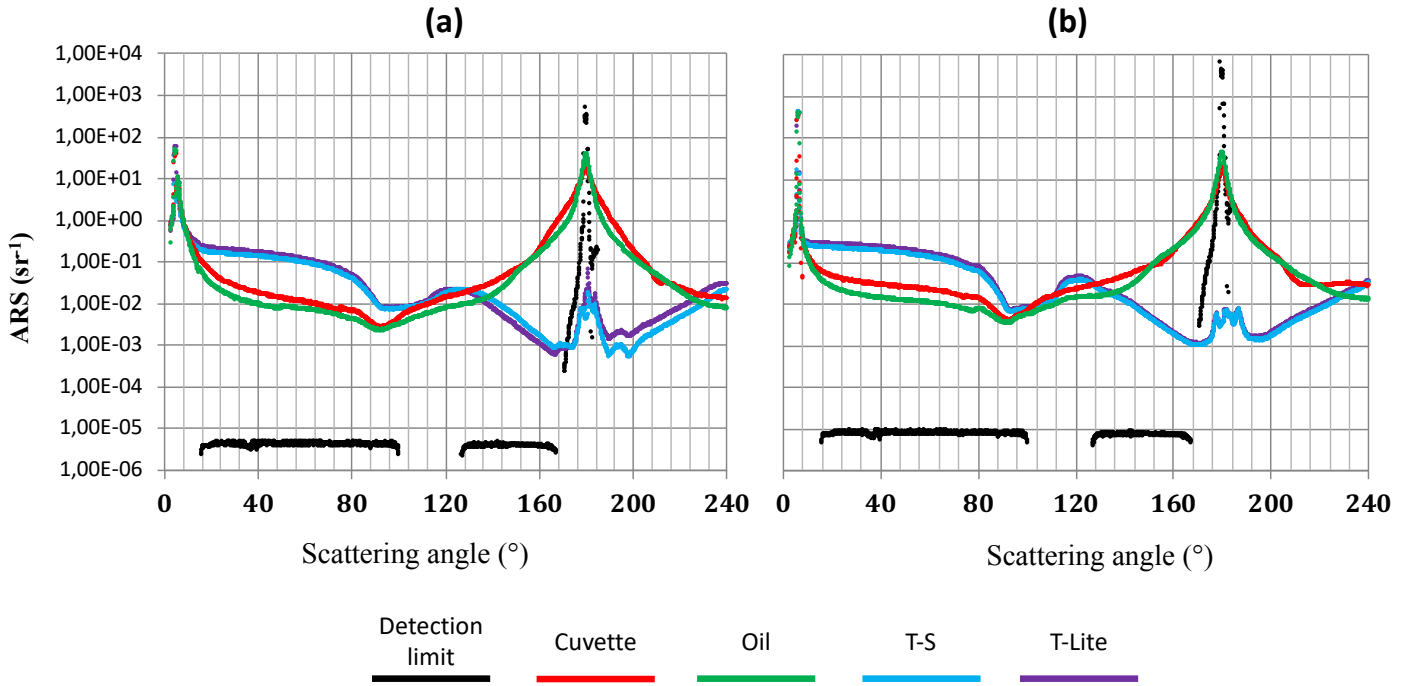


**Figure 5.8:** ARS measurements and calibration measurement (black) with vertical (a) and horizontal (b) polarization, T-Lite (violet); T-S (blue); empty cuvette (red) and cuvette filled with pure oil phase (green).

## 5.7 Total scattering and absorption calculation

In order to obtain the total reflected and transmitted scattered light, angular scattering intensity was integrated in all the measurement space, named *Total Integrated Scattering* (TIS) and described by the equation (12):

$$TIS = \sum_{\theta_i}^{\theta_n} 2\pi \cdot (I_{(\theta)} \cdot \sin \theta) \Delta\theta \quad (12)$$

This formula was obtained from a scalar theory<sup>160</sup> in which we imposed the further assumption that particle rugosity contribution is negligible. To determine the total reflected scattering light intensity, we performed the calculation for  $\theta$  going from  $9^\circ$  to  $90^\circ$ , and from  $95^\circ$  to  $180^\circ$  for the total transmitted scattered intensity. The fraction of light absorbed by the ENMs oily dispersions was thus obtained by the relation (13)

$$A + T + R = 1 \quad (13)$$

Where A stands for absorption, T for transmissive scattering and R for reflective scattering. Equation (13) is derived from the Kirchhoff's relation and it is a consequence of the conservation energy law<sup>161</sup>. The results of the calculation for both T-S and T-Lite oily dispersion, with vertical and horizontal polarization of the incident light, are reported in **Figure 4.9**.

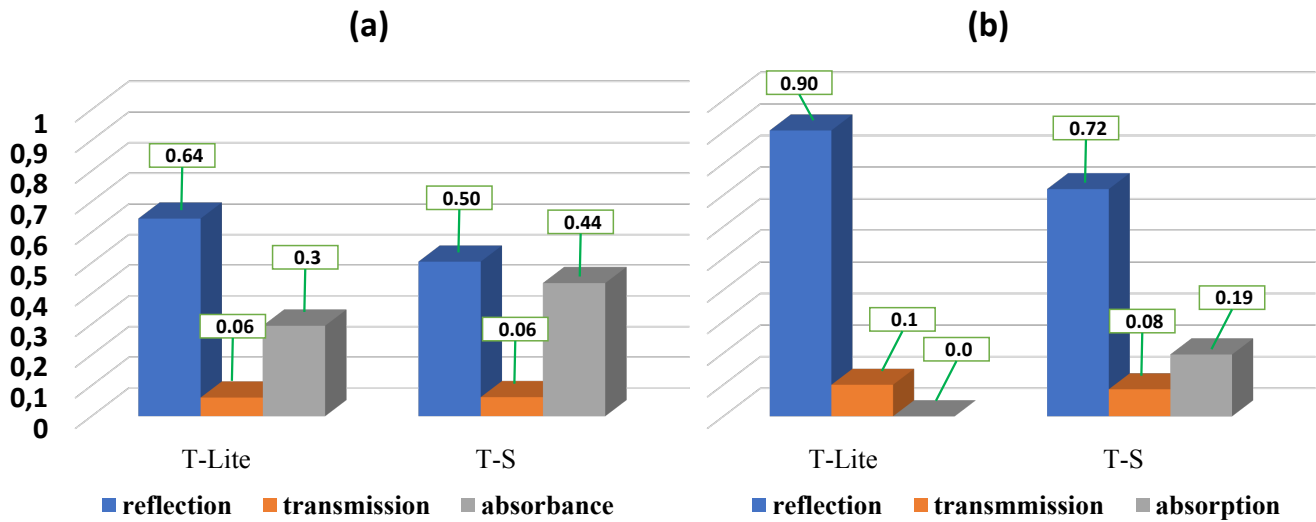


**Figure 5.9:** Ratios of transmitted, reflected and absorbed radiation, in vertical (a) and horizontal (b) polarization, by T-S and T-Lite ENMs oily dispersions.

## 5.8 Results discussion

ARS spectra presented in **Figure 5.8** show a sensible difference between ENMs formulations and reference samples (empty cuvette and pure oil phase). No differences of pure reflective phenomena, detected between 3° and 9°, are observed between the samples and could be thus ascribed to the interaction between the incident beam and the quartz cuvette. However, from 9° to 90° (reflective scattering), ARS of T-S and T-Lite formulations (blue and grey lines)

has a magnitude 10 times greater than the ENMs free samples (cuvette and pure oil phase), proving the efficiency of these mineral filters to physically reflect the near UV radiation. Still, reference samples have a huge reflective scattering effect as their ARS is  $\approx 1000$  times higher than the one of the calibration measures recorded in the vacuum. Transmitted ARS (from  $90^\circ$  to  $180^\circ$ ) shows a similar trend between the four samples until  $\theta \approx 130^\circ$ , while for superior scattering angles, the curves of ENMs dispersions and reference samples start to diverge. Light transmitted by reference samples is in fact increasing going from  $130^\circ$  to  $180^\circ$  while for filter dispersions it is decreasing. This difference of trends could likely be a consequence of the superior reflective scattering of ENMs containing samples, which will decrease the amount of light transmitted near  $180^\circ$ . On the contrary, intensity of the light transmitted around  $180^\circ$  by empty cuvette and pure oil phase is only mildly lower than the beam profile intensity recorded without sample (black line in **Figure 5.8**) with both light polarizations.

Overall, T-S and T-Lite dispersions ARS, shows a similar/superimposable trend suggesting that their different aggregation state observed in Chapters III and IV does not modify the scattering properties of the ENMs at 405 nm wavelength incident radiation. This could be due to the fact that this wavelength is too short to distinguish the contributions of aggregates in the micrometric domain, as in the case of T-S ENMs aggregates in the sunscreen oil medium observed in Chapter III. In fact, scattering response of particle dispersions is more effective when the particle (or the aggregates) are of a size comparable to the wavelength<sup>162</sup>. Also, Liu & Mishchenko<sup>163</sup>, demonstrates computationally that random variations in size and shapes of monomers composed a cluster of dust particles, does not have a significative effect in the scattering properties of the cluster itself, at least in the visible part of the spectrum. Indeed, in Chapters III and VI, we showed that there are negligible differences in the size and shapes of primary particles between T-S

and T-Lite ENMs, which would likely not influence the ARS of the two ENMs dispersion especially at wavelengths far above their average primary particle longer size length ( $\approx 60$  nm).

While the shapes of the ARS curves are almost the same between the two ENMs dispersions at both polarization of the incident radiation, significative differences are instead observed in the total scattering and absorption intensities reported in **Figure 5.9**. With a vertical polarization of the incident beam, **(a)**, T-Lite sample TIS most important contribution is represented by reflection phenomena (64%) followed by absorption (30%) and low transmission scattering (6%). For T-S sample, instead, reflection and absorption contributions are quite similar (50 and 44 % respectively) while a lower transmission contribution (6%) is detected as in the case of T-Lite sample. With a horizontal polarization, **(b)**, reflective scattering contribution is far more relevant. For T-Lite sample, in fact, it represents the 90% of the total ARS with only a minor transmitted scattering (10%) and no absorption. For T-S formulation, reflective scattering is still dominant, followed by absorption (20%) and transmission (6%).

In these presented results, absorption contribution should be not considered as the classical absorption of quantum radiation by a semiconductor (like  $\text{TiO}_2$ ) of sufficient energy to promote the jump of an electron through its band-gap<sup>164</sup>, as a 405 nm wavelength radiation have not enough energy to be absorbed by the  $\text{TiO}_2$  ENMs used for these experiments. It is thus more correct in this case to speak about “macroscopic absorption”<sup>165</sup>, which is a mechanism of light absorption often occurring when the irradiated system is capable of causing multiple scattering<sup>166</sup>, as concentrated ENMs dispersion. The cuvette transmitted path length that the light radiation had to travel along the sample was of 10 mm, which is long enough to determine a significative increase of multiple scattering process

along the way. In other words, macroscopic absorption means that part of the incident radiation, after passing through the first layers of the sample thickness, remains trapped into the colloidal matrix due to multiple scattering phenomena, being thus incapable to reach the detector.

The higher reflective scattering observed for T-Lite dispersion compared to the T-S one, could be explained by the finer T-Lite ENMs dispersion in the oil phase already discussed in Chapter IV. Reflective phenomena are more likely to happen at the beginning of the light interaction with the sample, that is before multiple scattering phenomena begins. Finer ENMs dispersions are indeed able to occupy a larger sample surface and should thus be more effective in the reflective scattering mechanism. In the bulk of the sample, instead, at the working ENMs concentrations the probability for the light radiation to encounter particles increase drastically, and the different aggregation state of T-S and T-Lite samples will probably be less influent. This could probably be the reason behind the similar transmitted scattering intensity between T-S and T-Lite sample even though they show significative differences in the reflective scattering intensities. The higher reflective efficiency of T-Lite sample is particularly evident with an incident radiation horizontal polarized than vertical polarized (**Figure 5.9 b**). These different scattered light intensities observed with both T-S and T-Lite samples, as function of the polarization could be due to the fact that we are in the Mie regime of scattering<sup>167</sup>. It mean that interacting particles size is too big compared to the incident radiation wavelength and its scattering properties could thus not be treated using the simpler Rayleigh theory<sup>168</sup>. In practice, in such conditions, the scattering mechanisms are influenced by the size and shape of the interacting particles and also by the polarization of the incident radiation, as already reported by Voarino *et al.* with microspheres particles<sup>169</sup>.

## 5.9 Conclusions and prospective

The instrumental design and set-up developed in this study, proved to be capable to finely describe the scattering and absorption properties of realistic nanoparticulate mineral UV filters dispersions. Experimental results were consistent with the current literature and with the findings described in chapters III and IV. Finer dispersed T-Lite ENMs were seen to be more effective in attenuate the incident radiation through reflective scattering mechanism. This preliminary study needs anyway further developments. In first place ARS measurement should be carried on using an UV laser source emitting around 300 nm, in order to be consistent with the type of radiation the mineral UV filters are supposed to attenuate. The sample should be also homogeneously spread on a PMMA plate support, mimic the user skin surface, which would be a more realistic condition to investigate and even more consistent with the current in vitro tests used to determine the SPF of commercial sunscreen formulation. In such experimental conditions, structural absorption contribution will be minimized, and the actual contributions of “chemical” absorption and reflective scattering to the entire UVR attenuation would be clearer. Also, to go further, different sizes and shapes of TiO<sub>2</sub> based ENMs should be tested, in order to select the ENMs physical features allowing the most efficient reflective scattering attenuation of UVR.





## **Part B: Environmental release and ecotoxicity**



## Chapter VI: Mineral UV filters exposure in the marine environment

After usage, sunscreens are released in the environment through different pathways. Among all, bathing activity represent one of the most important release pathways. Knowing realistic release and concentration of UV filters in aquatic environment is a key step in the LCA of sunscreens nanoprodukt. However, due to several practical and technical issues (e.g. sensitivity of the analytical methods; co-occurrence of natural and anthropogenic chemicals), few field campaign studies have been performed to date, and most of them were focused on the quantification of organic UV filters. For this reason, in this chapter, we studied the release of both mineral and organic UV filters in marine environment during the peak of recreational activities in three of the major beaches of Marseille sea-shore. The main tasks of this field campaign were: to estimate the daily flux of sunscreen and UV filters transferred from beachgoers into the bathing water on a standard summer day; to study the possible co-occurrence of organic and mineral UV filters in seawater, both in the water top surface layer and water column. Also, for the first time, a social survey of consumer habits was released in concomitance with the field sampling, in order to obtain information about: number of people in the beaches and bathers into water; types and amount of sunscreen used during recreational activities. Such data were then used to better interpret the results of water chemical analysis.

The study revealed that, during the peak of recreational activities at the three beaches, both mineral and organic UV filters were detected in higher concentrations near the bathing area than in the offshore. In general, higher concentrations were recovered in the water top surface layer than in the water column, giving respectively 100–900 and 20–50 µg/L for TiO<sub>2</sub>, 10–15 and 1–3

µg/L for ZnO, 40–420 and 30–150 ng/L for octocrylene, and 10–15 and 10–350 ng/L for avobenzone. Also, the social survey revealed that more than 75% of the interviewees reported bathing every time they go to the beach, with 68% using a suncare product 2.6 times on average. From these data we estimated that an average mass of 52 kg/day or 1.4 t/month of sun-care products are possibly released into bathing water for a beach attended by 3000 people daily.

***Paper III :***

Assessing UV filter inputs into beach waters during recreational activity: A field study of three French Mediterranean beaches from consumer survey to water analysis (Published in Science of Total Environment)



Contents lists available at ScienceDirect

Science of the Total Environment

journal homepage: [www.elsevier.com/locate/scitotenv](http://www.elsevier.com/locate/scitotenv)

## Assessing UV filter inputs into beach waters during recreational activity: A field study of three French Mediterranean beaches from consumer survey to water analysis

Jérôme Labille <sup>a,\*</sup>, Danielle Slomberg <sup>a</sup>, Riccardo Catalano <sup>a</sup>, Samuel Robert <sup>b</sup>, Marie-Laure Apers-Tremelo <sup>b</sup>, Jean-Luc Boudenne <sup>c</sup>, Tarek Manasfi <sup>c</sup>, Olivier Radakovitch <sup>a,d</sup>

<sup>a</sup> Aix Marseille Univ, CNRS, IRD, INRAE, Coll France, CEREGE, Aix-en-Provence, France

<sup>b</sup> Aix-Marseille Univ, Avignon Univ, Univ Côte d'Azur, CNRS, ESPACE, Avignon, France

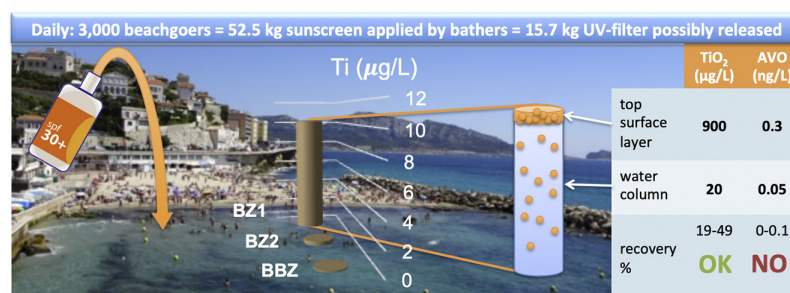
<sup>c</sup> Aix Marseille Univ, CNRS, LCE UMR7376, Marseille, France

<sup>d</sup> Institut de Radioprotection et de Sécurité Nucléaire (IRSN), PSE-ENV/SRTE/LRTA, BP 13, 13115 Saint Paul les durance, France

### HIGHLIGHTS

- 68% of beachgoers use sunscreen 2.6 times per visit to the beach.
- 3000 beachgoers/day = 52.5 kg sunscreen applied by bathers = 15.7 kg UV filter potentially released
- Mineral UV filters recovered in top surface layer and water column at 19 and 49% of PEC
- Low levels (ng/L) of organic UV filters recovered in seawater
- No use of sun care products labeled as eco-friendly, despite consumer awareness

### GRAPHICAL ABSTRACT



### ARTICLE INFO

#### Article history:

Received 29 October 2019

Received in revised form 4 December 2019

Accepted 6 December 2019

Available online 09 December 2019

Editor: Damia Barcelo

#### Keywords:

Sunscreen

Marine contamination

Nanomaterial fate

UV filter

Titanium dioxide

Environmental social issue

### ABSTRACT

In order to assess the release of UV filters from the sunscreen used by beachgoers into seawater within the bathing zone, a field campaign was carried out during the summer of 2017 at three beaches in Marseille, along the French Mediterranean coast. A social survey analyzed beachgoer attendance, the quantities and types of sun care products used and the bathing frequencies, while the bathing water was analyzed spatially and temporally so as to quantify both mineral and organic UV filters directly released and recovered.

During the peak recreational time at the three beaches, both mineral and organic UV filters were detected in higher concentrations in the bathing area than offshore. In general, higher concentrations were recovered in the water top surface layer than in the water column, giving respectively 100–900 and 20–50 μg/L for TiO<sub>2</sub>, 10–15 and 1–3 μg/L for ZnO, 40–420 and 30–150 ng/L for octocrylene, and 10–15 and 10–350 ng/L for avobenzone.

More than 75% of the 471 interviewees reported bathing every time they go to the beach, with 68% using a sun care product 2.6 times on average. From these data we estimated that an average mass of 52 kg/day or 1.4 t/month of sun care products are possibly released into bathing water for a beach attended by 3000 people daily. The mass ratio of UV filters in such products typically ranges from 0.03 to 0.1, allowing us to propose theoretical maximum concentrations in the beach water. Our recovery of measured UV filter concentrations in seawater compared to the theoretical concentrations revealed two distinct scenarios for the mineral and organic

\* Corresponding author.

E-mail address: [labille@cerege.fr](mailto:labille@cerege.fr) (J. Labille).

filters. While up to 49% of the mineral filters used by beachgoers may be released into the seawater, the organic filters were minimally recovered in the environment, most likely due to internalization through the skin barrier or partial photodegradation.

© 2019 The Authors. Published by Elsevier B.V. This is an open access article under the CC BY-NC-ND license (<http://creativecommons.org/licenses/by-nc-nd/4.0/>).

## 1. Introduction

Sunscreens are of emerging concern regarding both human and environmental health. Their regulation is constantly evolving, largely due to the potential risks related to the ingredients they contain. They typically consist of an oil-in-water emulsion in which the major active ingredients are UV filters, incorporated in high concentration. The UV filters can be organic or mineral in nature, depending on country specific regulations, and provide the desired sun protection factor (SPF) that is labeled on the product packaging (Steinberg, 2007).

A debate has taken place as to the risks associated with UV filters regarding both consumer health and environmental impact. After application to the consumer's skin, such ingredients are potentially internalized and transported by the blood throughout the body (Schlumpf et al., 2004; Gulson et al., 2010; Gulson et al., 2012; Matta et al., 2019). Several UV filters are blamed for having an endocrine disrupting capacity, including benzophenone-3, ethylhexyl methoxycinnamate, octocrylene, and 4-methylbenzylidene camphor (Schlumpf et al., 2004; Kunz and Fent, 2006; Calafat et al., 2008; Bluthgen et al., 2012). Benzophenone and its derivatives are also known to cause adverse effects on fecundity and reproduction in fish and rodents (Calafat et al., 2008; Kunz and Fent, 2009). Furthermore, once leaving the skin either through bathing or cleaning, the UV filters contained in the sunscreen can be released into rivers, lakes, coastal waters, and/or sewage treatment plants (Giokas et al., 2007; Hopkins and Blaney, 2016). Their fate and impact in these different systems are largely determined by their chemical properties, persistence, and transformation (Auffan et al., 2010; Labille et al., 2010; Botta et al., 2011). The scenario of direct release into the marine environment during recreational activity is of particular interest since UV filters have been repeatedly blamed for harmful effects toward coral reef areas (Danovaro et al., 2008; Downs et al., 2016; Fel et al., 2019) and other marine systems (Sanchez-Quiles and Tovar-Sanchez, 2014; Sendra et al., 2017; Rodriguez-Romero et al., 2019; Tovar-Sanchez et al., 2019; Calafat et al., 2008; Kunz and Fent, 2009).

Organic UV filters are synthetic molecules, generally dissolved in the sunscreen formulation. To date, only a few field-sampling campaigns have been completed in different coastal waters around the world to assess their environmental concentration and associated risk (Tashiro and Kameda, 2013; Bargar et al., 2015; Rodriguez et al., 2015; Downs et al., 2016; Tsui et al., 2017; Kung et al., 2018; Mitchelmore et al., 2019). While the presence of organic UV filters is commonly observed in the ng/L range in areas with recreational activities, it is still unclear how these molecules partition and degrade within the different environmental compartments, and how this will impact their resulting lifetime. Degradation is mainly induced by photoisomerization and photodegradation processes in the presence of sunlight, processes which are known to be influenced by the presence of certain water constituents, such as natural organic matter, chlorides, nitrates, and bicarbonates (Giokas et al., 2007; Santos et al., 2012).

The mineral UV filters present in sunscreens consist of ultrafine titanium dioxide (TiO<sub>2</sub>) or zinc oxide (ZnO) particles, often used in the nanoparticulate size range for improved UV blocking efficiency and transparency. These two types of minerals are both efficient UV blockers, favoring UV reflection and absorption over a wide range of wavelengths. While the environmental impact of nanotechnology has led to both tremendous lab and field research during the last 15 years, only a few studies have evaluated real mineral UV filters as found in sunscreens (Auffan et al., 2010; Labille et al., 2010; Virkutyte et al.,

2012). Although mineral UV filters are generally considered as inert, ZnO and TiO<sub>2</sub> minerals possess a photocatalytic character (Imanishi et al., 2007) and are thus always surface functionalized in order to suppress the formation of undesired reactive oxygen species (King et al., 2008) as well as favor dispersion in the formulation (Faure et al., 2013). This industrial surface coating controls the environmental fate, exposure, and hazard of these nanomaterials, making the bare TiO<sub>2</sub> or ZnO species widely studied elsewhere an inappropriate reference (Sani-Kast et al., 2016).

Moreover, the detection of anthropogenic TiO<sub>2</sub> and ZnO minerals (nano or non-nano) in aquatic environments where both Ti and Zn elements naturally occur in varying background concentrations remains an analytical challenge. Different proxies have been tested to distinguish the natural, terrigenous materials from those that are man-made. Al and Si are the most often used elements in mineral UV filter coatings, but are difficult to use as a proxy for anthropogenic emission due to their abundance in natural systems (Gondikas et al., 2014; Gondikas et al., 2018). Elemental ratios using Ti, V or rare earth elements (Ga, Y, Nb, Eu, Ho, Er, Tm, Yb, Ta) have also been proposed as proxies for terrigenous material behavior in aquatic systems (Gondikas et al., 2014; Reed et al., 2017).

An alternative to traditional proxies can be considered based on the simultaneous release of mineral and organic UV filters in bathing water. Both filter types may be found together in the environment, as a result of being associated in a common sunscreen or originating from different products. The organic UV filters, which are not present in the natural background, can be detected more easily and may be used as a proxy for the mineral filters. Indeed, the co-evolution of organic and mineral UV-filters has been measured in near shore fresh waters with time-dependent concentrations (Tovar-Sanchez et al., 2013; Reed et al., 2017). However, a lack of knowledge remains regarding the respective environmental fate and persistence of these two types of UV-filters, which may be contrasting. The fate of mineral UV filters depends on both their solubility and their tendency to disperse or aggregate and sediment (Labille and Brant, 2010). In addition, the hydrophilic or hydrophobic character of the particle surface will also affect its propensity to remain individually dispersed in the aqueous environment or to adsorb to the surface of natural suspended matter (Giokas et al., 2007).

Overall, despite the rising interest in the environmental concern of UV filters, very few data are available on the quantification of the source of UV filter inputs in the field. Social surveys on consumer sunscreen use in recreational areas are needed to better understand the relation between the quantities of sunscreen used and the environmental concentrations of the UV filters actually detected in the water. Keller et al. (2014) estimated the amount of engineered nanomaterials released from personal care products based on a survey of consumer habits in the USA and China. For the USA, they calculated a total sunscreen consumption of 90,000 metric tons per year, involving an estimated potential release of 2300–2700 mt/yr of nanomaterials. Ficheux et al. performed a large survey of the French population's cosmetics consumption, including skincare products. They revealed that 40–46% of adults use sunscreen, with 80% of the consumption being concentrated during summer time (Ficheux et al., 2015). Using volunteers, they also determined that an average range of 15–18 g of the sunscreen product is consumed during one application of sunscreen on the entire adult body (Ficheux et al., 2016). Extrapolating this to the entire adult French population (49 million adults), this gives 21 million users consuming 350 metric tons of sunscreen per application.



In this context, the aims of this work were (i) to estimate the daily flux of sunscreen and UV filters transferred from beachgoers into the bathing water on a standard summer day; (ii) to study the possible co-occurrence of organic and mineral UV filters in seawater, both in the water top surface layer and water column; and (iii) to determine, for the first time, the patterns of UV filter occurrence in the bathing water at three French Mediterranean beaches. This study is the first field campaign coupling chemical water analysis to quantify both organic and mineral UV filters in seawater, with a simultaneous social survey of consumer's habits on the beach. Thus, both the release and exposure to UV filters in such littoral systems could be evaluated.

## 2. Methodological approach

### 2.1. Beach description

The three urban beaches selected as study sites were chosen based on geographical and socio-demographic criteria. They are located in

various stretches of Marseille's seafront (900,000 inh.) (Fig. 1). To the north, the Lave Beach belongs to the seaside park of Corbière, the only recreational bathing area in the northern half of the city. Located beyond the northern tip of the commercial port, at the foot of limestone cliffs, it mainly welcomes people from working class neighborhoods. To the south, Pointe Rouge Beach is part of the recreational waterfront of the city's shoreline. It is characterized by high attendance and an urban environment. In the center, the Prophète Beach is characteristic of the rocky Provençal coast. Nestled at the foot of the coastal road and below a wealthy neighborhood, most of its users come from downtown Marseille. The present work focuses more on Prophète Beach than the two other beaches because its restricted access allowed us to count the exact daily attendance, and its relatively closed bathing zone enabled us to estimate the volume of bathing water. Despite their small size (less than 1 ha), each of the three beaches is intensely frequented during the summer season, which requires specific management by local authorities from June to September (beach patrol, user services, additional cleaning and maintenance, etc.).

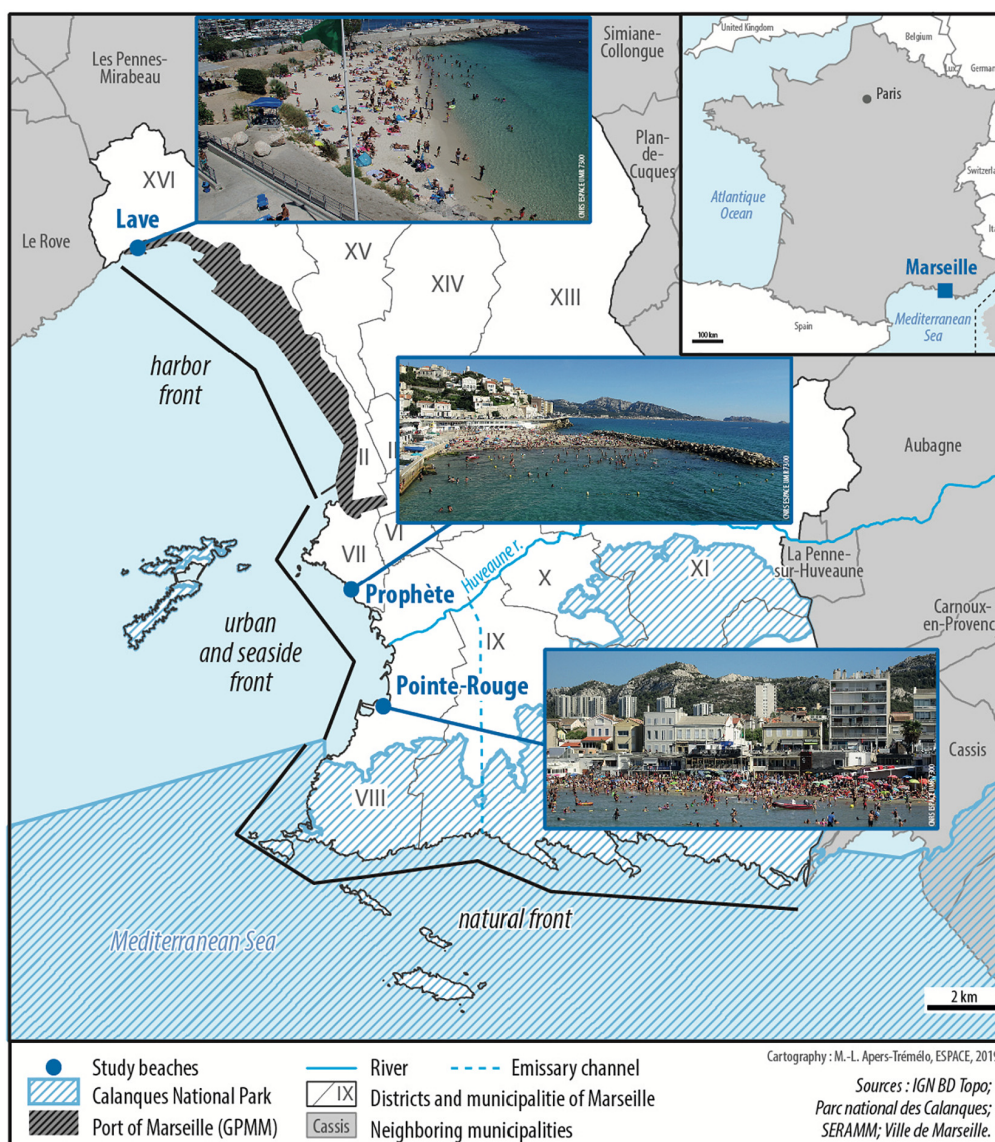


Fig. 1. Localization of the three urban beaches studied in this field campaign in the Marseille city area, along the French Mediterranean coast.



## 2.2. Seawater analysis

### 2.2.1. Water sampling

On Saturday, July 15th, 2017, water samples were collected at 4:00 pm, during peak recreational activity. The spatial distribution of any UV filters in the waters was assessed by sampling at three distances from the beach shoreline in Bathing Zone 1 (BZ1), Bathing Zone 2 (BZ2) and beyond the Bathing zone (BBZ). BZ1 and BZ2 were selected to sample the bathing water at the closest and farthest distance from the shoreline, respectively (Fig. 2). The water depth at these sampling points ranged from 0.4 to 1.9 m over the three beaches, depending on the coast slope (Table S1).

BBZ was selected to sample water beyond the bathing zone that gives a footprint of the local geochemical background. The seawater local background composition may result from several contributions, of natural or anthropogenic origin, that cannot be distinguished. Since the release of UV filters from sources other than beachgoer recreational activity could cause interference with this study, it should be noted that Marseille's treated urban wastewater is emitted into the sea > 4 km away from the studied sites, in another bay (Fig. 1). Here we assume that the BBZ water composition represents a local background, respective to each studied beach, and that any change in the bathing zone water composition can be related back to swimming activity on that beach.

Water samples were collected at two depths. The top surface layer (~1 cm), where hydrophobic compounds would likely be concentrated, was collected separately (250 mL) using a homemade sampler consisting of a plastic plate connected to a funnel. Samples were stored in high-density polyethylene bottles. To represent the average water column and obtain comparable data, a constant sampling depth was selected at 40 cm, which was always above the bottom of the water column. ~20 L of water was pumped directly from the 40 cm depth into pre-cleaned plastic drums carried on a kayak. During pumping, transects across the entire beach width were realized in order to pool the

water along the BZ1, BZ2, or BBZ lines (Fig. 2). Agitation due to recreational activity, waves, and wind may likely cause homogenization of the water composition over the entire water column height in the bathing zone (Table S1). Nevertheless, we assume that any contrasts in the composition between the two layers sampled (1 cm and 40 cm), should reflect the relative hydrophobic character of the components analyzed. In order to avoid any manipulation artifacts, the collaborators involved in water sampling and preparation did not use any sun care products during the campaign. Immediately following sampling, all collected waters were conserved at 4 °C in the dark until further treatment for chemical analysis.

To verify that recreational activity has an immediate impact on the bathing water composition in terms of UV filter concentration, the temporal variability of organic UV filter concentrations was assessed for the seawater at Prophète Beach. Additional samplings were conducted at 8:00 am on Saturday, July 15 and Sunday, July 16, 2017, i.e. just before and after the studied peak attendance on July 15th at 4:00 pm.

### 2.2.2. Seawater sample pre-treatment and analysis for UV filter quantification

**2.2.2.1. Mineral UV filters.** To provide insight as to whether any mineral UV filters (i.e.,  $\text{TiO}_2$  and  $\text{ZnO}$ ) present were aggregated or well-dispersed, the waters collected at a depth of 40 cm were fractionated into particulate ( $>0.5 \mu\text{m}$ ) and colloidal ( $0.02 < x < 0.5 \mu\text{m}$ ) fractions.

The raw waters from each sampling point (~20 L) were first processed with a KrosFlow Research Ili Tangential Flow Filtration System (Spectrum Laboratories, Rancho Dominguez, CA, USA) utilizing a  $0.5 \mu\text{m}$  membrane cut-off (mPES MiniKros Module: N04-P50U-10-N, 5–50L, Spectrum Laboratories), until the  $>0.5 \mu\text{m}$  particulate fraction had been concentrated ~100×. The resulting filtrate ( $<0.5 \mu\text{m}$ , ~20 L) was then fractionated a second time using a membrane with a 500-kD ( $\sim 0.02 \mu\text{m}$ ) cut-off (Spectrum Laboratories, mPES MiniKros Module:

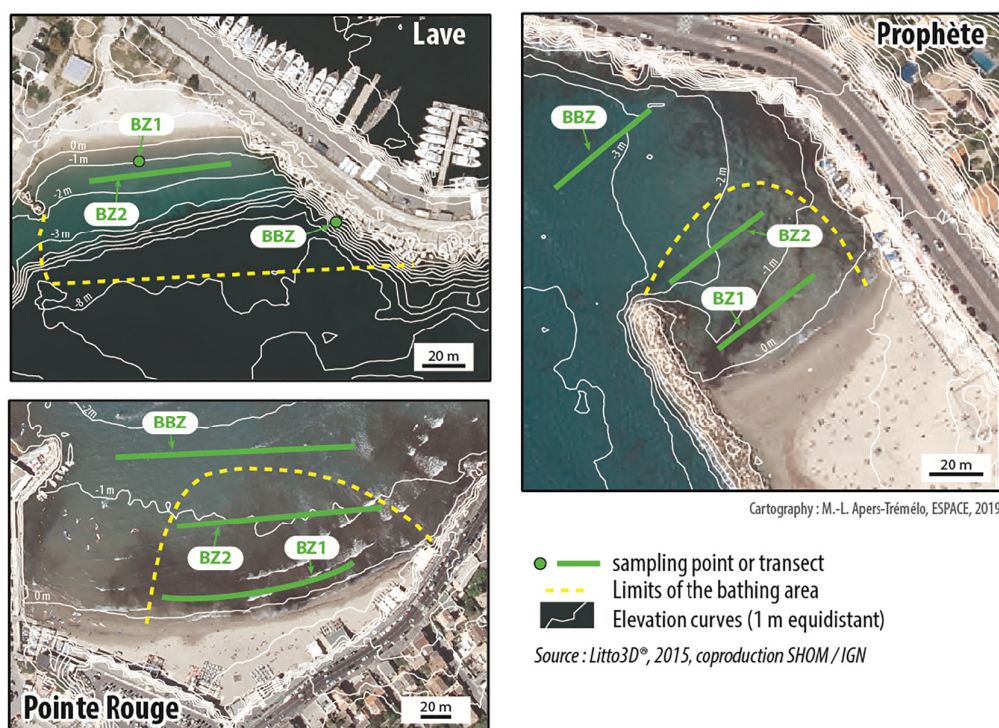


**Fig. 2.** Localization of the sampling points (green) in Bathing Zone 1 (BZ1), Bathing Zone 2 (BZ2) and Beyond Bathing Zone (BBZ) on the three beaches studied. The yellow dotted line shows the limit of the bathing zone. (For interpretation of the references to color in this figure legend, the reader is referred to the web version of this article.)

N04-E500-05-N, 5–50L) until the  $0.02 < x < 0.5 \mu\text{m}$  colloidal fraction had been concentrated  $\sim 100\times$ .

All water fractions (i.e.,  $>0.5 \mu\text{m}$  and  $0.02 < x < 0.5 \mu\text{m}$ ), as well as surface layer samples, were subjected to total decomposition using microwave-assisted acid digestion. The samples (2 g) were digested in an UltraWAVE microwave system (Milestone Inc.) with 1 mL hydrogen peroxide ( $\text{H}_2\text{O}_2$ , 30%), 1 mL nitric acid ( $\text{HNO}_3$ ), and 0.5 mL hydrofluoric acid (HF). After digestion, excess HF was immediately neutralized with boric acid (0.4 g) and the resulting digest was diluted to 25 mL with 5%  $\text{HNO}_3$ . Using quadrupole ICP-MS (Perkin Elmer Nexion 300 $\times$ ), samples were then analyzed for Ti and Zn concentrations as indicators of mineral UV filter occurrence. Al, Fe, and V elements were also quantified as potential proxies for terrestrial materials in order to better distinguish the UV filter signal apart from the local background. V, showing stable local background levels at all sampled distances, was selected for this purpose.

**2.2.2.2. Organic UV filters.** We investigated the occurrence of five commonly used organic UV filters, namely dioxybenzone (DIOXY), oxybenzone (OXY), avobenzone (AVO), 2-ethylhexyl-4-methoxycinnamate (OMC), and octocrylene (OC) (Table 1) using liquid chromatographic/mass spectrometric analyses.

Standards of OXY, DIOXY, AVO, OMC, OC and the internal standard benzophenone-d10 were purchased from Sigma-Aldrich Fluka (purity  $> 98\%$ ). Standard solutions of UV filters were prepared with methanol (Ultra Chromasolv, purity  $> 99.9\%$ ). Sodium sulfate (ACS reagent grade) was purchased from Sigma-Aldrich, India. Sulfuric acid (analytical grade) was purchased from Fisher Scientific, UK. Methyl tert-butyl ether (MTBE, Chromosolv, HPLC grade, Sigma-Aldrich, Germany) was used for extraction. Reconstituted seawater was prepared according to the ASTM International standard practice for the preparation of substitute ocean water (ASTM-International, 2013).

Seawater samples (50 mL) were filtered using cellulose filters papers, then adjusted to pH 3.0 using concentrated sulfuric acid, and an internal standard (benzophenone-d10) was added. Liquid-liquid extraction (LLE) of the filtrates was then conducted with 5 mL MTBE by shaking vigorously for 2 min. Sodium sulfate (10 g) was added to enhance separation of the organic and aqueous phases. Extracts (5 mL) were further concentrated by exposing them to a gentle stream of nitrogen to a final volume of 0.5 mL at  $50^\circ\text{C}$ . The total concentration factor thus obtained was 100 (10 by LLE and 10 by reduction of MTBE volume). Recovery ranged between 89 and 117%. Within the studied concentration range, the calibration curves were linear ( $r^2 > 0.99$ ). Limits of

quantification (LOQ) were determined as a signal-to-noise ratio 3:1 and ranged between 1 and 8 ng/L. Further details on the UPLC MS/MS analytical procedure followed for UV filter quantification is given in the Supplementary material file (Section S1, Table S2).

### 2.3. Social survey

We assessed beach attendance through user counts and photographic images. At Prophète Beach, which is only accessible via two narrow stairways, the exact number of people entering and exiting the beach was counted at the beach entrance from 8:00 am until 8:00 pm each day. This was not possible at the other two studied beaches because of their wide and open access. Meanwhile, hourly photographic images were taken at the three beaches from 8:00 am until 8:00 pm and analyzed in order to count people on the beach and bathers into the water. Simultaneously, a questionnaire was carried out on-site between 8:00 am and 8:00 pm. We surveyed 471 people, corresponding to 112, 103 and 256 interviewees at La Lave, Pointe Rouge and Prophète beaches respectively. Our survey strategy was aimed at having equal representation of respondents by gender and age group. In addition to questions concerning their visits to the beach (frequency), activities generally practiced, individual behaviors, and the perception of the beach management by local authorities, beachgoers were asked specific questions about their sunscreen use (type, frequency, and time of application) and their opinion regarding the possible effects of these products on the marine environment (Table S3). When applicable, the containers of the sunscreen products used by the interviewees were photographed and the information on the packaging, such as brand, SPF, and composition were recorded. A total of 124 sunscreen product compositions were reported. This enabled us to estimate the average composition and maximum UV filter (i.e., organic and mineral) quantity that could be released daily into the beach water.

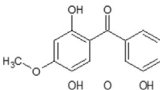
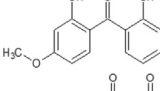
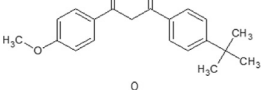
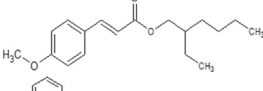
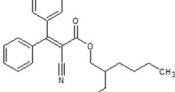
## 3. Results and discussion

### 3.1. UV filter quantification in seawater

#### 3.1.1. Time evolution of organic UV filter concentrations in beach water

Fig. 3 shows the temporal impact of bathing activity on the water chemistry by plotting the time dependent trend of the organic filter concentrations in Prophète Beach water. Three different sampling times are compared in terms of OC, AVO, and OXY concentrations. Only one sampling time corresponds to bathing activity, on Saturday,

**Table 1**  
Chemical structure and relevant data of the target organic UV filters.

| Compound/CAS number  | Formula   | Molecular weight | Chemical structure  | pKa  | Log K <sub>OW</sub> |
|--|---|------------------|---|------|---------------------|
| Benzophenone-3 (or oxybenzone)/131-57-7                              | C <sub>14</sub> H <sub>12</sub> O <sub>3</sub>  | 228.247          |  | 7.56 | 3.79                |
| Benzophenone-8 (or dioxybenzone)/131-53-3                            | C <sub>14</sub> H <sub>12</sub> O <sub>4</sub>  | 244.246          |  | 7.11 | 4.31                |
| Butyl-methoxy-dibenzoylmethane (or avobenzone)/70356-09-1            | C <sub>20</sub> H <sub>22</sub> O <sub>3</sub>  | 310.393          |  | 9.74 | 2.41                |
| Ethylhexyl-methoxycinnamate (or octyl methoxycinnamate)/5466-77-3    | C <sub>18</sub> H <sub>26</sub> O <sub>3</sub>  | 290.403          |  | –    | 5.80                |
| 2-Ethylhexyl-2-cyano-3,3 diphenylacrylate (or octocrylene)/6197-30-4 | C <sub>24</sub> H <sub>27</sub> NO <sub>2</sub> | 361.485          |  | –    | 7.35                |

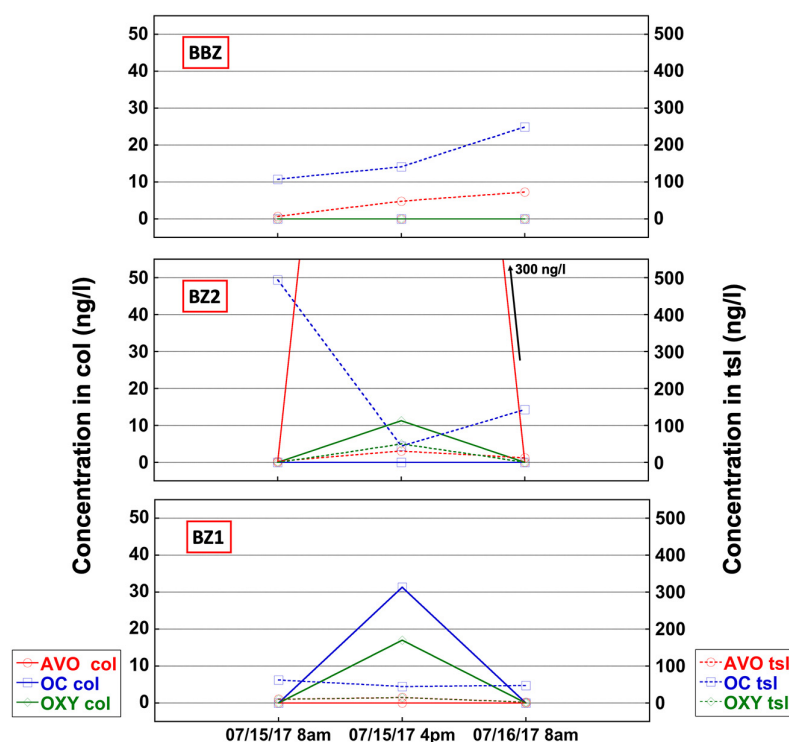


Fig. 3. Time evolution of organic UV filter concentrations at the three distances from shore line at Prophète Beach. Concentrations in water column (col) are compared to those in the top surface layer (tsl).

July 15th at 4:00 pm, while the two other sampling times were at 8:00 am the morning of the same day and 8:00 am the following day (July 16th). This clearly shows that the three UV filters are found in the water column only in the bathing zone (BZ) and during recreational activity. At 4:00 pm on July 15th, in the water column of BZ1 and BZ2, OXY, OC and AVO levels were 15, 30, 0 and 0, 10, 300 ng/L, respectively. At the same time, they were not detected beyond the bathing zone (BBZ, Fig. 2), and at the two other time points associated with low bathing activity there was also low occurrence. This trend was not as clearly observed in the top surface layer (tsl), where other factors certainly play a role, such as sun radiation, wind-induced water renewal, and tides (maximum tidal amplitude of 15 cm on July 15th). Faster photodegradation of the molecules certainly takes place, coupled with easier UV filter transport over long distances. OC has been proven to be photostable, unlike AVO and OXY, with OXY easily being photodegraded into 2,4-dimethylanisole under natural sunlight, especially in presence of natural organic matter (Santos et al., 2012; Manasfi et al., 2017). Indeed, OC was always detected at 8:00 am in the top surface layer at all the distances from the shoreline (50 to 500 ng/L), probably resulting from its release in the bathing zone the day before and its subsequent transport. This was not the case for the two other molecules that were always detected in lower concentrations in the top surface layer compared to the OC.

These results show not only the impact of bathing activity on the water chemistry, they also suggest that the residence time of the organic UV filters in the water column is quite short, since no detectable concentration was measured before, nor remained in the morning following peak attendance. Molecule degradation coupled with vertical and horizontal migration is probably the main driving factor. For this reason, in order to assess the overall UV filter release into the beach water, we focused further on the water composition during peak attendance at the three beaches, and also included the analysis of inorganic UV filters.

### 3.1.2. UV filter detection during peak bathing activity

The concentrations of Ti and Zn recovered in the seawater at the different distances (i.e., BZ1, BZ2, and BBZ) and depths (i.e., top surface layer and 40 cm) of the bathing zone of the three beaches give insight as to the occurrence of mineral UV filters suspended in the water (Fig. 4, Table 2). Since these elements occur naturally in the marine environment, it can be challenging to distinguish Ti and Zn originating from sunscreen. However, our hypothesis is that the chemical composition of the waters measured far beyond the bathing zone (BBZ), can be considered as the local background, while the waters in the bathing zone are more likely to be significantly impacted by recreational activity, and thus sun care products. Any enrichment in Zn or Ti in the bathing zone of the three studied sites as compared to BBZ concentrations could thus be attributed to mineral UV filters. Moreover, since resuspension of terrigenous materials from the sediments may likely occur in the bathing zone due to recreational activities and lead also to enrichment in those elements (Reed et al., 2017), distinction between natural and anthropogenic Zn and Ti was performed by tracking V element as a proxy of terrigenous materials (Gondikas et al., 2014).

In the three beaches studied, both Zn and Ti were detected in higher concentrations in the bathing zone, i.e. at BZ1 and BZ2, compared to the BBZ site. Prophète and La Lave displayed similar patterns of Ti concentration in the bathing zone, with a very high range of 70–500 µg/L in the water top surface layer and a lower range of 10–30 µg/L in the water column, while a much lower concentration was measured beyond the bathing zone (approx. 5 µg/L) (Table 2). Zn concentrations leveled off at lower values than Ti, around 10 µg/L, and were also more concentrated, at 80–90% in the bathing zone nearest the shore (i.e., BZ1). The Ti and Zn concentrations recovered in the waters of Pointe Rouge Beach indicated very few occurrences of mineral UV filters in the top surface layer, but similar concentrations to those observed at the other beaches were found in the water column. The geographic

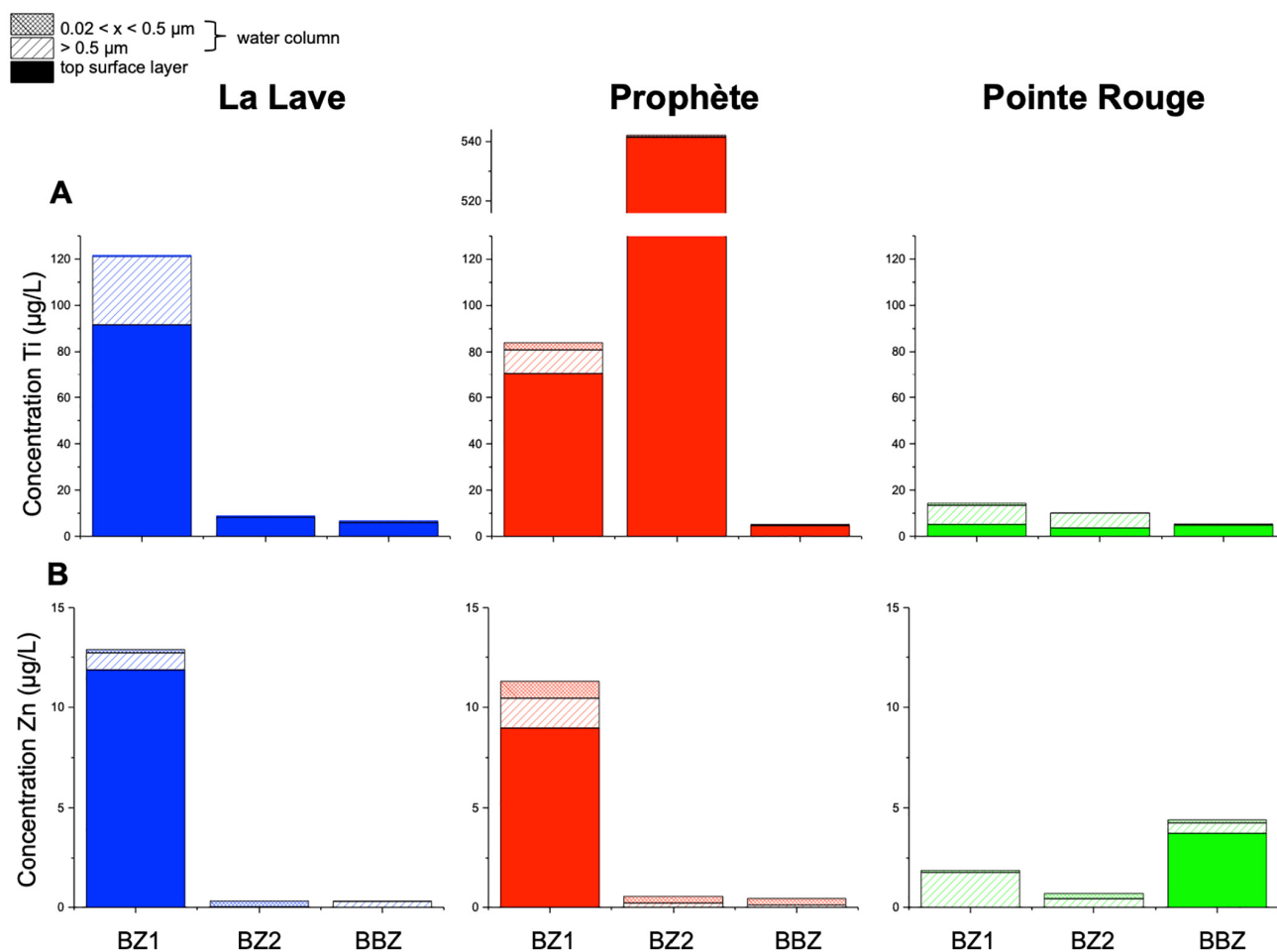


Fig. 4. Concentrations of Ti (A) and Zn (B) found in different water fractions at 4:00 pm on July 15, 2017 in Bathing Zone 1 (BZ1), Bathing Zone 2 (BZ2), and Beyond Bathing Zone (BBZ).

profile of the Pointe Rouge Beach makes it more exposed to local marine currents and winds than the two other beaches, which are more protected by artificial dikes. This likely implies a more constant renewal of the water's top surface layer and thus a more limited UV filter accumulation.

The sampled water column was further fractionated into two size classes in order to distinguish the nanoparticulate UV filters free in suspension ( $0.02 < x < 0.5 \mu\text{m}$  fraction) from those existing as a part of larger aggregates ( $>0.5 \mu\text{m}$  fraction). Indeed, this analysis revealed that the mineral UV filters are mostly concentrated in the larger size fraction,

i.e. behaving in an aggregated form (Fig. 4, Table 2). This size can correspond to either the original size of the sunscreen residues washed of the user's skin, or to the aggregation of the smaller mineral filters after their release in water. Salt-induced homo-aggregation of these filters or hetero-aggregation with natural particulate matter can indeed take place in such natural systems (Botta et al., 2011; Labille et al., 2015). Finally, the attribution of Ti and Zn patterns to the occurrence of mineral UV filters in seawater was well supported by Ti/V and Zn/V elemental ratios, with V being used as a proxy for geogenic materials (Figs. S1 and S2). If the enrichments in Ti and Zn in the bathing area were only

Table 2

Ti and Zn concentrations ( $\mu\text{g/L}$ ) measured in beach water for the three beaches, three distances from the shoreline and three compartments top surface layer (tsl), size fraction larger than  $0.5 \mu\text{m}$  and size fraction comprised between  $0.02$  and  $0.5 \mu\text{m}$ . Element concentrations are also converted in terms of equivalent  $\text{TiO}_2$  and  $\text{ZnO}$  concentrations, based on molar masses ( $\mu\text{g/L}$ ).

|                | Distance | La Lave |                    |                        | Prophète |                    |                        | Pointe Rouge |                    |                        |
|----------------|----------|---------|--------------------|------------------------|----------|--------------------|------------------------|--------------|--------------------|------------------------|
|                |          | tsl     | $>0.5 \mu\text{m}$ | $0.02-0.5 \mu\text{m}$ | tsl      | $>0.5 \mu\text{m}$ | $0.02-0.5 \mu\text{m}$ | tsl          | $>0.5 \mu\text{m}$ | $0.02-0.5 \mu\text{m}$ |
| Ti             | BZ1      | 91.7    | 29.4               | 0.5                    | 70.7     | 10.2               | 3.1                    | 5.1          | 8.3                | 0.8                    |
|                | BZ2      | 8.3     | 0.2                | 0.3                    | 541.4    | 0.3                | 0.4                    | 3.6          | 6.4                | 0.1                    |
|                | BBZ      | 5.9     | 0.6                | 0.2                    | 4.7      | 0.1                | 0.4                    | 4.8          | 0.5                | 0.1                    |
| Zn             | BZ1      | 11.9    | 0.8                | 0.2                    | 9.0      | 1.5                | 0.9                    | <LD          | 1.7                | 0.1                    |
|                | BZ2      | <LD     | 0.0                | 0.3                    | <LD      | 0.2                | 0.3                    | <LD          | 0.4                | 0.3                    |
|                | BBZ      | <LD     | 0.3                | 0.0                    | <LD      | 0.1                | 0.3                    | 3.7          | 0.5                | 0.2                    |
| $\text{TiO}_2$ | BZ1      | 152.9   | 49.1               | 0.9                    | 117.9    | 17.0               | 5.1                    | 8.6          | 13.9               | 1.4                    |
|                | BZ2      | 13.8    | 0.4                | 0.6                    | 903.1    | 0.6                | 0.7                    | 6.0          | 10.7               | 0.2                    |
|                | BBZ      | 9.9     | 1.0                | 0.4                    | 7.8      | 0.2                | 0.7                    | 8.0          | 0.8                | 0.2                    |
| ZnO            | BZ1      | 14.8    | 1.1                | 0.2                    | 11.2     | 1.8                | 1.1                    | <LD          | 2.2                | 0.1                    |
|                | BZ2      | <LD     | 0.0                | 0.3                    | <LD      | 0.3                | 0.4                    | <LD          | 0.5                | 0.3                    |
|                | BBZ      | <LD     | 0.4                | 0.0                    | <LD      | 0.1                | 0.4                    | 4.6          | 0.6                | 0.2                    |



due to natural sediment resuspension, Ti, Zn, and V would demonstrate a co-evolution. Here the elemental ratios followed trends with the different sampled distances similar to those of Ti and Zn alone, confirming that these enrichments are not of terrigenous origin. Moreover, the fact that the same pattern of Ti and Zn is obtained for the three beaches at the same time of peak recreational activity also supports the assumption that UV filters from the recreational area are the main contributors to this pattern.

Among the five organic UV filters analyzed in the beach water samples, DIOXY was never detected and OMC only occurred once, but OC, AVO, and OXY were often observed in the bathing water (Fig. 5, Table 3). Regarding the fractionation between the top surface layer and the water column or the spatial distribution with distance from the shoreline, there was no clear pattern for these molecules as was observed with the mineral filters. This is certainly due to the respective behavior and lifetime of the molecules at the two sampled water depths. OC and AVO were always detected in the bathing zone of the three beaches, totaling 75–425 ng/L and 10–350 ng/L, respectively. OC was generally equally distributed at both depths while AVO was mostly concentrated in the water column with a small amount in the top surface layer. OXY was only detected at Pointe Rouge and Prophète, ranging from 50 to 75 ng/L, with a significant contribution in the top surface layer. At La Lave and Prophète beaches, the occurrence of these molecules in the water column clearly showed again a higher concentration in the bathing zone, while they were not detected at BBZ. This was not as clear in the top surface layer, which may have been more impacted by winds that could rapidly push the UV filters offshore (e.g. OC and AVO in Prophète at BBZ).

### 3.2. Consumer habits regarding bathing and sunscreen use

For the 471 people interviewed at the three beaches, their habits regarding bathing activity are depicted in Fig. 6. Bathing is a very common practice, with >75% of respondents having a bath every time they go to the beach and <3% never bathing (Fig. 6). When going to the beach, attendees (40–60%) bathe 2.6 times on average and 91.5% of them practice whole body immersion. These data reflect how bathing provides an opportunity to refresh the body in a Mediterranean climate. Of note, the average air temperature measured over the week of the field campaign between 9:00 am and 7:00 pm was 25 °C (Fig. S3).

**Table 3**

Organic UV filter concentrations (ng/L) measured in beach water for the three beaches, three distances from the shoreline and two depth compartments top surface layer (tsl) and water column (col).

|     | Distance | La Lave |       | Prophète |       | Pointe Rouge <sup>a</sup> |       |
|-----|----------|---------|-------|----------|-------|---------------------------|-------|
|     |          | tsl     | col   | tsl      | col   | tsl                       | col   |
| OC  | BZ1      | 85.0    | 148.4 | 44.8     | 31.4  |                           | 149.8 |
|     | BZ2      | 419.9   | 0.0   | 44.4     | 0.0   |                           | 0.0   |
|     | BBZ      | 0.0     | 0.0   | 141.6    | 0.0   |                           | 141.4 |
| AVO | BZ1      | 10.3    | 12.8  | 15.3     | 0.0   |                           | 23.5  |
|     | BZ2      | 0.0     | 10.7  | 31.1     | 309.1 |                           | 0.0   |
|     | BBZ      | 0.0     | 0.0   | 48.1     | 0.0   |                           | 6.1   |
| OXY | BZ1      | 0.0     | 0.0   | 37.9     | 17.0  |                           | 78.3  |
|     | BZ2      | 0.0     | 0.0   | 50.0     | 11.3  |                           | 31.0  |
|     | BBZ      | 0.0     | 0.0   | <LD      | 0.0   |                           | 26.7  |
| OMC | BZ1      | 0.0     | 0.0   | <LD      | 0.0   |                           | 8.8   |
|     | BZ2      | 0.0     | 0.0   | <LD      | 0.0   |                           | 2.6   |
|     | BBZ      | 0.0     | 0.0   | <LD      | 0.0   |                           | 0.0   |

<sup>a</sup> Top surface layer samples were not analyzed for Pointe Rouge.

The use of sun care products on the beach is depicted in Fig. 7. On average, 68.4% of the interviewees use a sun care product and apply it to their skin 2.6 times per visit to the beach. Details on sunscreen application and bathing frequencies are depicted in Fig. S4. Of note, contrasting practices were observed between La Lave and the two other beaches, which might be related to the ethnic origins and socio-professional status of the respondents (Fig. 7). Only 50% of the interviewees at La Lave Beach, which is mostly attended by people living in the nearby working class neighborhoods and having North African as well as sub-Saharan roots, use sun care products. This is compared to 70% of attendees reporting sun care product use at the two other beaches which welcome tourists and city center inhabitants. However, no clear difference was observed regarding the part of body on which the sun care product is applied, with 80% of all consumers applying it to the whole body.

Among the list of UV filters authorized in Annex VI of the EU Cosmetic Regulation (European, 2009; Sobek et al., 2013), Fig. 8 displays their occurrence in the sun care products consumed by the interviewees at the three beaches. Some organic UV filters are clearly more favored by the manufacturers. The six most common being avobenzone > bemotrizinol > octocrylene > octisalate > ethylhexyl

40 cm depth  
top surface layer

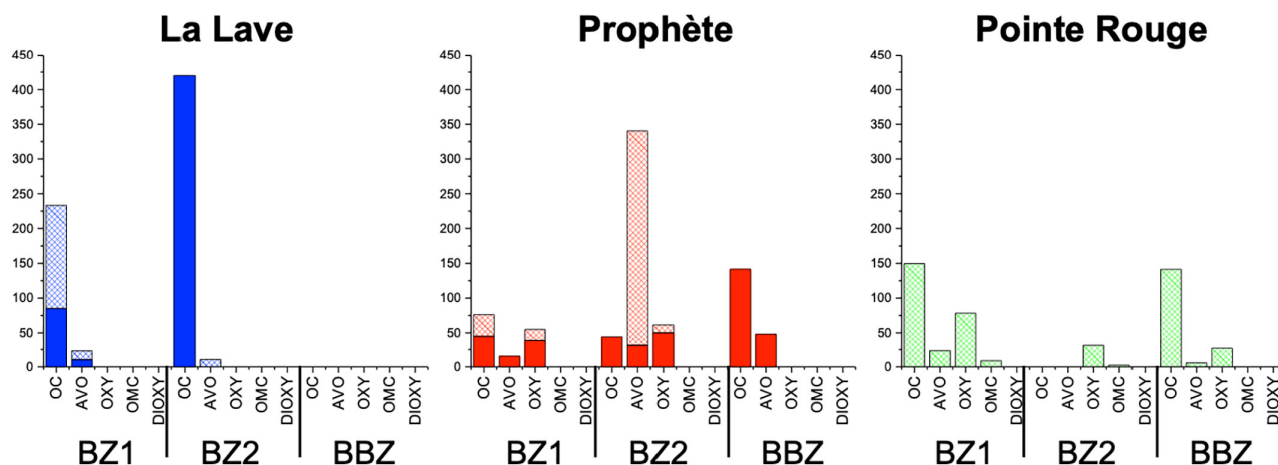


**Fig. 5.** Concentrations of organic UV filters (ng/L) OC, AVO, OXY, OMC, and DIOXY found in water at 40 cm depth and top surface layer at 4:00 pm on July 15, 2017 in Bathing Zone 1 (BZ1), Bathing Zone 2 (BZ2), and Beyond Bathing Zone (BBZ). Top surface layer samples were not analyzed for Pointe Rouge.

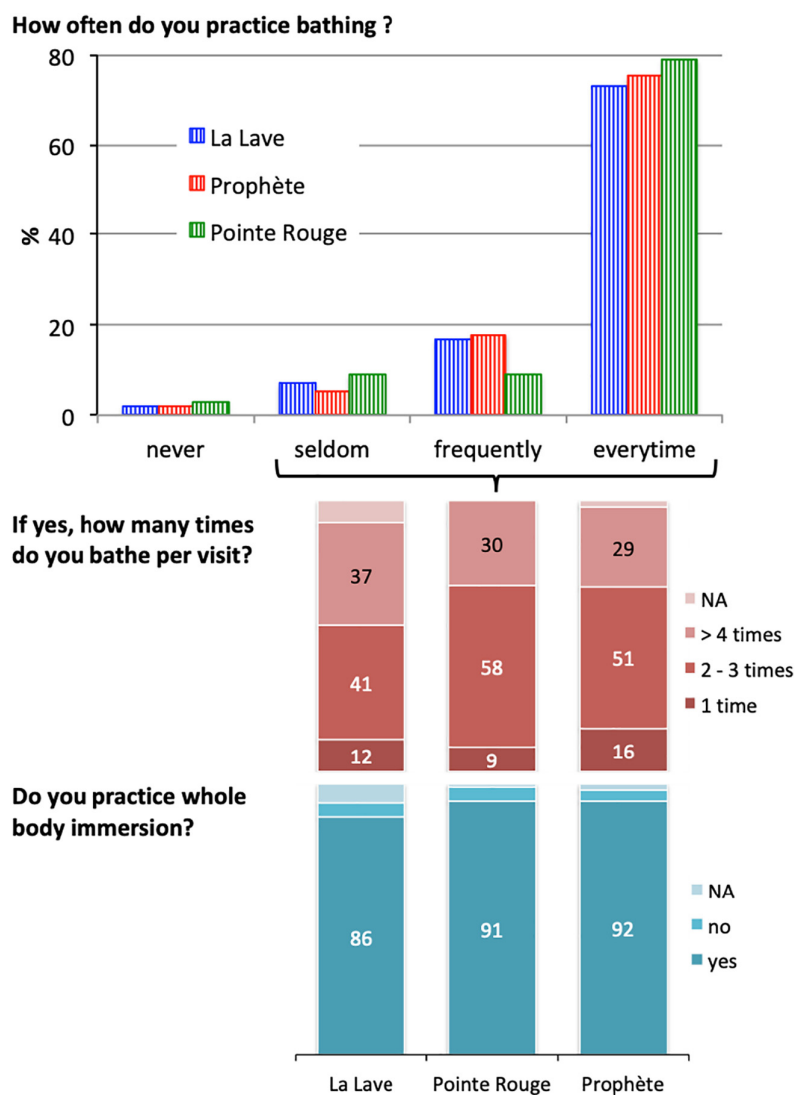


Fig. 6. Beachgoer habits regarding bathing activity at the beach.

triazone > homosalate, which are found in 78 to 31% of the products, respectively. These percentages logically correspond to protections against both UVB and UVA ranges which are usually desired together in the formulation. Nevertheless, since UVA specific filters are available

in a more limited choice for the manufacturers, the preferred candidate avobenzone is statistically more abundant on the market. The mineral UV filters,  $\text{TiO}_2$  and  $\text{ZnO}$ , were found in 19% and 2% of the products, respectively.

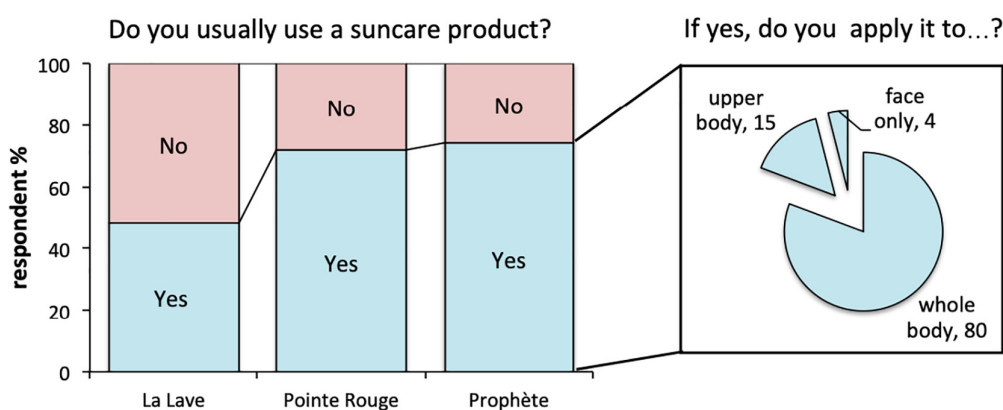
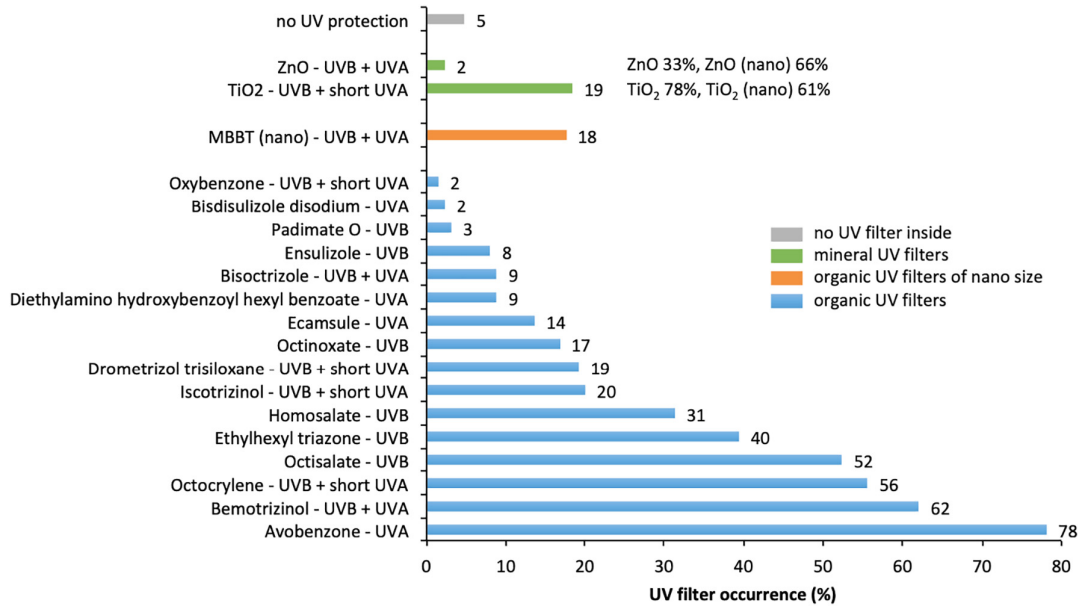


Fig. 7. Suncare product consumption habits on the beach. The inset presents average values over the three beaches studied.



**Fig. 8.** UV filter occurrence among the sunscreen products used on the three beaches. Data recovered from photographs of 124 products. Specific UV absorption range of each filter is also given as /filter name - UV range/. For mineral UV filters, the occurrence of non-nano and nano forms are given; an overlap exists for TiO<sub>2</sub> as both forms are labeled on certain products.

### 3.3. Estimation of the UV filter flux from consumer skin to beach water

#### 3.3.1. Average UV filter flux

From the data collected on the field through the consumer survey, an assessment of the daily UV filter mass used on the consumer skin and possibly transferred to the beach water was performed. Here any retention of the product on the skin through bathing was not taken into account, so that a worst-case contamination scenario could be estimated. The flux of the sunscreen product,  $m_{\text{sunscreen}}$ , consumed and transferred to the bathing water can be obtained from Eq. (1).

$$m_{\text{sunscreen}} = N \cdot \chi \cdot \gamma \cdot m \quad (1)$$

where  $N$  is the total number of people attending the beach,  $\chi$  is the % of people that reported using sunscreen products before bathing,  $\gamma$  is the average number of times the product is applied to the skin per visit to the beach, and  $m$  is the mass of product consumed during each application to the entire body. The lowest and highest values recovered from the survey over the three beaches were used for  $\chi$  and  $\gamma$  considerations to obtain a reasonable range for  $m_{\text{sunscreen}}$ . People who reported applying a sunscreen product before bathing represented 29, 47 and 53% of the attendees at La Lave, Prophète, and Pointe Rouge beaches, respectively, and the average number of applications was 2.8, 2.4 and 2.9 respectively. A daily beach attendance of  $N = 3000$  people was used for this estimation as it is typical for the Prophète Beach studied in this work (Fig. S5). Finally,  $m = 15$  g was taken as the mass of sunscreen product used for each application to the entire body (Ficheux et al., 2016). We thus obtained:

$$m_{\text{sunscreen}} = 52.5 \pm 16.5 \text{ kg/day} = 367 \pm 114 \text{ kg/week} \\ = 1.45 \pm 0.45 \text{ t/month} \quad (2)$$

From  $m_{\text{sunscreen}}$ , the corresponding mass of UV filter  $i$  involved,  $m_{UVi}$ , can be obtained from the composition of the products used, following Eq. (3)

$$m_{UVi} = \%_{UVi} \cdot \phi_{UVi} \cdot m_{\text{sunscreen}} \quad (3)$$

where  $\%_{UVi}$  corresponds to the occurrence of the UV filter  $i$  within the panel of sunscreen product compositions used, given in Fig. 8, and  $\phi_{UVi}$  is

the average mass fraction of the UV filter  $i$  used in the product formulation.  $\phi_{UVi}$  is not usually provided in Europe on the product packaging, only the list of components. Here, we propose a range  $0.03 < \phi_{UVi} < 0.1$  as a reasonable estimation, considering literature data (Botta et al., 2011; Matta et al., 2019), maximum UV filter concentrations authorized by EU regulation, and the fact that most of the sunscreen products registered in our survey display a high SPF ranging from 30 to 50+. From these values of  $\%_{UVi}$ ,  $\phi_{UVi}$  and  $m_{\text{sunscreen}}$ , the average and a relevant range of  $m_{UVi}$  were obtained.

These values are presented in Table 4 for the six most abundant organic UV filters and the mineral filters, ZnO and TiO<sub>2</sub>. Estimated consumption of organic UV filters is more than 1 kg/day each, and 83 and 633 g/day for the mineral filters, ZnO and TiO<sub>2</sub> respectively. Summing all the UV filters quantified in Fig. 8 results in a total mass of 15.7 kg/day potentially released into the beach water. This large quantity of cosmetic product may be released or remain on the skin through bathing activity, depending on the retention factor of the product. This value accounts for a beach welcoming 3000 users per day.

#### 3.3.2. Predicted environmental concentration and measured concentration

From the  $m_{UVi}$ , based on our survey analysis, we calculated a predicted environmental concentration for the UV filter  $i$  in the bathing

**Table 4**

UV filter mass consumed and potentially entering the bathing area, given in g/day, with average ( $m_{UVi}$  av), and total range. These values account for a daily attendance of 3000 beachgoers. The total mass is obtained from the sum of all the UV filters quantified in Fig. 8.

| UV filter $i$       | $m_{UVi}$ av | $m_{UVi}$ range |
|---------------------|--------------|-----------------|
| Avobenzene          | 2669         | 845–5398        |
| Bemotrizinol        | 2119         | 671–4285        |
| Octocrylene         | 1899         | 601–3840        |
| Octisalate          | 1789         | 566–3617        |
| Ethylhexyl triazone | 1348         | 427–2727        |
| Homosalate          | 1073         | 340–2170        |
| TiO <sub>2</sub>    | 633          | 200–1280        |
| ZnO                 | 83           | 26–167          |
| Total mass          | 15,742       | 4982–31,829     |

water,  $PEC_{UVi}$  (Eq. (4))

$$PEC_{UVi} = m_{UVi}/V \quad (4)$$

where  $V$  is the volume of water in the bathing zone.

Our aim was to investigate whether  $PEC_{UVi}$  could be compared to the actual UV filter concentrations  $C_{UVi}$ , measured in this work in the bathing zone, and used to interpret any eventual divergence in terms of UV filter retention, release, or fate. The estimation of  $PEC_{UVi}$  was only completed for the Prophète Beach, where the bathing zone is delimited between a dike and the shoreline, facilitating the estimation of  $V$ . We used 85 m length x 64 m width and bathymetric data ranging from 0 to 3 m depth, giving 4530 cubic meters of water (Fig. S8). In a coastal system such as this, constant water renewal should be considered as a source of dilution, but here water renewal is limited by the dike. To compensate for this effect, we used an average water residence time of 24 h (Basterretxea et al., 2007), giving a renewal of 29% of this volume after 7 h of recreation time cumulated at the 4:00 pm sampling time. This gave a total water column volume of  $V_{col} = 5850 \text{ m}^3$ . As for the top surface layer, the sampling consisted of roughly 1 cm of water layer thickness and the measured surface area of the bathing zone was  $4114 \text{ m}^2$ . This gave  $V_{tsl} = 53 \text{ m}^3$  including 29% renewal.

In order to compare our estimation of the filter concentration,  $PEC_{UVi}$ , based on the survey, to the actual UV filter concentration measured in the bath water,  $C_{UVi}$ ,  $PEC_{UVi}$  was further refined regarding the actual attendance and bathing activity at Prophète Beach during the sampling time. Indeed, the declarations from our survey reflect the users' habits, and thus do not take into account any punctual events that may disturb those habits, such as bad weather. On July 15th, 2017, the day of water sampling at the recreational peak, a cumulated beach attendance of  $N = 2700$  people was measured at 4:00 pm, which is close to the average daily attendance (Fig. S5). However, the actual number of bathers was unusually low because of the colder water temperature resulting from cold and windy weather the previous day (Figs. S5–7) (water temperature on 07/15/17 =  $18^\circ\text{C}$ ). Our daily survey during the entire week enabled us to estimate that bath practice was two times lower on July 15th than on warm days on average. A correction factor of 0.5 was thus applied to  $m_{suncare}$ , to obtain  $PEC_{UVi}$ , on July 15th at 4:00 pm, giving Eq. (5) for water column.

$$PEC_{UVi, \text{July } 15.4 \text{ pm}} = \frac{\%_{UVi} \cdot \phi_{UVi} \cdot N \cdot \chi \cdot \gamma \cdot m}{V} \times 0.5$$

$$= \frac{\%_{UVi} \times 0.065 \times 2700 \times 0.47 \times 2.4 \times 15 \times 10^6 \times 0.5}{5850 \times 10^3} \quad (5)$$

$C_{UVi}$  values are obtained from Tables 3 and 4. Note that the  $C_{UVi}$  values for  $\text{TiO}_2$  and  $\text{ZnO}$  were calculated by subtracting the geochemical

background measured in BBZ from the value measured in BZ1. A recovery value  $\alpha_{UVi}$  could then be calculated in both the water column and the top surface layer by normalizing  $PEC_{UVi, \text{July } 15, 4 \text{ pm}}$  to  $C_{UVi}$  (Table 5). If  $\alpha_{UVi} \approx 100\%$  was recovered, then the worst-case scenario previously described, where the totality of UV filters consumed are released into the bathing water, would be reality. Here, relatively high values of  $\alpha_{UVi}$  were obtained for the mineral UV filters, with 49 and 19% of  $\text{TiO}_2$  recovered in the water column and top surface layer, respectively. The same order of recovery was obtained for  $\text{ZnO}$  in the water column ( $\alpha_{\text{ZnO, col}} = 31.7\%$ ) but a lower amount was detected in the top surface layer ( $\alpha_{\text{ZnO, tsl}} = 1.3\%$ ). This may be attributed to the very low number of products containing  $\text{ZnO}$  UV filters reported in our survey ( $\%_{\text{ZnO}} = 3\%$ ), which resulted in a limited range of cosmetic formulation types. Apparently these few products dispersed rather well in the water column. As for  $\text{TiO}_2$  mineral UV filters,  $\%_{\text{TiO}_2} = 17\%$  resulted in a wider variety of environmental fates, leading to the filter occurrence in both the water column and the top surface layer. Different causes may be discussed to explain why the UV filter recovery is not complete. The rapid sedimentation of the UV filters at the bottom of the water column once washed off the skin is rather unlikely because the water in the bathing zone is constantly agitated during the recreation peak. The retention factor of the cosmetic product on the consumer skin certainly plays a major role in  $\alpha_{UVi}$ . Values from 25 to 50% have been proposed (Danovaro et al., 2008; Slijkerman and Keur, 2018), which fall in the same order as the  $\alpha_{\text{TiO}_2}$  and  $\alpha_{\text{ZnO}}$  values obtained here.

As for the organic UV filters, the concentrations measured,  $C_{UVi}$ , fall in the ng/L range. Despite these concentrations being in agreement with the existing literature (Tashiro and Kameda, 2013; Tovar-Sanchez et al., 2013; Bargar et al., 2015; Rodriguez et al., 2015; Downs et al., 2016; Tsui et al., 2017; Kung et al., 2018; Mitchelmore et al., 2019), they fall two orders of magnitude below our predicted concentrations  $PEC_{UVi}$ . Recoveries as low as 0.3, 0.15, 0.02 and 0.0% were obtained for OXY, AVO, OC and OMC respectively in the water column and always 0.0% in the top surface layer. Such divergence with the mineral UV filters was not expected. Even if photodegradation of these molecules is a known mechanism, here, water sampling was realized precisely during the peak of recreation, which should limit this effect in the present results. Our hypothesis is that the retention factor on the skin for these molecules is much higher since they are known to penetrate through the skin barrier (Matta et al., 2019). A few field campaigns focusing on both mineral and organic UV filters have already shown, in agreement with our data, that mineral UV filters are found in bath water in concentrations 1000 times higher than organic UV filters (Tovar-Sanchez et al., 2013; Reed et al., 2017). However, this is the first time that the proportion of both types of UV filters at the time of potential release (i.e. during consumer bathing), is known. These results clearly demonstrate the contrasted fates of mineral and organic UV filters once spread on the skin.

#### 3.4. Consumer awareness and manufacturer choice

During the survey,  $66 \pm 6\%$  of the interviewees believed that suncare products do alter the quality of the bathing water, arguing first that the product is washed off and floats as an oily surface layer (28%), that the chemical components involved are of concern (37%), can pollute the environment (12%) or are bad for the aquatic fauna and flora (13%) (Fig. 9). A little >19% of the interviewees were not aware of the issue, as they did not have any opinion. Finally, a minority but non-negligible fraction of the respondents,  $14 \pm 6\%$ , think that suncare products have no effect on bathing water quality because the sea is too large and dilution effects minimize the impact. Some of them also argued that the sunscreen composition is certainly adapted by the manufacturer or regulators to take this into account. These results indicate a certain discrepancy between the claimed awareness of the consumers regarding the environmental impact of suncare products and the quasi-total absence of any product labeled as eco-friendly among those actually

**Table 5**

Estimation of UV filters fluxes on Prophète Beach on Saturday 07/15/17, 4:00 pm, in terms of occurrence among the products surveyed  $\%_{UVi}$ , estimated mass involved  $m_{UVi}$ , predicted environmental concentration in bath water  $PEC_{UVi}$ , and actual concentrations measured  $C_{UVi}$  at 40 cm depth (col) and in the top surface layer (tsl).

| UV filter i                | $\%_{UVi}$ | $m_{UVi}/\text{g}$ | $PEC_{UVi}/\mu\text{g/L}$ | $C_{UVi}/\mu\text{g/L}$ | $\alpha_{UVi}/\%$ recov. |
|----------------------------|------------|--------------------|---------------------------|-------------------------|--------------------------|
| $\text{TiO}_{2\text{col}}$ | 17         | 251                | 43                        | 21                      | 49.0                     |
| $\text{TiO}_{2\text{tsl}}$ |            |                    | 4724                      | 117–895                 | 19.0                     |
| $\text{ZnO}_{\text{col}}$  | 3          | 44                 | 7.6                       | 2.4                     | 31.7                     |
| $\text{ZnO}_{\text{tsl}}$  |            |                    | 834                       | 11                      | 1.3                      |
| $\text{AVO}_{\text{col}}$  | 80         | 1181               | 202                       | 0.3                     | 0.15                     |
| $\text{AVO}_{\text{tsl}}$  |            |                    | 22,230                    | 0.015–0.05              | 0                        |
| $\text{OC}_{\text{col}}$   | 57         | 842                | 144                       | 0.03                    | 0.02                     |
| $\text{OC}_{\text{tsl}}$   |            |                    | 15,840                    | 0.04–0.14               | 0                        |
| $\text{OMC}_{\text{col}}$  | 17         | 251                | 43                        | 0                       | 0                        |
| $\text{OMC}_{\text{tsl}}$  |            |                    | 4724                      | 0                       | 0                        |
| $\text{OXY}_{\text{col}}$  | 2          | 30                 | 5                         | 0.015                   | 0.30                     |
| $\text{OXY}_{\text{tsl}}$  |            |                    | 556                       | 0.04–0.05               | 0.01                     |



## Do you think that sun care products can impact the quality of marine bath water ?

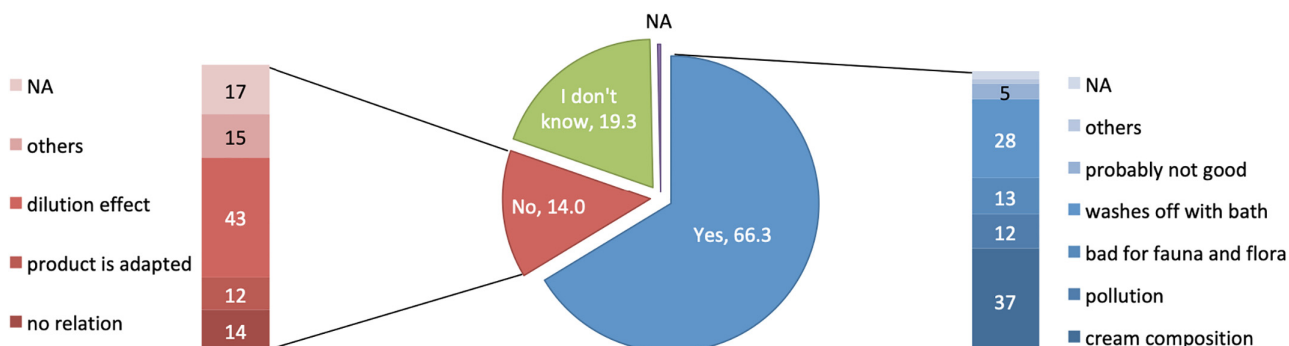


Fig. 9. Answers of the interviewees to the question "Do you think that sun care products can impact the quality of marine bath water?"

consumed (only 2 out of 170 products). Product composition comes as the criteria number 4 (12% of the consumers) in selecting a sun care product (Fig. 10c). However, it shall be noted that only 3% of those respondents actually mention environmental concerns, while 19% of them worry about the product composition because of a possible impact on their own health. More than half, 57%, did not give any explanation and 22% mentioned their preference for the products labeled as organic (BIO). For 73% of respondents, the sun protection factor (SPF) is their paramount consideration in selecting and buying a sun care product (Fig. 10c). The distribution of sunscreen SPF labels found on the packaging of the interviewees revealed a clear majority of medium and high

levels of protection, namely SPF 30 and SPF 50+ (Fig. 10a). This likely reflects the different expectations from the users, with high sun protection wanted on the one hand, and tanning preferred with a lower sun protection on the other hand. It also indicates a real awareness of the potential harmful effects of the sun. Sunscreens with SPF values between 15 and 20 were less preferred (13%), probably because the protection they provide is considered too low. The cosmetic products with SPF values from 4 to 10, found in 6% of the panel, were not considered as sunscreens. Likewise for the UV filter-free skin care products, such as monoï or other moisturizing oils, that constituted 4% of the products consumed.

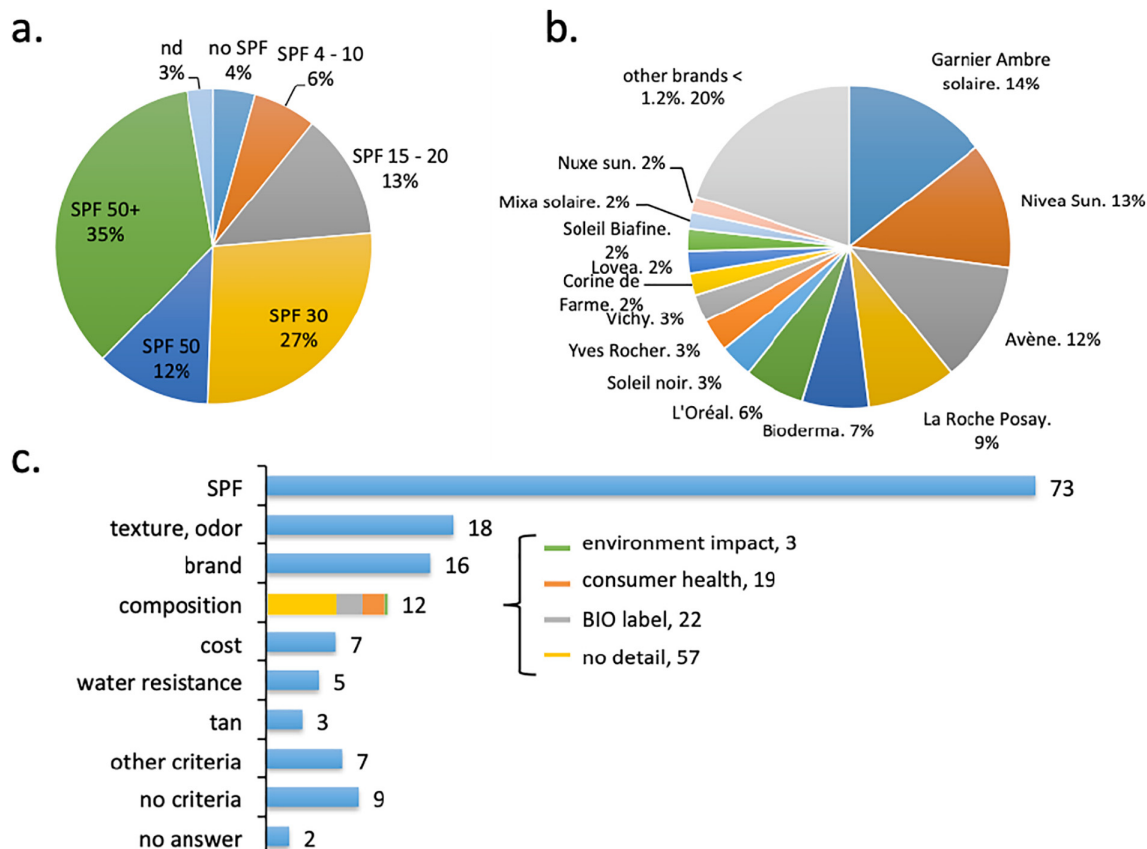


Fig. 10. Distribution in % of the sun protection factors (SPF) of the sun care products used on the beach (a), of the cosmetic brands providing these products (b), and of the consumer's three primary criteria for selecting a sun care product. Data shown are averages over the three beaches studied.

The frequency of different sunscreen product brands used on the beach is depicted in Fig. 10b. It shows that >50% of the local sunscreen product consumption is dominated by only 5 well-known brands, Garnier Ambre Solaire (L'Oréal), Nivea Sun (Beiersdorf), Avene (Lab. Pierre Fabre), La Roche Posay (L'Oréal) and Bioderma (NAOS), in accordance with the French sunscreen market (Euromonitor, 2015).

This suggests that consumers buy the most well-known brands, those that are more heavily advertised, or those that are the most present at points of sale. Looking for effective sun protection, and lacking means of comparison, some consumers may move toward these well-known brands because they are often associated with efficacy. Brand comes as the third most important criteria in selecting a sunscreen product, with 16% of the consumers actively paying attention to the brand they buy (Fig. 10c). Lacking the advertising influence and financial means of many well-known brands, organic (BIO) and/or eco-designed products are often distributed by small or medium businesses which is the most likely reason for why they represent only a minority of the products consumed on the beach.

Of note, only mineral UV filters are currently allowed within products labeled as organic (BIO). This agrees with the minority of this type of filter recovered in Fig. 8, namely 19% and 2% of products containing TiO<sub>2</sub> and ZnO respectively. ZnO is used more rarely within the European sunscreen market, partly due to questions regarding its high solubility and bioavailability, which may lead to higher risk. TiO<sub>2</sub> has been widely used as the main mineral option for organic (BIO) UV filters. Nevertheless, its under representation among the products used here suggests that manufacturers still prefer synthetic organic UV filters. This is likely due to easier formulation processes, preferred texture, and simpler regulation. Indeed, mineral UV filters constitute a significant particle loading in the cosmetic formulation, which increases the challenge in stabilizing the product emulsion (Tyner et al., 2011), results in a less appreciated sensation on skin, and product whiteness in some cases. In addition, the ultrafine particles used to create more transparent formulations often fall under the definition of a nanomaterial, nanosubstance or nanoform and formulators using such materials have to deal with complex and continually changing local regulations (SCCP, 2008; French-Government, 2012; Sobek et al., 2013; SCCS, 2014; REACH, 2018). Of note, 61% of the products containing TiO<sub>2</sub> UV filters were labeled with the (nano) form on their component list, while 78% were labeled as containing TiO<sub>2</sub> without the (nano) characteristic (Fig. 8). The sum of both labels corresponds to 139% of the products containing TiO<sub>2</sub>. The overlap is due to manufacturers labeling both nano and non-nano forms on the same packaging, which is likely false and misleading. This illustrates some of the difficulties encountered by the manufacturers and product formulators in characterizing their material size in order to respect regulation. Nevertheless, since regulation should contribute to making our environment safer, the balance between organic and mineral UV filters should be further evaluated in terms of their respective cost/benefit ratio.

#### 4. Conclusion

A field campaign was carried out during the summer of 2017 at three beaches in Marseille along the French Mediterranean coast, with the aim of quantifying the fluxes of UV filters released from the sunscreen on the beachgoer's skin to the bathing seawater.

In the three beaches studied, both Zn and Ti were detected in higher concentrations in the bathing zone than beyond it, and behaved independently of terrigenous materials. Their occurrence could be attributed to the presence of TiO<sub>2</sub> and ZnO mineral UV filters in the seawater, with ranges of 100–900 and 20–50 µg/L for TiO<sub>2</sub> and 10–15 and 1–3 µg/L for ZnO in the top surface layer and in the water column, respectively.

Octocrylene, avobenzone, and oxybenzone were mostly observed in the bathing water during peak recreation time only at concentration ranges of 75–425, 10–350 and 50–75 ng/L respectively. They followed

diverging behaviors likely due to multiple factors like molecule lifetime, water currents, transport in the water column vs surface layer, and distance from the shoreline.

The environmental concentrations of UV filters evidenced here can be put into perspective by considering the predicted no effect concentrations (NOEC) for marine organisms. Slijkerman and Keur recently reviewed these values for different UV filters from the existing literature (Slijkerman and Keur, 2018). The NOEC for nano-TiO<sub>2</sub> on crustacean mortality at 48 h of exposure was 1000 µg/L, while it was 10 µg/L for nano-ZnO at 72 h of exposure. The NOEC for OC on mollusks and on algal growth inhibition at 96 h of exposure was 20 and 40 µg/L, respectively. These values are higher than the UV filter concentrations measured here in seawater, suggesting that no acute effect would be expected on these living organisms. Nevertheless, since the NOEC values only represent short-term exposures, questions remain regarding UV filter chronic effects in the marine environment neighboring recreational areas.

Despite the fact that consumer awareness of this issue is rising, with 66% of the interviewees considering that sunscreen products can impact the quality of bathing water, the sunscreen composition does not appear to be a priority concern for them when buying a product. The protection efficacy of the product against sun radiation remains their paramount consideration. We were able to estimate the product quantities used on the consumer skin and those being possibly transferred to the bathing water, giving an average mass of 52 kg/day or 1.4 t/month of sunscreen products for a beach attended by 3000 people daily. Their composition was determined from the products used by the interviewees, revealing a cumulated mass of about 15.7 kg of UV filters per day, with a net majority of organic UV filters, at the expense of mineral ones found in only 20% of the products.

Comparing our predicted environmental concentration of UV filters to the actual concentrations measured in bathing water revealed two distinct scenarios for mineral and organic filters. About 30 to 49% of the estimated mineral UV filter flux was effectively quantified in the bathing water, in the water column. This recovery is in agreement with the approaches developed here and suggests a retention factor of the product on the skin lower than 70%, in agreement with the literature (Danovaro et al., 2008; Slijkerman and Keur, 2018). On the other hand, our recovery in organic UV filters is much lower, ranging between 0 and 0.3%. This suggests a much higher retention factor for organic molecules on the skin, possibly due to trans-cutaneous internalization.

These results suggest that a new compromise could come into consideration when selecting sunscreen products, between mineral UV filters released to the marine environment and organic UV filters that are able to pass the skin barrier. These two aspects should be heavily weighed in future attempts toward safer-by-design sunscreen products that will have minimal impact on both human and environmental health.

#### Declaration of competing interest

The authors declare that they have no known competing financial interests or personal relationships that could have appeared to influence the work reported in this paper.

#### Acknowledgements

This work was funded by Labex DRIHM (ANR-11-LABX-0010) funded by the French Government's Investissements d'Avenir Program, through OHM Littoral Méditerranéen. It was also a contribution to the Cofund DOC2AMU fellowship and to the Labex Serenade (ANR-11-LABX-0064) funded by the French Government's "Investissements d'Avenir" ANR program, through the A\*MIDEX project (ANR-11-IDEX-0001-02). The authors acknowledge people who contributed to the field survey (CEREGE: Camille De Garidel; ESPACE: colleagues from HSM laboratory) and to the chemical analyses (LCE: Sylvain Ravier).

## Appendix A. Supplementary data

Supplementary data to this article can be found online at <https://doi.org/10.1016/j.scitotenv.2019.136010>.

## References

- ASTM-International, 2013. Standard Practice for the Preparation of Substitute Ocean Water. ASTM D1141 - 98. ASTM International.
- Auffan, M., Pedetour, M., Rose, J., Masion, A., Ziarelli, F., Borschneck, D., Chaneac, C., Botta, C., Chaurand, P., Labille, J., Bottero, J.Y., 2010. Surface structural degradation of TiO<sub>2</sub>-based nanomaterial used in cosmetics. *Environ. Sci. Technol.* 44 (7), 2689–2694.
- Bargar, T.A., Alvarez, D.A., Garrison, V.H., 2015. Synthetic ultraviolet light filtering chemical contamination of coastal waters of Virgin Islands national park, St. John, US Virgin Islands. *Mar. Pollut. Bull.* 101 (1), 193–199.
- Basterretxea, G., Garces, E., Jordi, A., Angles, S., Maso, M., 2007. Modulation of nearshore harmful algal blooms by in situ growth rate and water renewal. *Mar. Ecol. Prog. Ser.* 352, 53–65.
- Bluthgen, N., Zucchi, S., Fent, K., 2012. Effects of the UV filter benzophenone-3 (oxybenzone) at low concentrations in zebrafish (*Danio rerio*). *Toxicol. Appl. Pharmacol.* 263 (2), 184–194.
- Botta, C., Labille, J., Auffan, M., Borschneck, D., Miche, H., Cabie, M., Masion, A., Rose, J., Bottero, J.-Y., 2011. TiO<sub>2</sub>-based nanoparticles released in water from commercialized sunscreens in a life-cycle perspective: structures and quantities. *Environ. Pollut.* 159 (6), 1543–1548.
- Calafat, A.M., Wong, L.Y., Ye, X.Y., Reidy, J.A., Needham, L.L., 2008. Concentrations of the sunscreen agent benzophenone-3 in residents of the United States: National Health and Nutrition Examination Survey 2003–2004. *Environ. Health Perspect.* 116 (7), 893–897.
- Danovaro, R., Bongiorno, L., Corinaldesi, C., Giovannelli, D., Damiani, E., Astolfi, P., Greci, L., Pusceddu, A., 2008. Sunscreens cause coral bleaching by promoting viral infections. *Environ. Health Perspect.* 116 (4), 441–447.
- Downs, C.A., Kramarsky-Winter, E., Segal, R., Fauth, J., Knutson, S., Bronstein, O., Ciner, F.R., Jeger, R., Lichtenfeld, Y., Woodley, C.M., Pennington, P., Cadenas, K., Kushmaro, A., Loya, Y., 2016. Toxicopathological effects of the sunscreen UV filter, oxybenzone (benzophenone-3), on coral planulae and cultured primary cells and its environmental contamination in Hawaii and the US Virgin Islands. *Arch. Environ. Contam. Toxicol.* 70 (2), 265–288.
- E. C. REACH, 2018. Commission regulation (EU) 2018/1881 of 3 December 2018 amending Regulation (EC) No 1907/2006 of the European Parliament and of the Council on the Registration, Evaluation, Authorisation and Restriction of Chemicals (REACH) as regards Annexes I, III, VI, VII, VIII, IX, X, XI, and XII to address nanoforms of substances. *Off. J. Eur. Union* 2018 (/1881).
- Euromonitor, 2015. Sunscreen in France. Passport. E. International.
- European, C., 2009. Regulation (EC) No 1223/2009 of the European Parliament and of the Council of 30 November 2009 on cosmetic products. *Off. J. Eur. Union* 1223 (/2009).
- Faure, B., Salazar-Alvarez, G., Ahnizay, A., Villaluenga, I., Beriozabal, G., De Miguel, Y.R., Bergstrom, L., 2013. Dispersion and surface functionalization of oxide nanoparticles for transparent photocatalytic and UV-protecting coatings and sunscreens. *Sci. Technol. Adv. Mater.* 14 (2).
- Fel, J.P., Lacherez, C., Bensetra, A., Mezzache, S., Beraud, E., Leonard, M., Allemand, D., Ferrier-Pages, C., 2019. Photochemical response of the scleractinian coral *Stylophora pistillata* to some sunscreen ingredients. *Coral Reefs* 38 (1), 109–122.
- Ficheux, A.S., Wesolek, N., Chevillotte, G., Roudot, A.C., 2015. Consumption of cosmetic products by the French population. First part: frequency data. *Food Chem. Toxicol.* 78, 159–169.
- Ficheux, A.S., Chevillotte, G., Wesolek, N., Morisset, T., Dornic, N., Bernard, A., Bertho, A., Romanet, A., Leroy, L., Mercat, A.C., Creusot, T., Simon, E., Roudot, A.C., 2016. Consumption of cosmetic products by the French population second part: amount data. *Food Chem. Toxicol.* 90, 130–141.
- French-Government, 2012. Décret no 2012-232 du 17 février 2012 relatif à la déclaration annuelle des substances à l'état nanoparticulaire pris en application de l'article L. 523-4 du code de l'environnement. Décret no 2012-232. D. D. D. MINISTÈRE DE L'ÉCOLOGIE, DES TRANSPORTS ET DU LOGEMENT. *Journal Officiel de la République Française* 43, 2863 4.
- Giokas, D.L., Salvador, A., Chisvert, A., 2007. UV filters: from sunscreens to human body and the environment. *TriAc Trends Anal. Chem.* 26 (5), 360–374.
- Gondikas, A.P., Kammer, F. von der, Reed, R.B., Wagner, S., Ranville, J.F., Hofmann, T., 2014. Release of TiO<sub>2</sub> nanoparticles from sunscreens into surface waters: a one-year survey at the Old Danube recreational lake. *Environ. Sci. Technol.* 48 (10), 5415–5422.
- Gondikas, A., Kammer, F. von der, Kaegi, R., Borovinskaya, O., Neubauer, E., Navratilova, J., Praetorius, A., Cornelis, G., Hofmann, T., 2018. Where is the nano? Analytical approaches for the detection and quantification of TiO<sub>2</sub> engineered nanoparticles in surface waters. *Environ. Sci. Nano* 5 (2), 313–326.
- Gulson, B., McCall, M., Korsch, M., Gomez, L., Casey, P., Oytam, Y., Taylor, A., McCulloch, M., Trotter, J., Kinsley, L., Greenoak, G., 2010. Small amounts of zinc from zinc oxide particles in sunscreens applied outdoors are absorbed through human skin. *Toxicol. Sci.* 118 (1), 140–149.
- Gulson, B., Wong, H., Korsch, M., Gomez, L., Casey, P., McCall, M., McCulloch, M., Trotter, J., Stauber, J., Greenoak, G., 2012. Comparison of dermal absorption of zinc from different sunscreen formulations and differing UV exposure based on stable isotope tracing. *Sci. Total Environ.* 420, 313–318.
- Hopkins, Z.R., Blaney, L., 2016. An aggregate analysis of personal care products in the environment: identifying the distribution of environmentally-relevant concentrations. *Environ. Int.* 92–93, 301–316.
- Imanishi, A., Okamura, T., Ohashi, N., Nakamura, R., Nakato, Y., 2007. Mechanism of water photooxidation reaction at atomically flat TiO<sub>2</sub> (rutile) (110) and (100) surfaces: dependence on solution pH. *J. Am. Chem. Soc.* 129 (37), 11569–11578.
- Keller, A.A., Vosti, W., Wang, H.T., Lazareva, A., 2014. Release of engineered nanomaterials from personal care products throughout their life cycle. *J. Nanopart. Res.* 16 (7).
- King, D.M., Liang, X.H., Burton, B.B., Akhtar, M.K., Weimer, A.W., 2008. Passivation of pigment-grade TiO<sub>2</sub> particles by nanothick atomic layer deposited SiO<sub>2</sub>(2) films. *Nanotechnology* 19 (25).
- Kung, T.A., Lee, S.H., Yang, T.C., Wang, W.H., 2018. Survey of selected personal care products in surfacewater of coral reefs in Kenting National Park, Taiwan. *Sci. Total Environ.* 635, 1302–1307.
- Kunz, P.Y., Fent, K., 2006. Multiple hormonal activities of UV filters and comparison of in vivo and in vitro estrogenic activity of ethyl-4-aminobenzoate in fish. *Aquat. Toxicol.* 79 (4), 305–324.
- Kunz, P.Y., Fent, K., 2009. Estrogenic activity of ternary UV filter mixtures in fish (*Pimephales promelas*) - an analysis with nonlinear isobolograms. *Toxicol. Appl. Pharmacol.* 234 (1), 77–88.
- Labille, J., Brant, J., 2010. Stability of nanoparticles in water. *Nanomedicine* 5 (6), 985–998.
- Labille, J., Feng, J.H., Botta, C., Borschneck, D., Sammut, M., Cabie, M., Auffan, M., Rose, J., Bottero, J.Y., 2010. Aging of TiO<sub>2</sub> nanocomposites used in sunscreen. Dispersion and fate of the degradation products in aqueous environment. *Environ. Pollut.* 158 (12), 3482–3489.
- Labille, J., Harns, C., Bottero, J.Y., Brant, J., 2015. Heteroaggregation of titanium dioxide nanoparticles with natural clay colloids under environmentally relevant conditions. *Environ. Sci. Technol.* 49 (11), 6608–6616. <https://doi.org/10.1021/acs.est.5b00357>.
- Manasfi, T., Coulomb, B., Ravier, S., Boudenne, J.L., 2017. Degradation of organic UV filters in chlorinated seawater swimming pools: transformation pathways and bromoform formation. *Environ. Sci. Technol.* 51 (23), 13580–13591.
- Matta, M.K., Zusterzeel, R., Pilli, N.R., Patel, V., Volpe, D.A., Florian, J., Oh, L., Bashaw, E., Zineh, I., Sanabria, C., Kemp, S., Godfrey, V., Adah, S., Coelho, S., Wang, J., Furlong, L.-A., Ganley, C., Michele, T., Strauss, D.G., 2019. Effect of sunscreen application under maximal use conditions on plasma concentration of sunscreen active ingredients: a randomized clinical trial. *Jama* 321 (21), 2082–2091. <https://doi.org/10.1001/jama.2019.5586>.
- Mitchellmore, C.L., He, K., Gonsior, M., Hain, E., Heyes, A., Clark, C., Younger, R., Schmitt-Kopplin, P., Feerick, A., Conway, A., Blaney, L., 2019. Occurrence and distribution of UV-filters and other anthropogenic contaminants in coastal surface water, sediment, and coral tissue from Hawaii. *Sci. Total Environ.* 670, 398–410.
- Reed, R.B., Martin, D.P., Bednar, A.J., Montano, M.D., Westerhoff, P., Ranville, J.F., 2017. Multi-day diurnal measurements of Ti-containing nanoparticle and organic sunscreen chemical release during recreational use of a natural surface water. *Environ. Sci. Nano* 4 (1), 69–77.
- Rodriguez, A.S., Sanz, M.R., Rodriguez, J.R.B., 2015. Occurrence of eight UV filters in beaches of Gran Canaria (Canary Islands). An approach to environmental risk assessment. *Chemosphere* 131, 85–90.
- Rodriguez-Romero, A., Ruiz-Gutierrez, G., Viguri, J., Tovar-Sanchez, A., 2019. Sunscreens as a new source of metals and nutrients to coastal waters. *Environ. Sci. Technol.* 53 (17), 10177–10187.
- Sanchez-Quiles, D., Tovar-Sanchez, A., 2014. Sunscreens as a source of hydrogen peroxide production in coastal waters. *Environ. Sci. Technol.* 48 (16), 9037–9042.
- Sani-Kast, N., Labille, J., Ollivier, P., Slomberg, D., Hungerbühler, K., Scheringer, M., 2016. Nanoparticles and dissolved organic matter: a network perspective reveals a decreasing diversity of the materials investigated. *PNAS* 114 (10), E1756–E1765.
- Santos, A.J.M., Miranda, M.S., Silva, J.C.G.E. da, 2012. The degradation products of UV filters in aqueous and chlorinated aqueous solutions. *Water Res.* 46 (10), 3167–3176.
- SCCP, E.U., 2008. Safety of Nanomaterials in Cosmetic Products Scientific Committee on Consumer Products Available. [SCCP/1147/07](https://doi.org/10.1001/jama.2019.5586).
- SCCS, 2014. OPINION ON Titanium Dioxide (nano form) COLIPA n° S75. Scientific Committee on Consumer Safety (SCCS/1516/13).
- Schlumpf, M., Schmid, P., Durrer, S., Conscience, M., Maerkel, K., Henseler, M., Gruetter, M., Herzog, I., Reolon, S., Ceccatelli, R., Faass, O., Stutz, E., Jarry, H., Wuttke, W., Lichtensteiger, W., 2004. Endocrine activity and developmental toxicity of cosmetic UV filters - an update. *Toxicology* 205 (1–2), 113–122.
- Sendra, M., Sanchez-Quiles, D., Blasco, J., Moreno-Garrido, I., Lubian, L.M., Perez-Garcia, S., Tovar-Sanchez, A., 2017. Effects of TiO<sub>2</sub> nanoparticles and sunscreens on coastal marine microalgae: ultraviolet radiation is key variable for toxicity assessment. *Environ. Int.* 98, 62–68.
- Slijkerman, D., Keur, M., 2018. Sunscreen Ecoproducts - Products Claims, Potential Effects and Environmental Risks of Applied UV Filters. Wageningen Marine Research, Wageningen Marine Research (report C056/18).
- Sobek, A., Bejgarn, S., Ruden, C., Molander, L., Breitholtz, M., 2013. In the shadow of the Cosmetic Directive - inconsistencies in EU environmental hazard classification requirements for UV-filters. *Sci. Total Environ.* 461, 706–711.
- Steinberg, D., 2007. Global regulations of sunscreens. *Int. J. Cosmet. Sci.* 29, 409–411.
- Tashiro, Y., Kameda, Y., 2013. Concentration of organic sun-blocking agents in seawater of beaches and coral reefs of Okinawa Island, Japan. *Mar. Pollut. Bull.* 77 (1–2), 333–340.
- Tovar-Sanchez, A., Sanchez-Quiles, D., Basterretxea, G., Benede, J.L., Chisvert, A., Salvador, A., Moreno-Garrido, I., Blasco, J., 2013. Sunscreen products as emerging pollutants to coastal waters. *PLoS One* 8 (6).
- Tovar-Sanchez, A., Sanchez-Quiles, D., Rodriguez-Romero, A., 2019. Massive coastal tourism influx to the Mediterranean Sea: the environmental risk of sunscreens. *Sci. Total Environ.* 656, 316–321.

- Tsui, M.M.P., Lam, J.C.W., Ng, T.Y., Ang, P.O., Murphy, M.B., Lam, P.K.S., 2017. Occurrence, distribution, and fate of organic UV filters in coral communities. *Environ. Sci. Technol.* 51 (8), 4182–4190.
- Tyner, K.M., Wokovich, A.M., Godar, D.E., Doub, W.H., Sadrieh, N., 2011. The state of nano-sized titanium dioxide (TiO<sub>2</sub>) may affect sunscreen performance. *Int. J. Cosmet. Sci.* 33 (3), 234–244.
- Virkutyte, J., Al-Abed, S.R., Dionysiou, D.D., 2012. Depletion of the protective aluminum hydroxide coating in TiO<sub>2</sub>-based sunscreens by swimming pool water ingredients. *Chem. Eng. J.* 191, 95–103.



## Chapter VII: TiO<sub>2</sub> based UV filters ecotoxicity: the Mediterranean Sea Urchin case study

Once released in the environment, nanoparticulate UV filters used in sunscreens formulation are transported through the water column and become potentially bioavailable and dangerous for the surrounding aquatic organisms. Until now, few studies were addressed on the evaluation of mineral UV filters toxicity toward marine organisms, mainly because of the complexity of the salty medium which leads to enhanced ENMs instability. Moreover, several studies were carried on in unrealistic experimental conditions, such as ENMs concentrations far above the environmental relevant ones and/or pure bare TiO<sub>2</sub> nanoparticles used as pollutants, instead of commercially available mineral filters.

In this chapter, we focus on the toxicity of different commercial nano-TiO<sub>2</sub> based UV filters toward the Mediterranean Sea-urchin development and immune response. We selected the UV filters based on their hydrophobic or hydrophilic surface properties and we selected the more realistic pre-dispersant medium (e.g. sunscreen oil phase or MQW) as function of these characteristic. The results obtained during the field campaign discussed in Chapter IV, inspired the experimental conditions of ENMs exposure, such as environmental relevant concentrations in both water column and surface layer.

None of the selected ENMs showed a significant harmful effect on the biological activities of the exposed embryos and cells at the environmental relevant concentrations (from 0.001 to 1 mg/L). Nonetheless, particles coatings shape and dispersing medium turned out to influence the sea urchin immunological state and development. Silica coated particles showed a superior immune compatibility among all the commercial nano-TiO<sub>2</sub> rutile-based UV filters tested.

It was also hypothesized that the interaction between hydrophobic nanoparticles and the ODX surfactant contained in the sunscreen oil phase, discussed in Chapter III, could modulate the transport and bioavailability of the ENMs during embryos development. Overall, in this chapter we highlight the need to develop new exposure strategy for both *in vitro* and *in vivo* eco-toxicological tests, in which the knowledge provided at all the lifecycle stages should be used, in order to better assess the risk associated to ENMs used in sunscreen formulations.

## **Paper IV:** Effect of nano-TiO<sub>2</sub> (rutile)-based UV filters used for sunscreen formulations on the immunological state and embryonic development of the sea urchin *Paracentrotus lividus* (submitted on Nanomaterials)

Riccardo Catalano<sup>a,b</sup>, Annalisa Pinsino<sup>c</sup>, Daniela Gaglio<sup>d-e</sup>, Andi Alijagic<sup>c</sup>, Elisabetta Napodano<sup>e</sup>; Andrea Campos<sup>f</sup>; Jerome Labille<sup>a,b</sup>

**Abstract:** Sunscreen are of emerging concern regard their environmental impact. Nano-TiO<sub>2</sub> (rutile)-based UV filters used for sunscreen formulations released from could have adverse effect toward the human health and marine environment. Few studies were addressed on the impact of commonly used commercial filters. Even-though these engineered nanomaterials (ENMs) do contain a rutile core, they are also enrobed with other compounds (*e.g.*, alumina, silica, polydimethylsiloxane, stearic acid), which modify their surface properties, possibly altering their transportation, bioavailability and toxicity. Here, the effect of three different commercial nano-TiO<sub>2</sub> rutile-based UV filters on development and immune response of the sea urchin (*Paracentrotus lividus*) were evaluated in comparison with bare rutile NPs. Milli-Q water and sunscreen oil phase were selected in turn as UV filters pre-dispersant mediums based on the surface properties (hydrophilicity; hydrophobicity) of each ENMs. None of the selected ENMs showed a significant harmful effect on the biological activities of the exposed embryos and cells at the environmental relevant concentrations (from 0.001 to 1 mg/L). Nonetheless, particles coatings shape and dispersant medium turned out to influence the sea urchin immunological state and development. Silica coated particles showed a superior immune compatibility among all the commercial nano-TiO<sub>2</sub> rutile-based UV filters tested.



## 1. Introduction

Ultraviolet (UV) radiation is a main risk factor for skin disorders such erythema, photoaging and keratinocyte cancer. As consequence effective photoprotection is of outmost importance to humans. Several skin protective approaches including organic (*e.g.*, benzophenone, octocrylene) and inorganic UV-filters (*e.g.*, zinc oxide, titanium dioxide), topically applicable antioxidants, DNA repair enzymes and oral photoprotective strategies based on nutritional supplements have been quickly developed<sup>116</sup>. Sunscreens are emulsions of water and oil-containing UV filters able to screen the human skin from the UV detrimental effects. In 2018, the Environmental Working Group stated that two-thirds of the sunscreens available in the United States are substances unsafe to the environment, mainly organic filters<sup>170</sup>.

As the coastal tourism reached his peak in the recent decades<sup>171</sup>, the use and consequently the emission of sunscreen products in the environment has increasead

<sup>79</sup>.

Recent reports have highlighted the organic filter potential impact (*e.g.*, benzophenones, camphor) on the marine environmental, particularly on coral reef and in marine organisms such as Crustaceans, Echinoderms, Algae <sup>69-71</sup>. Thus, inorganic UV-filters become dominant in discussions about photoprotection. Based on a few evidences, zinc oxide (ZnO) and titanium dioxide (TiO<sub>2</sub>)-containing sunscreens are safe alternatives to organic filters but a clear knowledge on their potential health risk remains scant. Among the mainly used inorganic filters, ZnO-based UV filters are generally considered the most unsafe because of their high solubility in salt water<sup>76,10,11</sup>. On the other hand, TiO<sub>2</sub>-based UV-filters are generally considered safer UV-filters, because their low solubility in aqueous mediums that would likely lead to a lower bioavailability and toxicity<sup>79,82</sup>.

ZnO and TiO NPs, both metal oxide particles, are used in sunscreens as nanoparticles (NPs) (a size <100 nm), growing their cosmetic acceptability by users, as they are much less visible after application. They are both the power to adsorb, reflect and refract UV photons, but function in photoprotection predominantly by scattering UV radiation<sup>107</sup>.

However, when utilized in the nanometric form, particles could become more unsafe because of the higher surface reactivity and bioavailability<sup>77</sup>. For example, an issue in the state of the art could be recognized in the type of nano-TiO<sub>2</sub> (n-TiO<sub>2</sub>) utilized in most of the studies concerning TiO<sub>2</sub> based UV filters toxicity on aquatic environment. Based on a review published in 2014 by Minetto *et al.*<sup>87</sup> on more than 200 articles, almost all the safety investigations were performed using Anatase or P25 TiO<sub>2</sub> NPs. Although these TiO<sub>2</sub> forms are consistent analogues of pigments used in self-cleaning paintings, cements and food, sunscreens n-TiO<sub>2</sub> based UV filters are in Rutile crystal phase, that would most likely modify its reactivity and toxicity<sup>173</sup>. Moreover, commercial n-TiO<sub>2</sub>-based UV-filters, are coated with different materials to prevent rutile photocatalytic activity (*e.g.*, Al<sub>2</sub>O<sub>3</sub>, SiO<sub>2</sub>) and enhancing the particles dispersion stability (*e.g.*, polydimethylsiloxane, stearic acid). While the transformation and environmental fate of such engineered nanomaterials (ENM) have already been addressed in the literature<sup>38,65,74</sup>, their effects on the aquatic environment remain a challenge. Researches are needed to better understand which ingredients are safe for the organisms and which pose a realistic threat to marine environment. Although the determination of mineral filters in natural environments remain an analytical challenge, the reported highest n-TiO<sub>2</sub> concentration seashore surface layer is 38 µg/l<sup>63</sup>. At this concentrations range, fish embryos of Japanese Medaka were one of the few marine species to be sensitive to n-TiO<sub>2</sub>, showing neurologic adverse symptoms<sup>90</sup>. Nevertheless, no environmental threshold level for n-TiO<sub>2</sub> is available yet. Therefore, it is mandatory to address which type of impact n-TiO<sub>2</sub>

may have both in the environment and in the organismal fitness. Notably, reproduction, development and immunity are three metabolically expensive traits, important determinant of fitness.

In the present work, we test the toxicity of three different n-TiO<sub>2</sub>- based UV filters commonly used in sunscreens, in comparison with pure bare TiO<sub>2</sub> rutile NPs. The tests were performed on the Mediterranean Sea Urchin (*Paracentrotus lividus*) biological model, using both environmental relevant (or near relevant) concentrations of UV filters (realistic) and extreme concentrations (unrealistic). The sea urchin is indeed an effective sentinel of environmental stress<sup>19</sup> which is found in almost all the marine environments. In order to obtain a clearer overview, the sea urchin immunological state and embryonic development were investigated. When the experimental condition allowed it, hydrophobic coated UV filters were pre-dispersed in a common, lab made, sunscreen oil phase, while hydrophilic UV filters and bare TiO<sub>2</sub> rutile NPs were pre-dispersed in Milli-Q water (MQW) medium using standard treatment procedures. The reason behind this choice was to be more consistent with the early stages of the mineral UV filters aging, after the sunscreen release in the marine environment, *vis-a-vis* of their different surface properties.

## **2. Materials and methods**

### 2.1 Commercial nano-TiO<sub>2</sub> based UV filters and Sunscreen Oil phase

The TiO<sub>2</sub>-based NPs utilized in this work were directly purchased from the suppliers as dry powders. The respective trade names together with the chemical compositions and primary particle size provided by the manufacturers are reported in Table 1. Three of these (called T-S, T-Lite, and T-AVO) were

commercial nanoparticulate UV filters commonly utilized in sunscreen formulations, while one were pure TiO<sub>2</sub> rutile NPs (Evonik Degussa, Essen, Germany), here chosen as non-coated n-TiO<sub>2</sub> UV filters. T-S and T-Lite UV filters contained a mineral internal coating of aluminium oxide and a hydrophobic external layer of stearic acid (T-S) or dimethicone (T-Lite), while T-AVO NPs only contained a unique coating of SiO<sub>2</sub>.

Each sunscreen oil phase (Phase A) was prepared by mixing together emollient oil and emulsifying agent (2:1), and gently homogenizing them by stirring agitation for 10 min. Product names, manufacturer, function, and chemical composition of the 3 components used here to prepare sunscreen oil medium (Phase A) are reported in Table 2.

**Table 4.** Product names, manufacturer and chemical composition provided by the supplier for the TiO<sub>2</sub>-based NPs utilized in this work.

| Product Name | Manufacturer   | Chemical composition   |
|--------------|----------------|--|
| T-Lite       | BASF           | TiO <sub>2</sub> (79-89%)/Al(OH) <sub>3</sub> /dimethicone             |
| T-AVO        | Merck          | TiO <sub>2</sub> (79.6%)/SiO <sub>2</sub>                              |
| T-S          | Merck          | TiO <sub>2</sub> (73-79%)/Al <sub>2</sub> O <sub>3</sub> /stearic acid |
| Rutile       | Evonik Degussa | TiO <sub>2</sub> (Rutile)  |

**Table 5.** Product names; manufacturer; function and chemical composition of the Phase A used as sunscreen oil medium.

| Product name | Manufacturer | Function          | Chemical composition  |
|--------------|--------------|-------------------|---|
| Tegosoft P   | Evonik       | Emollient oil     | Isopropyl palmitate   |
| Cetiol LC    | BASF         | Emollient oil     | Coco-Caprylate/Caprates   |
| Easynov      | SEPPIC       | Emulsifying agent | Octyldodecanol; Octyldodecyl xyloside; PEG-30 Dipolyhydroxystearate |

## 2.2 Adult sea urchin immune cell exposure

Adult sea urchins (*Paracentrotus lividus*) were collected along the Northwest coast of Sicily and were acclimatized and maintained under controlled conditions of temperature ( $16 \pm 2^\circ\text{C}$ ), pH ( $8.1 \pm 0.1$ ), salinity (38–39‰), and density ( $1.028\text{--}1.030\text{ g/cm}^3$ ) in oxygenated Artificial Seawater (Aqua Ocean Reef Plus Marine Salt, Aquarium Line, Italy)<sup>95</sup>. Animals were fed every 7 days with the green alga *Ulva lactuca*. Approximately 0.5 ml of Coelomic Fluid containing freely circulating immune cells, were collected from each sea urchin using a 1 ml sterile syringe already containing 0.5 ml of anticoagulant solution namely Coelomocyte Culture Medium (CCM), composed of 1 M NaCl, 10mM MgCl<sub>2</sub>, 40mM Hepes, 2mM EGTA pH 7.2. After collection, the immune cells were counted in a Fast-Read chamber (Biosigma), and morphological analysis of cells was performed using an optical microscope, Olympus CKX31 (Olympus, Japan). The Trypan Blue exclusion test was used to determine the number of viable cells present in the cell suspension. After counting, immune cells were plated at a density of  $1 \times 10^5$  cells/well in a 96-well white, opaque-walled plate (Thermo Fisher Scientific) and exposed to T-AVO NPs, final volume of 100  $\mu\text{l}$ . T-AVO NPs were pre-dispersed in stock solutions of MQW (1 and 100 mg/l nominal concentration) and sterilized under UV light and vortexed for 5 min in order to homogenize the dispersions. The NPs were added to each cell culture medium reaching five different concentrations (0.1, 1, 10, 100, 500 mg/L final concentration). Culturing was performed in the dark at  $16 \pm 2^\circ\text{C}$ . Cell viability and cytotoxicity were measured using RealTime-Glo MT Cell Viability Assay (Promega, USA) and the non-lytic CellTox™ Green Cytotoxicity Assay (Promega, USA) respectively, as previously described<sup>175</sup>. Luminescence and fluorescence were detected using GloMax Discover high-performance Microplate Reader (Promega). All assays involved at least five biological replicates (specimens).

### 2.3 Sea Urchin *Paracentrotus lividus* embryo exposure during development

Six males and six females were induced to spawn by injecting 1-2 ml of 0.1 M KCl into the sea urchin body cavity, through the peristomial membrane surrounding the mouth. Eggs were collected by placing spawning females on 100 mL beakers with 0.45µm filtered ASW. Egg quality and sperm motility were inspected by observing the gametes under an optical microscope (OLYMPUS CKX31); 10µL seminal fluid was added to the egg suspension (sperm/egg ratio 50:1) and the success of the fertilization was verified under the microscope (formation of the fertilization membrane with a fertilization rate > 95%). After fertilization, embryonic culture (500 embryos per mL) was transferred in 50 mL disposable sterile tubes (10 mL in each tube), and embryos were immediately exposed for 48 hours (h) to increasing environmentally relevant concentrations (between 0.001 and 1 mg/L) of pure TiO<sub>2</sub> rutile and T-AVO NPs, which were pre-dispersed in MQW.

Tests using hydrophobic nano-TiO<sub>2</sub> based UV filters (T-S and T-Lite) were performed similarly, by pre-dispersing them in sunscreen oil phase. These oily emulsions were diluted in MQW to obtain an oil/MQW emulsion of 5 mL/L nominal concentration. A pure oil phase/MQW emulsion was used as oil control reference. These emulsions were then added to the embryo culture medium at the nominal concentrations of 0.005, 0.05, and 0.5 mg/L. Tests were accepted if the percentage of control embryos at 48 h of development was ≥ 80% as recommended by standard procedure (ASTM, 2012).

The degree of toxicity per each treatment was calculated using the standard criteria of evaluation based on the calculation of the percentage of normal *versus* abnormal embryos in a one hundred 100 embryos (in triplicate), by an optical microscopy (48 h of development end-point). Embryonic development was also kept under observation to evaluate the happening and timing of several

morphological events related to the endoderm, ectoderm and mesoderm (germ layers) development and differentiation, as reported by Pinsino et al 2017<sup>23</sup>.

#### 2.4 Metabolite renewal analysis by mass spectrometry in untargeted liquid chromatography

Liquid chromatography-mass spectroscopy (LC-MS analysis) was performed to analyse the metabolite profile of sea urchin cells exposed to hydrophilic n-TiO<sub>2</sub> based UV filters, according to previously established protocols<sup>95</sup>. Metabolites were isolated in 0.5 mL ice-cold 1% acetic acid water-acetonitrile solution (70:30 v/v). Supernatant were recovered in glass inserts for solvent evaporation, dried at 30 °C for about 2.5 h (Concentrator plus/Vacufoam® plus, Eppendorf), re-suspended in 150 µL of H<sub>2</sub>O LC-MS grade and injected in UHPLC-MS system for RPLC chromatography. Samples were analysed using an UHPLC system (Agilent 1290 Infinity UHPLC system) coupled with a quadrupole-time of flight hybrid mass spectrometer (Agilent 6550 iFunnel Q-TOF), and equipped with an electrospray Dual JetStream source. Data analysis and isotopic natural abundance correction were performed with MassHunter ProFinder and Mass Profiler Professional software (Agilent).

#### 2.5 Characterization of the NPs by High-resolution Scanning Electron Microscopy

3-4 milligrams of the four pristine TiO<sub>2</sub>-based NPs (T-AVO; T-S; T-Lite; Rutile) were dispersed on carbon adhesive tabs and analysed through High-resolution Scanning Electron Microscopy (HR-SEM) using a Zeiss Gemini500-Field emission SEM. To obtain surface sensitive imaging at nanoscale resolution, images were recorded at low voltage (1-5 kV) with an in-lens secondary electron detector.

## 2.6 Characterization of the NPs dispersions by Dynamic Light Scattering

Rutile and T-AVO NPs MQW water dispersion with a nominal concentration of 50 mg/L were prepared from the pristine dry powders. This concentration has proved to be the lower possible concentration allowing acceptable sizes distributions. The measurements were performed in triplicates at 25 °C with 11 runs per measurement, normal resolution analysis and 0.01 cumulant fit error tolerance.

The oily dispersion of T-S and T-Lite NPs were prepared by dispersing the UV filters in Phase A by mechanical agitation at 1000 rpm rotation speed for 10 min, at a nominal NPs concentration of 25 g/L (intermediate between the lowest and the highest concentration used in the *in vivo* essays), using a *Heidolph Hei-Torque* 400 stirrer equipped with a pitcher blade impeller. Size measurement were performed in the same way as for the aqueous dispersions but changing the medium parameters.

## 2.7 Statistical analysis on biological assays

Statistical analyses were performed by GraphPad Prism Software 6.01 (USA). Statistical differences among selected groups were estimated by one-way ANOVA (followed by the multiple comparison tests). The p-value lower than 0.05 was deemed statistically significant. Data were expressed as mean±standard deviation (SD)



### 3. Results and discussion

#### 3.1 Pristine TiO<sub>2</sub>-based NP Characterization and Particle Dynamic Light Scattering Distribution

Scanning Electron Microscopy images results are reported in **Figure 2**, and the sizes (longer side length) determined from these images are reported in **Table 3**. TiO<sub>2</sub> pure rutile NPs showed a non-uniform spherical morphology (**Figure 2a**) with a diameter of  $\cong 23$  nm. T-AVO (silica coated) NPs presented a more spherical/elongated shape (**Figure 2b**) and a higher particle size ( $\cong 50$  nm), whereas both hydrophobic n-TiO<sub>2</sub> based UV filters, T-Lite (dimethicone) and T-S (stearic acid), presented similar primary particle sizes ( $58.3 \pm 10.7$  and  $64.4 \pm 11.4$  diameter) with a rod-like shape (**Figure 2c, 2d**).

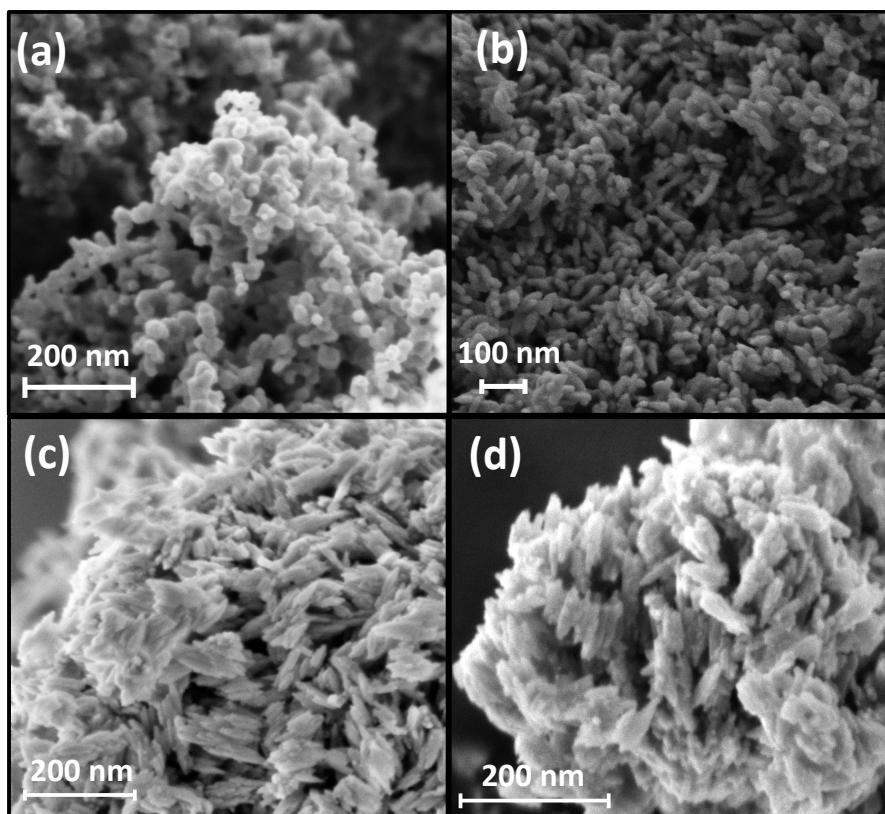


**Figure 15.** High-resolution scanning electron microscopy (HR-SEM) analysis of the pristine TiO<sub>2</sub>-based NPs. (a) Rutile; (b) T-AVO, (c) T-Lite and (d) T-S.

**Table 3.** Primary particle sizes of the pristine **TiO<sub>2</sub>-based NPs** determined from SEM images

| <b>TiO<sub>2</sub>-based NPs</b> | <b>Primary particle size</b> |
|----------------------------------|------------------------------|
| Rutile                           | 22.7 ± 4.3                   |
| T-AVO                            | 51.0 ± 10.6                  |
| T-Lite                           | 58.3 ± 10.7                  |
| T-S                              | 64.4 ± 11.4                  |

The **dynamic light scattering** (DLS) intensity distributions are reported in **Figure 2**. The hydrophilic filters, T-AVO and **TiO<sub>2</sub>** rutile NPs, dispersed in MQW showed similar aggregation states (**Figure 2a**). Both distributions appeared bimodal at 160 and 600 nm, indicating a large and polydisperse aggregation of the primary particles in suspensions. However, it is worthwhile noting that the size values reported here are intensity-weighted, which over-expresses larger sizes to the power 6. Any slight difference in the lower size range of the distribution should then be considered significant in a number weight consideration. The average size values reported in **Table 4** obtained on three different measurements, shows that T-AVO NP aggregation state, although still standing in the micro-scale, is slightly finer dispersed (1217 nm) than **TiO<sub>2</sub>** rutile NPs (1952). This suggests that the SiO<sub>2</sub> particle coating, or the more elongated shape of primary particle, may slightly enhance the dispersion of T-AVO compared to pure bare **TiO<sub>2</sub>** rutile NPs, but still does not prevent a severe particle aggregation of the NPs in aqueous medium. On the contrary, the hydrophobic T-S and T-Lite NPs showed a significant different aggregation state in oil, although they are both hydrophobic filters. T-Lite NPs size distribution present a wide signal centred a 100 nm while T-S NPs appeared to be more aggregated and polydisperse with a bimodal distribution at 200 and 1300 nm. In this case, as both NPs have similar primary particle size and shape, the difference in the aggregation state should come from their respective organic coatings. On the one hand, the

stearic acid coating of T-S NPs certainly has a low affinity for the oil dispersing medium, which favours NP homo-aggregation, so that the surface area of interaction with the solvent is minimized. On the other hand, dimethicone surface of T-Lite leads to a higher affinity with the dispersing medium, which favour NP dispersion stability<sup>176</sup>.

It is unclear how the dispersion states of the different UV filters measured here in pure water or sunscreen oil are altered after dispersion and dilution in the culture medium. NP fate is then characterized by co-evolving size and concentration of the suspended NPs. Such mechanism is challenging to track *in situ* in the exposure medium because the NP concentration decreases close to zero while the composition of the complex medium can lead to multiple scenarios of interaction such as hetero-aggregation<sup>61,90</sup>. This was not investigated here. However, aggregation and sedimentation will surely occur in artificial seawater for the hydrophilic TiO<sub>2</sub> pure rutile and T-AVO NPs pre-dispersed in water because salt-induced aggregation is a well-known effect in such system<sup>177</sup>. For T-S and T-Lite UV filters instead, further aggregation is not expected. Although no experimental proofs are provided in the present study, it is fair to hypothesize that these hydrophobic filters may remain in the oil phase during the exposure without entering in contact with the aqueous culture medium. This was evidenced on field in bathing seawater that hydrophobic UV filters tend to remain floating in a surface layer<sup>63,178</sup>. For these reasons, we assume that the DLS distributions reported for the hydrophobic UV filters dispersed in oil (**Figure 3b**) were mostly preserved during the embryos exposition, while those returned with the hydrophilic UV filters pre-dispersed in MQW (**Figure 3a**) did not remain and should not be argued in the result discussion.

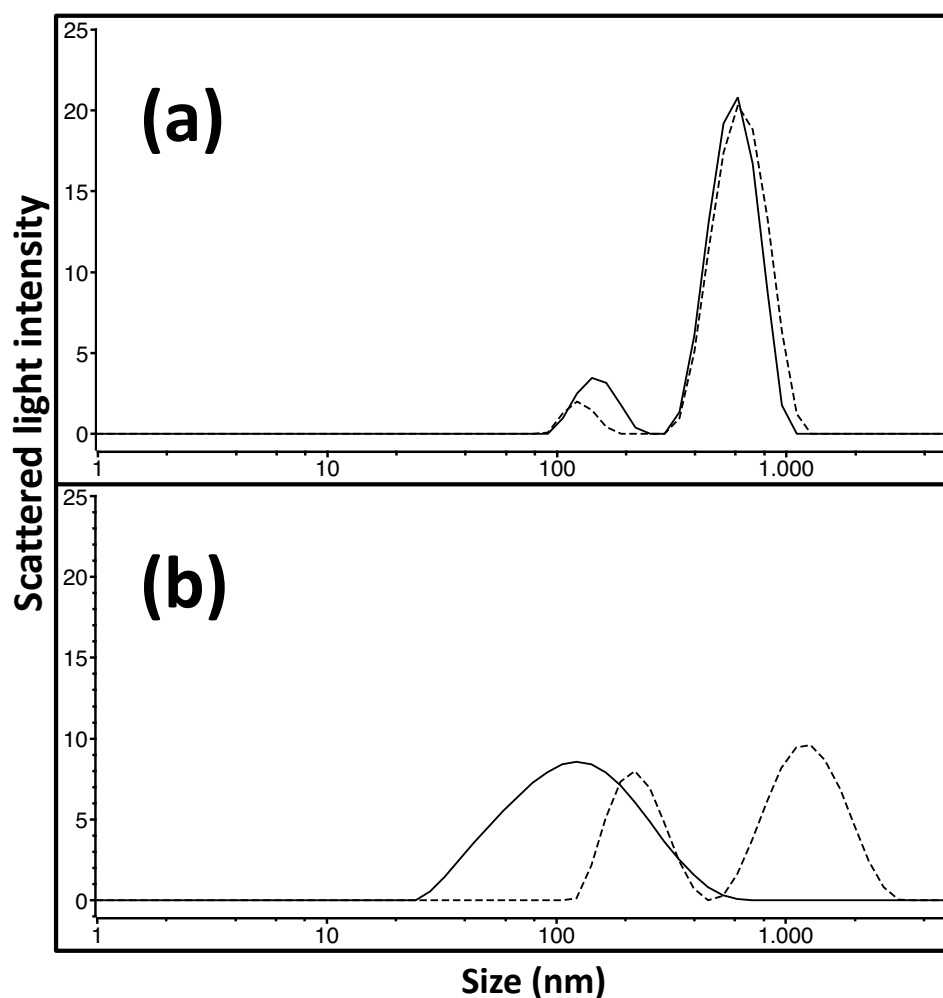


**Figure 16.** DLS size measurement of hydrophilic and hydrophobic n-TiO<sub>2</sub> (rutile)-based UV filters. a) DLS intensity distributions in MQW (50 mg/l) for Rutile (solid line) and T-AVO (dashed line) nanoparticles; b) DLS intensity distributions in sunscreen oil phase (25 g/l) for T-Lite (solid line) and T-S (dashed lines) nanoparticles.

**Table 4.** Average intensity sizes distribution of particle aggregates for the different UV filters detected through DLS measurements

| Nanoparticle (dispersant medium) | Average aggregate size (nm) |
|----------------------------------|-----------------------------|
| Rutile (ASW)                     | 1952.7 ± 542.3              |
| T-AVO (ASW)                      | 1217.0 ± 169.1              |
| T-Lite (Phase A)                 | 173.9 ± 63.5                |
| T-S (Phase A)                    | 857.3 ± 131.7               |

### 3.2 Effects of Nano-TiO<sub>2</sub>-based UV filters on sea urchin embryonic development

Here, we investigated the effects of exposure to increasing concentrations of n-TiO<sub>2</sub>-based UV filters on *P. lividus* embryonic development. Embryos were classified as normal only when they satisfied all the following morphological criteria: i) acceptable schedule in reaching the developmental endpoint; ii) dorso/ventral and left/right embryonic axis symmetry; iii) correct differentiation of oral/aboral endoderm and ectoderm; iv) correct mesenchyme differentiation, distribution pattern and shape. At the gastrula stage (24 h of development), embryos exposed from fertilization maintained regular time schedule and proper sites of spicule elongation at all concentrations used (not shown). In agreement, at the pluteus stage (48 h), n-TiO<sub>2</sub>-based UV filter-exposed embryos displayed a low number of abnormalities (**Figure 4**). A weak but significant increase in the incidence of potential teratogenic effects was observed only in embryos exposed to 1 mg L<sup>-1</sup> T-AVO hydrophilic UV filter and 0.05 mg L<sup>-1</sup> T-Lite hydrophobic UV filter. Specifically, about 20% of embryos exhibited problems on arm and skeleton rod development, and/or atypical big cells randomly distributed (**Figure 5**). The most common skeletal malformations observed were: i) crossed or separated tips at the hood apex arms (**Figure 5** - red arrows); ii) asymmetrical arm lengths; iii) decrease or increase in arm growth and supporting skeletal rods (**Figure 5** - black arrows, oral and post-oral skeletal rods). Similar skeleton-defective embryos have been previously observed in *P. lividus* embryos exposed to other types of NPs, suggesting that skeleton abnormalities could be used as sensitive target upon NP exposure<sup>179,180</sup>. Besides, the formation of big cells or masses (**Figure 5** - blue arrows) is in agreements with results previously obtained by Pinsino *et al.*<sup>181</sup> in *P. lividus* embryos exposed to PS-NH<sub>2</sub> and by Magesky and Pelletier<sup>182</sup> in *Strongylocentrotus droebachiensis* embryos exposed to Ag NPs. These cells could

be mesodermal cells involved in NP internalization (immune defenses) as already suggested by Pinsino et al<sup>181</sup>.

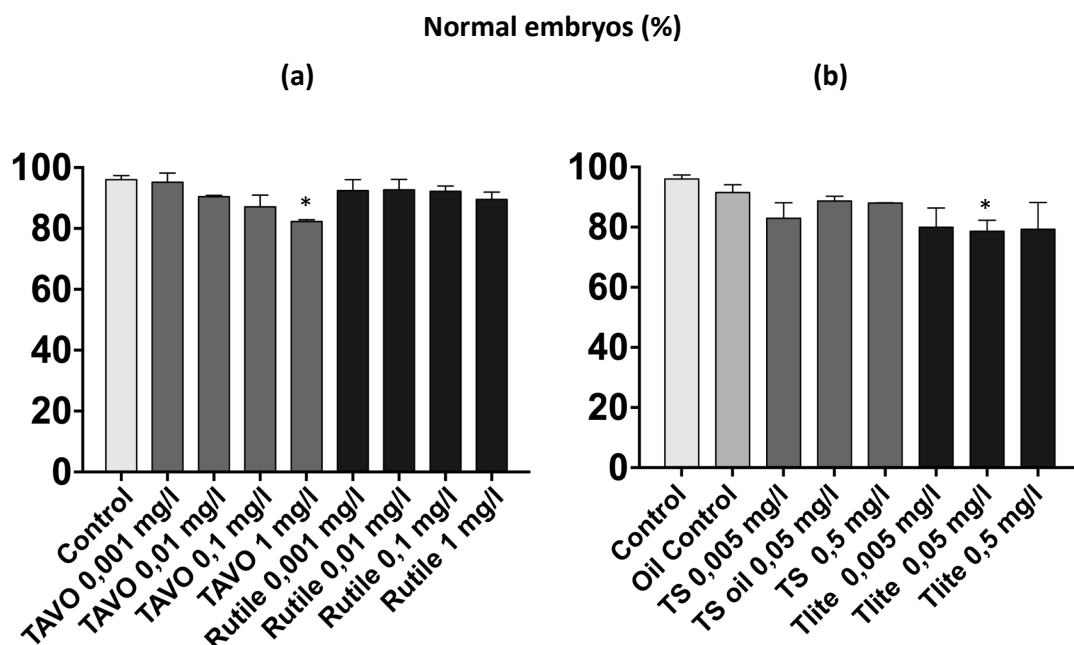


**Figure 4.** Sea urchin embryonic development evaluated according to standard criteria. Histograms represent the results expressed as mean percentage (%) of abnormal embryos  $\pm$  standard deviation after 48 h of exposure to the (a) hydrophilic (T-AVO and Rutile) and (b) hydrophobic (T-S and T-Lite) n-TiO<sub>2</sub>-based UV filters.

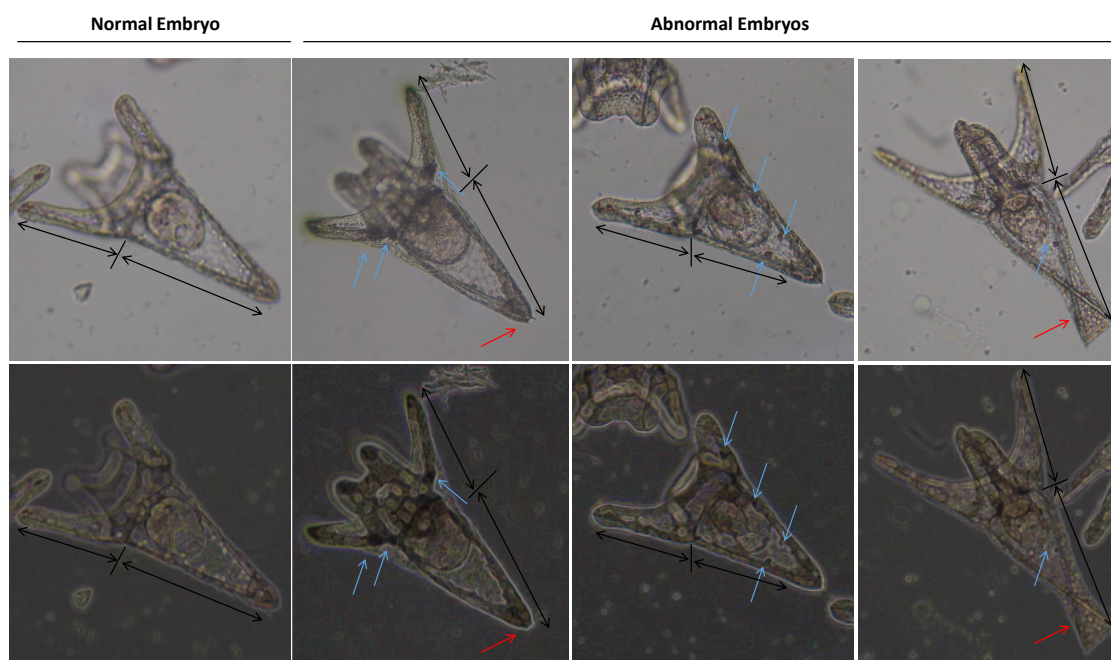


**Figure 5.** Pictures of representative sea urchin *P. lividus* exposed embryos compared with a normal embryo development. Black arrows indicate decrease or increase in arm growth and supporting skeletal rods; Red arrows indicate crossed or separated tips at the hood apex arms, and the blue arrows indicate the atypical big cells found in abnormal developed embryos.

The embryonic coating layer (membrane of fertilization) may function as a selective barrier (amphiphilic) from chemical and mechanical injury related to the NPs and interfere the particle-cellular interaction or the particle-body interaction. The hatching enzymes secreted at the blastula stage (12 h) proteolyzes this membrane, thereby allowing the embryo to hatch and to start swimming. Li *et al.*<sup>183</sup> proposed that hydrophobic NPs are thermodynamically stable around the core of the bilayer hydrophobic membrane, and their insertion lead to the lipid molecule deformation and distribution. On the contrary, hydrophilic NPs are adsorbed on the membrane surface (ready to be phagocytized) rather than entering the hydrophobic core of the membrane. In agreement, under hydrophilic NP (1 mg L<sup>-1</sup> T-AVO hydrophilic UV filter) exposure, perturbed embryos mainly exhibited big cells/masses (probably phagocytizing), while under hydrophobic NP (0.05 mg L<sup>-1</sup> T-Lite hydrophobic UV filter) exposure, skeleton-defective embryos were predominant. It is unclear why T-AVO NPs and Rutile NPs did not impact the sea urchin embryonic development in the same way. The relative aggregation states measured in MQW are certainly not maintained in both particle types and NPs are expected to be largely aggregated in the exposure conditions. Thus, here, any characteristic determining the internalisation should be seek at the interface between NP and the membrane. The primary particle shape could likely influence and modulate the ecotoxicity of NPs. Indeed, ZnO and TiO<sub>2</sub> NPs, with rod-shaped structures (or in general containing sharper edges) have been shown to induce a higher cytotoxicity<sup>9,184</sup> than round-shape ones, probably due to a specific phagocytic process that depends on the NP shape. Particle shape can also modulate the interaction with the fertilization membrane. Brown *et al.*<sup>185</sup> argued that rod-shaped NPs could interact stronger with biological systems than round-shape NP, because the van der Waals interaction forces in lengthwise oriented NPs increase proportionally to their length, typically reaching values several orders in magnitude above that of spheres. Thus,

compared to the rutile, the rod shape of T-AVO NPs may be facilitate to interact with the fertilization membrane, in agreement with more frequent internalization within the embryonic cells.

The small differences on the impact of T-S and T-Lite hydrophobic filters (**Figure 4 b**) on embryonic development, may arise from a different mechanism compared to the hydrophilic filters. Here, the filters remain mostly concentrated in the oil phase through the exposition duration, likely floating on the ASW medium surface, i.e. with a minimal mixing within the aqueous exposure medium. This should likely limit the putative interaction between embryos and NPs to the area close to the oil/water interface. In addition, the migration of the NPs from the oil phase to the water phase may be facilitated by some interactions with amphiphilic components from the oil, such as surfactants. It was recently evidenced that T-Lite NPs interact stronger than T-S<sup>176</sup> with the octyldodecyl xyloside (ODX) surfactant present in the emulsifier employed in the Phase A (**Table 2**). The ODX molecule adsorbs at the NP surface, leading to the finer dispersion in oil measured here (**Figure 3b**). This may also lead to an amphiphilic character of the T-Lite surface, which could favour its transport into the water phase and thus lead to a higher probability of interaction with the embryos hydrophobic membrane.

Overall, our results confirm that both hydrophilic and hydrophobic nano-TiO<sub>2</sub> based UV filters used for sunscreen formulations do not elicit significant harmful effects on sea urchin embryonic development. Of note, we were not fully satisfied on the efficacy of our evaluation assay with the hydrophobic UV filters pre-dispersed in oil. Increasing the NP concentration in oil also increased the viscosity, which reduced the extendibility of the assays to the higher concentration and to the other assays performed at static conditions (*e.g.*, primary immune cell culture). For this reason, only hydrophilic nano-TiO<sub>2</sub> based UV filters were used in the further assays on immune cells culture.



### 3.3 Sea urchin adult immune cells: healthy state and metabolic typing under hydrophilic nano-TiO<sub>2</sub>-based UV filters

It is known that when the surface of TiO<sub>2</sub> fine powder is coated with dense and uniform thin-layer of silica it is possible to obtain a broad-spectrum sunscreen with enhanced UV absorption characteristics<sup>186</sup>. Thus, in order to focus on the silica coated nano-TiO<sub>2</sub> based UV filters capability of keeping good immunological tolerance, we assessed the viability and cytotoxicity of the exposed immune cells to the hydrophilic T-AVO NPs for 48 h, and we characterized their metabolic profile at 72 h of exposure. Cell viability and cytotoxicity were monitored in real-time measurement for cells exposed at increasing concentrations of the T-AVO NPs (0.1, 1, 10, 100, 500 mg L<sup>-1</sup>). Only the measurement points at 48 h are shown (Figure 6).

Our results confirmed those obtained from sea urchin embryonic development assay, in which no significant toxic effects were found at concentrations that could be found in marine environment (from 0.1 to 10 mg/L). However, at the two highest T-AVO exposure concentrations (100 and 500 mg/L), a significant decrease in viability and a high cell toxicity were measured. At these concentrations, a faster NP aggregation is expected, leading to the suspension destabilization and sedimentation. Here, toxicity could thus be related to some physical effects caused by the aggregates sedimented on the cell culture. For samples exposed to 0.1-10 mg/L T-AVO, the RealTime-Glo MT cell viability assay indicated an increased tendency (not statistically significant) in cell viability/metabolic activity compared to unexposed controls. This result may be due to a hysteresis response usually known under drug administration, in which the effect of a drug declines despite its continuing presence (drug tolerance)<sup>36</sup>. Notably, the assay chemistry is based on the reducing potential of the cell, which is a known metabolic marker of cell viability. Studies elucidating metabolic

profiles of immune cells exposed to T-AVO have been carried out to clarify this indication of an increased metabolic activity, as reported below.

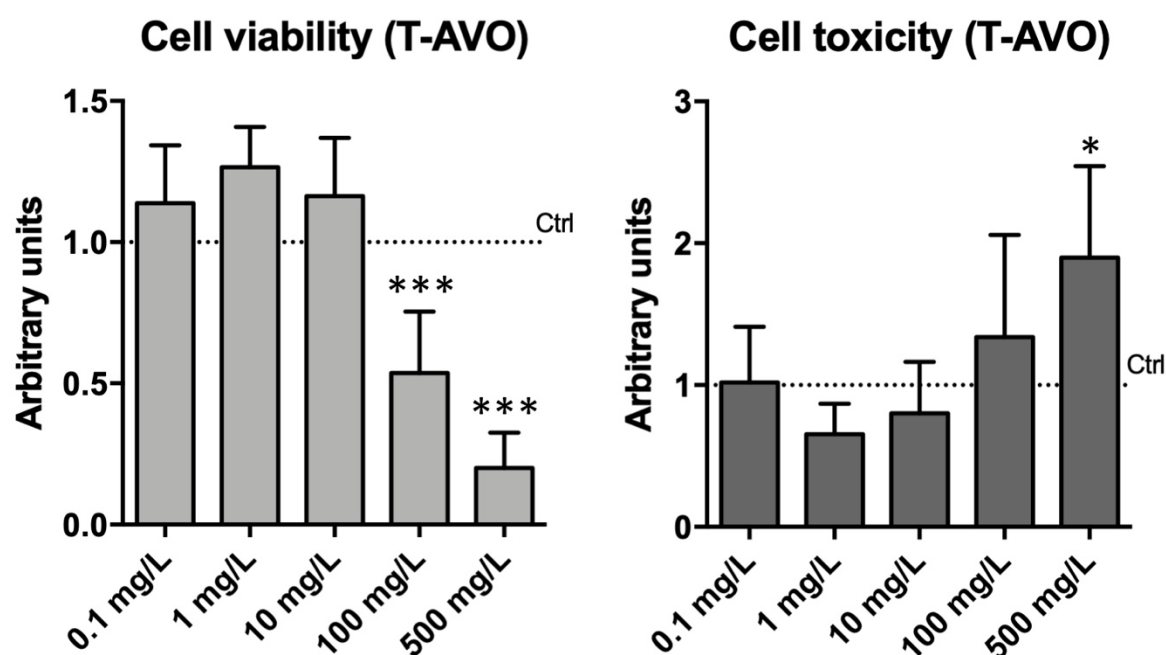


**Figure 6.** Impact of T-AVO-based UV filters on the sea urchin immune cell viability and toxicity.

Real-time viability during the 2 days of continuous monitoring, of which 1 measurement point (48) is shown (0.1, 1, 10, 100, 500 mg/L final concentration). The highest doses (100 and 500 mg/L) provoke decrease in cell viability and increase in cell toxicity. Levels are expressed in arbitrary units as fold increase or decrease compared to controls assumed as 1 (dot line). Data are reported as the mean  $\pm$  SD; stars (\*) indicate significant differences among groups (\* $p < 0.05$ ; \*\*\* $p < 0.001$ ).

Immune functions are bio-energetically expensive, requiring accurate management of metabolites coordinated by intracellular and extracellular signals, which direct the uptake, storage, and utilization of substrates (e.g.,

glucose, amino acids, fatty acids). In turn, metabolites renew and control immune responses<sup>187</sup>. In order to obtain integrated data on sea urchin immune metabolic state under hydrophilic nano-TiO<sub>2</sub> based UV filter exposure and related tolerance state, here we characterized the metabolic profile of cells exposed to T-AVO and compared with both the profile of cells exposed to Rutile and un-exposed cells (72 h in culture) (Figure 7). To this purpose we used an initial higher dose of particles (2 mg L<sup>-1</sup>, loading dose) to drop down to a lower maintenance dose (1 mg L<sup>-1</sup>).

Metabolite profiling identified level changes of only 8 metabolites among groups (Group 1: T-AVO 1-day exposure at 2 mg L<sup>-1</sup> followed by 2-days exposure at 1 mg L<sup>-1</sup>; Group 2: control, 3 days; Group 3: Rutile 1-day exposure at 2 mg L<sup>-1</sup> followed by 2-days exposure at 1 mg L<sup>-1</sup>), including proteinogenic amino acids (Serine, Glutamine), amino acid derivatives (L-Pyroglutamic acid), organic acids (L-Lactic acid, Glutaric acid, Pyruvic acid), sulfate metabolites (sulfate), acetamides (Acetamidovalerate). Sea urchin T-AVO-responsive metabolites were found predominantly involved in mediating inflammatory signals and phagocytosis. Specifically, Glutamine and Acetamidovalerate were found significantly increased compared to unexposed controls, while L-Pyroglutamic acid and L-Lactic acid were found significantly decreased. It is well known that to re-establish a normal cellular and molecular function, immune cells have higher glutamine necessities during inflammatory states<sup>188</sup>. Notably, acetamides are known to relieve inflammatory events; in-fact they are used as chemotherapeutic agents for inflammation-associated cancers<sup>189</sup>.

Lactic acid is produced in high amounts by innate immune cells during inflammatory activation (anaerobic glycolysis product). A reduction in its amount may be translated in a negative feedback signal to silence or to attenuate inflammatory responses<sup>190</sup>.

Increased levels of Pyroglutamic acid (also called 5-oxoproline) are able to promote lipid and protein oxidation and to enhance hydrogen peroxide content,

thus promoting oxidative stress<sup>191</sup>. Consequently, the significant decreased Pyroglutamic acid levels observed under T-AVO exposure may be considered a signal of an increased defence antioxidant metabolic activity. Although weakly, L-Serine and Pyruvic acid were found also increased compared to unexposed cells. Serine racemase enzyme catalyzes the  $\alpha,\beta$ -elimination of water from L-serine to produce pyruvate and ammonia<sup>192</sup>. Notably, L-serine metabolism is required to fuelling one-carbon metabolism and nucleotide biosynthesis, and it is known to lower the inflammatory responses in mice during infection<sup>193</sup>.

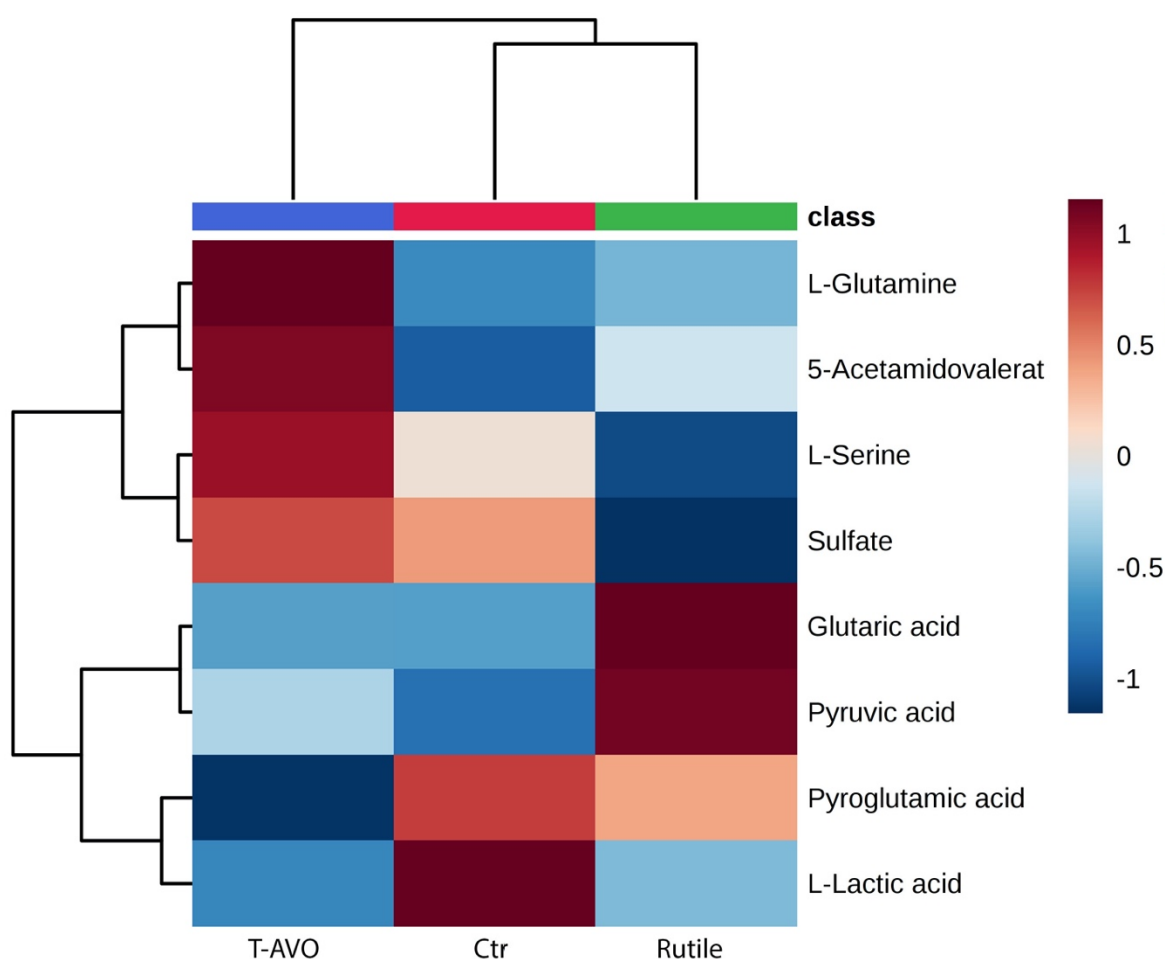


**Figure 7.** Sea urchin immune cell metabolic profile under hydrophilic nano-TiO<sub>2</sub>-based UV filters.

Untargeted metabolic profiling of T-AVO and Rutile exposed and un-exposed immune cells (CTR) for 72 h. Hierarchical clustering heatmaps display

significantly ( $p \leq 0.05$ ) different intracellular metabolites by LC-MS. Metabolic typing was performed on *P. lividus* primary immune cell cultures obtained from five individual donors.

TiO<sub>2</sub> fine powder (Rutile) has been used here as a negative control for T-AVO (Functionalized TiO<sub>2</sub> particle). In our recent studies we demonstrated that under TiO<sub>2</sub>NP-exposure (1 mg/L TiO<sub>2</sub>NPs nominal concentration, 24 h ending point) sea urchin innate immune system is able to control inflammatory signalling, excite antioxidant metabolic activity and acquire immunological tolerance<sup>95,175</sup>. Notably, sea urchin immune system metabolic typing under Rutile exposure for 72 h (1-day exposure at 2 mg/L followed by 2-days exposure at 1 mg/L) highlighted a different scenario compared with the respective T-AVO and control groups. L-glutamine, Acetamidovalerate and Pyrroglutamic acid levels present a trend similar to control, Lactic acid levels are similar to T-AVO exposed cells and Pyruvic acid levels are much more increased. Interestingly, L-serine, Sulfate and Glutaric acid levels present a trend completely different to both T-AVO and control groups. Specifically, L-serine, Sulfate were found reduced compared to controls, while Glutaric acid was found increased, highlighting an on-going inflammatory state. These findings show the superior immune-compatibility of T-AVO compared to Rutile when particles stay in contact with the sea urchin immune cells for 72 h (1-day exposure at 2 mg/L, and 2 days exposure at the half dose).

## 4. Conclusions

Our results overall demonstrate that the commercial n-TiO<sub>2</sub>-based UV filters tested in this work do not show any significant harmful impact towards the development, and **immunity** of the Mediterranean Sea Urchin (*P. lividus*) at environmental relevant concentrations. These results are in accordance with the majority of the risk assessment studies performed in the literature upon different marine organisms using pure rutile or anatase NPs summarized in the most relevant reviews<sup>79,87</sup>. The different coatings of the commercial UV filters, together with particle shape and original dispersant phase, seem to slightly modulate the effects toward the embryo development without still causing a relevant developmental impairment. In this context, the particle shape of hydrophilic NPs (bare rutile and T-AVO), pre-dispersed in MQW, seemed to predominantly influence the interaction with sea urchin embryos compared with other physical features such as primary particle size or aggregation state. Particularly, rod-shaped T-AVO NPs had slightly impact on the development compared to the spherical rutile NPs. The effects of hydrophobic UV filters (T-S and T-Lite) instead, were in line with their respective dispersion capacity in the former sunscreen oily dispersant medium, which is only related to their different particle external coatings. Finer dispersed T-Lite NPs showed a few visible effects compared to the T-S NPs, probably because of specific interactions with the octyldodecyl xyloside surfactant present in the sunscreen oily medium, which would likely ease its transportation inside the culture ASW culture medium.

Viability and toxicity tests on immune cells showed no toxicity of T-AVO NPs at environmental relevant concentrations. Furthermore, metabolic profile characterization performed on bare rutile and silica coated (T-AVO NPs) showed that these latter have a superior immune compatibility after 72h of interaction with sea urchin immune cells, ultimately proving the safety of this type of

commercial TiO<sub>2</sub> based UV filter on the immunological state and embryonic development of the Mediterranean-sea urchin.

This study highlighted the interest to utilize commercial mineral-based UV filters, rather than the pure bare counterpart, at environmental relevant concentrations, in order to assess more realistically their eco-toxicological impact. Further studies with a similar approach need to be performed in the future, on different biological models and at different experimental conditions, in order to fully confirm the safety of these nano-products.





## Chapter VIII: General conclusions and prospective

### 8.1 Conclusions

The present PhD work was inscribed into the wider project ECO-SUN, funded by SERENADE excellence initiative of Aix-Marseille University. The aim of the project was the evaluation of the risk associated to engineered nanomaterials (ENM) used in sunscreen formulation at all lifecycle stages of the product, together with the minimization and anticipation of the risk by application of a safer-by-design approach. After careful analysis of the current state-of-the-art, we decided to focus on some particular key-steps of the sunscreen lifecycle assessment (LCA) that, in our opinion, needed to be further investigated and clarified.

In the fabrication and usage stages of the product lifecycle, we studied three different aspects:

- determination of dispersion and aggregation state of  $\text{TiO}_2$  based ENM UV filters in complete sunscreen formulations;
- the optimization of these UV filters content in the formulation by the identification of the sunscreen component able to enhance their dispersion stability;
- the elucidation of the scattering and absorption pathway of light attenuation provided by the same UV filters.

In the release and environmental fate of the sunscreen lifecycle, we decided to look at two main problematics which are rarely investigated in the literature:

- the release and realistic concentrations of UV filters in the coastal marine environment;

- the eco-toxicological impact of commercially available nanoparticulate UV filters toward marine organism, at coastal marine environmental relevant concentrations.

A novel methodology, based on the use of 2D X-Ray Nano Tomography (XRNT), for the detection of mineral UV filters in sunscreen formulation is presented Chapter III of the manuscript. Indeed, this methodology proved to be suitable for determining the aggregation state of different  $\text{TiO}_2$  based ENMs without significantly alter the original sunscreen matrix, which is of crucial interest as such alterations during the treatment can also likely affect the original aggregation state of the ENMs, thus leading to artefact results. Even-though this methodology does not allow the determination of the primary particle size of the ENMs, contrarywise to finer characterization techniques as Cryogenic Transmission Electron Microscopy (Cryo-TEM), compared to this latter it is less expensive and time consuming and it is also able to provide accurate and representative information on the homogeneity of the entire emulsion. Indeed, ENMs aggregation state and emulsion homogeneity demonstrate to dramatically affect the efficiency of UV attenuation of the product. Moreover, it was observed that increasing the ENMs content eventually leads to an increase ENMs aggregate size and a loss of formulation homogeneity. The 2D XRNT based methodology presented in this manuscript could thus be useful not only for the mineral filter characterization, but also for the determination of the optimal ENMs concentration allowing the best dispersion stability and UVR attenuation efficiency.

Control the stability of the ENMs dispersion is thus a key step in the eco-design prospective of sunscreen nanoproduct. We studied this particular aspect in Chapter IV of the manuscript. The dispersion capacity of 4 four commercially available nano- $\text{TiO}_2$  based UV filters, characterized by different external and

internal coatings, were studied in the very first step of the sunscreen fabrication, that is during the dispersion in the oil phase of the formulation. It was observed that the emulsifying agent, and in particular the surfactant octyldodecyl xyloside (ODX), have preferential interaction for the ENMs surface and were able to stabilize all the 4 four UV filters tested. The extent of stabilization depends on the nature of external and internal coatings. In particular, aluminium (hydro)oxides internal coatings were hypothesised to be the elective interaction surfaces for the ODX substrate, which is interesting as this type of mineral coating is used in commercial mineral UV filters as passivating agent for the photo-reactivity of  $\text{TiO}_2$  nanoparticles. Such interaction with surfactant species contained in the formulation could also alter the transport and bioavailability of these ENMs at the moment of the environmental release of the nanoproduct, which makes such type of knowledge highly important also in a risk assessment prospective. Increase the ENMs dispersion stability was also seen to increase the UVR attenuation of the oily formulations until a factor 2 in certain cases. Controlling these parameters would thus enable the fabricants to produce more performant sunscreens with lower ENMs but similar protection efficiency. In other words, lower environmental foot-print nanoproducts.

Mineral filters could have two different UVR attenuation pathways: chemical absorption and physical scattering. The first one enables the photocatalytic generation of ROS at particle surfaces, which is the main toxicity pathways of  $\text{TiO}_2$  based UV filters. Such mechanism should be thus minimized in favour of the less impactful scattering interaction. In order to do this, it is mandatory to be able to distinguish between the two screening pathways. In Chapter V we focus on this problematic, designing and test-out an angular scatterometer able to detect the angular resolved scattering (ARS) of different  $\text{TiO}_2$  ENMs oily dispersions. After fabrication and optimisation of this novel analytical tool, preliminary results

showed that it enables to distinguish between structural absorption, transmitted and reflected scattering of the samples at wavelength of 405 nm. Nonetheless further development and analysis should be done in the future. In the first place, the laser source at 405 nm should be replaced by a laser source emitting in the UVB range, which will have the right frequency to be chemically absorbed by TiO<sub>2</sub>-based ENMs. Also, the set-up should be adapted for the analysis of oily dispersions spread on a PMMA plate in place of a quartz cuvette, in a similar way as standard used for *in vitro* SPF analysis. Such thinner device will likely minimize the structural absorption contribution of the sample, put more in evidence the chemical absorption of the ENMs. Finally, analysing different sized and shaped TiO<sub>2</sub> ENMs will eventually permit to elucidate how the morphology of these nanomaterials affect one or another UVR attenuation pathway.

The release in the marine environment of sunscreen nanoproducts, and the subsequent transportation and impact of the ENMs filters is a problematic which requires further investigation. Sampling and analysis of ENMs in marine environment present different technical obstacles and still represent an analytical challenge. During this PhD work, a sea water sampling campaign was realized in three major beaches of the Marseille sea shore, during the summer recreational activities. It is presented in Chapter VI. We quantified the coastal environmental concentration of both mineral and organic UV filters on both water column and surface microlayer. TiO<sub>2</sub> concentration range went from 10 to 900 ug/l, with a significant increase of the concentration near the bathing zone. Interestingly, in two of the three sampling sites, TiO<sub>2</sub> concentration in the surface microlayer was  $\approx$  10 times higher than in the water column. Such difference could be, among other, ascribed to the strong hydrophobicity of commercially available TiO<sub>2</sub> ENMs, which could probably remain stuck for a certain amount of time in the oily microlayer formed after the sunscreen release.

Such knowledge, inspired the following experimental design to determine the ecotoxicological impact of different commercial nano-TiO<sub>2</sub> based UV filters, on the immune system and embryos development of Sea Urchin biological model. This work is presented in Chapter VII. We used the same concentration range of ENMs detected in the sampling campaign, putting also particular attention to the hydrophobic or hydrophilic properties of the ENMs used. Hydrophobic ENMs were specifically pre-dispersed in sunscreen oil phase before the exposition to embryos culture medium, trying to reproduce the first stages of sunscreen aging after the environmental release, while hydrophilic filters were pre-dispersed in Milli-Q water. Although no warning toxicity for any of the tested ENMs was observed on both immune system and embryos of Mediterranean Sea-Urchin, interesting differences of harmful effect during the embryos development tests were observed between the filters as function of their shape, coating and dispersant medium. Among hydrophilic filters pre-dispersed in MQW, rod-shaped ENMs (T-AVO) showed slightly higher harmful effect than spherical counterpart (bare rutile), while among hydrophobic filters pre-dispersed in sunscreen oil phase, dimethicone coated ENMs (T-Lite) had a slightly higher impact than the stearic acid coated ones (T-S), which did not show any toxicity. Indeed, as discussed in chapter IV, T-Lite ENMs are more finely dispersed in the oil phase, because of their more favourable interaction with the ODX surfactant. It could thus be probable that, during the embryo development tests, that lasted 48h, the ODX surfactant could have favoured the transportation of these ENMs from the surface to the water column, making them more bioavailable toward the embryos. In prospective, eco-toxicological tests of mineral UV filters should be performed preferentially toward surface microlayer organisms (mostly fish egg and larvae), as it is becoming more and more evident that in this ecosystem, sunscreen ENMs impact could be more important.

We can develop the discussion in order to highlight this point. In Chapter VI we showed that the  $\text{TiO}_2$  concentration in coastal water is higher in the surface microlayer than in the water column during the summer recreational activity, in some sites even 1000 times higher. The knowledge provided in Chapters I, III and IV on the physical-chemical properties and preferential dispersing media of sunscreens ENMs, leads us to assume that such surface accumulation can be partially associated to the hydrophobicity of the mineral UV filters. During sunscreen aging in aquatic environment, the hydrophobic UV filters likely tend to remain in the oily surface layer rather than to disperse in the aqueous system. Moreover, at the smaller scale of the oil drop, the ENMs might even reach higher concentrations, potentially approaching that in the original oil phase of the sunscreen formulation. This raises the question of the environmental concentration at which the organisms living close the bathing area are actually exposed, and in particular those living under low water depth. Such local hot-spots highly concentrated in ENMs may have unexpected hazardous effects on marine and fresh water eco-systems. Putting together all these evidences and assumptions, made possible to design eco-toxicological experiments using different concentration ranges, each one representing a realistic scenario: from 1 to 10  $\mu\text{g/l}$  for the water column, from 100 to 1000  $\mu\text{g/l}$  for the surface microlayer and even  $> 1 \text{ mg/l}$  if we want to take into account also the oily hot-spot of ENMs.

Another example of close correlation between different stages of the sunscreen LCA, could be observed between Chapters III, IV and VI. Based on the social survey performed on three beaches of the Marseille sea-shore, we reported that a maximum of 1.3 kg of  $\text{TiO}_2$  could be released from the sunscreen consumed to the environment each day during the recreational activity on a beach attended by 3000 people (article III, Table 4). On another hand, we evidenced (chapter III)

how T-Lite ENM loaded sunscreen, given their finer ENMs dispersion and homogeneity, has a higher UV attenuation efficiency compared to T-S loaded sunscreens. Finely controlling the ENMs dispersion in sunscreen oil phase, as approached in Chapter IV, can help increasing twofold the screening efficiency with T-Lite ENMs. Reasoning *ad absurdum*, in our field study, if all the sunscreens containing TiO<sub>2</sub> were not optimised formulations (i.e. low stability and high aggregation state) but were replaced by optimized ingredients selection and dosage, an equivalent SPF level could be maintained with half the ENMs content. This could lead to decrease the maximum quantity of TiO<sub>2</sub> released to 650 g instead of 1.3 kg, and thus accordingly to a lower exposure of marine organisms. Although this is pure speculative reasoning, it gives an idea of how a fine analysis of the ENMs physical-chemical behaviour at the sunscreen fabrication stage can ultimately have a relevant positive effect on the environmental impact of sunscreen nanoproduct at the end-of-life stage.

In sum this PhD work highlighted how a lifecycle analysis could be a powerful tool to anticipate and assess the risk of nano-enabled products. Interdisciplinary studies could allow a better understanding of the inside mechanisms behind the potential risks of the nanoproduct starting from its fabrication till the end-of-life. In particular, knowing the physical-chemical properties of the nanomaterials and their interaction with the product components, will not only help us to anticipate and minimize the risk associated, but will also allow a more precise evaluation of their environmental fate together with a more realistic design and interpretation of the different eco-toxicological tests.

## 8.2 Prospective

The studies performed during this PhD work highlighted, among all, how the knowledge regarding the interactions and behaviour of ENMs in sunscreen formulation is still scarce and needs further understandings. In chapter III and IV we demonstrate how determining the surface interaction between the sunscreen components and the ENMs, is essential to control the aggregation state of the latter, optimize their concentrations and maximize the screening performances of the product. However, the study presented in Chapter IV needs to be further developed, by confirming and elucidate the mechanism of interaction between TiO<sub>2</sub> based UV filters and the ODX surfactants. With this purpose, it could be interesting to analyse the ENMs treated with the same aging procedure presented in Chapter IV, by X-Rays Photoelectron spectroscopy (XPS). XPS is a surface-sensitive quantitative spectroscopic technique able to give insight of the empirical formula, chemical state and electronic state of the elements that exist within a material. This characterization method will eventually allow the observation of new covalent bond created at the nanoparticle surface after the aging in the oil phase, and thus better understand the role of aluminium (hydro)oxide coating in the reaction mechanism.

Then, it could be also interesting to analyse the effects on ENMs dispersion stability of other types of bio-sourced emulsifying agents and emollient oils, different from the one used in the present work, using an optimized methodology inspired from the one presented in Chapter IV. The optimized methodology should first of all give insight of the effects of the recovery treatment, mediated by the use of cyclo-hexane, on the coating stability of the ENMs after the aging in oil phase. Particular attention should be also paid on performing the subsequent <sup>13</sup>C NMR characterization quantitatively, in order to precisely determine the



amount of oil phase remained attached on the surface and the amount of external coating loss during the treatment. The set of these studies will permit select the best ingredients (emollients, emulsifier and particle coating) that allow an optimal ENMs dispersion in the oil phase of the formulation during the initial stages of the sunscreen fabrication. The different oily dispersion could then be used to formulate full sunscreen formulations to be further analysed using the characterization methodology presented in Chapter III, in order to evaluate if the ENMs dispersion state in oil is maintained through the formulation process. Then, various  $\text{TiO}_2$  concentrations could be tested, in order to find out the optimal dose, which provides efficient UVR attenuation with minimal aggregation phenomena.

The optical properties of the different formulations, (simplified oily systems and/or full sunscreen formulations) could be then studied using the experimental set-up presented in Chapter V, implemented with UVB laser source and PMMA plate loaded with the sample to analyse as already suggested in the previous subchapter. Knowing the respective contributions of light scattered and absorbed is a crucial information to optimize a UV filter performance. Although the passivating coating  $\text{Al}_2\text{O}_3$  or  $\text{SiO}_2$  can minimize the photocatalytic activity of  $\text{TiO}_2$  based UV filters, it was observed that  $\text{SiO}_2$  could be rapidly degraded in aqueous media after the environmental release<sup>34</sup>. For this reason, it is still important to minimize the absorption pathways in favour of the scattering one. Among the scattered light, transmitted scattering mechanism should also be minimized, as such scattering radiation it is still susceptible to reach the user skin afterwards. Playing on the size and shape of the ENMs as well as on their aggregation state could likely be useful to favour one or another light interaction mechanism, and it could be definitely an interesting point to investigate. Eventually, the sum of all these studies during the fabrication stage of nano-enable sunscreens, will lead to

the development of new safer-by design nanoproducts with a lower environmental footprint.

New eco-toxicological test methodology could be also explored in order to better understand the environmental impact of these ENMs. A new insight could be to study the concomitant effects of organic and inorganic UV filters used together and separately, during the eco-toxicological tests, first of all to determine which one is more toxic. Moreover, as already mentioned in Chapter 1.2.2,  $\text{TiO}_2$  can exhibit a *carrier function*, meaning that it can interact with other molecules. Any attractive interaction between the ENM and the organic UV filters, may increase or decrease the bioavailability of the former. Besides, the interaction with organic filters can also modify the surface chemistry and reactivity of the  $\text{TiO}_2$  based ENMs, likely leading to unpredictable new effects towards target organisms. In this regard, aquatic organisms belonging to the surface microlayer of marine environment (i.e. proteobacteria; microplankton), should be preferentially used as biological model. As explained in Chapter 1.2.1, also confirmed by the results obtained during the field campaign in Chapter VI, in this particular ecosystem the highest  $\text{TiO}_2$  and  $\text{ZnO}$  concentrations are detected, and it will probably be the one more impacted by sunscreen UV filters pollution also in the near future. Microorganism in surface microlayer are also more exposed to detrimental factors as UV solar radiation<sup>194</sup>, which is an interesting variable to include in the design of new eco-toxicological tests.

With the aim of clarifying the UV filters eco-toxicity in more realistic environmental conditions, cocktail effect studies should be also performed. Once released into the aquatic environment, UV filters does not in fact represent the only pollutant species. For example, the presence of heavy and transition metals, as well as microplastics, in the environment could in some cases enhance the

impact of mineral UV filters, as was already observed by Santaella et al.<sup>195</sup> with aged TiO<sub>2</sub> based UV filters increasing the sensitivity of E.coli bacteria to cadmium exposition. The chronic impact of ENMs aging and cocktail effect should be more extensively studied by performing for example mesocosm experiments. Mesocosms are experimental systems designed to simulate specific ecosystems and proved to be really useful to assess the chronic fate and toxicity of different ENMs nanomaterials in complex environmental matrix<sup>196</sup>. Using mesocosm, we could also be able to test various organisms belonging to different marine ecosystems at the same time. For example, besides common organisms belonging to the water column, it would be interesting to add in the system organisms belonging to surface microlayer and sediment. This will allow to evaluate three different types of ENMs exposition: floating on the surface; transportation through the water column and sediment deposition.

It should be clear that in order to pursue all these goals and minimize the risk associated to ENMs used in sunscreen formulation, interdisciplinarity represents a fundamental mean. All the different studies, from microbiology to physical-chemistry, will need to be linked by an invisible string, seen as a piece of the same puzzle. This could be achieved only by networking and collaboration between all the scientists involved and the definition of common language and procedural protocols.



## References:

- (1) Oberdörster, G.; Maynard, A.; Donaldson, K.; Castranova, V.; Fitzpatrick, J.; Ausman, K.; Carter, J.; Karn, B.; Kreyling, W.; Lai, D.; Olin, S.; Monteiro-Riviere, N.; Warheit, D.; Yang, H. Principles for Characterizing the Potential Human Health Effects from Exposure to Nanomaterials: Elements of a Screening Strategy. *Part. Fibre Toxicol.* **2005**, *2* (1), 8. <https://doi.org/10.1186/1743-8977-2-8>.
- (2) Nanotechnology: The Next Big Thing, or Much Ado about Nothing? *Ann. Occup. Hyg.* **2006**. <https://doi.org/10.1093/annhyg/mel071>.
- (3) Yellepeddi, V. K.; Joseph, A.; Nance, E. Pharmacokinetics of Nanotechnology-Based Formulations in Pediatric Populations. *Adv. Drug Deliv. Rev.* **2019**, *151–152*, 44–55. <https://doi.org/10.1016/j.addr.2019.08.008>.
- (4) He, X.; Deng, H.; Hwang, H. The Current Application of Nanotechnology in Food and Agriculture. *J. Food Drug Anal.* **2019**, *27* (1), 1–21. <https://doi.org/10.1016/j.jfda.2018.12.002>.
- (5) Mu, L.; Sprando, R. L. Application of Nanotechnology in Cosmetics. *Pharm. Res.* **2010**, *27* (8), 1746–1749. <https://doi.org/10.1007/s11095-010-0139-1>.
- (6) Market Value of Nanotechnology Worldwide from 2010 to 2020. Statista <https://www.statista.com/statistics/1073886/global-market-value-nanotechnology/>.
- (7) Global Nanotechnology Market Outlook 2024. Research and Markets. <https://www.researchandmarkets.com/reports/4991720/global-nanotechnology-market-outlook-2024>.
- (8) Maynard, A. D. Nanotechnology: Assessing the Risks. *Nano Today* **2006**, *1* (2), 22–33. [https://doi.org/10.1016/S1748-0132\(06\)70045-7](https://doi.org/10.1016/S1748-0132(06)70045-7).
- (9) Hsiao, I.-L.; Huang, Y.-J. Effects of Various Physicochemical Characteristics on the Toxicities of ZnO and TiO<sub>2</sub> Nanoparticles toward Human Lung Epithelial Cells. *Sci. Total Environ.* **2011**, *409* (7), 1219–1228. <https://doi.org/10.1016/j.scitotenv.2010.12.033>.
- (10) Yen, H.; Hsu, S.; Tsai, C. Cytotoxicity and Immunological Response of Gold and Silver Nanoparticles of Different Sizes. *Small* **2009**, *5* (13), 1553–1561. <https://doi.org/10.1002/smll.200900126>.
- (11) Royal Society (London, G. B.; Royal Academy of Engineering (London, G. B. *Nanoscience and Nanotechnologies: Opportunities and Uncertainties*; Royal Society: London, 2004.
- (12) Adams, L. K.; Lyon, D. Y.; Alvarez, P. J. J. Comparative Eco-Toxicity of Nanoscale TiO<sub>2</sub>, SiO<sub>2</sub>, and ZnO Water Suspensions. *Water Res.* **2006**, *40* (19), 3527–3532. <https://doi.org/10.1016/j.watres.2006.08.004>.
- (13) Kato, H.; Suzuki, M.; Fujita, K.; Horie, M.; Endoh, S.; Yoshida, Y.; Iwahashi, H.; Takahashi, K.; Nakamura, A.; Kinugasa, S. Reliable Size Determination of Nanoparticles Using Dynamic Light

- Scattering Method for in Vitro Toxicology Assessment. *Toxicol. In Vitro* **2009**, 23 (5), 927–934. <https://doi.org/10.1016/j.tiv.2009.04.006>.
- (14) Singhal, A.; Skandan, G.; Wang, A.; Glumac, N.; Kear, B. H.; Hunt, R. D. On Nanoparticle Aggregation during Vapor Phase Synthesis. *Nanostructured Mater.* **1999**, 11 (4), 545–552. [https://doi.org/10.1016/S0965-9773\(99\)00343-8](https://doi.org/10.1016/S0965-9773(99)00343-8).
- (15) Labille, J.; Harns, C.; Bottero, J.-Y.; Brant, J. Heteroaggregation of Titanium Dioxide Nanoparticles with Natural Clay Colloids. *Environ. Sci. Technol.* **2015**, 49 (11), 6608–6616. <https://doi.org/10.1021/acs.est.5b00357>.
- (16) Wagner, S.; Gondikas, A.; Neubauer, E.; Hofmann, T.; von der Kammer, F. Spot the Difference: Engineered and Natural Nanoparticles in the Environment-Release, Behavior, and Fate. *Angew. Chem. Int. Ed.* **2014**, n/a-n/a. <https://doi.org/10.1002/anie.201405050>.
- (17) Kammer, F. von der; Ferguson, P. L.; Holden, P. A.; Masion, A.; Rogers, K. R.; Klaine, S. J.; Koelmans, A. A.; Horne, N.; Unrine, J. M. Analysis of Engineered Nanomaterials in Complex Matrices (Environment and Biota): General Considerations and Conceptual Case Studies. *Environ. Toxicol. Chem.* **2012**, 31 (1), 32–49. <https://doi.org/10.1002/etc.723>.
- (18) Handy, R. D.; Cornelis, G.; Fernandes, T.; Tsyusko, O.; Decho, A.; Sabo-Attwood, T.; Metcalfe, C.; Steevens, J. A.; Klaine, S. J.; Koelmans, A. A.; Horne, N. Ecotoxicity Test Methods for Engineered Nanomaterials: Practical Experiences and Recommendations from the Bench: Ecotoxicity Test Methods for Engineered Nanomaterials. *Environ. Toxicol. Chem.* **2012**, 31 (1), 15–31. <https://doi.org/10.1002/etc.706>.
- (19) American Society for Testing and Materials. Standard Guide for Conducting Acute Toxicity Tests on Test Materials with Fishes, Macro- Invertebrates, and Amphibians. Annual Book of ASTM Standards. 2007, pp 79–100.
- (20) U.S. Environmental Protection Agency. Methods for Measuring the Acute Toxicity of Effluents and Receiving Waters to Freshwater and Marine Organisms. 5th ed. EPA. 2007.
- (21) Crane, M.; Handy, R. D.; Garrod, J.; Owen, R. Ecotoxicity Test Methods and Environmental Hazard Assessment for Engineered Nanoparticles. *Ecotoxicology* **2008**, 17 (5), 421–437. <https://doi.org/10.1007/s10646-008-0215-z>.
- (22) Wang, J.; Gerlach, J. D.; Savage, N.; Cobb, G. P. Necessity and Approach to Integrated Nanomaterial Legislation and Governance. *Sci. Total Environ.* **2013**, 442, 56–62. <https://doi.org/10.1016/j.scitotenv.2012.09.073>.
- (23) Poças, F.; Franz, R. Overview on European Regulatory Issues, Legislation, and EFSA Evaluations of Nanomaterials. In *Nanomaterials for Food Packaging*; Elsevier, 2018; pp 277–300. <https://doi.org/10.1016/B978-0-323-51271-8.00010-3>.
- (24) Bergeson LL, Hester T. *Nanotechnology Deskbook.*, Environmental Law Institute.; Eli Press, 2008.
- (25) Guidance for Industry CGMP for Phase 1 Investigational Drugs. 20.

- (26) Zheng, N.; Sun, D. D.; Zou, P.; Jiang, W. Scientific and Regulatory Considerations for Generic Complex Drug Products Containing Nanomaterials. *AAPS J.* **2017**, *19* (3), 619–631. <https://doi.org/10.1208/s12248-017-0044-1>.
- (27) EPA. *Life Cycle Assessment: Principles and Practice*, National Risk Management Research Laboratory, USEPA.; 2006.
- (28) Baccile, N.; Babonneau, F.; Bejoy, T.; Coradin, T. Introducing Ecodesign in Silica Sol–Gel Materials. *J. Mater. Chem.* **2009**, *19* (45), 8515. <https://doi.org/10.1039/b911318e>.
- (29) Asmatulu, E.; Twomey, J.; Overcash, M. Life Cycle and Nano-Products: End-of-Life Assessment. *J. Nanoparticle Res.* **2012**, *14* (3), 720. <https://doi.org/10.1007/s11051-012-0720-0>.
- (30) The Woodrow Wilson Center’s Project on Emerging Nano-; technologies (PEN); <http://www.nanotechproject.org/inventories/consumer/browse/categories/>. Consumer Products/Categories. <http://www.nanotechproject.org/inventories/consumer/browse/categories/>. 2010.
- (31) Gavankar, S.; Suh, S.; Keller, A. F. Life Cycle Assessment at Nanoscale: Review and Recommendations. *Int. J. Life Cycle Assess.* **2012**, *17* (3), 295–303. <https://doi.org/10.1007/s11367-011-0368-5>.
- (32) Romero-Franco, M.; Godwin, H. A.; Bilal, M.; Cohen, Y. Needs and Challenges for Assessing the Environmental Impacts of Engineered Nanomaterials (ENMs). *Beilstein J. Nanotechnol.* **2017**, *8*, 989–1014. <https://doi.org/10.3762/bjnano.8.101>.
- (33) Giese, B.; Klaessig, F.; Park, B.; Kaegi, R.; Steinfeldt, M.; Wigger, H.; von Gleich, A.; Gottschalk, F. Risks, Release and Concentrations of Engineered Nanomaterial in the Environment. *Sci. Rep.* **2018**, *8* (1), 1565. <https://doi.org/10.1038/s41598-018-19275-4>.
- (34) Slomberg, D. L.; Catalano, R.; Ziarelli, F.; Viel, S.; Bartolomei, V.; Labille, J.; Masion, A. Aqueous Aging of a Silica Coated TiO<sub>2</sub> UV Filter Used in Sunscreens: Investigations at the Molecular Scale with Dynamic Nuclear Polarization NMR. *RSC Adv.* **2020**, *10* (14), 8266–8274. <https://doi.org/10.1039/D0RA00595A>.
- (35) Masion; Auffan; Rose. Monitoring the Environmental Aging of Nanomaterials: An Opportunity for Mesocosm Testing? *Materials* **2019**, *12* (15), 2447. <https://doi.org/10.3390/ma12152447>.
- (36) Auffan, M.; Liu, W.; Brousset, L.; Scifo, L.; Pariat, A.; Sanles, M.; Chaurand, P.; Angeletti, B.; Thiéry, A.; Masion, A.; Rose, J. Environmental Exposure of a Simulated Pond Ecosystem to a CuO Nanoparticle-Based Wood Stain throughout Its Life Cycle. *Environ. Sci. Nano* **2018**, *5* (11), 2579–2589. <https://doi.org/10.1039/C8EN00712H>.
- (37) Scifo, L.; Chaurand, P.; Bossa, N.; Avellan, A.; Auffan, M.; Masion, A.; Angeletti, B.; Kieffer, I.; Labille, J.; Bottero, J.-Y.; Rose, J. Non-Linear Release Dynamics for a CeO<sub>2</sub> Nanomaterial Embedded in a Protective Wood Stain, Due to Matrix Photo-Degradation. *Environ. Pollut.* **2018**, *241*, 182–193. <https://doi.org/10.1016/j.envpol.2018.05.045>.

- (38) Botta, C.; Labille, J.; Auffan, M.; Borschneck, D.; Miche, H.; Cabié, M.; Masion, A.; Rose, J.; Bottero, J.-Y. TiO<sub>2</sub>-Based Nanoparticles Released in Water from Commercialized Sunscreens in a Life-Cycle Perspective: Structures and Quantities. *Environ. Pollut.* **2011**, *159* (6), 1543–1550. <https://doi.org/10.1016/j.envpol.2011.03.003>.
- (39) Kaegi, R.; Ulrich, A.; Sinnet, B.; Vonbank, R.; Wichser, A.; Zuleeg, S.; Simmler, H.; Brunner, S.; Vonmont, H.; Burkhardt, M.; Boller, M. Synthetic TiO<sub>2</sub> Nanoparticle Emission from Exterior Facades into the Aquatic Environment. *Environ. Pollut.* **2008**, *156* (2), 233–239. <https://doi.org/10.1016/j.envpol.2008.08.004>.
- (40) Walker, G. W.; Kookana, R. S.; Smith, N. E.; Kah, M.; Doolette, C. L.; Reeves, P. T.; Lovell, W.; Anderson, D. J.; Turney, T. W.; Navarro, D. A. Ecological Risk Assessment of Nano-Enabled Pesticides: A Perspective on Problem Formulation. *J. Agric. Food Chem.* **2018**, *66* (26), 6480–6486. <https://doi.org/10.1021/acs.jafc.7b02373>.
- (41) Diffey, B. L. Sunscreens and Melanoma: The Future Looks Bright. *Br. J. Dermatol.* **2005**, *153* (2), 378–381. <https://doi.org/10.1111/j.1365-2133.2005.06729.x>.
- (42) Krickler, A.; Armstrong, B. K.; English, D. R. Sun Exposure and Non-Melanocytic Skin Cancer. *Cancer Causes Control* **1994**, *5* (4), 367–392. <https://doi.org/10.1007/BF01804988>.
- (43) Sowa, P.; Rutkowska-Talipska, J.; Rutkowski, K.; Kosztyla-Hojna, B.; Rutkowski, R. Optical Radiation in Modern Medicine. *Postępy Dermatol. Alergol.* **2013**, *6*.
- (44) Moyal, D. Prevention of Ultraviolet-Induced Skin Pigmentation. *5*.
- (45) Osterwalder, U.; Sohn, M.; Herzog, B. Global State of Sunscreens: Global State of Sunscreens. *Photodermatol. Photoimmunol. Photomed.* **2014**, *30* (2–3), 62–80. <https://doi.org/10.1111/phpp.12112>.
- (46) Diffey, B. L.; Tanner, P. R.; Matts, P. J.; Nash, J. F. In Vitro Assessment of the Broad-Spectrum Ultraviolet Protection of Sunscreen Products. *J. Am. Acad. Dermatol.* **2000**, *43* (6), 1024–1035. <https://doi.org/10.1067/mjd.2000.109291>.
- (47) Ferrero, L.; Pissavini, M.; Dehais, A.; Marguerie, S.; Zastrow, L. Importance of Substrate Roughness for in Vitro Sun Protection Assessment. *Int. J. Cosmet. Sci.* **2007**, *29* (1), 59–59. [https://doi.org/10.1111/j.1467-2494.2007.00340\\_2.x](https://doi.org/10.1111/j.1467-2494.2007.00340_2.x).
- (48) Diffey, B. L.; Robson, J. A New Substrate to Measure Sunscreen Protection Factors throughout the Ultraviolet Spectrum. *J. Soc. Cosmet. Chem.* *7*.
- (49) Gottschalk, F.; Sonderer, T.; Scholz, R. W.; Nowack, B. Possibilities and Limitations of Modeling Environmental Exposure to Engineered Nanomaterials by Probabilistic Material Flow Analysis. *Environ. Toxicol. Chem.* **2010**, n/a-n/a. <https://doi.org/10.1002/etc.135>.
- (50) Gottschalk, F.; Lassen, C.; Kjoelholm, J.; Christensen, F.; Nowack, B. Modeling Flows and Concentrations of Nine Engineered Nanomaterials in the Danish Environment. *Int. J. Environ. Res. Public Health* **2015**, *12* (5), 5581–5602. <https://doi.org/10.3390/ijerph120505581>.



- (51) Keller, A. A.; Vosti, W.; Wang, H.; Lazareva, A. Release of Engineered Nanomaterials from Personal Care Products throughout Their Life Cycle. *J. Nanoparticle Res.* **2014**, *16* (7), 2489. <https://doi.org/10.1007/s11051-014-2489-9>.
- (52) Boxall, A. B.; Tiede, K.; Chaudhry, Q. Engineered Nanomaterials in Soils and Water: How Do They Behave and Could They Pose a Risk to Human Health? *Nanomed.* **2007**, *2* (6), 919–927. <https://doi.org/10.2217/17435889.2.6.919>.
- (53) Gottschalk, F.; Sun, T.; Nowack, B. Environmental Concentrations of Engineered Nanomaterials: Review of Modeling and Analytical Studies. *Environ. Pollut.* **2013**, *181*, 287–300. <https://doi.org/10.1016/j.envpol.2013.06.003>.
- (54) Zhang, M.; J. H. Yang; Z. X. Cai; Y. D. Feng; Y. F. Wang; D. Y. Zhang; X. L. Pan. Detection of Engineered Nanoparticles in Aquatic Environments: Current Status and Challenges in Enrichment, Separation, and Analysis. *Environ. Sci.-Nano* **2019**, *6*, 709–735. <https://doi.org/10.1039/C8EN01086B>.
- (55) Tashiro, Y.; Kameda, Y. Concentration of Organic Sun-Blocking Agents in Seawater of Beaches and Coral Reefs of Okinawa Island, Japan. *Mar. Pollut. Bull.* **2013**, *77* (1–2), 333–340. <https://doi.org/10.1016/j.marpolbul.2013.09.013>.
- (56) Bargar, T. A.; Alvarez, D. A.; Garrison, V. H. Synthetic Ultraviolet Light Filtering Chemical Contamination of Coastal Waters of Virgin Islands National Park, St. John, U.S. Virgin Islands. *Mar. Pollut. Bull.* **2015**, *101* (1), 193–199. <https://doi.org/10.1016/j.marpolbul.2015.10.077>.
- (57) Mitchelmore, C. L.; He, K.; Gonsior, M.; Hain, E.; Heyes, A.; Clark, C.; Younger, R.; Schmitt-Kopplin, P.; Feerick, A.; Conway, A.; Blaney, L. Occurrence and Distribution of UV-Filters and Other Anthropogenic Contaminants in Coastal Surface Water, Sediment, and Coral Tissue from Hawaii. *Sci. Total Environ.* **2019**, *670*, 398–410. <https://doi.org/10.1016/j.scitotenv.2019.03.034>.
- (58) Giokas, D. L.; Salvador, A.; Chisvert, A. UV Filters: From Sunscreens to Human Body and the Environment. *TrAC Trends Anal. Chem.* **2007**, *26* (5), 360–374. <https://doi.org/10.1016/j.trac.2007.02.012>.
- (59) Santos, A. J. M.; Miranda, M. S.; Esteves da Silva, J. C. G. The Degradation Products of UV Filters in Aqueous and Chlorinated Aqueous Solutions. *Water Res.* **2012**, *46* (10), 3167–3176. <https://doi.org/10.1016/j.watres.2012.03.057>.
- (60) Gondikas, A.; von der Kammer, F.; Kaegi, R.; Borovinskaya, O.; Neubauer, E.; Navratilova, J.; Praetorius, A.; Cornelis, G.; Hofmann, T. Where Is the Nano? Analytical Approaches for the Detection and Quantification of TiO<sub>2</sub> Engineered Nanoparticles in Surface Waters. *Environ. Sci. Nano* **2018**, *5* (2), 313–326. <https://doi.org/10.1039/C7EN00952F>.
- (61) Domingos, R. F.; Baalousha, M. A.; Ju-Nam, Y.; Reid, M. M.; Tufenkji, N.; Lead, J. R.; Leppard, G. G.; Wilkinson, K. J. Characterizing Manufactured Nanoparticles in the Environment: Multimethod Determination of Particle Sizes. *Environ. Sci. Technol.* **2009**, *43* (19), 7277–7284. <https://doi.org/10.1021/es900249m>.
- (62) Simonet, B. M.; Valcárcel, M. Monitoring Nanoparticles in the Environment. *Anal. Bioanal. Chem.* **2009**, *393* (1), 17–21. <https://doi.org/10.1007/s00216-008-2484-z>.

- (63) Tovar-Sánchez, A.; Sánchez-Quiles, D.; Basterretxea, G.; Benedé, J. L.; Chisvert, A.; Salvador, A.; Moreno-Garrido, I.; Blasco, J. Sunscreen Products as Emerging Pollutants to Coastal Waters. *PLoS ONE* **2013**, *8* (6), e65451. <https://doi.org/10.1371/journal.pone.0065451>.
- (64) Reed, R. B.; Martin, D. P.; Bednar, A. J.; Montañó, M. D.; Westerhoff, P.; Ranville, J. F. Multi-Day Diurnal Measurements of Ti-Containing Nanoparticle and Organic Sunscreen Chemical Release during Recreational Use of a Natural Surface Water. *Environ. Sci. Nano* **2017**, *4* (1), 69–77. <https://doi.org/10.1039/C6EN00283H>.
- (65) Labille, J.; Feng, J.; Botta, C.; Borschneck, D.; Sammut, M.; Cabie, M.; Auffan, M.; Rose, J.; Bottero, J.-Y. Aging of TiO<sub>2</sub> Nanocomposites Used in Sunscreen. Dispersion and Fate of the Degradation Products in Aqueous Environment. *Environ. Pollut.* **2010**, *158* (12), 3482–3489. <https://doi.org/10.1016/j.envpol.2010.02.012>.
- (66) Sendra, M.; Sánchez-Quiles, D.; Blasco, J.; Moreno-Garrido, I.; Lubián, L. M.; Pérez-García, S.; Tovar-Sánchez, A. Effects of TiO<sub>2</sub> Nanoparticles and Sunscreens on Coastal Marine Microalgae: Ultraviolet Radiation Is Key Variable for Toxicity Assessment. *Environ. Int.* **2017**, *98*, 62–68. <https://doi.org/10.1016/j.envint.2016.09.024>.
- (67) A Giraldo; Rosa Montes; R Rodil; J B Quintana; Leticia Vidal-Liñán. Ecotoxicological Evaluation of the UV Filters Ethylhexyl Dimethyl P-Aminobenzoic Acid and Octocrylene Using Marine Organisms *Isochrysis Galbana*, *Mytilus Galloprovincialis* and *Paracentrotus Lividus*. *Arch. Environ. Contam. Toxicol.* **2017**, *72*, 4. <https://doi.org/10.1007/s00244-017-0399-4>.
- (68) Danovaro, R.; Bongiorno, L.; Corinaldesi, C.; Giovannelli, D.; Damiani, E.; Astolfi, P.; Greci, L.; Pusceddu, A. Sunscreens Cause Coral Bleaching by Promoting Viral Infections. *Environ. Health Perspect.* **2008**, *116* (4), 441–447. <https://doi.org/10.1289/ehp.10966>.
- (69) Paredes, E.; Perez, S.; Rodil, R.; Quintana, J. B.; Beiras, R. Ecotoxicological Evaluation of Four UV Filters Using Marine Organisms from Different Trophic Levels *Isochrysis Galbana*, *Mytilus Galloprovincialis*, *Paracentrotus Lividus*, and *Siriella Armata*. *Chemosphere* **2014**, *104*, 44–50. <https://doi.org/10.1016/j.chemosphere.2013.10.053>.
- (70) Fent, K.; Kunz, P. Y.; Zenker, A.; Rapp, M. A Tentative Environmental Risk Assessment of the UV-Filters 3-(4-Methylbenzylidene-Camphor), 2-Ethyl-Hexyl-4-Trimethoxycinnamate, Benzophenone-3, Benzophenone-4 and 3-Benzylidene Camphor. *Mar. Environ. Res.* **2010**, *69*, S4–S6. <https://doi.org/10.1016/j.marenvres.2009.10.010>.
- (71) Downs, C. A.; Kramarsky-Winter, E.; Segal, R.; Fauth, J.; Knutson, S.; Bronstein, O.; Ciner, F. R.; Jeger, R.; Lichtenfeld, Y.; Woodley, C. M.; Pennington, P.; Cadenas, K.; Kushmaro, A.; Loya, Y. Toxicopathological Effects of the Sunscreen UV Filter, Oxybenzone (Benzophenone-3), on Coral Planulae and Cultured Primary Cells and Its Environmental Contamination in Hawaii and the U.S. Virgin Islands. *Arch. Environ. Contam. Toxicol.* **2016**, *70* (2), 265–288. <https://doi.org/10.1007/s00244-015-0227-7>.
- (72) Tiede, K.; Hassellöv, M.; Breitbarth, E.; Chaudhry, Q.; Boxall, A. B. A. Considerations for Environmental Fate and Ecotoxicity Testing to Support Environmental Risk Assessments for Engineered Nanoparticles. *J. Chromatogr. A* **2009**, *1216* (3), 503–509. <https://doi.org/10.1016/j.chroma.2008.09.008>.

- (73) Lowry, G. V.; Gregory, K. B.; Apte, S. C.; Lead, J. R. Transformations of Nanomaterials in the Environment. *Environ. Sci. Technol.* **2012**, *46* (13), 6893–6899. <https://doi.org/10.1021/es300839e>.
- (74) Auffan, M.; Pedeutour, M.; Rose, J.; Masion, A.; Ziarelli, F.; Borschneck, D.; Chaneac, C.; Botta, C.; Chaurand, P.; Labille, J.; Bottero, J.-Y. Structural Degradation at the Surface of a TiO<sub>2</sub>-Based Nanomaterial Used in Cosmetics. *Environ. Sci. Technol.* **2010**, *44* (7), 2689–2694. <https://doi.org/10.1021/es903757q>.
- (75) Peijnenburg, W. J. G. M.; Baalousha, M.; Chen, J.; Chaudry, Q.; Von der kammer, F.; Kuhlbusch, T. A. J.; Lead, J.; Nickel, C.; Quik, J. T. K.; Renker, M.; Wang, Z.; Koelmans, A. A. A Review of the Properties and Processes Determining the Fate of Engineered Nanomaterials in the Aquatic Environment. *Crit. Rev. Environ. Sci. Technol.* **2015**, *45* (19), 2084–2134. <https://doi.org/10.1080/10643389.2015.1010430>.
- (76) Yung, M. M. N.; Wong, S. W. Y.; Kwok, K. W. H.; Liu, F. Z.; Leung, Y. H.; Chan, W. T.; Li, X. Y.; Djurišić, A. B.; Leung, K. M. Y. Salinity-Dependent Toxicities of Zinc Oxide Nanoparticles to the Marine Diatom *Thalassiosira pseudonana*. *Aquat. Toxicol.* **2015**, *165*, 31–40. <https://doi.org/10.1016/j.aquatox.2015.05.015>.
- (77) Wang, J.; Wang, W. Significance of Physicochemical and Uptake Kinetics in Controlling the Toxicity of Metallic Nanomaterials to Aquatic Organisms. *J. Zhejiang Univ. Sci. A* **2014**, *15* (8), 573–592. <https://doi.org/10.1631/jzus.A1400109>.
- (78) St, B. Marina A. Dobrovolskaia\* and Scott E. McNeil. *Nat. Nanotechnol.* **2007**, *2*, 10.
- (79) IMARES Onderzoeksformatie; Slijkerman, D. M. E.; Keur, M. *Sunscreen Ecoproducts: Product Claims, Potential Effects and Environmental Risks of Applied UV Filters*; Wageningen Marine Research: Den Helder, 2018. <https://doi.org/10.18174/457209>.
- (80) Wong, S. W. Y.; Leung, P. T. Y.; Djurišić, A. B.; Leung, K. M. Y. Toxicities of Nano Zinc Oxide to Five Marine Organisms: Influences of Aggregate Size and Ion Solubility. *Anal. Bioanal. Chem.* **2010**, *396* (2), 609–618. <https://doi.org/10.1007/s00216-009-3249-z>.
- (81) Trevisan, R.; Delapiedra, G.; Mello, D. F.; Arl, M.; Schmidt, É. C.; Meder, F.; Monopoli, M.; Cargnin-Ferreira, E.; Bouzon, Z. L.; Fisher, A. S.; Sheehan, D.; Dafre, A. L. Gills Are an Initial Target of Zinc Oxide Nanoparticles in Oysters *Crassostrea gigas*, Leading to Mitochondrial Disruption and Oxidative Stress. *Aquat. Toxicol.* **2014**, *153*, 27–38. <https://doi.org/10.1016/j.aquatox.2014.03.018>.
- (82) Miller, R. J.; Lenihan, H. S.; Muller, E. B.; Tseng, N.; Hanna, S. K.; Keller, A. A. Impacts of Metal Oxide Nanoparticles on Marine Phytoplankton. *Environ. Sci. Technol.* **2010**, *44* (19), 7329–7334. <https://doi.org/10.1021/es100247x>.
- (83) Sánchez-Quiles, D.; Tovar-Sánchez, A. Sunscreens as a Source of Hydrogen Peroxide Production in Coastal Waters. *Environ. Sci. Technol.* **2014**, *48* (16), 9037–9042. <https://doi.org/10.1021/es5020696>.

- (84) Sharma, V. K. Aggregation and Toxicity of Titanium Dioxide Nanoparticles in Aquatic Environment—A Review. *J. Environ. Sci. Health Part A* **2009**, *44* (14), 1485–1495. <https://doi.org/10.1080/10934520903263231>.
- (85) Farkas, J.; Bergum, S.; Nilsen, E. W.; Olsen, A. J.; Salaberria, I.; Ciesielski, T. M.; Bączek, T.; Konieczna, L.; Salvenmoser, W.; Jenssen, B. M. The Impact of TiO<sub>2</sub> Nanoparticles on Uptake and Toxicity of Benzo(a)Pyrene in the Blue Mussel (*Mytilus Edulis*). *Sci. Total Environ.* **2015**, *511*, 469–476. <https://doi.org/10.1016/j.scitotenv.2014.12.084>.
- (86) Ren, X.; Zhao, X.; Duan, X.; Fang, Z. Enhanced Bio-Concentration of Tris(1,3-Dichloro-2-Propyl) Phosphate in the Presence of Nano-TiO<sub>2</sub> Can Lead to Adverse Reproductive Outcomes in Zebrafish. *Environ. Pollut.* **2018**, *233*, 612–622. <https://doi.org/10.1016/j.envpol.2017.10.101>.
- (87) Minetto, D.; Libralato, G.; Volpi Ghirardini, A. Ecotoxicity of Engineered TiO<sub>2</sub> Nanoparticles to Saltwater Organisms: An Overview. *Environ. Int.* **2014**, *66*, 18–27. <https://doi.org/10.1016/j.envint.2014.01.012>.
- (88) Mueller, N. C.; Nowack, B. Exposure Modeling of Engineered Nanoparticles in the Environment. *Environ. Sci. Technol.* **2008**, *42* (12), 4447–4453. <https://doi.org/10.1021/es7029637>.
- (89) Clément, L.; Hurel, C.; Marmier, N. Toxicity of TiO<sub>2</sub> Nanoparticles to Cladocerans, Algae, Rotifers and Plants – Effects of Size and Crystalline Structure. *Chemosphere* **2013**, *90* (3), 1083–1090. <https://doi.org/10.1016/j.chemosphere.2012.09.013>.
- (90) Paterson, G.; Ataria, J. M.; Hoque, M. E.; Burns, D. C.; Metcalfe, C. D. The Toxicity of Titanium Dioxide Nanopowder to Early Life Stages of the Japanese Medaka (*Oryzias Latipes*). *Chemosphere* **2011**, *82* (7), 1002–1009. <https://doi.org/10.1016/j.chemosphere.2010.10.068>.
- (91) Hu, J.; Wang, J.; Liu, S.; Zhang, Z.; Zhang, H.; Cai, X.; Pan, J.; Liu, J. Effect of TiO<sub>2</sub> Nanoparticle Aggregation on Marine Microalgae *Isochrysis Galbana*. *J. Environ. Sci.* **2018**, *66*, 208–215. <https://doi.org/10.1016/j.jes.2017.05.026>.
- (92) Pinsino, A.; Matranga, V. Sea Urchin Immune Cells as Sentinels of Environmental Stress. *Dev. Comp. Immunol.* **2015**, *49* (1), 198–205. <https://doi.org/10.1016/j.dci.2014.11.013>.
- (93) Falugi, C.; Aluigi, M. G.; Chiantore, M. C.; Privitera, D.; Ramoino, P.; Gatti, M. A.; Fabrizi, A.; Pinsino, A.; Matranga, V. Toxicity of Metal Oxide Nanoparticles in Immune Cells of the Sea Urchin. *Mar. Environ. Res.* **2012**, *76*, 114–121. <https://doi.org/10.1016/j.marenvres.2011.10.003>.
- (94) Pinsino, A.; Russo, R.; Bonaventura, R.; Brunelli, A.; Marcomini, A.; Matranga, V. Titanium Dioxide Nanoparticles Stimulate Sea Urchin Immune Cell Phagocytic Activity Involving TLR/P38 MAPK-Mediated Signalling Pathway. *Sci. Rep.* **2015**, *5* (1), 14492. <https://doi.org/10.1038/srep14492>.
- (95) Alijagic, A.; Gaglio, D.; Napodano, E.; Russo, R.; Costa, C.; Benada, O.; Kofroňová, O.; Pinsino, A. Titanium Dioxide Nanoparticles Temporarily Influence the Sea Urchin Immunological State Suppressing Inflammatory-Related Gene Transcription and Boosting Antioxidant Metabolic Activity. *J. Hazard. Mater.* **2020**, *384*, 121389. <https://doi.org/10.1016/j.jhazmat.2019.121389>.

- (96) Brant, J.; Lecoanet, H.; Wiesner, M. R. Aggregation and Deposition Characteristics of Fullerene Nanoparticles in Aqueous Systems. *J. Nanoparticle Res.* **2005**, *7* (4–5), 545–553. <https://doi.org/10.1007/s11051-005-4884-8>.
- (97) French, R. A.; Jacobson, A. R.; Kim, B.; Isley, S. L.; Penn, R. L.; Baveye, P. C. Influence of Ionic Strength, PH, and Cation Valence on Aggregation Kinetics of Titanium Dioxide Nanoparticles. *Environ. Sci. Technol.* **2009**, *43* (5), 1354–1359. <https://doi.org/10.1021/es802628n>.
- (98) Mintel Group Ltd. Global New Products Database. Personal Care Portal. 2013. Available at <Http://Www.Gnpd.Com/>. Restricted Access, Accessed 18 October 2013.
- (99) Barrett C.; Gripp A. Solubilizing Avobenzone in Sunscreen Formulations without C12–15 Alkyl Benzoate. *SOFW Journal*. 2009, pp 28–33.
- (100) Evonik. Tegosoft P - Technical Information. 2018.
- (101) Cole CA; Vollhardt J; Mendrok C. Formulation and Stability of Sunscreen Products. *Lim HW, Draelos ZD, eds. Clinical guide to sunscreens and photoprotection, Basic and clinical dermatology*. 2009, pp 39–52.
- (102) Bonda C. Sunscreen Photostability. *Happi*. 2009, pp 72–75.
- (103) Brock, T. D.; Mosser, J. L. Rate of Sulfuric-Acid Production in Yellowstone National Park. *5*.
- (104) Carlson, R. W.; Anderson, M. S.; Johnson, R. E.; Schulman, M. B.; Yavrouian, A. H. Sulfuric Acid Production on Europa: The Radiolysis of Sulfur in Water Ice. *Icarus* **2002**, *157* (2), 456–463. <https://doi.org/10.1006/icar.2002.6858>.
- (105) Herzog B. Prediction of Sun Protection Factors and UV-A Parameters by Calculation of UV Transmissions Through Sunscreen Films of Inhomogeneous Surface Structure. *Sunscreens – regulations and commercial development, cosmetic science and technology, 3rd edn, Series 28*. Boca Raton: Taylor & Francis. 2005, pp 881–902.
- (106) Osterwalder, U.; Sohn, M.; Herzog, B. Global State of Sunscreens. *Photodermatol. Photoimmunol. Photomed.* **2014**, *30* (2–3), 62–80. <https://doi.org/10.1111/phpp.12112>.
- (107) Cole, C.; Shyr, T.; Ou-Yang, H. Metal Oxide Sunscreens Protect Skin by Absorption, Not by Reflection or Scattering. *Photodermatol. Photoimmunol. Photomed.* **2016**, *32* (1), 5–10. <https://doi.org/10.1111/phpp.12214>.
- (108) Wakefield, G.; Lipscomb, S.; Holland, E.; Knowland, J. The Effects of Manganese Doping on UVA Absorption and Free Radical Generation of Micronised Titanium Dioxide and Its Consequences for the Photostability of UVA Absorbing Organic Sunscreen Components. *Photochem. Photobiol. Sci.* **2004**, *3* (7), 648. <https://doi.org/10.1039/b403697b>.
- (109) Fujishima, A.; Zhang, X.; Tryk, D. TiO<sub>2</sub> Photocatalysis and Related Surface Phenomena. *Surf. Sci. Rep.* **2008**, *63* (12), 515–582. <https://doi.org/10.1016/j.surfrep.2008.10.001>.

- (110) King, D. M.; Liang, X.; Zhou, Y.; Carney, C. S.; Hakim, L. F.; Li, P.; Weimer, A. W. Atomic Layer Deposition of TiO<sub>2</sub> Films on Particles in a Fluidized Bed Reactor. *Powder Technol.* **2008**, *183* (3), 356–363. <https://doi.org/10.1016/j.powtec.2008.01.025>.
- (111) Faure, B.; Salazar-Alvarez, G.; Ahniyaz, A.; Villaluenga, I.; Berriozabal, G.; De Miguel, Y. R.; Bergström, L. Dispersion and Surface Functionalization of Oxide Nanoparticles for Transparent Photocatalytic and UV-Protecting Coatings and Sunscreens. *Sci. Technol. Adv. Mater.* **2013**, *14* (2), 023001. <https://doi.org/10.1088/1468-6996/14/2/023001>.
- (112) Roweczyk, L.; Duclairoir-Poc, C.; Barreau, M.; Picard, C.; Hucher, N.; Orange, N.; Grisel, M.; Feuilloley, M. Impact of Coated TiO<sub>2</sub>-Nanoparticles Used in Sunscreens on Two Representative Strains of the Human Microbiota: Effect of the Particle Surface Nature and Aging. *Colloids Surf. B Biointerfaces* **2017**, *158*, 339–348. <https://doi.org/10.1016/j.colsurfb.2017.07.013>.
- (113) Dzumedzey, Y.; Labille, J.; Cathala, B.; Moreau, C.; Santaella, C. Polysaccharide Coating on Environmental Collectors Affects the Affinity and Deposition of Nanoparticles. *NanoImpact* **2017**, *5*, 83–91. <https://doi.org/10.1016/j.impact.2016.12.004>.
- (114) Schulz, J.; Hohenberg, H.; Pflücker, F.; Gärtner, E.; Will, T.; Pfeiffer, S.; Wepf, R.; Wendel, V.; Gers-Barlag, H.; Wittern, K.-P. Distribution of Sunscreens on Skin. *Adv. Drug Deliv. Rev.* **2002**, *54*, S157–S163. [https://doi.org/10.1016/S0169-409X\(02\)00120-5](https://doi.org/10.1016/S0169-409X(02)00120-5).
- (115) Berube, D. M. Rhetorical Gamesmanship in the Nano Debates over Sunscreens and Nanoparticles. *J. Nanoparticle Res.* **2008**, *10* (S1), 23–37. <https://doi.org/10.1007/s11051-008-9362-7>.
- (116) Schneider, S. L.; Lim, H. W. A Review of Inorganic UV Filters Zinc Oxide and Titanium Dioxide. *Photodermatol. Photoimmunol. Photomed.* **2018**, phpp.12439. <https://doi.org/10.1111/phpp.12439>.
- (117) Smijs, T.; Pavel. Titanium Dioxide and Zinc Oxide Nanoparticles in Sunscreens: Focus on Their Safety and Effectiveness. *Nanotechnol. Sci. Appl.* **2011**, 95. <https://doi.org/10.2147/NSA.S19419>.
- (118) Egerton, T. A.; Tooley, I. R. UV Absorption and Scattering Properties of Inorganic-Based Sunscreens: Absorption and Scattering by TiO<sub>2</sub>. *Int. J. Cosmet. Sci.* **2012**, *34* (2), 117–122. <https://doi.org/10.1111/j.1468-2494.2011.00689.x>.
- (119) Tyner, K. M.; Wokovich, A. M.; Godar, D. E.; Doub, W. H.; Sadrieh, N. The State of Nano-Sized Titanium Dioxide (TiO<sub>2</sub>) May Affect Sunscreen Performance: Nano-Sized TiO<sub>2</sub> and Sunscreen Performance. *Int. J. Cosmet. Sci.* **2011**, *33* (3), 234–244. <https://doi.org/10.1111/j.1468-2494.2010.00622.x>.
- (120) Karlsson, R.; Luttrupp, C. EcoDesign: What's Happening? An Overview of the Subject Area of EcoDesign and of the Papers in This Special Issue. *J. Clean. Prod.* **2006**, *14* (15–16), 1291–1298. <https://doi.org/10.1016/j.jclepro.2005.11.010>.
- (121) Rossano, M.; Hucher, N.; Picard, C.; Colletta, D.; Le Foll, F.; Grisel, M. Effects of Aging on Structure and Stability of TiO<sub>2</sub> Nanoparticle-Containing Oil-in-Water Emulsions. *Int. J. Pharm.* **2014**, *461* (1–2), 89–96. <https://doi.org/10.1016/j.ijpharm.2013.11.039>.

- (122) Chevalier, Y.; Bolzinger, M.-A. Emulsions Stabilized with Solid Nanoparticles: Pickering Emulsions. *Colloids Surf. Physicochem. Eng. Asp.* **2013**, *439*, 23–34. <https://doi.org/10.1016/j.colsurfa.2013.02.054>.
- (123) Roweczyk, L.; Picard, C.; Duclairoir-Poc, C.; Hucher, N.; Orange, N.; Feuilleley, M.; Grisel, M. Development of Preservative-Free Nanoparticles-Based Emulsions: Effects of NP Surface Properties and Sterilization Process. *Int. J. Pharm.* **2016**, *510* (1), 125–134. <https://doi.org/10.1016/j.ijpharm.2016.06.014>.
- (124) Imae, T.; Muto, K.; Ikeda, S. The PH Dependence of Dispersion of TiO<sub>2</sub> Particles in Aqueous Surfactant Solutions. *Colloid Polym. Sci.* **1991**, *269* (1), 43–48. <https://doi.org/10.1007/BF00654658>.
- (125) Loosli, F.; Stoll, S. Effect of Surfactants, PH and Water Hardness on the Surface Properties and Agglomeration Behavior of Engineered TiO<sub>2</sub> Nanoparticles. *Environ. Sci. Nano* **2017**, *4* (1), 203–211. <https://doi.org/10.1039/C6EN00339G>.
- (126) Núñez-Rojas, E.; Domínguez, H. Computational Studies on the Behavior of Sodium Dodecyl Sulfate (SDS) at TiO<sub>2</sub>(Rutile)/Water Interfaces. *J. Colloid Interface Sci.* **2011**, *364* (2), 417–427. <https://doi.org/10.1016/j.jcis.2011.08.069>.
- (127) Tovar-Sánchez, A.; Sánchez-Quiles, D.; Rodríguez-Romero, A. Massive Coastal Tourism Influx to the Mediterranean Sea: The Environmental Risk of Sunscreens. *Sci. Total Environ.* **2019**, *656*, 316–321. <https://doi.org/10.1016/j.scitotenv.2018.11.399>.
- (128) Skoglund, S.; Lowe, T. A.; Hedberg, J.; Blomberg, E.; Wallinder, I. O.; Wold, S.; Lundin, M. Effect of Laundry Surfactants on Surface Charge and Colloidal Stability of Silver Nanoparticles. *Langmuir* **2013**, *29* (28), 8882–8891. <https://doi.org/10.1021/la4012873>.
- (129) Oberdörster, G.; Oberdörster, E.; Oberdörster, J. Nanotoxicology: An Emerging Discipline Evolving from Studies of Ultrafine Particles. *Environ. Health Perspect.* **2005**, *113* (7), 823–839. <https://doi.org/10.1289/ehp.7339>.
- (130) Monteiro-Riviere, N. A.; Wiench, K.; Landsiedel, R.; Schulte, S.; Inman, A. O.; Riviere, J. E. Safety Evaluation of Sunscreen Formulations Containing Titanium Dioxide and Zinc Oxide Nanoparticles in UVB Sunburned Skin: An In Vitro and In Vivo Study. *Toxicol. Sci.* **2011**, *123* (1), 264–280. <https://doi.org/10.1093/toxsci/kfr148>.
- (131) Zhang, L. W.; Monteiro-Riviere, N. A. Toxicity Assessment of Six Titanium Dioxide Nanoparticles in Human Epidermal Keratinocytes. *Cutan. Ocul. Toxicol.* **2019**, *38* (1), 66–80. <https://doi.org/10.1080/15569527.2018.1527848>.
- (132) Wang, S.; Lu, W.; Tovmachenko, O.; Rai, U. S.; Yu, H.; Ray, P. C. Challenge in Understanding Size and Shape Dependent Toxicity of Gold Nanomaterials in Human Skin Keratinocytes. *Chem. Phys. Lett.* **2008**, *463* (1–3), 145–149. <https://doi.org/10.1016/j.cplett.2008.08.039>.
- (133) Peltonen, L. Practical Guidelines for the Characterization and Quality Control of Pure Drug Nanoparticles and Nano-Cocrystals in the Pharmaceutical Industry. *Adv. Drug Deliv. Rev.* **2018**, *131*, 101–115. <https://doi.org/10.1016/j.addr.2018.06.009>.

- (134) Tyner, K. M.; Wokovich, A. M.; Doub, W. H.; Buhse, L. F.; Sung, L.-P.; Watson, S. S.; Sadrieh, N. Comparing Methods for Detecting and Characterizing Metal Oxide Nanoparticles in Unmodified Commercial Sunscreens. *Nanomed.* **2009**, *4* (2), 145–159. <https://doi.org/10.2217/17435889.4.2.145>.
- (135) Lu, P. J.; Cheng, W. L.; Huang, S. C.; Chen, Y. P.; Chou, H. K.; Cheng, H. F. Characterizing Titanium Dioxide and Zinc Oxide Nanoparticles in Sunscreen Spray. *Int. J. Cosmet. Sci.* **2015**, *37* (6), 620–626. <https://doi.org/10.1111/ics.12239>.
- (136) Wokovich, A.; Tyner, K.; Doub, W.; Sadrieh, N.; Buhse, L. F. Particle Size Determination of Sunscreens Formulated with Various Forms of Titanium Dioxide. *Drug Dev. Ind. Pharm.* **2009**, *35* (10), 1180–1189. <https://doi.org/10.1080/03639040902838043>.
- (137) Butler, M. K.; Prow, T. W.; Guo, Y.-N.; Lin, L. L.; Webb, R. I.; Martin, D. J. High-Pressure Freezing/Freeze Substitution and Transmission Electron Microscopy for Characterization of Metal Oxide Nanoparticles within Sunscreens. *Nanomed.* **2012**, *7* (4), 541–551. <https://doi.org/10.2217/nmm.11.149>.
- (138) Philippe, A.; Košík, J.; Welle, A.; Guigner, J.-M.; Clemens, O.; Schaumann, G. E. Extraction and Characterization Methods for Titanium Dioxide Nanoparticles from Commercialized Sunscreens. *Environ. Sci. Nano* **2018**, *5* (1), 191–202. <https://doi.org/10.1039/C7EN00677B>.
- (139) Schilling, K.; Bradford, B.; Castelli, D.; Dufour, E.; Nash, J. F.; Pape, W.; Schulte, S.; Tooley, I.; van den Bosch, J.; Schellauf, F. Human Safety Review of “Nano” Titanium Dioxide and Zinc Oxide. *Photochem. Photobiol. Sci.* **2010**, *9* (4), 495. <https://doi.org/10.1039/b9pp00180h>.
- (140) Litter, M. Heterogeneous Photocatalysis Transition Metal Ions in Photocatalytic Systems. *Appl. Catal. B Environ.* **1999**, *23* (2–3), 89–114. [https://doi.org/10.1016/S0926-3373\(99\)00069-7](https://doi.org/10.1016/S0926-3373(99)00069-7).
- (141) Pitkethy, M. J. Nanoparticles as Building Blocks? *Mater. Today* **2003**, *6* (12), 36–42. [https://doi.org/10.1016/S1369-7021\(03\)00022-1](https://doi.org/10.1016/S1369-7021(03)00022-1).
- (142) Chatterjee, R. The Challenge of Regulating Nanomaterials. *Environ. Sci. Technol.* **2008**, *42* (2), 339–343. <https://doi.org/10.1021/es0870909>.
- (143) Bijker, W. E.; de Beaufort, I. D.; van den Berg, A.; Borm, P. J. A.; Oyen, W. J. G.; Robillard, G. T.; van Dijk, H. F. G. A Response to ‘Nanotechnology and the Need for Risk Governance’, O. Renn & M.C. Roco, 2006. J. Nanoparticle Research 8(2): 153–191. *J. Nanoparticle Res.* **2007**, *9* (6), 1217–1220. <https://doi.org/10.1007/s11051-007-9261-3>.
- (144) Catalano, R.; Masion, A.; Ziarelli, F.; Slomberg, D.; Laisney, J.; Unrine, J. M.; Campos, A.; Labille, J. Optimizing the Dispersion of Nanoparticulate TiO<sub>2</sub>-Based UV Filters in a Non-Polar Medium Used in Sunscreen Formulations – The Roles of Surfactants and Particle Coatings. *Colloids Surf. Physicochem. Eng. Asp.* **2020**, 124792. <https://doi.org/10.1016/j.colsurfa.2020.124792>.
- (145) Xu, Z.; Liu, Q.; Ling, J. An Evaluation of the van Oss-Chaudhury-Good Equation and Neumann’s Equation of State Approach with Mercury Substrate. *Langmuir* **1995**, *11* (3), 1044–1046. <https://doi.org/10.1021/la00003a058>.



- (146) Henke, B. L.; Gullikson, E. M.; Davis, J. C. X-Ray Interactions: Photoabsorption, Scattering, Transmission and Reflection. 174.
- (147) Hubbell, J. H.; Veigele, Wm. J.; Briggs, E. A.; Brown, R. T.; Cromer, D. T.; Howerton, R. J. Atomic Form Factors, Incoherent Scattering Functions, and Photon Scattering Cross Sections. *J. Phys. Chem. Ref. Data* **1975**, *4* (3), 471–538. <https://doi.org/10.1063/1.555523>.
- (148) Chou, J.; Robinson, T. J.; Doan, H. Rapid Comparison of UVB Absorption Effectiveness of Various Sunscreens by UV-Vis Spectroscopy. *J. Anal. Bioanal. Tech.* **2017**, *08* (02). <https://doi.org/10.4172/2155-9872.1000355>.
- (149) van Oss, C. J. The Extended DLVO Theory. In *Interface Science and Technology*; Elsevier, 2008; Vol. 16, pp 31–48. [https://doi.org/10.1016/S1573-4285\(08\)00203-2](https://doi.org/10.1016/S1573-4285(08)00203-2).
- (150) Sambandan, D. R.; Ratner, D. Sunscreens: An Overview and Update. *J. Am. Acad. Dermatol.* **2011**, *64* (4), 748–758. <https://doi.org/10.1016/j.jaad.2010.01.005>.
- (151) Martínez-López, F.; Cabrerizo-Vílchez, M. A.; Hidalgo-Álvarez, R. Colloidal Interaction at the Air–Liquid Interface. *J. Colloid Interface Sci.* **2000**, *232* (2), 303–310. <https://doi.org/10.1006/jcis.2000.7172>.
- (152) Stiller, S.; Gers-Barlag, H.; Lergenmueller, M.; Pflücker, F.; Schulz, J.; Wittern, K. P.; Daniels, R. Investigation of the Stability in Emulsions Stabilized with Different Surface Modified Titanium Dioxides. *Colloids Surf. Physicochem. Eng. Asp.* **2004**, *232* (2–3), 261–267. <https://doi.org/10.1016/j.colsurfa.2003.11.003>.
- (153) Everett, D. H. Basic Principles of Colloids Science. In *RSC Paperbacks*; Royal Society of Chemistry: Cambridge, 2007; pp P009-P015. <https://doi.org/10.1039/9781847550200-FP009>.
- (154) Kollias, N.; Baqer, A.; Naqvi, K. R. Fiber Optic Spectrophotometer for Noninvasive Transmission and Diffuse Reflection Studies. *Spectrosc. Lett.* **1986**, *19* (2), 149–165. <https://doi.org/10.1080/00387018608069228>.
- (155) Goebel, D. G. Generalized Integrating-Sphere Theory. *Appl. Opt.* **1967**, *6* (1), 125. <https://doi.org/10.1364/AO.6.000125>.
- (156) Clarke, F. J. J.; Compton, J. A. Correction Methods for Integrating-Sphere Measurement of Hemispherical Reflectance. *Color Res. Appl.* **1986**, *11* (4), 253–262. <https://doi.org/10.1002/col.5080110406>.
- (157) Roos, A.; Ribbing, C. G. Interpretation of Integrating Sphere Signal Output for Non-Lambertian Samples. *Appl. Opt.* **1988**, *27* (18), 3833. <https://doi.org/10.1364/AO.27.003833>.
- (158) Payne, D. N. R.; Charlton, M. D. B.; Bagnall, D. M. Broadband Wavelength and Angle-Resolved Scattering Characterization for Nanophotonics Investigations. *Appl. Opt.* **2015**, *54* (24), 7224. <https://doi.org/10.1364/AO.54.007224>.
- (159) Amra, C.; Grezes-Besset, C.; Roche, P.; Pelletier, E. Description of a Scattering Apparatus: Application to the Problems of Characterization of Opaque Surfaces. *Appl. Opt.* **1989**, *28* (14), 2723. <https://doi.org/10.1364/AO.28.002723>.

- (160) Elson, J. M.; Rahn, J. P.; Bennett, J. M. Relationship of the Total Integrated Scattering from Multilayer-Coated Optics to Angle of Incidence, Polarization, Correlation Length, and Roughness Cross-Correlation Properties. *Appl. Opt.* **1983**, 22 (20), 3207. <https://doi.org/10.1364/AO.22.003207>.
- (161) Snyder, W. C.; Wan, Z.; Li, X. Thermodynamic Constraints on Reflectance Reciprocity and Kirchhoff's Law. *Appl. Opt.* **1998**, 37 (16), 3464. <https://doi.org/10.1364/AO.37.003464>.
- (162) Pollack, J. B.; Cuzzi, J. N. Scattering by Nonspherical Particles of Size Comparable to a Wavelength: A New Semi-Empirical Theory and Its Application to Tropospheric Aerosols. *Journal of the atmospheric science*. 1980, pp 868–881.
- (163) Liu, L. Effects of Aggregation on Scattering and Radiative Properties of Soot Aerosols. *J. Geophys. Res.* **2005**, 110 (D11), D11211. <https://doi.org/10.1029/2004JD005649>.
- (164) Vos, K.; Krusemeyer, H. J. Reflectance and Electreflectance of TiO<sub>2</sub>single Crystals. I. Optical Spectra. *J. Phys. C Solid State Phys.* **1977**, 10 (19), 3893–3915. <https://doi.org/10.1088/0022-3719/10/19/023>.
- (165) McCoy, D. E.; Feo, T.; Harvey, T. A.; Prum, R. O. Structural Absorption by Barbule Microstructures of Super Black Bird of Paradise Feathers. *Nat. Commun.* **2018**, 9 (1), 1. <https://doi.org/10.1038/s41467-017-02088-w>.
- (166) Tao, H.; Lin, J.; Hao, Z.; Gao, X.; Song, X.; Sun, C.; Tan, X. Formation of Strong Light-Trapping Nano- and Microscale Structures on a Spherical Metal Surface by Femtosecond Laser Filament. *Appl. Phys. Lett.* **2012**, 100 (20), 201111. <https://doi.org/10.1063/1.4719108>.
- (167) Wriedt, T. Mie Theory: A Review. In *The Mie Theory*; Hergert, W., Wriedt, T., Eds.; Springer Series in Optical Sciences; Springer Berlin Heidelberg: Berlin, Heidelberg, 2012; Vol. 169, pp 53–71. [https://doi.org/10.1007/978-3-642-28738-1\\_2](https://doi.org/10.1007/978-3-642-28738-1_2).
- (168) Young, A. T. Rayleigh Scattering. *Appl Opt* **1981**, 20 (4), 533–535. <https://doi.org/10.1364/AO.20.000533>.
- (169) Voarino, P.; Zerrad, M.; Deumié, C.; Amra, C. Multidielectric Quarter-Wave Coatings on Microspheres: A Study in Colorimetric Space. *Appl. Opt.* **2006**, 45 (7), 1469. <https://doi.org/10.1364/AO.45.001469>.
- (170) EWG's Sunscreen Guide, 2018; <https://www.ewg.org/sunscreen/report/executive-summary/#.WxcjvVMvxmB>.
- (171) *Sustainable Coastal Tourism: An Integrated Planning and Management Approach ; [Priority Actions Programme]*; UNEP, Ed.; UNEP manuals on sustainable tourism; United Nations Environment Programme: Nairobi, 2009.
- (172) Corinaldesi, C.; Marcellini, F.; Nepote, E.; Damiani, E.; Danovaro, R. Impact of Inorganic UV Filters Contained in Sunscreen Products on Tropical Stony Corals (*Acropora* Spp.). *Sci. Total Environ.* **2018**, 637–638, 1279–1285. <https://doi.org/10.1016/j.scitotenv.2018.05.108>.

- (173) Gerloff, K.; Fenoglio, I.; Carella, E.; Kolling, J.; Albrecht, C.; Boots, A. W.; Förster, I.; Schins, R. P. F. Distinctive Toxicity of TiO<sub>2</sub> Rutile/Anatase Mixed Phase Nanoparticles on Caco-2 Cells. *Chem. Res. Toxicol.* **2012**, *25* (3), 646–655. <https://doi.org/10.1021/tx200334k>.
- (174) Matranga, V.; Toia, G.; Bonaventura, R. Cellular and Biochemical Responses to Environmental and Experimentally Induced Stress in Sea Urchin Coelomocytes. *Cell Stress* **2000**, *8*.
- (175) Alijagic, A.; Benada, O.; Kofroňová, O.; Cigna, D.; Pinsino, A. Sea Urchin Extracellular Proteins Design a Complex Protein Corona on Titanium Dioxide Nanoparticle Surface Influencing Immune Cell Behavior. *Front. Immunol.* **2019**, *10*, 2261. <https://doi.org/10.3389/fimmu.2019.02261>.
- (176) Catalano R.; Masion A.; Ziarelli F.; Slomberg D.; Laisney J.; Unrine J. M.; Campos A.; Labille J. Optimizing the Dispersion of Nanoparticulate TiO<sub>2</sub>-Based UV Filters in a Non-Polar Medium Used in Sunscreen Formulations - the Roles of Surfactants and Particle Coatings. (Accepted). *Colloids and Surfaces A: Physicochemical and Engineering Aspects*. 2020.
- (177) Labille, J.; Brant, J. Stability of Nanoparticles in Water. *Nanomed.* **2010**, *5* (6), 985–998. <https://doi.org/10.2217/nnm.10.62>.
- (178) Jérôme Labille; Danielle Slomberg; Riccardo Catalano; Samuel Robert; Marie-Laure Apers-Tremelo; Jean-Luc Boudenne; Tarek Manasfi; Olivier Radakovitch. Assessing UV Filter Inputs into Beach Waters during Recreational Activity: A Field Study of Three French Mediterranean Beaches from Consumer Survey to Water Analysis. *Sci. Total Environ.* **2019**.
- (179) Gambardella, C.; Aluigi, M. G.; Ferrando, S.; Gallus, L.; Ramoino, P.; Gatti, A. M.; Rottigni, M.; Falugi, C. Developmental Abnormalities and Changes in Cholinesterase Activity in Sea Urchin Embryos and Larvae from Sperm Exposed to Engineered Nanoparticles. *Aquat. Toxicol.* **2013**, *130–131*, 77–85. <https://doi.org/10.1016/j.aquatox.2012.12.025>.
- (180) Carballeira, C.; Ramos-Gómez, J.; Martín-Díaz, L.; DelValls, T. A. Identification of Specific Malformations of Sea Urchin Larvae for Toxicity Assessment: Application to Marine Pisciculture Effluents. *Mar. Environ. Res.* **2012**, *77*, 12–22. <https://doi.org/10.1016/j.marenvres.2012.01.001>.
- (181) Pinsino, A.; Bergami, E.; Della Torre, C.; Vannuccini, M. L.; Addis, P.; Secci, M.; Dawson, K. A.; Matranga, V.; Corsi, I. Amino-Modified Polystyrene Nanoparticles Affect Signalling Pathways of the Sea Urchin ( *Paracentrotus Lividus* ) Embryos. *Nanotoxicology* **2017**, *11* (2), 201–209. <https://doi.org/10.1080/17435390.2017.1279360>.
- (182) Magesky, A.; Pelletier, É. Toxicity Mechanisms of Ionic Silver and Polymer-Coated Silver Nanoparticles with Interactions of Functionalized Carbon Nanotubes on Early Development Stages of Sea Urchin. *Aquat. Toxicol.* **2015**, *167*, 106–123. <https://doi.org/10.1016/j.aquatox.2015.07.011>.
- (183) Li, Y.; Chen, X.; Gu, N. Computational Investigation of Interaction between Nanoparticles and Membranes: Hydrophobic/Hydrophilic Effect. *J. Phys. Chem. B* **2008**, *112* (51), 16647–16653. <https://doi.org/10.1021/jp8051906>.
- (184) Yamamoto, A.; Honma, R.; Sumita, M.; Hanawa, T. Cytotoxicity Evaluation of Ceramic Particles of Different Sizes and Shapes. *J. Biomed. Mater. Res.* **2004**, *68A* (2), 244–256. <https://doi.org/10.1002/jbm.a.20020>.

- (185) Brown, S. C.; Kamal, M.; Nasreen, N.; Baumuratov, A.; Sharma, P.; Antony, V. B.; Moudgil, B. M. Influence of Shape, Adhesion and Simulated Lung Mechanics on Amorphous Silica Nanoparticle Toxicity. *Adv. Powder Technol.* **2007**, *18* (1), 69–79. <https://doi.org/10.1163/156855207779768214>.
- (186) Jaroenworarluck, A.; Sunsaneeyametha, W.; Kosachan, N.; Stevens, R. Characteristics of Silica-Coated TiO<sub>2</sub> and Its UV Absorption for Sunscreen Cosmetic Applications. *Surf. Interface Anal.* **2006**, *38* (4), 473–477. <https://doi.org/10.1002/sia.2313>.
- (187) Ganeshan, K.; Chawla, A. Metabolic Regulation of Immune Responses. *Annu. Rev. Immunol.* **2014**, *32* (1), 609–634. <https://doi.org/10.1146/annurev-immunol-032713-120236>.
- (188) de Oliveira, D. C.; da Silva Lima, F.; Sartori, T.; Santos, A. C. A.; Rogero, M. M.; Fock, R. A. Glutamine Metabolism and Its Effects on Immune Response: Molecular Mechanism and Gene Expression. *Nutrire* **2016**, *41* (1), 14. <https://doi.org/10.1186/s41110-016-0016-8>.
- (189) Rani, P.; Pal, D.; Hegde, R. R.; Hashim, S. R. Acetamides: Chemotherapeutic Agents for Inflammation-Associated Cancers. *J. Chemother.* **2016**, *28* (4), 255–265. <https://doi.org/10.1179/1973947815Y.00000000060>.
- (190) Ratter, J. M.; Rooijackers, H. M. M.; Hooiveld, G. J.; Hijmans, A. G. M.; de Galan, B. E.; Tack, C. J.; Stienstra, R. In Vitro and in Vivo Effects of Lactate on Metabolism and Cytokine Production of Human Primary PBMCs and Monocytes. *Front. Immunol.* **2018**, *9*, 2564. <https://doi.org/10.3389/fimmu.2018.02564>.
- (191) Pederzoli, C. D.; Mescka, C. P.; Zandoná, B. R.; de Moura Coelho, D.; Sgaravatti, Â. M.; Sgarbi, M. B.; de Souza Wyse, A. T.; Duval Wannmacher, C. M.; Wajner, M.; Vargas, C. R.; Dutra-Filho, C. S. Acute Administration of 5-Oxoproline Induces Oxidative Damage to Lipids and Proteins and Impairs Antioxidant Defenses in Cerebral Cortex and Cerebellum of Young Rats. *Metab. Brain Dis.* **2010**, *25* (2), 145–154. <https://doi.org/10.1007/s11011-010-9190-1>.
- (192) Foltyn, V. N.; Bendikov, I.; De Miranda, J.; Panizzutti, R.; Dumin, E.; Shleper, M.; Li, P.; Toney, M. D.; Kartvelishvili, E.; Wolosker, H. Serine Racemase Modulates Intracellular D-Serine Levels through an  $\alpha,\beta$ -Elimination Activity. *J. Biol. Chem.* **2005**, *280* (3), 1754–1763. <https://doi.org/10.1074/jbc.M405726200>.
- (193) He, F.; Yin, Z.; Wu, C.; Xia, Y.; Wu, M.; Li, P.; Zhang, H.; Yin, Y.; Li, N.; Zhu, G.; Ren, W.; Peng, Y. L-Serine Lowers the Inflammatory Responses during *Pasteurella Multocida* Infection. *Infect. Immun.* **2019**, *87* (12), e00677-19, [/iai/87/12/IAI.00677-19.atom](https://doi.org/10.1128/IAI.00677-19). <https://doi.org/10.1128/IAI.00677-19>.
- (194) AgoguÃ©, H.; Casamayor, E. O.; Bourrain, M.; Obernosterer, I.; Joux, F.; Herndl, G. J.; Lebaron, P. A Survey on Bacteria Inhabiting the Sea Surface Microlayer of Coastal Ecosystems. *FEMS Microbiol. Ecol.* **2005**, *54* (2), 269–280. <https://doi.org/10.1016/j.femsec.2005.04.002>.
- (195) Santaella, C.; Allainmat, B.; Simonet, F.; Chanéac, C.; Labille, J.; Auffan, M.; Rose, J.; Achouak, W. Aged TiO<sub>2</sub>-Based Nanocomposite Used in Sunscreens Produces Singlet Oxygen under Long-Wave UV and Sensitizes *Escherichia Coli* to Cadmium. *Environ. Sci. Technol.* **2014**, *48* (9), 5245–5253. <https://doi.org/10.1021/es500216t>.

- (196) Auffan, M.; Tella, M.; Santaella, C.; Brousset, L.; Paillès, C.; Barakat, M.; Espinasse, B.; Artells, E.; Issartel, J.; Masion, A.; Rose, J.; Wiesner, M. R.; Achouak, W.; Thiéry, A.; Bottero, J.-Y. An Adaptable Mesocosm Platform for Performing Integrated Assessments of Nanomaterial Risk in Complex Environmental Systems. *Sci. Rep.* **2015**, *4* (1), 5608. <https://doi.org/10.1038/srep05608>.

